

Mass Transfer Mechanisms during the Solvent Recovery of Heavy Oil

by

Lesley Anne James

A thesis  
presented to the University of Waterloo  
in fulfilment of the  
thesis requirement for the degree of  
Doctor of Philosophy  
in  
Chemical Engineering

Waterloo, Ontario, Canada, 2009

©Lesley Anne James 2009

# **Author's Declaration**

I hereby declare that I am the sole author of this thesis. This is a true copy of the thesis, including any required final revisions, as accepted by my examiners.

I understand that my thesis may be made electronically available to the public.

# Abstract

Canada has the second largest proven oil reserves next to Saudi Arabia which is mostly located in Alberta and Saskatchewan but is unconventional heavy oil and bitumen. The tar sands are found at the surface and are mined, yet 80% of the 173 billion barrels of heavy oil and bitumen exist in-situ according to the Canadian Association of Petroleum Producers (CAPP). Two factors inhibit the economic extraction and processing of Canadian heavy oil; its enormous viscosity ranging from 1000 to over 1 million mPa.s and the asphaltene content (high molecular weight molecules containing heavy metals and sulphur). Heavy oil and bitumen were only included in the reserves estimates through the efforts of Canadian enhanced oil recovery (EOR) research.

Viscosity reduction is the one common element of in-situ methods of heavy oil recovery with the exception of cold production. Currently, steam assisted gravity drainage (SAGD) and cyclic steam stimulation (CSS) are being used commercially in the field where the oil's viscosity is reduced by injecting steam. Thermal methods are energy intensive requiring vast volumes of water such that any improvement would be beneficial. Solvent extraction is one alternative requiring no water, the solvent is recoverable and reusable, and depending on the mode of operation the heavy oil is upgraded in-situ. Vapour Extraction (VAPEX) and enhanced solvent extraction (N-Solv<sup>TM</sup>) are two such methods. VAPEX and N-Solv reduce the bitumen's viscosity via mass transfer and a combination of mass and heat transfer, respectively. A light hydrocarbon solvent (instead of steam) is injected into an upper horizontal well where the solvent mixes with the heavy oil, reduces its viscosity and allows the oil to drain under gravity to a bottom production well. The idea of using solvents for heavy oil extraction has been around since the 1970s and both VAPEX and N-Solv are patented processes. However, there is still much to be learned about how these processes physically work. Research to date has focused on varying system parameters (including model dimensions, permeability, heavy oil viscosity, solvent type and injection rate, etc.) to observe the effect on oil production from laboratory scale models.

Based on an early mass balance model by Butler and Mokrys (1989) and an improvement by Das (1995), molecular diffusion alone cannot account for the produced oil rates observed from laboratory models. Until recently, very little progress had been made towards qualifying and quantifying the mass transfer mechanisms with the exception of the diffusivity of light hydrocarbons in heavy oil. Mass transfer can only be by diffusion and convection. Differentiating and quantifying the contribution of each is complex due to the nature and

viscosity of the oil. **The goal of this thesis is to investigate the mass transfer mechanisms during the solvent recovery of heavy oil.**

Quantifying the diffusion of light hydrocarbon solvents has been an active topic of research with limited success since the mid 1990's. The experimental approach presented here focused on capturing the rate of solvent mass transfer into the bitumen by measuring the bitumen swelling and the butane uptake independently. Unlike early pressure decay methods, the pressure is held constant to not violate the assumed equilibrium solvent concentration at the interfacial boundary condition. The high solubility of solvent in heavy oil complicates the physical modeling because simplifying assumptions of a constant diffusion coefficient, constant density and a quiescent liquid should not be used. The model was developed from first principles to predict the bitumen swelling. The form of the concentration dependent diffusivity was assumed and the diffusivity coefficients initially guessed. The swelling (moving boundary) was fixed by defining a new dimensionless space coordinate and the set of partial differential equations solved using the method of lines. Using the non-linear regression (`lsqnonlin`) function in MATLAB®, optimising for the difference in predicted and experimentally found bitumen heights and independently validating the result using the solvent uptake, the diffusivity of butane in heavy oil (at 25°C) was found to be  $D_{sb} = 4.78 \times 10^{-6}\omega_s + 4.91 \times 10^{-6} \text{ cm}^2/\text{s}$  where  $\omega_s$  is the solvent mass fraction.

Diffusion alone has proven inadequate in predicting oil recovery rates from laboratory scale models. It is logical to assume that convective mass transfer plays a role at mixing the solvent and bitumen while draining via gravity through the reservoir porous matrix. Solvent extraction experiments were conducted in etched glass micromodels to observe the pore scale phenomena. The pore scale mechanisms were found to differ depending on how the solvent extraction was operated, with non-condensing (VAPEX) or condensing (N-Solv™) solvent. Observations show increased convective mixing and an increased rate of interface advancement when the solvent condenses on the bitumen surface. Evidence of trapped butane vapour being mobilised with the draining live oil and a technique of observing solvent extraction using UV light confirm that the draining live oil is on average one pore deep. While the interface appears from a distance to be uniform, at the pore scale it is not. Live oil can drain from one to two pores via capillary displacement mechanisms in one section of the interface and via film flow only in another area (James and Chatzis 2004; James *et al.* 2008). This work also shows the detrimental impact of having a non-condensable gas present during solvent extraction (James and Chatzis 2008). In summary, this work emphasises the mass transfer and drainage displacement mechanisms of non-condensing (VAPEX) and condensing (N-Solv) solvent extraction methods of heavy oil recovery.

# Acknowledgements

Would have, could have, and should have. Some may have questioned, doubted and wondered but no more than myself. I am here now at the end of a road less travelled and am fortunate that I have few regrets and many thanks.

I would like to thank my supervisor and teacher Dr. Ioannis Chatzis whose supervisory approach and fortuitous personal characteristics have inspired me to continue questioning and learning.

My wonderful mentors have coached and guided me to achieve more in all aspects of my research and career prospects. Thank you to Dr. Mario Ioannidis for providing so much more assistance than deserved, the motivation, detailed technical attention, and support. Dr. Christine Moresoli has been my woman in engineering, friend and someone on whom I rely for great advice, thank you. I appreciate and value Dr. Maurice Dusseault for helping me see the “bigger” picture, and look forward to ongoing heavy oil discussions.

The financial support provided by NSERC, the Postdoctoral Graduate Scholarship and research grants, Dr. Chatzis, the University of Waterloo and my husband are gratefully acknowledged.

I'd like to thank the Department of Chemical Engineering staff for providing countless assistance over many years. I will miss my friends and colleagues in the department, the many conversations, hallway chats, technical discussions and friendly atmosphere created.

How do you truly thank your family who has given so much? My love and gratitude extend from my husband Arman, son Esmé, the perfectly timed birth of my daughter Olwyn, parents, siblings and friends who I rely on like family. Your unending support was crucial in my completion. Thank you.

This thesis is dedicated to my son Esmé and daughter Olwyn;  
may they be inspired to question and learn.

# Table of Contents

List of Tables.....	ix
List of Figures .....	x
Nomenclature .....	xiii
<b>Chapter 1: Introduction.....</b>	<b>1</b>
1.1 Global Oil Consumption and Production.....	1
1.2 Canada's Heavy Oil .....	5
1.3 In-Situ Extraction of Heavy Oil .....	6
1.4 Objectives .....	8
<b>Chapter 2: Literature Review of Solvent Extraction Processes.....</b>	<b>9</b>
2.1 History of Solvent Processes.....	9
2.2 Summary of Vapour Extraction (VAPEX) Literature Results.....	10
2.3 Effect of Heat on the VAPEX Process.....	18
2.4 Depth of the Viscosity Reduced Oil at the VAPEX Interface .....	19
2.5 Solvents Mixed with Non-Condensable Gas .....	23
2.6 Hybrid (Steam-Solvent) Processes.....	24
2.7 N-Solv <sup>TM</sup> .....	25
2.8 Economic and Environmental Advantages .....	28
2.9 Asphaltene Precipitation .....	29
2.10 Pore Scale Phenomena .....	31
<b>Chapter 3: Differentiating Solvent Processes .....</b>	<b>33</b>
3.1 Introduction and Objectives .....	33
3.2 Condensing & Non-condensing Solvent Processes .....	33
3.2.1 Experimental Procedure using Glass Micromodels.....	33
3.2.2 Experimental Results and Discussion.....	40
3.2.2.1 Interface Velocity / Sweep Efficiency .....	41
3.2.2.2 Mass Transfer Mechanisms at the Pore Scale.....	45
3.2.2.3 Asphaltene Precipitation .....	51
3.2.2.4 Drainage Mechanisms and Priority.....	55
3.2.2.5 Depth of the Draining Live Oil .....	62
3.2.2.6 Residual Oil .....	66
3.3 Effect of Non-Condensable Gas on VAPEX .....	67
3.3.1 Experimental Procedure using Unconsolidated Glass Beads .....	67
3.3.2 Results and Discussion .....	69

<b>Chapter 4: One Dimensional Diffusion of n-Butane in Heavy Oil.....</b>	<b>71</b>
4.1 Literature.....	72
4.1.1 Pressure Decay Methods.....	72
4.1.2 Dynamic Pendant Drop Volume Analysis (DPDVA) .....	75
4.1.3 NMR and CAT Scanning.....	80
4.1.4 Oil Phase Swelling.....	84
4.1.5 Solubility in Heavy Oil.....	85
4.2 Experimental Procedure.....	87
4.3 Experimental Results .....	90
4.3.1 Change in Bitumen and Solvent Heights.....	90
4.3.2 Experimental Error .....	93
4.4 Mathematical Model .....	96
4.4.1 Development of the Partial Differential Equations.....	96
4.4.2 Dimensionless Position ( $\xi=x/x_s(t)$ ).....	102
4.4.3 Discretized Set of Equations.....	104
4.4.4 Change in Solvent Height.....	109
4.4.5 Numerical Model Methodology .....	109
4.5 Model Validation .....	110
4.6 Comparison and Discussion.....	111
<b>Chapter 5: Conclusions and Recommendations.....</b>	<b>119</b>
5.1 Conclusions.....	119
5.2 Recommendations.....	121
References .....	122
<b>Appendices</b>	
Appendix A: Micromodel Characterisation.....	127
Appendix B: Effect of Non-Condensable Gas on VAPEX.....	135



# List of Tables

Table 2.2.1: Summary of Laboratory Scale VAPEX Experiments .....	10
Table 3.2.1: Fluid Properties for Solvent Extraction Experiments in Micromodels .....	38
Table 3.2.2: Micromodel Characterisation .....	40
Table 3.2.3: VAPEX Interface Velocity ( $U_p^x$ ) and .....	42
Table 3.2.4: Estimated Average Depth of the Draining Live Oil and Bitumen .....	64
Table 4.1.1: Diffusivity and Oil Swelling Factor Results for Different Solvents in Lloydminster Heavy Oil at 23.9°C (Yang, C. and Gu, Y 2006b).....	79
Table 4.2.1: Experimental Data.....	89
Table 4.3.1: Average and Standard Deviation for the Differences in Height between the Replicate Experiments .....	94
Table 4.3.2: Experimental Error Propagation.....	95
Table 4.6.1: Optimised Diffusion Coefficients .....	115

# List of Figures

Figure 1.1.1: World Historical & Projected Energy Consumption (EIA) .....	2
Figure 1.1.2: Historical & Projected Unconventional Oil Production (EIA) .....	3
Figure 1.1.3: World Heavy Oil Resources (modified from Smalley 2000).....	4
Figure 1.1.4: Viscosity of Heavy Oil and Bitumen (Smalley 2000) .....	4
Figure 1.2.1: Canada's Heavy Oil and Bitumen (Wikimedia Commons 2006).....	6
Figure 1.3.1: Schematic Representation of Solvent Based EOR using Two Horizontal Wells .....	7
Figure 2.2.1: Photo of the Swept Area (Solvent Chamber) and Remaining Oil at End of Experiment ( $k = 16 \mu\text{m}^2$ ) (Moghadam <i>et al.</i> 2009) .....	21
Figure 2.2.2: Comparison of Experimental and Calculated Cumulative Production (Moghadam <i>et al.</i> 2009).....	22
Figure 2.2.3: Square-Root Dependence of Experimentally Found Production Rates on Permeability (data from Moghadam <i>et al.</i> 2009) .....	23
Figure 2.2.4: Dew Point versus Bubble Point at Typical Alberta Reservoir Conditions (Nenniger and Dunn 2008).....	26
Figure 2.2.5: Solvent Based Gravity Drainage Correlation (Nenniger and Dunn 2008).....	27
Figure 2.2.6: Bitumen Viscosity as a Function of Asphaltene Content (Luo and Gu 2005).....	30
Figure 2.2.7: Valleys and Peaks at the uneven VAPEX Interface (Chatzis 2002).....	31
Figure 2.2.8: A Closer Look at the VAPEX Interface (Chatzis, 2002) .....	32
Figure 3.2.1: Micromodel Patterns Etched in Glass (James and Chatzis, 2004).....	36
Figure 3.2.2: Investigating Pore Scale Mechanisms – Experimental Apparatus.....	38
Figure 3.2.3: VAPEX Interface Advancement in Model DC-1.....	41
Figure 3.2.4: VAPEX Interface Advancement in Micromodels DL-1, DC-1 and OC-1 .....	42
Figure 3.2.5: VAPEX Interface Velocity in model DL-1 with and without Condensation.....	44
Figure 3.2.6: The Solvent - Bitumen Interface.....	46
Figure 3.2.7: Disappearing Trapped Solvent Vapour Bubbles Indicate Dilution by Diffusion with Non-Condensing Solvent.....	47
Figure 3.2.8: Effect of Temperature and Solvent on the Viscosity of Athabasca Bitumen (Badamchi-Zadeh <i>et al.</i> 2009) .....	49
Figure 3.2.9: Stripping of Bitumen by Condensed Solvent – Convective Mass Transfer.....	51
Figure 3.2.10: Asphaltene Precipitation .....	52
Figure 3.2.11: Live Oil Draining Around Precipitated Asphaltenes .....	54
Figure 3.2.12: Interface Positions during VAPEX Drainage in Model OC-1 .....	56

Figure 3.2.13: Live Oil Drainage at the Interface of Model OC-1 .....	57
Figure 3.2.14: Live Oil Drainage at the Interface of Model DC-1 .....	58
Figure 3.2.15: Model DC-1 Bubble Formation during Live Oil Drainage 1/3 (series 7-1).....	59
Figure 3.2.16: Model DC-1 Bubble Formation during Live Oil Drainage 2/3 (series 7-1).....	60
Figure 3.2.17: Model DC-1 Bubble Formation during Live Oil Drainage 3/3 (series 7-1).....	61
Figure 3.2.18: Solvent Extraction in Two-Dimensional Models.....	63
Figure 3.2.19: Depth of Mobile Live Oil in Consolidated Media using Florescence.....	65
Figure 3.2.20: Residual Oil Trapped in Extracted Parts of Models with Non-Condensing Solvent (VAPEX).....	66
Figure 3.3.1: Plexiglas Channels used for holding Unconsolidated Glass Beads .....	67
Figure 3.3.2: Experimental Set-up for Examining the Effect of Non-Condensable Gas.....	68
Figure 3.3.3: Live Oil Production Rates with Methane Present .....	69
Figure 4.1.1: Schematic Diagram of the Pressure Decay Method for Determining Diffusivities .....	73
Figure 4.1.2: Experimental Apparatus for the Dynamic Pendant Drop Volume Analysis (Yang, C. and Gu, Y. 2005a, 2005b, 2006a, 2006b, 2007) .....	76
Figure 4.1.3: a) Experimental Schematic and b) Concentration Dependent Diffusivity for Heptane in Heavy Oil (Luo <i>et al.</i> 2007) .....	81
Figure 4.1.4: Excess Volume of Mixing for Heptane in Heavy Oil (Luo and Kantzas 2007) .....	81
Figure 4.1.5: Comparison of Effective and Molecular Diffusivities for a Homogeneous Sand Pack (Luo, H. and Kantzas, A. 2008).....	82
Figure 4.1.6: Solubility of Butane in Frog Lake Bitumen (Yazdani and Maini 2007).....	86
Figure 4.2.1: Schematic Diagram of Solvent Diffusion into Heavy Oil .....	88
Figure 4.3.1: Experimental Increase in Bitumen Height .....	91
Figure 4.3.2: Experimental Decrease in Solvent Height .....	91
Figure 4.3.3: Solvent Concentration in the Bitumen Phase as a Function of Time.....	92
Figure 4.3.4: Change in Height is Square Root Dependent on Time .....	93
Figure 4.3.5: Temperature Profile for the Solvent and Bitumen Water Baths .....	94
Figure 4.3.6: Increase in Bitumen Height is Independent of Cross-Sectional Area.....	96
Figure 4.4.1: Solubility Predicted using the PR EOS for n-Butane in Athabasca Bitumen .....	106
Figure 4.5.1: Predicted Increase in Bitumen as a function of Time & Initial Height.....	111
Figure 4.6.1: Bitumen Increase - Comparison of Experimental and Model Results .....	112
Figure 4.6.2: Solvent Decrease - Comparison of Experimental and Model Results .....	112
Figure 4.6.3: Predicted Concentration Profiles .....	113

Figure 4.6.4: Optimised Diffusivity Functions as per Table 4.6.1 .....	115
Figure 4.6.5: Comparison of the Increase in Bitumen using Different Diffusivities.....	116
Figure 4.6.6: Comparison of the Decrease in Solvent using Different Diffusivities.....	117
Figure 4.6.7: Comparison of Bitumen Phase Density using Different Diffusivities .....	118

# Nomenclature

Symbol	Description	Units
A	Area	cm <sup>2</sup> , m <sup>2</sup>
C	Concentration	g/mol
D	Diffusivity	cm <sup>2</sup> /s, m <sup>2</sup> /s
d	Depth	cm, m, mm, μm
g	Gravitational constant	m/s <sup>2</sup> , cm/s <sup>2</sup>
h	Height	cm, m, mm
k	Permeability	Darcy, μm <sup>2</sup>
L	Length	cm, m, mm
m	Mass	g, kg
$\dot{m}$	Mass flow rate	g/min,
N	Flux	g/cm <sup>2</sup> .s, kg/m <sup>2</sup> .s
P	Pressure	kPa, MPa, psi
PV	Pore volume	cm <sup>3</sup> cm <sup>3</sup> /min,
Q	Volumetric flow rate	barrels/day (bb/d)
S	Saturation	%
SOI	Initial oil saturation	%
SOR	Residual oil saturation	%
t	Time	day, hour, min, s
U	Velocity	m/s, cm/s
V	Volume	m <sup>3</sup> , cm <sup>3</sup> , barrels, bb
V <sup>m</sup>	Mass average velocity	m/s, cm/s
v	Volume fraction	
w	Width	M, cm
X	Mole fraction	
<b>Greek</b>		
δ	Depth of the draining live oil	μm, mm, pores
δ <sub>etch</sub>	Depth of etching in micromodels	μm, mm, pores
Δ	Change in, i.e. ΔS <sub>o</sub> = change in oil saturation	%
φ	Porosity	%
μ	Viscosity	mPa.s, cP
θ	Dip or contact angle	°
ρ	Density	kg/m <sup>3</sup> , g/cm <sup>3</sup>
σ	Surface tension	N/m, dyne/cm
ω	Mass fraction	
<b>Subscripts</b>		
b	Bitumen	
c	Capillary	
c	Calculated	

<b>Symbol</b>	<b>Description</b>	<b>Units</b>
eq	Equivalent	
f	Falling	
g, G	Gas	
i	Interface or nodal position	
l, L	Liquid	
lo	Live oil	
m	Cementation factor	
max	Maximum	
n	Exponent	
o	Oil	
p	Pore	
x	Cross sectional	
s	Solvent or spreading phase	
v	Vapour	
wb	Water bath	
wc	Connate water	
or	Residual oil	
sys	System	

### **Superscripts**

*	Solubility limit, i.e. $\omega_s^*$ or $P_v^*$
i	Interfacial
imb	Imbibition
dr	Drainage
x	X-direction

# Chapter 1: Introduction

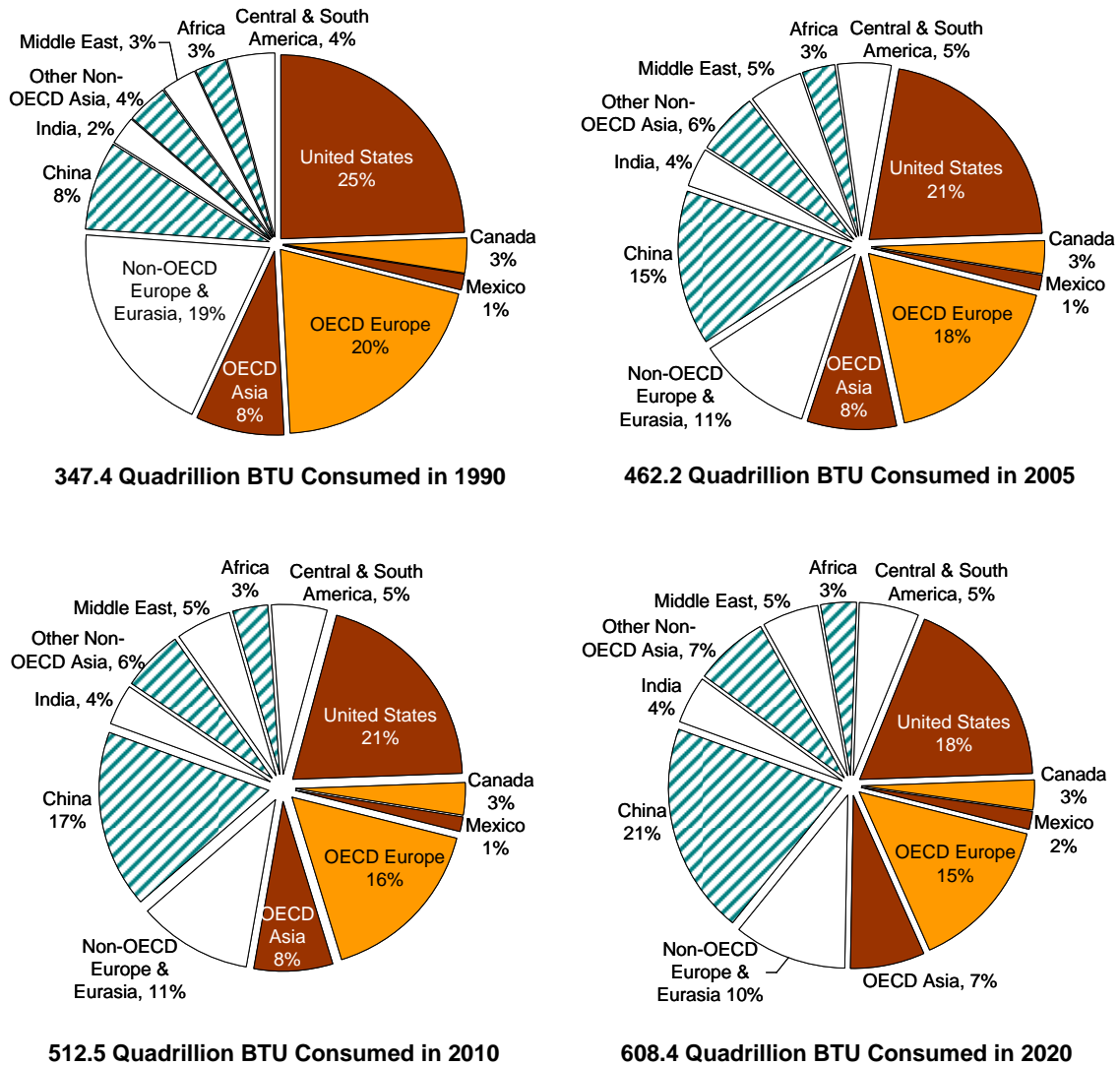
Advancing the technical understanding of the in-situ heavy oil recovery using light hydrocarbon solvents has major economic and environmental importance for Canada and the rest of the oil consuming world. Most of the world's large easily accessible conventional oil reserves are already being produced. This leaves more costly, geologically and geographically challenging, smaller deposits of conventional oil and unconventional liquid fuels to fill the gap of the world's increasing consumption of oil and oil products. Heavy oil and bitumen are thick or viscous oils that cannot be efficiently produced using conventional oil production technologies. VAPEX (VAPour EXtraction) and N-Solv<sup>TM</sup> (eNhanced SOLvent extraction) are two emerging heavy oil production methods invented and developed in Canada. They are enhanced oil recovery (EOR) techniques to produce in-situ heavy oil and bitumen by first reducing the viscosity through the addition of a light hydrocarbon solvent into the heavy oil. This thesis aims to qualify and illustrate the mass transfer mechanisms by which the heavy oil viscosity is reduced and quantify the diffusivity of butane in heavy oil in applications such as VAPEX and N-Solv.

## 1.1 *Global Oil Consumption and Production*

Oil and petroleum products will continue to play an important and dominant role in society for the foreseeable future. While the exploration and advancement of sustainable, emerging, alternative energy sources and bio-products are environmentally important, the reality is that petroleum products are still cheaper and more energy efficient than many alternatives. The United States is the largest gross consumer of energy in the world, but Canada is the largest per capita. Rapidly industrialising countries with huge populations like China and India (second and fifth largest oil consumers in 2007) are quickly consuming more and more energy.

Figure 1.1.1 shows the total energy consumed historically in 1990 and 2005 and total projected energy consumption in 2010 and 2020. OECD is the organisation for economic co-operation and development. An OECD member must be a democratic country committed to a global market economy that supports sustainable economic growth, improved living standards, maintenance of financial stability, etc. and can be viewed as a sign of a modern, developed country. In 1990 non-OECD Asian countries consumed only 14% of the world's 347.4 quadrillion BTUs consumed. By 2010, 15 years later, they are expected to consume 27% of the world's 512.5 quadrillion BTUs and 32% by 2020. The shift in energy consumption is coming primarily from China and India. In 1990, OECD countries accounted for 57% of the energy consumption which is expected

to drop to 45% by 2020. In the same time period oil consumption is only expected to drop from 37% of the 347.4 quadrillion BTUs in 1990 to 34% of the 608.4 quadrillion BTUs in 2020. Transportation followed by industrial use of liquid fuels makes up over 85% of the world's consumption of liquid fuels and 90% of the United State's liquid fuels consumption. The projected forecasts indicate that liquid fuel consumption will continue to increase at an average rate of 1.2% annually worldwide and even faster, at a rate of 2.8% annually in non-OECD Asia.

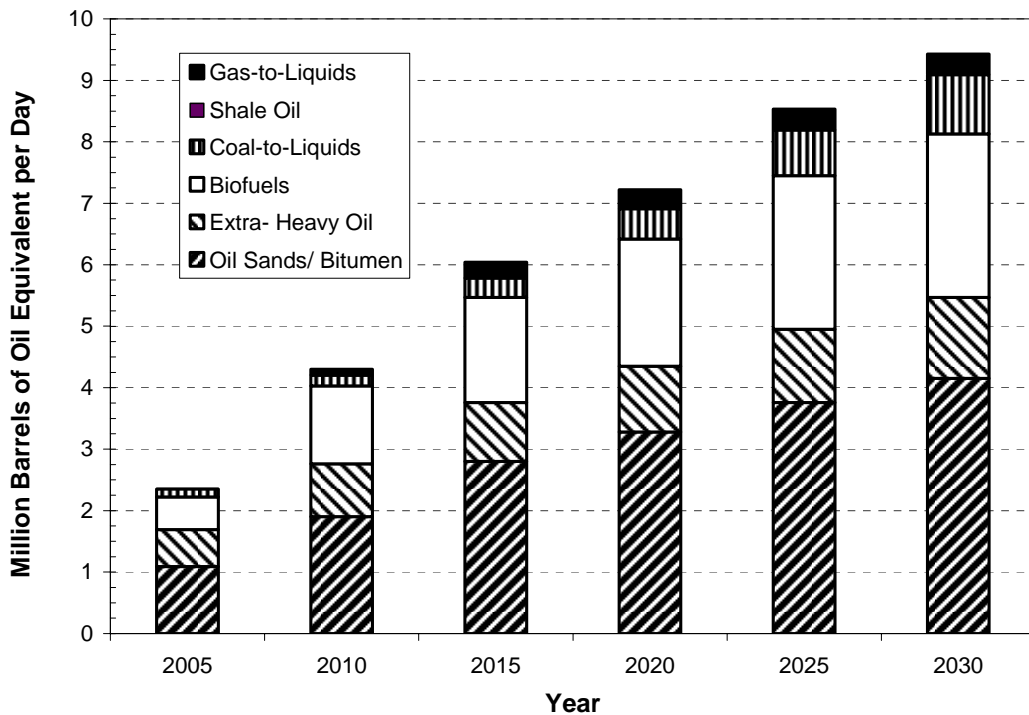


**Figure 1.1.1: World Historical & Projected Energy Consumption (EIA)**

Every year the Oil and Gas Journal updates the proven oil reserves worldwide. In December 2008,  $2.13 \times 10^{11} \text{ m}^3$  (1.34 trillion barrels) of oil were recorded (Radler 2008). Annual changes occur due to re-estimating an already producing reserve less the annual production, radical developments in production technology and any well discoveries. Experts agree that most of the



world's large oil reserves have been already discovered and now it takes more effort to find smaller reserves of oil that is less easily recovered. The physical location, geology, and physical properties of the oil all play an important role in the cost and actual percentage of oil that can be recovered from a particular reserve. Oil that is deep offshore or in a low permeability, fractured formation is more difficult and costly to produce than the same quality oil found in homogeneous sandstone in the desert. As oil demand continues to rise and cheap, conventional oil is being produced, the world is turning towards less accessible, smaller reserves of conventional oil and unconventional oil.



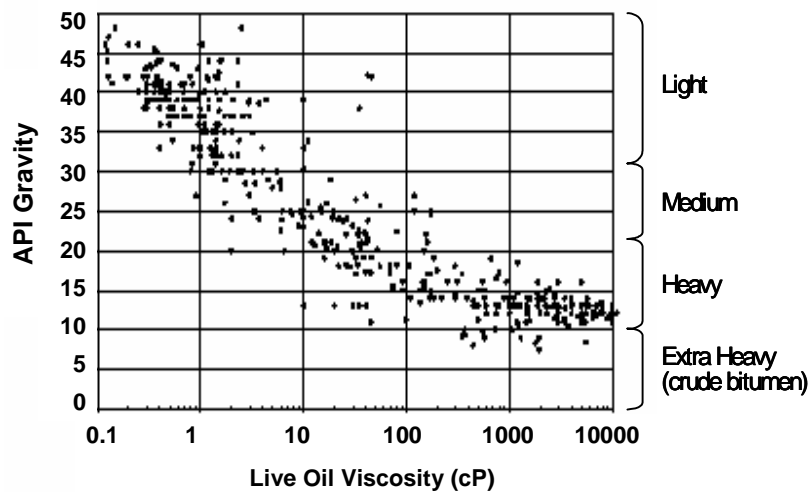
**Figure 1.1.2: Historical & Projected Unconventional Oil Production (EIA)**

Unconventional liquid fossil fuels are oils that aren't produced by drilling conventional, vertical wells and using the earth's pressure along with secondary oil recovery techniques to extract the oil. Unconventional oil consists of shale oil, tar sands, heavy oil, bitumen, gas to oil and includes biofuels. Figure 1.1.2 shows the projected significance of unconventional oil production over the next 21 years. Overall, unconventional oil production is expected to increase from  $0.375 \times 10^6 \text{ m}^3$  (2.36 million barrels) of oil equivalent per day in 2005 to  $1.50 \times 10^6 \text{ m}^3$  (9.43 million barrels) of oil equivalent per day in 2030. As shown in Figure 1.1.2, heavy oil and bitumen are expected to comprise of more than 60% of the unconventional oils until at least 2020. The countries with significant heavy oil and extra-heavy oil reserves are shown in Figure 1.1.3 where estimates are for initial oil in place not proven recoverable oil.



**Figure 1.1.3: World Heavy Oil Resources (modified from Smalley 2000)**

Significant changes in the estimated proven oil reserves occurred in 2002 when Canadian heavy oil and bitumen were included at amount of  $27.8 \times 10^9 \text{ m}^3$  (174.8 billion barrels) (Radler 2002). The addition of Canadian heavy oil in the reserves estimates positioned Canada as second behind Saudi Arabia as countries with the most oil reserves. Since 2002, Venezuelan proven reserves have been steadily climbing to  $15.8 \times 10^9 \text{ m}^3$  (99.4 billion barrels) in 2008. The heavy oil in both countries is not newly discovered and the initial oil in place is much greater. The difference is proving that current technology is capable of producing the “proven” quantity. The commercialisation of the oil sands, proven in-situ heavy oil recovery methods such as cold heavy oil production with sand (CHOPS) and steam assisted gravity drainage (SAGD) and committed heavy oil research in Canada are the governing reasons for the inclusion of Canada’s heavy oil in worldwide reserves estimates.



**Figure 1.1.4: Viscosity of Heavy Oil and Bitumen (Smalley 2000)**

Heavy oil and bitumen are much thicker or viscous than conventional oil. The tar sands are heavy oil and bitumen deposits found in unconsolidated sand close enough to the earth's surface that they can be mined. Figure 1.1.4 shows the range of API gravity and viscosity of different grade oils found around the world. Heavy oil is often defined as having an API gravity less than 20 and a viscosity greater than 1000 mPa.s (water is 1 mPa.s). The oil is considered bitumen if the API gravity is less than 10 and the viscosity is greater than 10,000 mPa.s (Dusseault 2006). The viscosity and shallow depth (pressure) of the heavy oil makes it very difficult to produce economically using conventional pressure-drive production techniques.

## **1.2 Canada's Heavy Oil**

Canada's heavy oil reserves are found in western Canada, mainly in Alberta and Saskatchewan, as shown in Figure 1.2.1. Situated north of Edmonton, AB, the three main deposits are the Athabasca, Cold Lake and Peace River oil sands. The geographic location of the reserve is indicative of the quality of the oil based on geology. The oil deposit is generally shallower and the oil's viscosity higher (with a lower °API density) the further east and north it is found (Dusseault 2006). Conventional oil has a low viscosity (< 100 mPa.s) and is typically found in deep, high pressure reservoirs where primary recovery is due to the pressure difference between the reservoir and well. In contrast, the heavy oil and bitumen in western Canada are:

- very viscous, ranging from a few hundred to over 1 million mPa.s and are often immobile at standard conditions
- found in thin oil seams, with 20 m pay zones on average
- found in unconsolidated sandstone ( $\sim 0.27 \times 10^{12} \text{ m}^3$ , 1.7 Tb) and fractured carbonates ( $\sim 0.08 \times 10^{12} \text{ m}^3$ , 0.5 Tb)
- unconsolidated sandstone porosity ranges from 26-32% and the permeability from 1200-7500 mD
- shallow, such that the reservoir pressure and temperature are low
- current producing fields are found at the surface to a maximum depth of 800-1000 m and have a reservoir temperature from 4 to 40°C

Sustainable use of heavy oil as an energy source depends not only on the price of oil, but also on our ability as Canadian researchers to develop an energy efficient and environmentally appropriate life cycle. Both surface mining of the tar sands and thermal methods of in-situ extraction are energy intensive processes requiring large volumes of water for separating the bitumen from the sand or providing heat in the form of steam for reducing the viscosity of the in-situ oil. Besides water consumption and the land footprint of mining the oil sands and tailings

ponds, heavy oil and bitumen is of lower quality than conventional crude oil. Heavy oil and bitumen contain 15-20 weight percent asphaltenes (heavy metals and sulphur) which must be removed from the oil during upgrading resulting in another energy intensive process with waste products. Any recovery process that can minimise water usage and upgrade the oil in-situ needs to be seriously considered economically and environmentally.



Figure 1.2.1: Canada's Heavy Oil and Bitumen (Wikimedia Commons 2006)

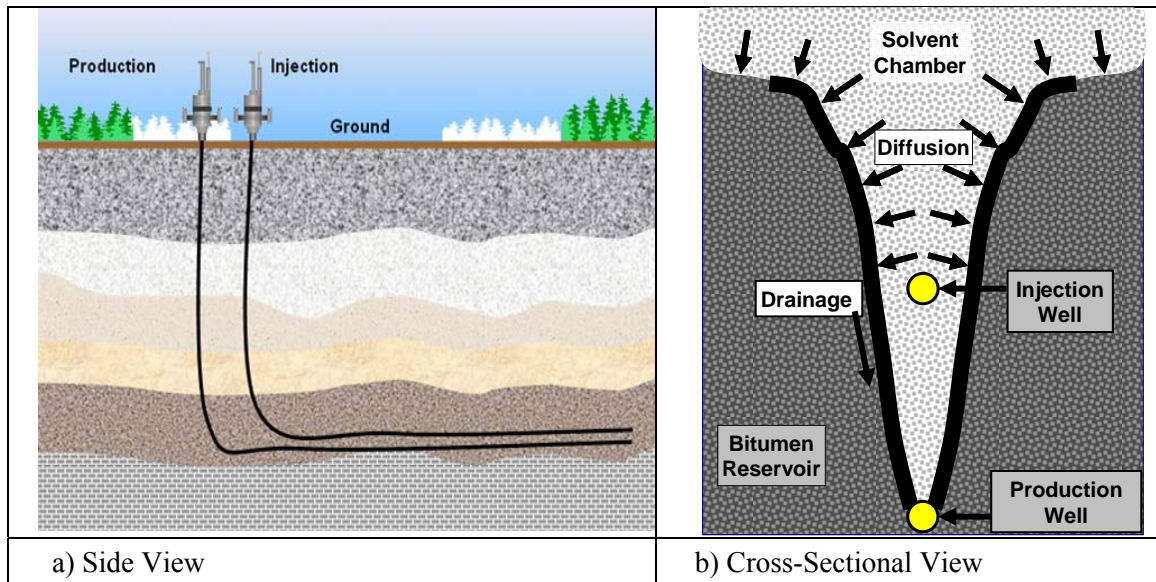
### 1.3 *In-Situ Extraction of Heavy Oil*

Canada is the world leader in developing EOR techniques for in-situ heavy oil production. Cold production of lower viscosity heavy oil is possible, but production rates are often low, with marginal recovery factors and high water cuts. Allowing sand to be produced along with the oil helps and is known as CHOPS – cold heavy oil production with sand. Sand production used to be considered disastrous but it does not pose the same risk with new technology and equipment capable of handling solids (Dusseault 2006). Otherwise, viscosity reduction is essential to economically produce oils with viscosities greater than a few thousand centipoises. New EOR techniques and combinations of techniques are constantly being investigated and compared where the ultimate goal is to maximise oil recovery.

Viscosity reduction can be achieved by thermally reducing the viscosity (heating), by mass transfer (solvent dilution), or by molecular scission (pyrolysis, *in-situ* hydrogenation, etc.). Thermal methods include steam-assisted gravity drainage (SAGD), cyclic steam stimulation (CSS), and in-situ combustion. The viscosity can be reduced by dilution or the mass transfer of a light hydrocarbon solvent into the heavy oil as in the case of vapour extraction (VAPEX) or N-Solv. VAPEX is considered the solvent analog to SAGD (Butler and Mokrys 1989). Both N-Solv and VAPEX involve injecting a solvent into a heavy oil reservoir to reduce the viscosity of the heavy oil via mass transfer. The solvent-enhanced live oil then drains via gravity drainage and is produced through a lower horizontal production well. The recent high oil prices experienced have motivated some researchers to consider combination thermal-solvent techniques. Many of these ideas may be more motivated by potential royalties than good science.

Figure 1.3.1 shows a typical representation of a thermal or solvent recovery method using horizontal wells. Solvent or steam is injected into the upper well where:

- the steam condenses on the cold bitumen surface, reducing the viscosity of the bitumen through heat conduction (steam assisted gravity drainage – SAGD, or other thermal steam processes),
- solvent vapour diffuses into the bitumen and reduces the viscosity (solvent processes operated in the vapour phase such as Vapour Extraction – VAPEX)
- solvent condenses on the bitumen interface and reduces the bitumen viscosity through heat conduction and mass transfer (when operated so the solvent condenses – N-Solv)



**Figure 1.3.1: Schematic Representation of Solvent Based EOR using Two Horizontal Wells**

The viscosity reduced mobile “live oil” drains via gravity to the bottom production well. The growth of the solvent or steam chamber is generally upwards first to the top of the oil “pay zone” during what’s called the chamber rising phase. Then the chamber starts to spread laterally outwards sweeping the oil bearing formation as the viscosity reduced oil drains downwards. The pores drained of oil become filled with solvent or steam known as the steam or solvent chamber which grows laterally in time, known as the chamber spreading phase. Finally, when the solvent/steam chamber reaches the extent of the oil formation, the height of the oil filled pores decreases during the chamber falling phase, as shown in Figure 1.3.1b.

## **1.4 Objectives**

The objectives of this doctoral thesis are to explore and understand the in-situ solvent extraction of heavy oil. Chapter 2 provides a detailed review of solvent EOR methods research to date and goes on to compare and contrast non-condensing (VAPEX) and condensing (N-Solv) solvent processes using experimental observations and results along with fundamental theory. Pore scale observations from experiments in etched glass micromodels provided direct evidence of the mass transfer of solvent in heavy oil, the pore scale events associated with VAPEX and N-Solv and the determination of how mass transfer and gravity drainage interact to advance the VAPEX interface (James and Chatzis 2004; James *et al.* 2008). Observations show that convective mixing plays an important role at the pore scale. The effect of solution gas or another non-condensable gas present in the solvent chamber is clearly shown to have a negative impact on production (James and Chatzis 2008).

Another long term objective has been to quantify the concentration dependent diffusivity of solvent into heavy oil. High solvent-bitumen mass transfer rates observed in laboratory scale experiments dictate that the dilute diffusion assumption often used is violated. Chapter 4 describes over a decade of research trying to quantify the diffusivity of solvent in heavy oil. The experimental approach and results are presented for the one-dimensional diffusion of butane in heavy oil where the rate of solvent mass transfer (bitumen swelling and solvent uptake) was measured with time. Finally, a mathematical model was developed to describe the bitumen swelling from first principles and is used to find the diffusivity function coefficients by optimising the predicted versus experimentally measured bitumen swelling. Both the experimental aspects and mathematical model were developed and perfected over time (James 2003). The fact that the optimised diffusivity is independently validated using the solvent mass balance differentiates this work.

# Chapter 2: Literature Review of Solvent Extraction Processes

## 2.1 History of Solvent Processes

Butler and Mokrys published their first VAPEX paper on the solvent analog of steam-assisted gravity drainage in 1989. Liquid toluene was used to extract two different oils (Athabasca and Suncor Coker) from Hele-Shaw cells. However, the idea of using solvent to produce heavy oil is derived from the 1970s, when Allen (1974) varied the ‘huff and puff’ process by alternating steam and solvents like butane and propane. Allen and Redford (1976) also used liquid solvent, along with a non-condensable gas, and injected these into the reservoir. Nenniger (1979) patented the injection of pure gas or a mixture of gases at or below the vapour pressure of the gaseous mixture in order to recover the heavy oil-in-place. At that time, he was thinking of carbon dioxide and ethane as the best options for the solvent due to their availability and lower cost. Dunn *et al.* (1989) investigated the recovery of heavy oil from sand using carbon dioxide and ethane. However, the discouraging production rates from these efforts proved uneconomical on paper and, therefore, were never tried in the field. The technological breakthrough of horizontal wells revitalised the idea of using solvent injection to produce heavy oil after a 10 year gap! Throughout the 1990s VAPEX research focused on performing laboratory-scale experiments in non-porous models (Hele-Shaw cells) and in porous media models such as unconsolidated sand or glass beads packed into various dimensioned models (Butler and Mokrys 1989, 1991, 1993; Das 1996; Jiang 1996; Jin 1999; Oduntan 2001; Ramakrishnan 2003; James 2003; James and Chatzis 2004; Karmaker and Maini 2003; Talbi and Maini 2004; Friedrich 2005; Yazdani and Maini 2005, 2006, Tam 2007; Rezaei and Chatzis 2008; and Moghadam *et al.* 2009).

The concept of using heated miscible solvents to recover heavy oil and bitumen commenced in the early 1970s. Farouq Ali and Snyder (1973) and Awang and Farouq Ali (1980) suggested hot miscible displacement using solvents. Instead of waterflooding a reservoir, the thought was to use a warm liquid solvent that was miscible in the heavy oil to help reduce the heavy oil viscosity and increase the recovery efficiency.

## 2.2 Summary of Vapour Extraction (VAPEX) Literature Results

Most VAPEX experiments have involved laboratory scale models where heavy oil is recovered from various shaped geometry systems filled with saturated porous media by injecting either vapour or liquid solvent. The following table summarises the majority of VAPEX experiments carried out to date and describes the VAPEX system used, the solvent used along with its state and method of injection and the experimental goals.

**Table 2.2.1: Summary of Laboratory Scale VAPEX Experiments**

Author & VAPEX System	Objectives and Results
<p><b>Butler and Mokrys (1989)</b>  <b>Hele-Shaw cell</b>            [7 cm x 2.6 cm x 7 cm]</p>	<ul style="list-style-type: none"> <li>- Observed asphaltene precipitation</li> <li>- Scaling equations were proposed for production rates</li> </ul>
<p><b>Butler and Mokrys (1993)</b>  <b>2-D Packed Model</b>            [3.46 cm x 21.7 cm x 69.8 cm]            1 mm beads, <math>\rho_{\text{beads}} = 1327 \text{ kg/m}^3</math>  <math>k = 1136 \mu\text{m}^2</math>  <math>\phi = 0.39</math></p> <p><b>Heavy oil</b>            Lloydminster (Tangleflags)  <math>\mu = 10,000 \text{ mPa}\cdot\text{s}</math> at <math>20^\circ\text{C}</math>  <math>\rho = 972 \text{ kg/m}^3</math> at <math>20^\circ\text{C}</math>            15.6 wt% asphaltenes (pentane, <math>20^\circ\text{C}</math>)</p> <p><b>Solvents</b>            Hot water &amp; propane            Constant propane (l) injection just below the dew point.            Propane            Ethane</p>	<p><b>Hot Water Flood and Propane Vapour Results:</b></p> <ul style="list-style-type: none"> <li>- <math>P = 1.34 - 1.38 \text{ MPa}</math> (196-200 psig), <math>T = 42 - 47^\circ\text{C}</math></li> <li>- Recovery = 60% in 7 hours</li> <li>- Production Rates = 500 g/hr (857 bbl/day) from 1h 46min to 2h 36min &amp; 150 g/hr (260 bbl/day) from 2h 36min to 6h. Rates are shown in parentheses are estimated scaled rates using a 10m pay zone and a 2-sided 457m horizontal well.</li> <li>- Observations = Some asphaltene precipitation</li> </ul> <p><b>Propane Results:</b></p> <ul style="list-style-type: none"> <li>- Pressure = 0.888 – 0.918 MPa (129-133 psig)</li> <li>- Temperature = 26 - 30°C</li> <li>- Recovery = 66% in 8 hours</li> <li>- The recovery resulted in two distinct scaled recovery rates starting at 155 g/hr (270 bbl/day) for the first 3 hours and ending at 72 g/hr (126 bbl/day) from 3 to 8 hours. Rates are shown in parentheses are estimated scaled rates using a 10m pay zone and a 2-sided 457m horizontal well.</li> <li>- The oil was upgraded from 10,000 to 2000 mPa.s</li> </ul> <p><b>Ethane Results:</b></p> <ul style="list-style-type: none"> <li>- Recovery = 26% in 7 hours</li> <li>- Two distinct laboratory scale rates resulted in scaled recovery rates starting at 140 g/hr (243 bbl/day) for the first 2 hours and ending at 38 g/hr (66 bbl/day) from 2 to 8 hours. Rates are shown in parentheses are estimated scaled rates using a 10m pay zone and a 2-sided 457m horizontal well.</li> <li>- There was no visible asphaltene precipitation.</li> </ul>



Author & VAPEX System	Objectives and Results
<p><b>Jiang and Butler (1996)</b></p> <p><b>2-D Packed Model</b> [3.2 cm x 21.6 cm x 35.6 cm] Alternate layers of Ottawa Sand: 20-30 mesh, <math>k = 214 \mu\text{m}^2</math> 30-50 mesh (fine), <math>k = 43 \mu\text{m}^2</math> <math>\phi = 0.35 - 0.37</math></p> <p><b>Heavy oil</b> Lloydminster (Tangleflags) <math>\mu = 7400 \text{ mPa}\cdot\text{s}</math> at ambient SOI: 0.79 – 0.82</p> <p><b>Solvent</b> n-Butane at its vapour pressure <math>T_{\text{wb}} \sim 20^\circ\text{C}</math>, <math>T_{\text{amb}} = 21\text{-}23^\circ\text{C}</math> <math>P_{\text{vap}}^* = 110\text{-}124 \text{ kPa}</math> (16-18 psig)</p>	<p><b>Goal:</b> Their goal was to investigate the effect heterogeneity using nine continuous layers of alternating high and low permeability as well as discontinuous lenses of low permeability zones.</p> <p><b>Results:</b></p> <ul style="list-style-type: none"> <li>- Oil production rates are lower for heterogeneous layered systems compared to homogeneous systems.</li> <li>- Vertical fractures and solvent injection from the top of the system both result in higher oil production rates due to better communication between the solvent and heavy oil.</li> <li>- The solvent chamber easily extends around discontinuous lenses of low permeability.</li> <li>- The solvent chamber advances into the higher permeability layers of the continuous layered model while growth into the low permeability layers is retarded by capillarity.</li> </ul>
<p><b>Das (1995), and Das and Butler (1996a, 1998)</b></p> <p><b>Hele-Shaw cell</b> <math>k = 1344 \text{ and } 5400 \mu\text{m}^2</math></p> <p><b>2-D Packed Model</b> [3.2 cm x 34 cm x 22 cm] Ottawa sand or Glass beads <math>k = 27, 43.5, 217, 432, 1032 \mu\text{m}^2</math> <math>\phi = 0.35 - 0.37</math></p> <p><b>Heavy oil (at 20°C)</b> Peace River, <math>\mu = 130,000 \text{ mPa}\cdot\text{s}</math> Lloydminster, <math>\mu = 10,000 \text{ mPa}\cdot\text{s}</math></p> <p><b>Solvents</b> Propane &amp; n-butane below and near their vapour pressures</p>	<p><b>Goal:</b> The goal was to assess VAPEX in terms of performance and impact of asphaltene precipitation</p> <p><b>Hele-Shaw Results:</b></p> <ul style="list-style-type: none"> <li>- Production rates increased with solvent partial pressure below the vapour pressure.</li> <li>- When the solvent was used at its vapour pressure de-asphalting occurred in regular patterns in the Hele-Shaw cell.</li> <li>- Production rates using propane and Peace River oil were increased 35% by the onset of de-asphalting.</li> </ul> <p><b>2-D Packed Model Results:</b></p> <ul style="list-style-type: none"> <li>- The production rates from the saturated 2-D models were found to be almost 10x higher than expected using scale-up predictions.</li> <li>- <math>Q \propto \sqrt{k}</math></li> <li>- They hypothesised that production rates were higher in porous media due to the increased surface area in the pores and the cross-current flow of the solvent and live oil drainage.</li> <li>- An effective diffusivity taking into account the ratio of the diffusion area to the fluid flow area may help account for differences between experimental and predicted production rates.</li> <li>- Increased production rates from porous media models may be attributed to imbibition of the live oil and higher spreading coefficients of the live oil over connate water.</li> </ul>

Author & VAPEX System	Objectives and Results
<p><b>Boustani &amp; Maini (2001)</b></p> <p><b>Hele-Shaw cell</b> [DxWxH] [10τ x 7.6 cm x 7.4 cm] k = 254 μm<sup>2</sup></p> <p><b>Heavy oil</b> Dover μ = 543,800 mPa.s at 20.5°C</p> <p>Panny μ = 51,676 mPa.s at 10.5°C, 10,800 mPa.s at 19.5°C, and 5918 mPa.s at 23°C</p> <p><b>Solvent</b> Propane</p>	<p><b>Goal:</b> The goal was to identify the main mass transfer processes at the VAPEX interface.</p> <p><b>Results:</b></p> <ul style="list-style-type: none"> <li>- Using the Hayduk <i>et al.</i> (1973) for the diffusivity of propane in Peace River bitumen where <math>D = 0.0591 \times 10^{-9} \mu^{-0.545} \text{ m}^2/\text{s}</math>, the Butler and Mokrys (1989) VAPEX parameter, <math>N_s</math>, was determined for the maximum solvent concentration. This proved to be 1-2 orders of magnitude different than <math>N_s</math> values back-calculated from the experiments.</li> <li>- When Taylor dispersion was taken into account in the effective diffusivity, the discrepancy between analytically found and experimentally determined values of <math>N_s</math> were minimised for equivalent Peclet numbers.</li> </ul>
<p><b>Oduntan (2001)</b></p> <p><b>2-D Troughs</b> [DxWxH] [1.9 cm x 1.6 cm x 21 cm, 42 cm, 84 cm, 160 cm, 247 cm]</p> <p><b>Unconsolidated Glass Beads</b> k = 25, 84, 134, 190 μm<sup>2</sup>, φ = 0.38 Dip Angle = 45°, 90°</p> <p><b>Heavy oil</b> μ = 40,550 mPa.s at <math>T_{\text{amb}}</math> ρ = 970.3 kg/m<sup>3</sup></p> <p><b>Solvent</b> Free flow C<sub>4</sub>H<sub>10</sub> at its <math>P_{\text{vap}}^*(T_{\text{amb}})</math> T = 19-22°C <math>P_{\text{vap}}^* = 110\text{-}124 \text{ kPa (16-18 psig)}</math></p>	<p><b>Goal:</b> The goal was to examine the effect of length, permeability, and heterogeneity on production using unconsolidated glass beads at a 45° dip angle using n-butane.</p> <p><b>Results:</b></p> <ul style="list-style-type: none"> <li>- <math>Q \propto \sqrt{kL}</math>, where L = length of the VAPEX model.</li> <li>- Cumulative live oil production was linear with time.</li> <li>- SOR was found to be 3-5% OIIP after blow down.</li> <li>- Live oil properties were found to be essentially independent of packing length and permeability: <math>\mu_{\text{lo}} = 2\text{-}3 \text{ mPa.s}</math>, <math>\omega_s = 0.40\text{-}0.42</math>, <math>\rho_{\text{lo}} = 700\text{-}870 \text{ kg/m}^3</math>.</li> <li>- Heterogeneous models exhibited higher residual oil saturation and lower live oil production rates compared to equivalent permeability homogeneous systems.</li> <li>- Asphaltene precipitation was visible near the production end.</li> </ul>
<p><b>Ramakrishnan (2003)</b></p> <p><b>2-D Troughs</b> [DxWxH] [1.9 cm x 1.6 cm x 84 cm]</p> <p><b>Unconsolidated Glass Beads</b> k = 25, 84, 134, 190 μm<sup>2</sup>, φ = 0.38 Dip Angle = 45°, 75°, 80°, 90°</p> <p><b>Heavy oil</b> μ = 70,000 mPa.s at ambient</p> <p><b>Solvent</b> Free flow C<sub>3</sub>H<sub>8</sub> at its <math>P_{\text{vap}}^*(T_{\text{WB}})</math> <math>T_{\text{wb}} = 20\text{-}24^\circ\text{C}</math>, <math>T_{\text{amb}} = 21\text{-}26^\circ\text{C}</math> <math>P_{\text{vap}}^* = 724\text{-}827 \text{ kPa (105-120 psig)}</math></p>	<p><b>Goal:</b> The goal was to examine the effect of permeability and dip angle on production using propane.</p> <p><b>Results:</b></p> <ul style="list-style-type: none"> <li>- Live oil production rates were found to be constant.</li> <li>- SOR = f(dip angle). SOR for 45° dip angles ranged from 10-13% whereas SOR for larger dip angles was found to be 5-7% pore volume after blow down.</li> <li>- <math>\mu_{\text{lo}} = 2.5\text{-}5 \text{ mPa.s}</math> (appeared to depend on permeability), <math>\omega_s = 0.35\text{-}0.40</math>, <math>\rho_{\text{lo}} = 450\text{-}850 \text{ g/m}^3</math>.</li> <li>- Heterogeneous models exhibited higher residual oil saturation and lower live oil production rates compared to equivalent permeability homogeneous systems.</li> </ul>

Author & VAPEX System	Objectives and Results
<p><b>Cuthiell et al. (2003)</b></p> <p><b>2-D Models</b> [DxWxH] [2.8 cm x 25 cm x 30 cm]</p> <p><b>Silica, sand and mixture of both</b> <math>k = 8, 87, 89 \mu\text{m}^2</math></p> <p><b>Heavy oil</b> Aberfeldy Lloydminster <math>\mu = 5500 \text{ mPa.s}</math> at <math>25^\circ\text{C}</math></p> <p><b>Solvent</b> Toluene (l)</p>	<p><b>Goal:</b> Their goal was to examine the diffusion/dispersion phenomena and viscous fingering in liquid toluene miscible flooding of heavy oil using a CT scanner to capture the effects.</p> <p><b>Results:</b></p> <ul style="list-style-type: none"> <li>- This was a solvent miscible flood experiment. The use of a dispersion coefficients and X-ray is interesting.</li> <li>- Growth of the solvent chamber and internal mixing in the dominant finger was observed using x-ray.</li> <li>- The dispersion coefficient was found by choosing different dispersion coefficients and simulating the results to match the experimentally observed viscous fingering qualitatively and quantitatively match post-breakthrough production rates using the Butler and Mokrys model although the model was derived for gravity drainage not miscible flooding.</li> <li>- The “best” dispersion coefficient matching experimental results was consistent with the transverse dispersion coefficients published by Blackwell (1962).</li> </ul>
<p><b>Karmaker and Maini (2003)</b></p> <p><b>3-D Models</b> [DxWxH] [3.2 cm x 67.3 cm x 15.3 cm]</p> <p><b>Silica, sand and mixture of both</b> <math>k = 326 \mu\text{m}^2</math> (330 Darcy), <math>\phi = 0.38</math></p> <p><b>Heavy oil</b> <math>\mu = 40,000 \text{ mPa.s}</math> at <math>10^\circ\text{C}</math> <math>\mu = 600 \text{ mPa.s}</math> at <math>20^\circ\text{C}</math> <math>\mu = 9000 \text{ mPa.s}</math> at <math>20^\circ\text{C}</math></p> <p><b>Solvent</b> Propane Connate Water = 3.5% Gas Cap = 3 cm</p>	<p><b>Goal:</b> The goal was to examine the effect of oil viscosity, well placement, gas cap and operating pressure on the production of dead oil from a laboratory scale model.</p> <p><b>Results:</b></p> <ul style="list-style-type: none"> <li>- Increasing the temperature decreased start-up time when the injection as placed opposite the production well at <math>P = 1048 \text{ kPa}</math> (152 psig) with a gas cap present). The increase in temperature from <math>10</math> to <math>19^\circ\text{C}</math> increased the cumulative production (2% rate increase for every <math>1^\circ\text{C}</math> rise). Although the solubility decreases, the viscosity decreases and mass transfer increases with increasing temperature.</li> <li>- Oil production more than doubled when the viscosity was decreased from <math>9000</math> to <math>600 \text{ mPa.s}</math> at <math>1048 \text{ kPa}</math> and <math>10^\circ\text{C}</math>.</li> <li>- The dead oil production increased 37% when the operating pressure was increased from <math>931</math>-<math>1034 \text{ kPa}</math> (135-150 psig) as the solubility and mass transfer are increased.</li> <li>- Well spacing (at opposite ends) effected the initial communication but resulted in the same cumulative production when no gas cap was present. Production rates were identical irrespective of well spacing with a gas cap.</li> <li>- Production increased with initial solvent injection rate.</li> </ul>

Author & VAPEX System	Objectives and Results
<p><b>James (2003) and James and Chatzis (2004)</b></p> <p><b>Consolidated &amp; Unconsolidated Glass Beads</b> k = see table</p> <p><b>Heavy oil</b> <math>\mu_O = 85,000</math> mPa.s at ambient <math>\mu_N = 70,000</math> mPa.s at ambient</p> <p><b>Solvent</b> n-butane supplied at its vapour pressure at water bath temperature <math>T_{wb} = 21.5^\circ\text{C}</math> and <math>23.0^\circ\text{C}</math> <math>P_{vap}^* = 114</math> and <math>131</math> kPa (16.6 psig and 19.0 psig)</p>	<p><b>Goal:</b> The goal was to examine the effect of length and dip angle on production from consolidated glass beads using butane and investigate the VAPEX interface advancement in unconsolidated glass beads.</p> <p><b>Consolidated Media Results:</b></p> <ul style="list-style-type: none"> <li>- <math>Q_{lo} = \text{constant}</math> with time, <math>Q_{lo} \propto L</math>, <math>Q_{lo} \propto \sin(\theta)</math></li> <li>- Live oil density and solvent concentration were independent of length and angle with <math>\rho_{lo} = 810\text{--}820</math> kg/m<sup>3</sup> and <math>\omega_s = 0.27\text{--}0.32</math>.</li> <li>- Residual oil saturation increased from 10-22% PV as the length of the system decreased.</li> </ul> <p><b>VAPEX Interface Advancement, <math>U_p^x</math></b></p> <ul style="list-style-type: none"> <li>- Except for the top 20% of the model and the capillary region, the rate of VAPEX interface advancement was found to be constant in higher permeability unconsolidated media. This agrees with the constant cumulative production of live oil. Using unconsolidated glass beads saturated with heavy oil, live oil production was found to be constant and did not slow until the height of the VAPEX interface was reduced to over half its original height (well into the chamber falling phase). The logical explanation for this phenomenon is that the VAPEX interface visible at the surface of the model advances more quickly than the pores where there is no wall/boundary effect.</li> </ul>

	Consolidated Glass Beads				Unconsolidated Troughs	
	S1	S3	L2	L1	D2	D3
<b>Height, H (cm)</b>	32.5	40.1	54.5	60.2	92	23.7
<b>Width, W (cm)</b>	3	4.8	4.8	4.8	0.96	0.65
<b>Permeability, <math>K_{eff}</math> (Darcy)</b>	74	68	66	76	285	350
<b>Porosity, <math>\phi</math></b>	0.30	0.30	0.30	0.30	0.38	0.38
<b>Q (cm<sup>3</sup>/min)</b>	0.11	0.2	0.24	0.31	0.2	0.11
<b>VAPEX Interface Velocity (cm/hr)</b>	n/a	n/a	n/a	n/a	0.29	0.53
<b>Live Oil Thickness, <math>\delta_f^*</math> (mm)</b>	0.74	0.67	0.72	0.72	0.60	0.66
<b>Diffusivity (cm<sup>2</sup>/s)</b>	<b>Time to Diffuse One Pore, <math>t_D</math> (s)</b>					
1.00E-06	416.7	341.6	394.5	394.5	273	336
1.00E-05	41.7	34.2	39.5	39.5	27	34
<b>Live Oil Velocity (cm/s)</b>						
Superficial Velocity, $V_{lo}$	0.0083	0.0104	0.0116	0.015	0.058	0.042
Predicted Velocity, $V_{lo}^*$	0.0116	0.0107	0.0104	0.012	0.045	0.055
<b>% Difference</b>	41%	3%	10%	20%	23%	30%

\* Based on experimental evidence that live oil drainage occurs in one pore, the live oil thickness was estimated as one pore diameter, approximately equal to the average particle diameter.

$$V_{lo}^* = \frac{K_{eff} \Delta \rho g}{\mu}$$

$$V_{lo} = \frac{Q_{exp}}{W \delta_f}$$

**Constants**

$\Delta \rho$ (g/cm <sup>3</sup> )	<b>0.812</b>
$g$ (cm/s <sup>2</sup> )	<b>981</b>
$\mu$ (g/cm.s)	<b>0.05</b>

Author & VAPEX System	Objectives and Results																																																																														
<p><b>Talbi and Maini (2004)</b></p> <p><b>Cylindrical Annulus</b> [DxWxH] [3.0 cm x 42.3 cm x 30 cm] 12-16 US mesh glass beads <math>k = 632 \mu\text{m}^2</math> (640 Darcy) <math>\phi = 0.35</math></p> <p><b>Heavy Oil</b> Oil #1 <math>\mu = 4500 \text{ mPa.s}</math> at 21°C <math>\rho = 982.6 \text{ kg/m}^3</math></p> <p>Oil #2 <math>\mu = 18,600 \text{ mPa.s}</math> at 21°C <math>\rho = 987.5 \text{ kg/m}^3</math></p> <p><b>Solvents</b> Propane &amp; CO<sub>2</sub> Propane &amp; CH<sub>4</sub> C<sub>3</sub>H<sub>8</sub> (l) injected at 40 cm<sup>3</sup>/h P = 1.38, 1.72, 2.76, 4.14 MPa (200, 250, 400, 600 psig) T = 21-25°C</p>	<p><b>Goal:</b> The goal was to examine the effect of non-condensable gas (CO<sub>2</sub> &amp; CH<sub>4</sub>) on production rates from laboratory scale models using two different viscosity oils at different operating pressures.</p> <table border="1" data-bbox="695 445 1380 909"> <thead> <tr> <th>Oil</th> <th>NCG</th> <th>Pressure (MPa)</th> <th>Duration (hours)</th> <th>Avg. Oil Rate (cm<sup>3</sup>/h)</th> <th>Oil Recovery</th> </tr> </thead> <tbody> <tr> <td>1</td> <td>CO<sub>2</sub></td> <td>1.72</td> <td>9</td> <td>85.69</td> <td>47.5%</td> </tr> <tr> <td>1</td> <td>CO<sub>2</sub></td> <td>1.72</td> <td>9</td> <td>85.42</td> <td>46.9%</td> </tr> <tr> <td>1</td> <td>CH<sub>4</sub></td> <td>1.72</td> <td>9</td> <td>94.85</td> <td>52.4%</td> </tr> <tr> <td>1</td> <td>CH<sub>4</sub></td> <td>4.14</td> <td>9</td> <td>59.56</td> <td>32.1%</td> </tr> <tr> <td>1</td> <td>CO<sub>2</sub></td> <td>4.14</td> <td>9</td> <td>79.11</td> <td>42.5%</td> </tr> <tr> <td>2</td> <td>CO<sub>2</sub></td> <td>1.38</td> <td>12</td> <td>34.33</td> <td>25.1%</td> </tr> <tr> <td>2</td> <td>CH<sub>4</sub></td> <td>1.38</td> <td>12</td> <td>41.51</td> <td>29.8%</td> </tr> <tr> <td>2</td> <td>CO<sub>2</sub></td> <td>2.76</td> <td>12</td> <td>40.76</td> <td>30.0%</td> </tr> <tr> <td>2</td> <td>CH<sub>4</sub></td> <td>2.76</td> <td>12</td> <td>36.03</td> <td>25.8%</td> </tr> <tr> <td>2</td> <td>CO<sub>2</sub></td> <td>4.14</td> <td>12</td> <td>44.26</td> <td>32.7%</td> </tr> <tr> <td>2</td> <td>CH<sub>4</sub></td> <td>4.14</td> <td>12</td> <td>29.58</td> <td>24.3%</td> </tr> <tr> <td>2</td> <td>CO<sub>2</sub> only</td> <td>4.14</td> <td>12</td> <td>21.69</td> <td>15.6%</td> </tr> </tbody> </table> <p>CO<sub>2</sub> used as a non-condensable gas results in higher production rates at mid to high operating pressures while CH<sub>4</sub> is more efficient at low pressures.</p>	Oil	NCG	Pressure (MPa)	Duration (hours)	Avg. Oil Rate (cm <sup>3</sup> /h)	Oil Recovery	1	CO <sub>2</sub>	1.72	9	85.69	47.5%	1	CO <sub>2</sub>	1.72	9	85.42	46.9%	1	CH <sub>4</sub>	1.72	9	94.85	52.4%	1	CH <sub>4</sub>	4.14	9	59.56	32.1%	1	CO <sub>2</sub>	4.14	9	79.11	42.5%	2	CO <sub>2</sub>	1.38	12	34.33	25.1%	2	CH <sub>4</sub>	1.38	12	41.51	29.8%	2	CO <sub>2</sub>	2.76	12	40.76	30.0%	2	CH <sub>4</sub>	2.76	12	36.03	25.8%	2	CO <sub>2</sub>	4.14	12	44.26	32.7%	2	CH <sub>4</sub>	4.14	12	29.58	24.3%	2	CO <sub>2</sub> only	4.14	12	21.69	15.6%
Oil	NCG	Pressure (MPa)	Duration (hours)	Avg. Oil Rate (cm <sup>3</sup> /h)	Oil Recovery																																																																										
1	CO <sub>2</sub>	1.72	9	85.69	47.5%																																																																										
1	CO <sub>2</sub>	1.72	9	85.42	46.9%																																																																										
1	CH <sub>4</sub>	1.72	9	94.85	52.4%																																																																										
1	CH <sub>4</sub>	4.14	9	59.56	32.1%																																																																										
1	CO <sub>2</sub>	4.14	9	79.11	42.5%																																																																										
2	CO <sub>2</sub>	1.38	12	34.33	25.1%																																																																										
2	CH <sub>4</sub>	1.38	12	41.51	29.8%																																																																										
2	CO <sub>2</sub>	2.76	12	40.76	30.0%																																																																										
2	CH <sub>4</sub>	2.76	12	36.03	25.8%																																																																										
2	CO <sub>2</sub>	4.14	12	44.26	32.7%																																																																										
2	CH <sub>4</sub>	4.14	12	29.58	24.3%																																																																										
2	CO <sub>2</sub> only	4.14	12	21.69	15.6%																																																																										
<p><b>Friedrich (2005)</b></p> <p><b>2-D Packed Model</b> [DxWxH] [0.95 cm x 10.5 cm x 44 cm] 590 <math>\mu\text{m}</math> glass beads Etched Glass Micromodels</p> <p><b>Heavy Oil</b> <math>\mu = 23,000 \text{ mPa.s}</math> at 22°C <math>\rho = 980 \text{ kg/m}^3</math> 18.3 wt% asphaltenes using C<sub>5</sub></p> <p><b>Solvent</b> Pentane &amp; air at ambient pressure <math>y_{C_5} = 0.65 - 0.86</math></p>	<p><b>Goal:</b> The goal was to examine production rates and properties of the live oil using in a pentane-air VAPEX process.</p> <p><b>Results:</b></p> <ul style="list-style-type: none"> <li>- The vapour fraction of pentane in air was varied from 0.65 to 0.86 mass fraction by varying the temperature of the liquid pentane. There was little to no effect on production rates over this range.</li> <li>- Production varied with the square root of time, possibly due to the diffusion boundary layer and/or model dimensions.</li> <li>- Live oil properties: <math>\mu = 4-6 \text{ mPa.s}</math>, <math>\omega_s = 0.46-0.48</math>, SOR = 3.8-6.0 % PV.</li> <li>- The effective diffusivity calculated from the VAPEX interface advancement and found to be on the order of 0.09-0.12 cm<sup>2</sup>/s.</li> <li>- Micromodel observations include drainage by film flow, trapping by snap-off and solvent trapping.</li> </ul>																																																																														

Author & VAPEX System	Objectives and Results																
<p><b>Yazdani &amp; Maini (2005, 2006)</b></p> <p><b>Cylindrical Annulus [DxWxH]</b> [3.0 cm x 42.3 cm x 30 cm] [3.2 cm x 84.6 cm x 60.1 cm]</p> <table border="1" data-bbox="240 422 613 579"> <thead> <tr> <th>Pack</th> <th>k (<math>\mu\text{m}^2</math>)</th> <th><math>\phi</math></th> <th><math>S_{wc}</math></th> </tr> </thead> <tbody> <tr> <td>1</td> <td>218</td> <td>0.35</td> <td>0.007</td> </tr> <tr> <td>2</td> <td>326</td> <td>0.36</td> <td>0.055</td> </tr> <tr> <td>3</td> <td>632</td> <td>0.37</td> <td>0.041</td> </tr> </tbody> </table> <p><b>Heavy Oil</b> <b>Dina:</b> <math>\mu = 18,648</math> mPa.s at <math>9^\circ\text{C}</math>, <math>\rho = 982.6</math> kg/m<sup>3</sup>, <math>P = 41.4</math> kPa (6 psig) <b>Elk Pt:</b> <math>\mu = 18,656</math> mPa.s at <math>21.6^\circ\text{C}</math>, <math>\rho = 987.5</math> kg/m<sup>3</sup>, <math>P = 110.3</math> kPa (16 psig)</p> <p><b>Solvent</b> n-butane at constant injection</p>	Pack	k ( $\mu\text{m}^2$ )	$\phi$	$S_{wc}$	1	218	0.35	0.007	2	326	0.36	0.055	3	632	0.37	0.041	<p><b>Goal:</b> The goal was to investigate the significance of the grain size parameter and drainage height.</p> <p><b>Results:</b></p> <ul style="list-style-type: none"> <li>- Asphaltene precipitation was observed.</li> <li>- The average solvent concentration was found to be 0.40 volume fraction</li> <li>- Dead oil production was found to scale with the square root of the grain size parameter (<math>k\phi^m</math>, where m is the cementation factor) and the drainage height raised to an exponent of 1.1-1.3 instead of 0.5:</li> </ul> $\frac{\left(\frac{Q}{\sqrt{k\phi^m}}\right)_2}{\left(\frac{Q}{\sqrt{k\phi^m}}\right)_1} = \left(\frac{h_2}{h_1}\right)^n, \quad \text{where } 1.1 \leq n \leq 1.3$
Pack	k ( $\mu\text{m}^2$ )	$\phi$	$S_{wc}$														
1	218	0.35	0.007														
2	326	0.36	0.055														
3	632	0.37	0.041														
<p><b>Tam (2007)</b></p> <p><b>Cylindrical Annulus [DxWxH]</b> [0.635 cm x 10 cm x 101 cm] <math>k = 296, 1108 \mu\text{m}^2</math> (300, 1123 Darcy)</p> <p><b>Heavy Oil</b> <math>\mu = 23,200</math> mPa.s at <math>22^\circ\text{C}</math> <math>\rho = 980</math> kg/m<sup>3</sup> 18.3 wt% asphaltenes using <math>C_5</math></p> <p><b>Solvent</b> Butane</p> <p>With and without condensation With and without connate water</p>	<p><b>Goal:</b> The goal was to examine the effect of connate water on VAPEX and compare non-condensing versus condensing solvent extraction.</p> <p><b>Results:</b></p> <ul style="list-style-type: none"> <li>- 5% connate water in <math>296 \mu\text{m}^2</math> system resulted in a minor decrease in live oil production from 0.66 to 0.57 cm<sup>3</sup>/min. Bitumen production decreased from 0.66 to 0.57 g/min and solvent content from 0.38 to 0.35 mass fraction.</li> <li>- 7% connate water in an <math>1108 \mu\text{m}^2</math> system resulted in an increase in live oil production from 1.15 to 1.25 cm<sup>3</sup>/min. Bitumen production decreased slightly from 0.754 to 0.749 g/min but solvent content increased from 0.25 to 0.30 mass fraction with connate water.</li> <li>- The effect of condensation was compared at <math>1108 \mu\text{m}^2</math> at <math>P_{\text{vap}}^* = 103.4-110.3</math> kPa (15-16 psig). The live oil production rate increased from 1.15 to 2.15 cm<sup>3</sup>/min while bitumen production increased from 0.754 to 0.96 g/min (a 27% increase over the non-condensing case). The solvent content jumped from 0.25 to 0.60 mass fraction with condensation and the horizontal interface advancement increased from 0.018 to 0.031 cm/min.</li> </ul>																

Author & VAPEX System	Objectives and Results
<p><b>Rezaei and Chatzis (2008)</b></p> <p><b>2-D Packed Model</b> [DxWxH] [1.91 cm x 7.62 cm x 41.9 cm] <math>k = 296, 987 \mu\text{m}^2</math> (300, 1000 Darcy)</p> <p><b>Heavy Oil (at 35°C)</b> Lloydminster blend: 4800 mPa.s Cold Lake: 36,000 mPa.s</p> <p><b>Solvent</b> Pentane at 35°C</p>	<p><b>Goal:</b> The goal was to systematically examine the effect of different oil, porous media properties and heat on the effect of production in both condensing and non-condensing solvent processes</p> <p><b>Results:</b></p> <ul style="list-style-type: none"> <li>- See section 2.3.</li> <li>- When compared to VAPEX, condensation was slightly more advantageous in the lower permeability system at both viscosities.</li> <li>- Production increased with condensation for a given permeability. The increase was more pronounced for the lower viscosity oil: 31% increase compared to 12.5% for the more viscous oil.</li> </ul>
<p><b>Haghighat and Maini (2008)</b></p> <p><b>Cylindrical Annulus</b> [DxWxH] [3.0 cm x 42.3 cm x 30 cm] <math>k = 2.7 \mu\text{m}^2</math>, <math>\phi = 0.37</math></p> <p><b>Elk Pt Heavy Oil</b> <math>\mu = 20,500 \text{ mPa.s}</math> at <math>T_{\text{amb}}</math> <math>\rho = 987.5 \text{ kg/m}^3</math></p> <p><b>Solvent</b> <math>\text{C}_3\text{H}_8</math> at <math>P = 750, 814, 850 \text{ kPa}</math>, <math>\text{C}_3\text{H}_8</math> at <math>P = 850 \text{ kPa}</math> &amp; toluene (l) at <math>1 \text{ cm}^3/\text{hr}</math>, and <math>\text{C}_4\text{H}_{10}</math> at <math>200 \text{ kPa}</math>.</p>	<p><b>Goal:</b> Using a realistic permeability of <math>2.7 \mu\text{m}^2</math>, the goal was to determine the affect of asphaltene precipitation on production.</p> <p><b>Results:</b></p> <ul style="list-style-type: none"> <li>- There was minimal difference in cumulative dead oil production for the three different propane injection pressures.</li> <li>- The average live oil solvent concentration was 0.5 volume fraction when propane was injected at 814 and 850 kPa but 0.3 volume fraction at 750 kPa injection pressure.</li> <li>- The asphaltene content decreased from 10 to 4% when operated at 814 or 850 kPa. There was no reduction in asphaltene when operated at 750 kPa.</li> </ul>
<p><b>Moghadam et al. (2009)</b></p> <p><b>2-D Packed Model</b> [D x W x H] [2.0 cm x 40 cm x 10 cm] <math>k = 16, 25, 49, 96, 103 \mu\text{m}^2</math></p> <p><b>Heavy Oil</b> <math>\mu = 11,900 \text{ mPa.s}</math> at <math>20.8^\circ\text{C}</math> <math>\rho = 978 \text{ kg/m}^3</math> at <math>20.8^\circ\text{C}</math></p> <p><b>Solvent</b> Propane at 800 kPa</p>	<p><b>Goal:</b> The goal was to model the VAPEX process and predict the depth of the draining live oil.</p> <p><b>Results:</b></p> <ul style="list-style-type: none"> <li>- See section 2.4 for a detailed discussion.</li> <li>- Experimental production rates were found to vary with the square root of permeability although the authors only compared cumulative production at the end of the experimental time.</li> <li>- Predicted and observed dip angles were in good agreement.</li> <li>- The depth of the draining live oil was determined to be in the range of 1 – 2 mm and increased with decreasing permeability.</li> </ul>

Author & VAPEX System	Objectives and Results
<p><b>El-Haj <i>et al.</i> (2009)</b></p> <p><b>Cylindrical Model [H x D]</b> [21 cm x 6 cm] k = 109, 155, 178 <math>\mu\text{m}^2</math> (110, 157, 180 Darcy) <math>\phi = 0.38</math></p> <p><b>Heavy Oil (room temperature)</b> <math>\mu = 280,000 \text{ mPa}\cdot\text{s}</math> <math>\rho = 860 \text{ kg/m}^3</math></p> <p><b>Solvent</b> Butane at <math>1-2^\circ\text{C} &lt; T_{\text{sys}}</math> <math>T_{\text{sys}} = 20.6, 21.8, 19.5^\circ\text{C}</math> <math>P_{\text{sys}} = 106.2, 107.6, 108.2 \text{ kPa}</math> (15.4, 15.6, 15.7 psig)</p>	<p><b>Goal:</b> The goal was to find the dispersion coefficient of butane in heavy oil during VAPEX by comparing predicted &amp; experimentally found production rates.</p> <p><b>Results:</b></p> <ul style="list-style-type: none"> <li>- The physical model incorporates oil being produced from a vertical standing core saturated with heavy oil.</li> <li>- The shape of the predicted and VAPEX interface is in agreement with observed advancement by James (2003).</li> <li>- The concentration dependent dispersivity was found to vary with permeability and values decreased with increasing permeability with values of: <math>9.8 \times 10^{-8} \omega_s</math>, <math>9.5 \times 10^{-8} \omega_s</math>, and <math>9.4 \times 10^{-8} \omega_s \text{ m}^2/\text{s}</math> for the 109, 155 and 178 <math>\mu\text{m}^2</math> systems.</li> <li>- The interfacial concentration of butane in heavy oil was predicted to be 0.71 mass fraction.</li> </ul>

### 2.3 Effect of Heat on the VAPEX Process

A solvent heated to a temperature greater than the reservoir temperature carries some sensible heat to the VAPEX interface where it condenses on the colder surface of the bitumen. The viscosity of the oil is reduced from the mass transfer of the solvent into the bitumen as well as the the sensible heat transfer from the solvent to the bitumen and via ‘thermal diffusion’ or the Soret effect. Butler and Jiang (2000) and Karmaker and Maini (2003) examined the effect of an increased reservoir temperature on production rates from laboratory scale models. Butler and Jiang (2000) conducted VAPEX experiments in a large rectangular packed glass bead model saturated with 870 mPa·s viscosity using Atlee Buffalo field oil. Using propane as the solvent, production rates increased 21.5% when the operating temperature was raised from 21°C to 27°C. Karmaker and Maini (2003) observed an 18% increase in oil production when the operating temperature was increased from 10°C to 19°C. Their system consisted of a 16-20 mesh sand packing with a permeability of 336  $\mu\text{m}^2$  (340 Darcy) saturated with 40,000 mPa·s oil (at 10°C). Both authors used constant solvent injection, so it is unknown whether or not the solvent condensed. Frauenfeld *et al.* (2006) compared condensing solvent and a solvent-steam hybrid VAPEX to normal VAPEX and stated that the goal of applying heat was to more quickly establish communication between the injection and production wells, as well as further reduce the viscosity of the oil near the well.



Rezaei and Chatzis (2008) have been working on understanding the effect of solvent condensation on production rates. They are systematically investigating the effect of condensation on production rates by examining parameters such as temperature above the boiling point of n-pentane (i.e. rate of condensation), oil viscosity, and permeability. The effect of each variable on the rate of oil production, solvent concentration and asphaltene precipitation is being compared to a non-condensing VAPEX process as a baseline. A 1.91 cm x 7.62 cm x 41.9 cm model packed with saturated glass beads equivalent to 296  $\mu\text{m}^2$  (300 Darcy) or 987  $\mu\text{m}^2$  (1000 Darcy) was extracted using n-pentane boiling at 35°C either in non-condensing or condensing solvent mode (i.e. model at 36.5 or 34.5°C) using two different viscosity oils (4800 and 36,000 mPa.s at 35°C). When compared to non-condensing VAPEX, solvent condensation proved to increase production. Condensation was slightly more advantageous in the lower permeability system (296  $\mu\text{m}^2$ ) at both viscosities. The effect of condensation was compared for different viscosity oils in different permeability systems. Using the average production rate increase over normal VAPEX for both permeability systems, the increase was more pronounced for the lower viscosity oil compared to the higher viscosity oil. The permeability averaged production rate increases were 31% for the 4800 mPa.s oil compared to 12.5% for the 36,000 mPa.s oil.

## **2.4 Depth of the Viscosity Reduced Oil at the VAPEX Interface**

The depth of the mobile live oil at the solvent-bitumen interface has been a key question with respect to scaling solvent process production rates. In a recent paper by Moghadam *et al.* (2009) the depth of the viscosity reduced live oil layer between the solvent and bitumen (i.e. the transition zone thickness) was determined. The depth of the live oil was assumed constant throughout the height of the solvent-bitumen interface and set as an adjustable parameter for which the difference in calculated and measured cumulative volumes were minimised.

Experimentally, a 400 mm wide by 100 mm high by 20 mm transparent laboratory model was filled with different permeability sand ( $k = 103, 96, 49, 25, 16 \mu\text{m}^2$ ) and saturated with heavy oil ( $\rho = 978 \text{ kg/m}^3$  and  $\mu = 11,900 \text{ mPa.s}$  both at 20.8°C). Propane set at 800 kPa was used as a solvent where the vapour pressure at 20.8°C is 854 kPa and it was allowed to flow freely as necessary into the model (following the practise of the Porous Media Group at the University of Waterloo although the authors did not reference this methodology). Experimentally, the permeability ( $k$ ), porosity ( $\phi$ ), cumulative production ( $Q_m$ ), solvent-oil ratio – SOR, final time ( $t_f$ ) were measured. Photos were taken to track the interface shape, dip angle ( $\theta_m$ ) and advancement.

Mathematically, two sets of expressions were derived for the calculated cumulative production dependent on the sweep phase, chamber spreading or chamber falling phases. The equations are dependent on the residence time (characteristic time) it takes the live oil to drain in the spreading chamber ( $\Delta t_s$ ) and falling chamber ( $\Delta t_f$ ) phases respectively, the depth of the live oil ( $\delta$  - set as an adjustable parameter), the dip angle ( $\theta_c$  - calculated), and properties of the system (height ( $h$ ), depth ( $d$ ), change in oil saturation ( $\Delta S_o$ ) and porosity ( $\phi$ )).

$$t(\text{spreading}) = \frac{h\Delta t_s}{2\delta} \left[ \frac{\cos \theta}{\sin^2 \theta} - \ln \left( \tan \frac{\theta}{2} \right) \right] \quad (2.4.1)$$

$$Q_c(\text{spreading}) = h^2 d \phi \Delta S_o \cot \theta \quad (2.4.2)$$

$$t(\text{falling}) = t_s + \frac{w\Delta t_f}{\delta} \left[ \frac{1 + \cos \theta_s \ln \left( \tan \frac{\theta}{2} \right)}{\cos \theta_s} - \frac{1 + \cos \theta \ln \left( \tan \frac{\theta}{2} \right)}{\cos \theta} \right] \quad (2.4.3)$$

$$Q_c(\text{falling}) = hwd \phi \Delta S_o (2 - \cot \theta_s \tan \theta) \quad (2.4.4)$$

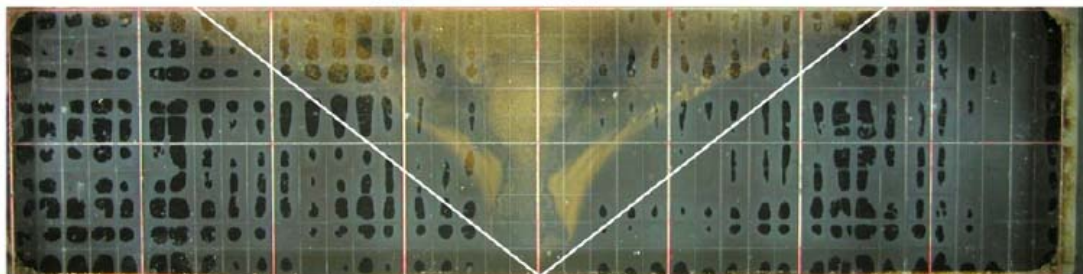
The characteristic time (using Darcy's Law) during the spreading and falling phases are functions of the maximum solvent concentration dependent viscosity ( $\mu_o(c_{\max})$ ) and density ( $\rho_o(c_{\max})$ ) assuming a vertical dip angle. The solubility is assumed to be 0.2606 g solvent/g oil with a corresponding density of 828 kg/m<sup>3</sup>, and a viscosity of 8.51 mPa.s.

$$\Delta t_s = \frac{h\phi\mu_o(c_{\max})}{K\rho_o(c_{\max})g} \quad (2.4.5)$$

$$\Delta t_f = \frac{w\phi\mu_o(c_{\max})}{K\rho_o(c_{\max})g} \quad (2.4.6)$$

Using the root mean square difference in the measured and calculated cumulative production at different times as the objective function for which to minimise, the depth of the transition zone was determined throughout the test time. The depth of the live oil varied from a constant value of 1 mm for the largest permeability of 103  $\mu\text{m}^2$  in test #1 to a slightly variable thickness with an average of almost 2 mm for tests #3, 4 and 5 ( $k = 16, 25$  and  $49 \mu\text{m}^2$ ) where the lowest permeability resulted in the thickest calculated draining live oil film. The resulting set of equations also solved for a calculated dip angle. When compared to experimentally observed dip angles, the calculated angles for the two lower permeabilities deviated from measured values by almost 18% but less than 10% for higher permeability tests (tests #1-3).

Figure 2.4.1 is a picture of experiment #5 ( $16 \mu\text{m}^2$  permeability) at the end of the experiment. There are three observations to consider when looking at this photograph: 1) From the picture it is easy to see that production is still within the chamber spreading phase as the swept area has not reached the top left most or top right most corners. Based on the model geometry, the end of the spreading phase should correspond to a  $27^\circ$  angle. The final measured angle of  $33^\circ$  (in Figure 2.4.1) is clearly still in the chamber spreading phase for which they predict it to take almost 102 hours to reach. 2) There is no capillary height shown even though the permeability is only  $16 \mu\text{m}^2$ . This could be for one of two reasons: a) the solvent is condensing in the model (see Observation #3) or b) the oil is not draining by gravity drainage. If the solvent was not condensing and the oil was draining by gravity drainage a fully saturated capillary region should be observed where the gravity forces are not sufficient to overcome the capillary height of imbibition ( $h_c$ ). Therefore, the pressure difference,  $\Delta P$ , must be greater than the capillary height difference ( $\Delta\rho gh_c$ ) where  $\Delta\rho$  is the difference in live oil and solvent vapour density and  $g$  is the gravitational constant. The authors do not mention what pressure the back pressure regulator is set at. The equations for the VAPEX model were developed assuming gravity drainage. 3) The third observation is that Figure 2.4.1 also shows evidence of asphaltene precipitation. The precipitation is only visible in the 18-25 hour range (dark zones close to the vertical middle line) yet production remains consistent throughout this time period (as shown in Figure 2.4.2). If the solvent was condensing everywhere in the model, asphaltene precipitation would be visible throughout and slightly higher production should be measured. The interfacial tension between the condensed solvent and solvent vapour is sufficiently small as to reduce a capillary region unlike the interfacial tension between “live” oil and solvent vapour.



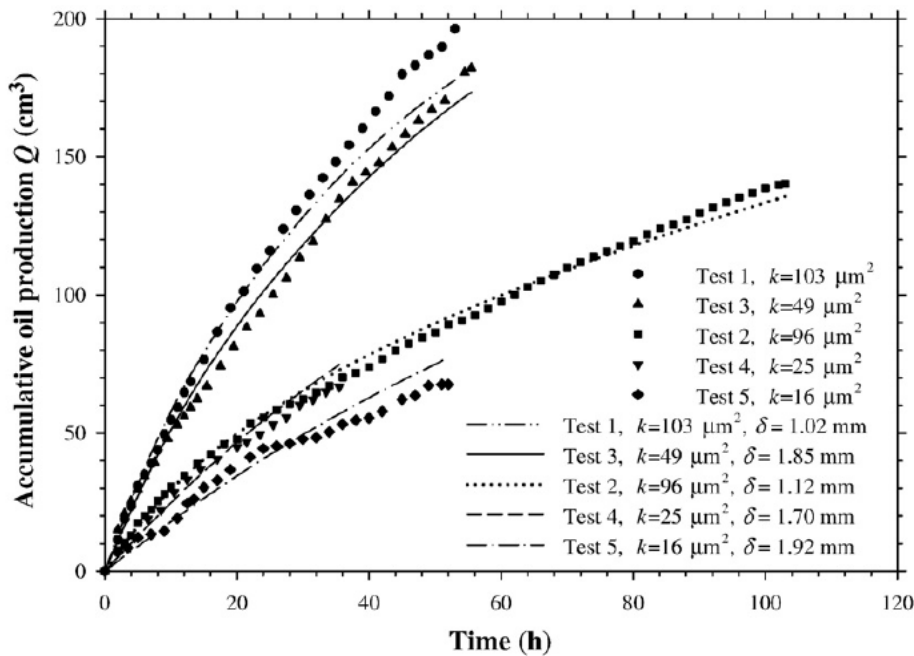
$$t_F = 52.0 \text{ h}, \theta_{Fm} = 33.0^\circ, \theta_{Fc} = 38.9^\circ$$

$$Q_{Fm} = 67.6 \text{ cm}^3, Q_{Fc} = 77.1 \text{ cm}^3$$

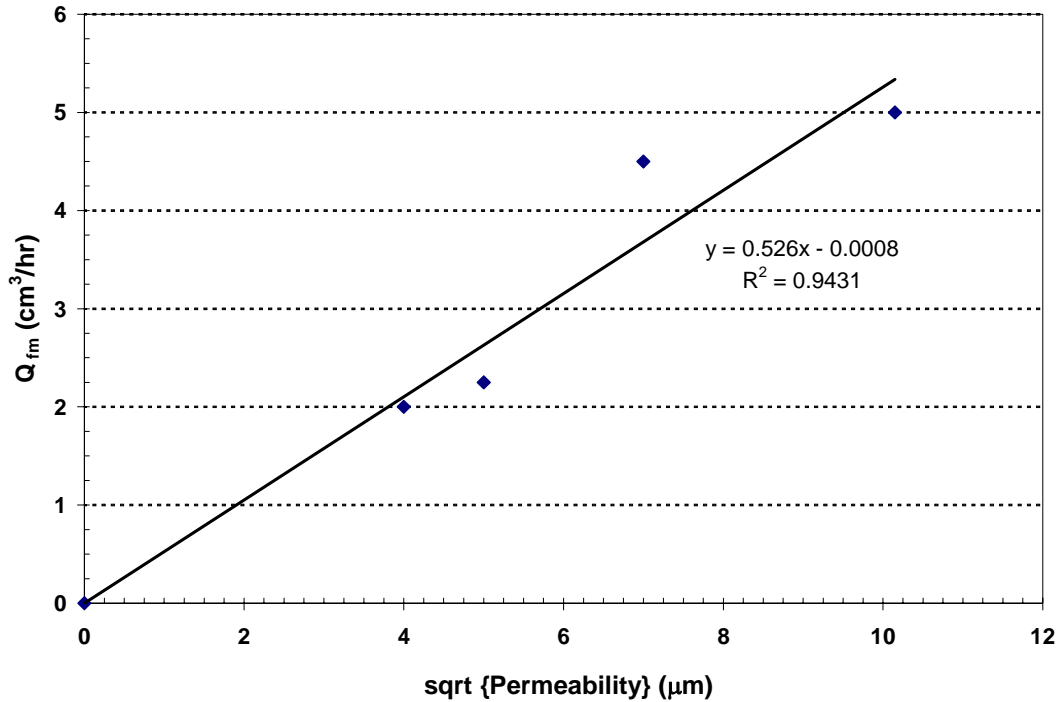
**Figure 2.4.1: Photo of the Swept Area (Solvent Chamber) and Remaining Oil at End of Experiment ( $k = 16 \mu\text{m}^2$ ) (Moghadam *et al.* 2009)**

Cumulative production is compared in Figure 2.4.2 yet the authors do not discuss rates but blame lower cumulative production on reduced permeability due to asphaltene precipitation in the lower permeability tests. In reality, the lower permeability test #5 was terminated prematurely and its cumulative production should not be compared to the cumulative production from the higher permeability tests (test #1-3). If one compares the production rates assuming linear cumulative production at 20 hours the data shows a square root dependence on permeability as shown in Figure 2.4.3. This is consistent with previous experimental results from laboratory scale models (Das and Butler 1998; Oduntan 2001, Ramakrishnan 2003) and do not indicate any asphaltene plugging issues at lower permeabilities.

The characteristic or residence time during the spreading and falling phases is dependent on the maximum concentration. The maximum concentration was assumed to be the solubility (0.2606 g solvent/g oil) yet the experimental solvent to oil ratios range from 0.33 to 0.63 g solvent/g oil. The authors should consider using the experimentally found average solvent concentrations to determine the live oil density and viscosity used in calculating the residence time.



**Figure 2.4.2: Comparison of Experimental and Calculated Cumulative Production (Moghadam *et al.* 2009)**



**Figure 2.4.3: Square-Root Dependence of Experimentally Found Production Rates on Permeability (data from Moghadam *et al.* 2009)**

## 2.5 Solvents Mixed with Non-Condensable Gas

While laboratory experiments are often carried out using pure solvent this may not be practical in the field. The vapour pressure of many of the solvents proposed for VAPEX (propane, butane, etc) is below the reservoir pressure. If one does not desire condensation, as in the VAPEX process, the hydrocarbon solvent can be mixed with a non-condensable gas such as methane (CH<sub>4</sub>) or carbon dioxide (CO<sub>2</sub>). This would reduce the solvent partial pressure to below its vapour pressure. The mixing of the solvent with a non-condensable gas has been promoted as advantageous for environmental reasons such as injecting CO<sub>2</sub> into the reservoir and economical reasons of reducing the solvent inventory required. However, there are two possible disadvantages of mixing the diffusing solvent with non-condensable gas: 1) the rate of solvent mass transfer into the heavy oil is lowered and 2) asphaltene precipitation is less likely to occur if the solvent is not at its dew point.

Talbi and Maini (2004) examined the effect of mixing propane with either methane or carbon dioxide on VAPEX production rates. Propane (l) was supplied at a constant rate of 40 cm<sup>3</sup>/h and mixed with either CH<sub>4</sub> or CO<sub>2</sub> to pressures of 1.38, 1.72, 2.76, and 4.14 MPa (200, 250, 400, and

600 psig) to recover two different viscosity oils (4500 and 18,600 mPa.s). Procedure wise, the annular model was filled with glass beads, packed via vibration resulting in a 35% porosity and  $632 \mu\text{m}^2$  (640 Darcy permeability), air removed via vacuum, saturated with brine and finally saturated to approximately 95% pore volume with the respective heavy oils. Free gas production was metered and measured by displacing water in a known volume cylinder.

The results are summarised in Table 2.2.1. There were five experiments performed with the lower viscosity oil and seven with the higher viscosity oil. The average oil production rates were consistently higher when the annulus was saturated with the lower viscosity oil (4500 mPa.s), at all pressures, regardless of non-condensable gas. At lower pressures (1.38 and 1.72 MPa), the average oil production rates were higher using methane as the non-condensable gas for both viscosity oils. At mid to high pressures (2.76 and 4.14 MPa), the average oil production rates were higher using CO<sub>2</sub> as the non-condensable gas. The authors concluded that at higher operating pressures the partial pressure of the non-condensable gas is increased and the solubility and diffusion of CO<sub>2</sub> is greater than CH<sub>4</sub>. At the same time, the partial pressure and solubility of the light hydrocarbon is decreased. The need to reduce greenhouse gas emissions via sequestration makes CO<sub>2</sub> economically and environmentally advantageous over methane.

## **2.6 Hybrid (Steam-Solvent) Processes**

Hybrid steam-solvent processes where they are co-injected or alternately injected, was also studied. Farouq Ali (1976) introduced the idea in 1976 and Mokrys and Butler (1993) compared SAGD to solvent-added steam-assisted gravity drainage with a 30% reduction in steam requirements and 99% propane recovery. Due to the higher dew point of water compared to light hydrocarbons, Mokrys and Butler (1993) also observed steam trapping, through a so-called self sealing mechanism, which is favourable as it reduces the steam-to-oil ratio and consequently the energy requirements. Researchers at Texas A&M University (Goite *et al.* 2001; Ferguson *et al.* 2001; Rivero and Mamora 2002; and Mamora *et al.* 2003) used steam to create a limited hot region at temperatures of 160-170°C, and the steam was co-injected with propane as the solvent. The results showed that, by adding some propane to the steam, steam injection is enhanced, the start-time decreases, oil production increases and energy requirements decrease considerably.

Computer-aided simulations have been performed by several groups in order to mimic reservoir condition. Deng (2005) and Mamora *et al.* (2003) used the STARS software module of the Computer Modelling Group Ltd. in order to integrate heat effects during a heat-assisted VAPEX

process. Zhao (2004) proposed a hybrid SAGD-VAPEX process in which steam and solvent were injected alternatively, with the same process configuration as SAGD. As mentioned earlier, Allen (1974) had also proposed a very similar idea, where he used a variation of the ‘huff and puff’ process with solvent injected in cycles. In the steam alternating solvent (SAS), Zhao (2004) found that, for the same oil production rate, the energy input decreased by 18% compared to SAGD. He used a commercial reservoir simulator (STARS by CMG Ltd.) to simulate typical Cold Lake Reservoir conditions and compared the performance of SAS to SAGD. He also found that the production rates with SAS were as high as, or even higher than, a conventional SAGD project. These simulation results were in agreement with several experiments and have shown promising features of the hybrid process.

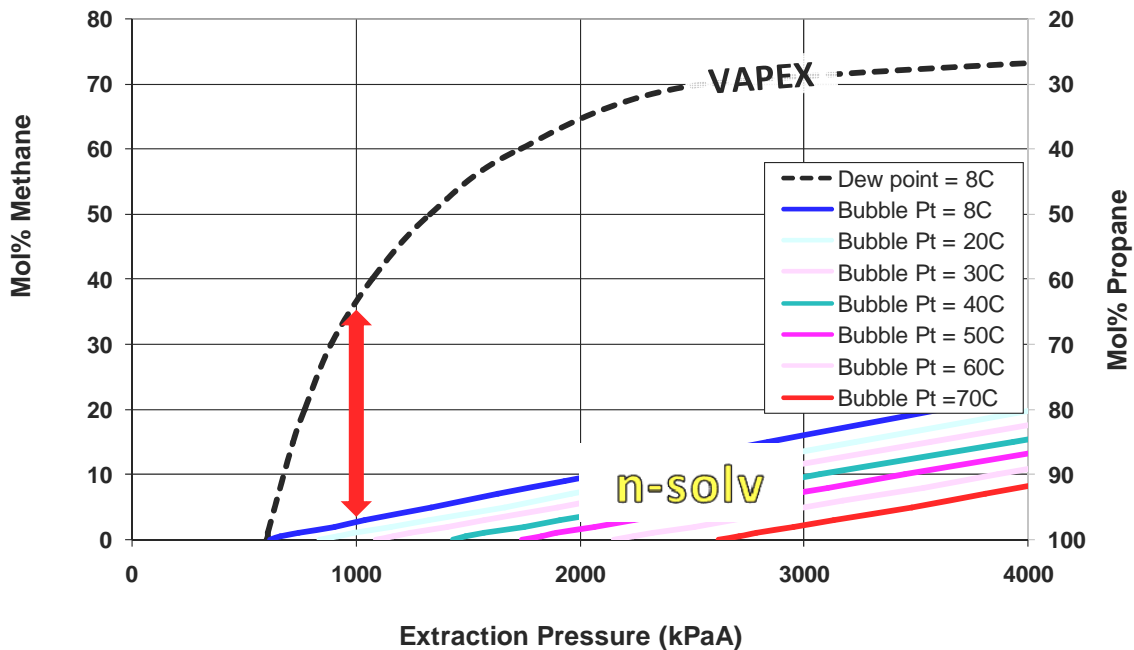
## **2.7 N-Solv<sup>TM</sup>**

The N-Solv<sup>TM</sup> process is a condensing solvent process that ensures a very low tolerance of solution gas and/or non-condensable gas is produced at the same time as the oil. N-Solv is patented by John Nenniger (CA2299790) and John and Emil Nenniger (CA2351148 and US6883607B2) and was publicly introduced by Nenniger and Dunn (2008) at the Canadian International Petroleum Conference. The key to N-Solv is that the process is operated to condense the solvent or solvent containing a small percentage of non-condensable gas below the bubble point. In conventional VAPEX, the solvent is kept in its vapour phase by operating at or above the dew point pressure of the solvent.

The patents for N-Solv imply that the phase envelope of the solvent/impurity between the reservoir and operating temperatures for the corresponding pressures is the key to a successful solvent recovery process. One should recall that the dew point is the temperature at which vapour first starts to condense when its cooled at constant pressure and the bubble point is when the last molecule in the vapour phase condenses to the liquid phase or conversely upon heating a liquid mixture when the first molecule of vapour appears. This patented criterion ensures that any impurities in the vapour phase will be condensed and removed from the solvent chamber during oil production. If solvent processes are operated at the dew point and especially with a solvent mixed with a non-condensable gas, the non-condensable gas builds up in the solvent chamber over time. This makes it more and more difficult for the solvent mass transfer to take place for two reasons: 1) it makes it more difficult for the injected solvent to reach the bitumen interface through the creation of a diffusion boundary layer throughout the solvent chamber and 2) the non-condensable gas reduces the partial pressure of the solvent and hence the solubility at the bitumen

interface is reduced making it inherently more difficult for the solvent to condense at the cold bitumen surface.

Figure 2.7.1 shows that if one wanted to operate VAPEX at its dew point at reservoir conditions of 8°C and 1000 kPa, the vapour should contain 65 mole% propane and 35 mole% methane whereas the condensed liquid would contain 97 mole % propane and only 3 mole% methane. In a short time the methane would build up greater than 35 mole % so that the propane would no longer condense. Alternatively, one could increase the operating pressure stepwise until it became uneconomical to do so. At these reservoir conditions, N-Solv could produce a liquid phase containing oil, propane, and 3 mole% methane from the solvent chamber. Consequently, it is not necessary to inject the solvent with a non-condensable gas, it is essential to have as little non-condensable gas present as possible. The solvent need only be heated.

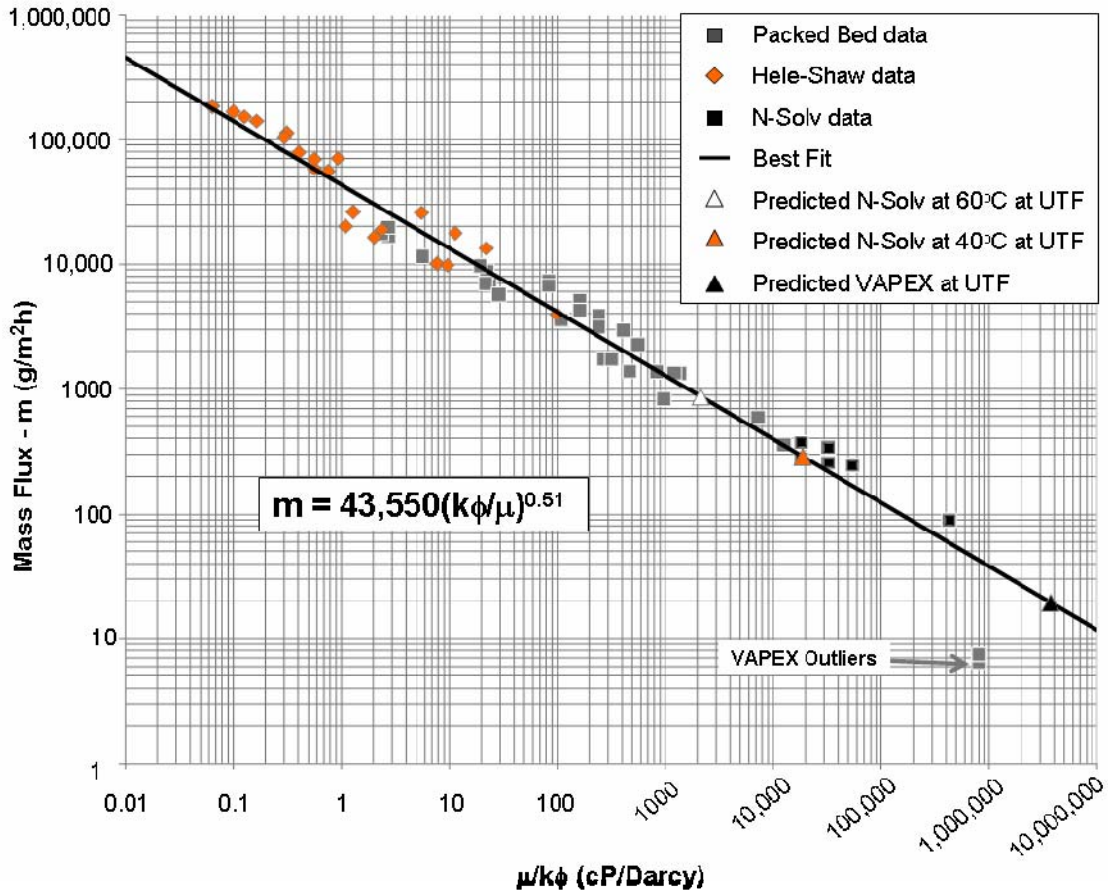


**Figure 2.7.1: Dew Point versus Bubble Point at Typical Alberta Reservoir Conditions (Nenniger and Dunn 2008)**

Heating the solvent has several advantages. The first advantage is that the vapour pressure increases allowing for the solvent to be injected into higher pressure (deeper) reservoir. The second advantage is simply the viscosity reduction of the oil at increased temperatures, as per section 2.2.1. The third is that the solvent delivers a latent heat of condensation to the cold



bitumen surface. Nenniger and Dunn (2008) discuss the fact that at only 30-50°C the vapour pressure of steam is less than 1 atm. The volume of propane required to heat the reservoir ( $\text{m}^3/\text{m}^3$ ) at 50°C is the same as the volume of steam at 250°C giving economic (both operating and capital savings) and environmental advantage (no water usage and an upgraded bitumen due to asphaltene precipitation) to N-Solv over SAGD. The main advantage is the effect of the solvent phase and temperature on the mass transfer mechanisms and viscosity reduction.



**Figure 2.7.2: Solvent Based Gravity Drainage Correlation (Nenniger and Dunn 2008)**

Nenniger and Dunn (2008) comprehensively reviewed most of the laboratory scale solvent experiments and compared the production rates in terms of mass fluxes with respect to the oil viscosity and permeability and porosity of the porous medium used. The results are shown in Figure 2.7.2. The mass flux is the rate of production ( $\text{g/h}$ ) divided by the bulk interfacial area for mass transfer ( $A = L \times W$ ,  $\text{m}^2$ ). They define an independent variable,  $\mu/k\phi$ , where  $\mu$  is the viscosity ( $\text{mPa}\cdot\text{s}$ ) of the dead oil at chamber temperature,  $k$  is the permeability (Darcy), and  $\phi$  is the porosity of the porous medium used. The authors acknowledge that the correlation does not

account for resistances to mass transfer, like the presence of a non-condensable gas or geological variability such as permeability or wettability heterogeneity. The authors concluded that the choice of solvent is not important and that a linear dependence on height resulted in a much better correlation. The insensitivity to the choice of solvent indicates that the draining layer is not the rate limiting step rather it is the viscosity of the original bitumen in place.

## **2.8 Economic and Environmental Advantages**

Solvent-aided processes offer advantages over SAGD. The advantages can be classified as improved energy efficiency, capital and operating costs and oil quality. In comparing VAPEX to SAGD, the energy requirements are less for VAPEX where the latent heat of vaporization is less for a hydrocarbon solvent compared to water. Also VAPEX operates at lower temperatures than SAGD. Some of the energy requirements are decreased when solvent is mixed with the steam (as described earlier). Singhal *et al.* (1996) found that the energy required for VAPEX was 3% of SAGD for the same project. A major problem with thermal operations is that the supplied heat transfers, not only to the reservoir fluid, but the solid structure and any connate water as well. Heat transfers, not only to the reservoir fluid, but to the solid as well. In steam applications, the reservoir temperature increases a lot while in VAPEX, the reservoir temperature increases are no more than 5 to 10°C (Singhal *et al.* 1996).

In 2003, Luhning *et al.* compared natural gas and fresh water requirements. It was estimated that SAGD would require  $1.15 \times 10^6$  m<sup>3</sup>/day of natural gas and 1700 m<sup>3</sup>/day of freshwater to produce 4000 m<sup>3</sup>/day, compared to VAPEX which would require  $8.5 \times 10^4$  m<sup>3</sup>/day of natural gas and 110 m<sup>3</sup>/day of freshwater. If one compares VAPEX to SAGD, then the capital costs for VAPEX are approximately 30% that of SAGD (Yazdani and Maini 2004). Additionally, the capital costs for VAPEX are approximately 30% of those for SAGD. The capital costs for a hybrid process would include equipment for both solvent and steam handling and may approach or exceed that of SAGD depending on the decrease in steam requirements.

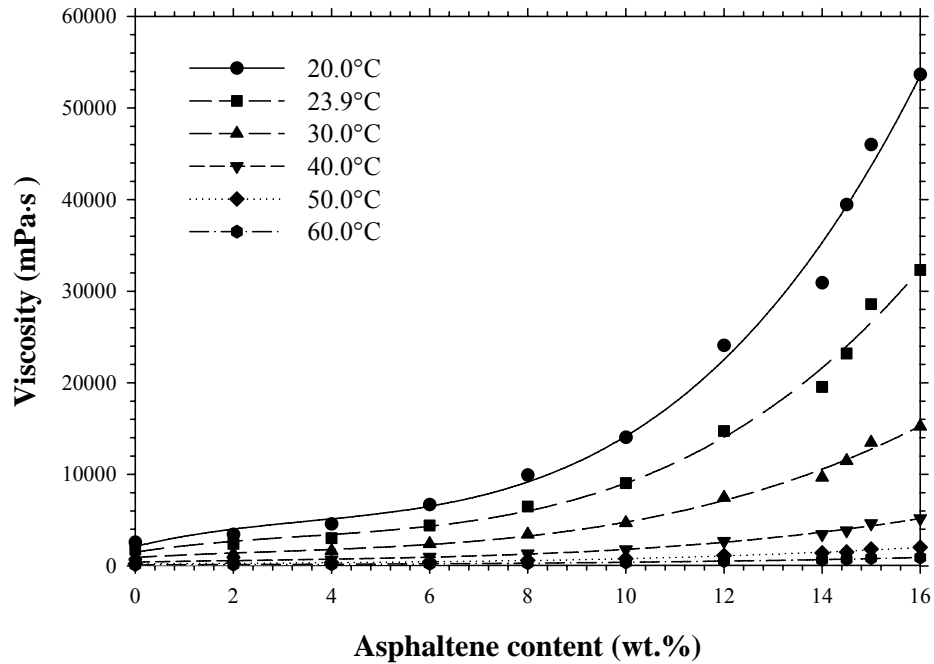
Energy requirements in a solvent extraction process would significantly decrease compared to SAGD with similar production rates. Operating costs include the purchase and handling of water and solvent, as well as the cost of separating the oil from the water and/or solvent. The typically high steam-to-oil ratio (SOR  $\cong$  3:1) in a SAGD well is reduced to less than one barrel of solvent per barrel of oil using VAPEX (Singhal *et al.* 1996). Light hydrocarbons are easily separated

from oil with a low temperature flash vaporizer unlike water-oil emulsions. Solvent recovery is at least 90%, not including the recovery after blow down (Singhal 1996).

Nenniger and Dunn (2008) compare N-Solv to SAGD at different temperatures using their empirical correlation (shown in Figure 2.7.2) relating the mass flux of oil produced per interfacial contact area to the square root of the permeability and porosity divided by the dead oil viscosity  $(k\phi/\mu)^{0.5}$  for 60 different experiments. The prediction suggests that for a 500m long horizontal well with a 20m pay zone and a permeability of 5 Darcy at 7°C, VAPEX would produce 8 m<sup>3</sup>/day with 95% confidence. Alternatively, N-Solv operated at 30°C would produce 70 m<sup>3</sup>/day or at 40°C maximum predicted production rates would 140 m<sup>3</sup>/day. They claim that the solvent to oil ratios on the order of 2-6 are equivalent to steam to oil ratios of 0.2-0.4 from an energy perspective, suggesting there is a 90% energy savings using N-Solv in the range of 30-50°C compared to SAGD (but the temperature is not mentioned). One counter-argument is the time value of money with respect to the solvent inventory whereby solvent costs increase and oil prices decrease. This may be the case if the solvent were lost in the reservoir. However, in the case of N-Solv where 97 mole% of the propane is recovered at 8°C and 1000 kPa, the propane is easily stripped and re-used.

## **2.9 Asphaltene Precipitation**

Asphaltenes precipitate from the heavy oil/bitumen if operating conditions depart from phase equilibrium conditions. Asphaltene precipitation greatly reduces the viscosity of heavy oil, as shown in Figure 2.9.1. By reducing the asphaltene content from 16% by mass to zero, the heavy oil viscosity at relatively low temperatures is reduced from several to over twenty orders of magnitude (Luo and Gu 2005). Asphaltene precipitation was observed when the operating pressure was above the vapour pressure for propane (Mokrys and Butler 1993) and show that the propane to oil ratio needs to be greater than 0.35 by mass in order to precipitate asphaltenes. While in-situ asphaltene precipitation reduces the operating and environmental expense of upgrading the oil thermally/catalytically some think that it will reduce permeability and have an impact on oil production and sweep efficiency. This was neither observed by Nenniger and Dunn (2008), Rezaei and Chatzis (2008) nor by James *et al.* (2007) and presented in the Results section of this chapter.



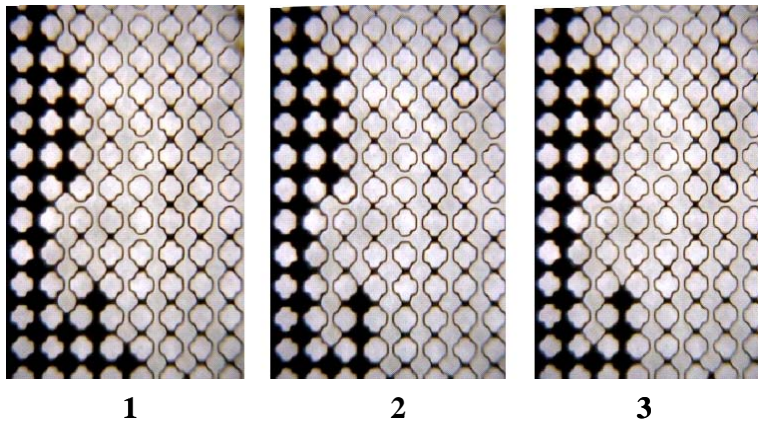
**Figure 2.9.1: Bitumen Viscosity as a Function of Asphaltene Content (Luo and Gu 2005)**

Some reservoirs are not conducive to SAGD. Reservoirs with bottom aquifers or an overlying water layer (in very viscous heavy oil reserves) decrease the energy efficiency of thermal production methods. The problem arises when steam tends to condense on the water layer and therefore heats the water. In the case of an overlying water layer, this problem is more serious as the intrusion of one barrel of water increases the steam requirements to be increased by half a barrel (Butler 2001). On the other hand, hydrocarbon solvents have very low solubility in water. The existence of bottom aquifers helps the communication between the injector and producer. It also changes the process scheme from gravity-dominated into a counter-current rising scheme, and consequently increases the production rate (Mokrys and Butler 1993a; Butler and Mokrys 1998; Das and Butler 1996). It is believed that VAPEX is the only viable technology for oil production from heavy oil reservoirs with bottom aquifers/overlying water layers (Das and Butler 1996; Karmaker and Maini 2003b). Shallow and thin reservoirs also suffer from too many thermal losses to the underburden and overburden. Reservoirs with high clay content can not be successfully exploited by SAGD. The problem arises from clay swelling caused by water condensates on the surface of the clay. It is believed that reservoirs with clay contents > 10% might be subject to formation damage due to clay swelling and they are not recommended for a SAGD project (Singhal *et al.* 1996), whereas this is not a problem for a typical VAPEX process.

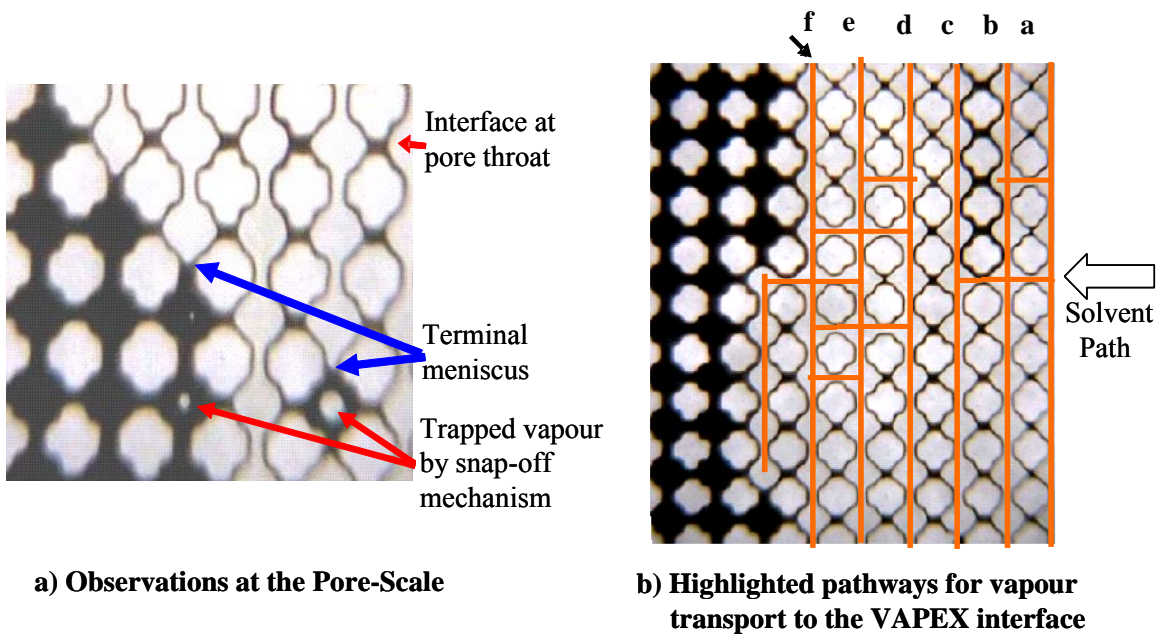
Some feel that low permeability maybe problematic for solvent processes because if asphaltenes precipitate they may reduce the permeability or plug the formation. Another reason is that it might be better to not upgrade the oil in-situ through the precipitation of asphaltenes because the reduction in asphaltenes ultimately means fewer barrels recovered. This philosophy is flawed for two reasons: 1) the upgraded oil sells for a higher price and 2) the environmental and energy implications required by surface upgrading of the oil are reduced if the asphaltenes are left in-situ.

## **2.10 Pore Scale Phenomena**

Chatzis (2002) investigated the pore scale phenomena associated with the VAPEX process using glass etched micromodels. He observed that the diluted oil drains preferentially over the solvent-heavy oil interface in the direction of gravity if a continuous oil film with reduced viscosity exists. Near the interface, oil drained into dead end pathways, causing the draining of oil film paths to redirect and the formation of peaks and valleys at the bitumen/solvent interface (see Figure 2.10.1). Away from the interface, diluted oil formed localised (close loop) films in pore throats and around pore bodies. The diluted oil films cannot drain until the weight of the oil (gravity forces) overcomes capillary and viscous forces. The oil in these closed loop films drained at a much slower rate than oil at the VAPEX interface because of reduced hydraulic conductivity. Live oil draining from above maintains oil continuity in the film and further solvent diffusion helps the closed loop films contribute to live oil production by gravity drainage. The closed loop formations create a tortuous pathway for the butane vapour to reach the main VAPEX interface, as shown in Figure 2.10.2. This may slow down the rate of diffusion when an inert gas is also present in the gas phase.



**Figure 2.10.1: Valleys and Peaks at the uneven VAPEX Interface (Chatzis 2002)**



**Figure 2.10.2: A Closer Look at the VAPEX Interface (Chatzis, 2002)**

# Chapter 3: Differentiating Solvent Processes

## 3.1 *Introduction and Objectives*

Since 2001, there has been renewed interest in exploring solvent combinations, solvent mixed with non-condensable gases, operating the solvent process so that the solvent condenses (N-Solv or thermal solvent reflux) and solvent-steam hybrid processes. The goal of mixing the solvent with a non-condensable gas such as methane or carbon dioxide is to 1) reduce the solvent inventory and/or 2) sequester the carbon dioxide. The goal of increasing the operating temperature greater than the reservoir temperature by either increasing the solvent temperature or combining the solvent with steam is to minimise the bitumen viscosity as quickly as possible and maximise the oil production rates. Unfortunately, there is very little is known about how either the pure solvent or steam processes physically work at the pore scale let alone the combination methods. Often, the combination is presented with some simulation results showing hopeful production rates without any true understanding of the process. This chapter strives to give the history of vaporized solvent processes (VAPEX), condensing solvent processes such as N-Solv and hybrid solvent-steam processes, and then compares and analyses the different methods, highlighting advantages and disadvantages, with a focus on the pore-scale mechanisms associated with non-condensing and condensing solvent processes.

## 3.2 *Condensing & Non-condensing Solvent Processes*

### 3.2.1 *Experimental Procedure using Glass Micromodels*

The Porous Media Laboratory at the University of Waterloo is well reputed for its groundbreaking work involving immiscible fluid flow characterisation in etched glass micromodels (Chatzis 1980, Chatzis and Dullien 1983, 1985). Using the same wet chemistry technique, different patterns were etched into glass creating a two-dimensional porous network used to simulate a porous medium. Etched glass micromodels offer the ability to visualise pore scale interactions and qualitatively understand the fluid interactions. Quantitatively, results from the 2-D micromodels shouldn't be scaled to predict results from 3-D reservoirs but results can be compared quantitatively between micromodels to gain an understanding of the effect of different pore structures. Fluid flow is expected to be different in 3-D models where film flow and the coordination number or pore inter-connectedness play more dominant roles. Several glass micromodels with different pore structure characteristics were used to investigate and compare

qualitatively the pore scale events and quantitatively the interface velocities of non-condensing and condensing solvent processes. The different micromodel patterns and characterisation of the micromodels are shown in Figure 3.2.1.

Before using the micromodels, they were characterised with respect to overall model dimensions, pore dimensions, porosity and permeability. The pore dimensions are illustrated in Figure 3.2.1, and the micromodel characteristics are summarised in Table 3.2.2 with details shown in Appendix A. There are two measurements in particular in glass etched micromodels which are inherently difficult to measure; the depth of etching ( $\delta_{etch}$ ) and the porosity ( $\phi$ ). Ideally, a profilometer would be used to measure the depth of etching; however, those available at the University of Waterloo are not suitable for translucent, deep, rough etched glass. The depth of etching was calculated from measuring the height of capillary imbibition in the models, and calculating an equivalent radius ( $r_{eq}$ ) of curvature from which the depth of etching was estimated.

$$P_c = \frac{2\sigma \cos \theta}{r_{eq}} \rightarrow r_{eq} = \frac{2\sigma \cos \theta}{\Delta\rho g h_c^{imb}} \quad (3.2.1)$$

Firstly, knowing that capillary imbibition is controlled by the pore body radius, the measured height of capillary imbibition ( $h_c^{imb}$ ) is related to the equivalent radius ( $r_{eq}$ ) of the assumed homogeneous pore bodies.  $\sigma$  is the surface tension between the fluids (water-air, or toluene-air),  $\theta$  is the contact angle and  $\Delta\rho$  is the difference in density between the fluids (water-air, or toluene-air). The radius of curvature is related to the two principle radii through (Dullien 1992):

$$\frac{2}{r_{eq}} = \left[ \frac{1}{r_{pore\ body}} + \frac{1}{r_{etch}} \right] \rightarrow \frac{2}{r_{eq}} = \left[ \frac{2}{Pore\ Body\ Width} + \frac{2}{\delta_{etch}} \right] \quad (3.2.2)$$

$$\delta_{etch} = \left[ \frac{1}{r_{eq}} - \frac{1}{Pore\ Body\ Width} \right]^{-1} \quad (3.2.3)$$

This depth of etching was then used to calculate the cross-sectional area perpendicular to fluid flow, i.e. across the width. The porosity is defined as the pore volume divided by the bulk volume. The pore volume was found from the difference in mass when saturated and dry. The bulk volume was calculated knowing the depth of etching, width (W) and length (L) of the model:



$$\phi = \frac{\text{Pore Volume}}{\text{Bulk Volume}} = \frac{V_{pore}}{(LW)_{model} \delta_{etch}} \quad (3.2.4)$$

Permeability (k) is the measure of flow through porous media and is measured in units “Darcy”. It is essentially a measure of the conductivity of the porous media. It can be related to the flow rate (Q) through the porous media and the corresponding pressure drop ( $\Delta P/L$ ) using Darcy’s Law, as shown in the next equation, where  $\mu$  is the liquid viscosity and A is the cross-sectional area. The permeability of a porous media can be found by experimentally manipulating Darcy’s Law or using any number of empirical correlations that exist for specific types of porous media.

$$Q = \frac{kA \Delta P}{\mu L} \quad (3.2.5)$$

### **Constant Head Permeability Measurement**

The permeability can be determined from a constant head steady state method where a hydrostatic head of water ( $\rho gh$ ) is maintained and the flow rate of water through the porous medium is measured. The pressure difference is defined as  $\Delta P = \rho gh$ , the length of the porous medium is L and Q is the measured volumetric flow rate. Using different hydrostatic pressures and measuring the corresponding different flow rates, the permeability can be determined from the slope of Q versus  $\Delta P/L$ . This method requires knowledge of the cross sectional area (A) which inherently requires knowledge of the depth of etching ( $\delta_{etch}$ ) of the micromodels.

### **Free Imbibition Interface Advancement Permeability Measurement**

The permeability of the glass etched micromodels is determined using the free imbibition advancing interface method and is derived from Darcy’s equation. Knowing the capillary height of imbibition in the model and the free imbibition interface position with respect to time, the advancing interface permeability can be calculated as shown:

$$\frac{dx}{dt} = v(x,t) = \frac{k \Delta P}{\mu x(t)} = \frac{k P_c^{imb}}{\mu x(t)} \quad (3.2.6)$$

$$\int x dx = \int \frac{k P_c^{imb}}{\mu} dt \rightarrow x^2 = \frac{2k P_c^{imb}}{\mu} t \quad (3.2.7)$$

If the imbibition front position squared ( $x^2$ ) is plotted versus time, then the permeability can be found from the slope ( $m$ ), the viscosity ( $\mu$ ) of the fluid and the imbibition capillary pressure.

$$m = \frac{2k P_c^{imb}}{\mu} \rightarrow k = \frac{\mu m}{2 P_c^{imb}} \rightarrow k = \frac{\mu m}{2 \Delta \rho g h_c^{imb}} \quad (3.2.8)$$

### Depth of the Draining Live Oil and Bitumen

Figure 3.2.1 shows some of the other dimensions used to characterise the micromodels such as the 1) pore to pore distance, 2) the pore width, 3) the pore throat width, 4) the particle size, 5) the diffusion distance and 6) the maximum flow path length from one pore to the one below it assuming film flow. The pore to pore distance is from the centre of one pore to the centre of the next or alternatively from the centre of one pore throat to the next. Model DL-1 is an example of a pore network with high permeability and negligible pore throat length. Models OC-1 and DC-1 have the same pore width but the pore to pore distance, diffusion distance, and flow path length are greater in OC-1 while the pore throat width in model DC-1 is greater, all attributing to a slightly larger permeability in model DC-1. The diffusion distance is essentially the distance from the centre of one pore to the edge of another pore and it signifies the distance solvent must diffuse in order to reach the next pore.

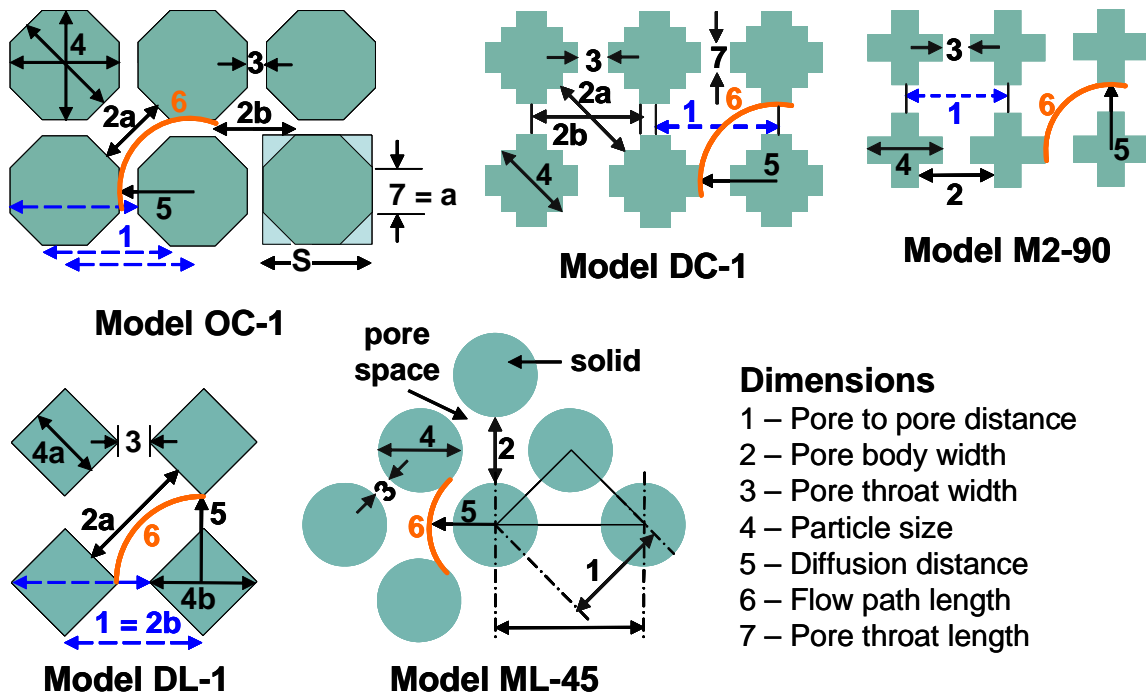


Figure 3.2.1: Micromodel Patterns Etched in Glass (James and Chatzis, 2004)

Figure 3.2.2 shows the experimental setup used for investigating the VAPEX process in etched pore network micromodels. The properties of the heavy oil and solvent used are shown in Table 3.2.1. The first step was filling or saturating the models with the heavy oil. The high viscosity of the oil and fairly low permeability of the models requires both pressurising and heating the oil to force it into the model. A small stainless steel pressure vessel was half filled with heavy oil and closed. The oil was then pressurised with nitrogen to approximately 103-138 kPa (15-20 psig). The heavy oil vessel was connected to the micromodel and both were placed in a low temperature oven (65°C). Once acclimatised, the valve was opened and the head of pressure provided enough force to push the heavy oil through the low permeability micromodel. The micromodels were constructed so that along one side of the pores and both ends a more permeable channel was etched to facilitate solvent injection and live oil production. While saturating the models the oil preferentially saturates the side with the channel. This was avoided by cooling the higher permeability side of the channel slightly (with a cold compress) to increase the viscosity of the oil and slow the flow rate of oil.

Before starting the VAPEX experiments, the heavy oil in the higher permeability side channel and entrance/exit channels was evacuated so that experimental time is not used to simply drain the channels. The overall model was cooled and all parts of the model covered with an insulating material except the channels. A heat gun was used to heat the channels and a syringe pump used to displace the warmed oil with air. The model was then placed in its holder, the collection tubing (flexible 0.635 cm, 1/4" Tygon® tubing and 2-way ball valve) and solvent line attached to it before placing the model in a constant temperature water bath.

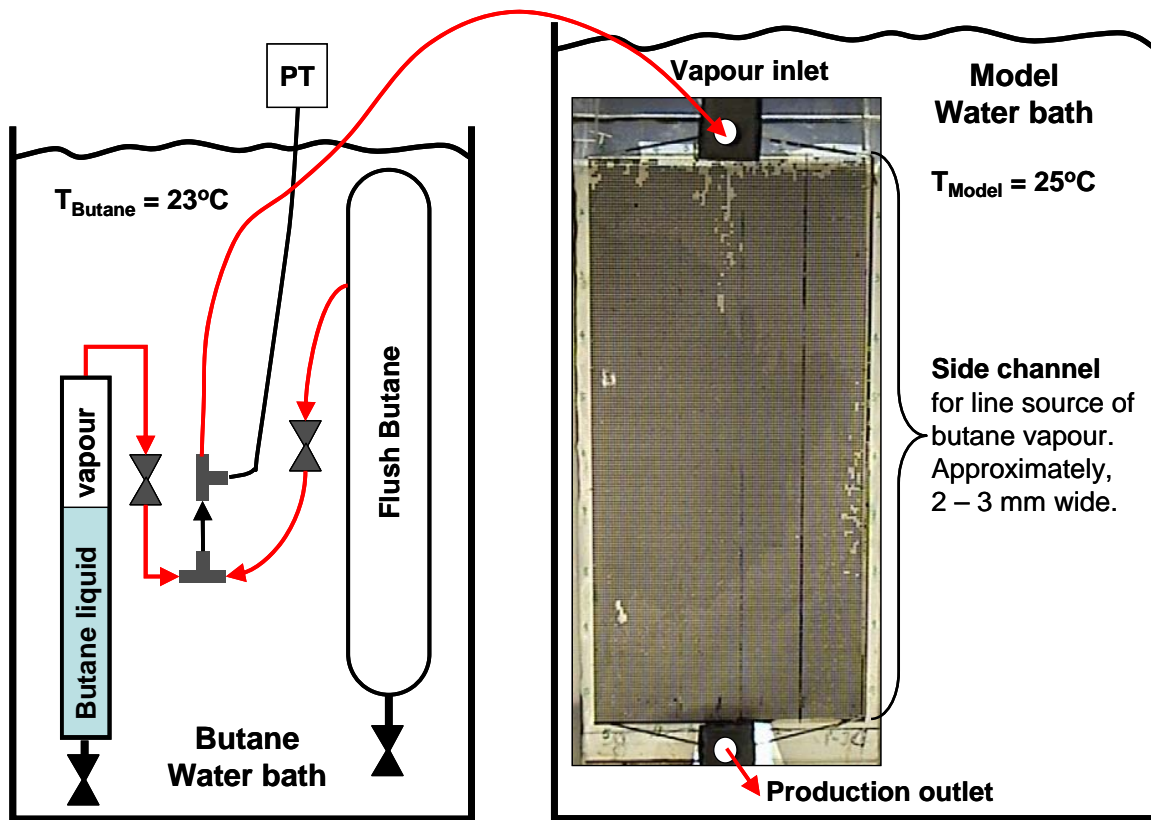


Figure 3.2.2: Investigating Pore Scale Mechanisms – Experimental Apparatus

Table 3.2.1: Fluid Properties for Solvent Extraction Experiments in Micromodels

Oil Properties	
<b>Density (kg/m<sup>3</sup>)</b>	
Bitumen, $\rho_b$	987.0
n-Butane (l) at 25°C, $\rho_s^l$	572.8
n-Butane (v) at 25°C, $\rho_s^v$	6.2
Live Oil, $\rho_{lo}$	811.1
$\Delta\rho_{lo}$	804.9
<b>Viscosity (mPa.s)</b>	
Bitumen, $\mu_b$	23,000
Live Oil, $\mu_{lo}$	5
<b>Concentration</b>	
Mass fraction, $\omega_s$	0.30
Volume fraction, $v_s$	0.425

During each experiment the butane vapour and the heavy oil filled micromodel were kept in separate water baths to ensure better control of their respective temperatures. Temperature control was essential to quantitatively compare results. The n-butane was maintained at 2°C less

than the micromodel to ensure that the butane did not condense for the non-condensing experiments. All were placed in the same water bath to facilitate solvent condensation when desired. The model was positioned close to the front wall of the rectangular water bath (constructed of 12 mm Plexiglas) in order to reduce parallax and increase the clarity for image capture compared to the curved glass of a normal water bath. Water was circulated around the model for better temperature control by using an auxiliary water bath pump attached with tubing that was positioned between the model and the water bath wall. The supplied butane (Praxair instrument grade) was transferred into two different supply cylinders as shown in Figure 3.2.2. A cathetometer was used to monitor the solvent flow rate by measuring the height of butane ( $\pm 0.005$  cm) in the small Plexiglas cylinder with an inner diameter of 12.7 mm and length of 324 mm ( $\frac{1}{2}$ " inner diameter by  $12\frac{3}{4}$ " long). The second butane cylinder (sized to fit in the water bath) was used for flushing the entire system of air prior to starting the experiment.






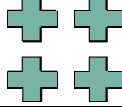
The micromodels were divided into cell blocks using a marker to simply allow for easier position recognition within the porous network without obstructing pore visibility. The size of the cell block was determined simply from the focus of the camera. Models DL-1 and OC-1 were divided into 15 horizontal rows and 5 vertical columns resulting in a model consisting of 75 cell blocks of 10 x 10 pores each except for the last rows/columns. 50 cell blocks of 20 x 20 pores or 10 rows and 5 columns were used in model DC-1. The VAPEX experiment started once communication between the solvent and saturated micromodel was established by opening the valve attached to the vapour cylinder, as shown in Figure 3.2.2. As solvent diffused into the heavy oil and reduced its viscosity, the live oil (viscosity reduced oil) drained in the direction of gravity to the production well. The data collected during the experiment included:

- the overall trace of the position of the VAPEX interface, recording the average position of the interface (# of pores that it has advanced) for every row (vertical group of 10 or 20 pores, depending on the model) with time
- digital photographs of the overall shape of the VAPEX/bitumen interface
- digital photographs and videos capturing detailed pore scale events
- monitoring the butane uptake using a cathetometer, as indicated by the decrease in liquid butane level in butane cylinder
- monitoring the temperature in each water bath

### 3.2.2 Experimental Results and Discussion

Glass micromodels with different pore structure characteristics were used to investigate the VAPEX process in order to discern pore scale events and compare interface velocities in different models and illustrate the effect pore structure. The dimensions and micromodel characterisation are shown in Table 3.2.2.

**Table 3.2.2: Micromodel Characterisation**

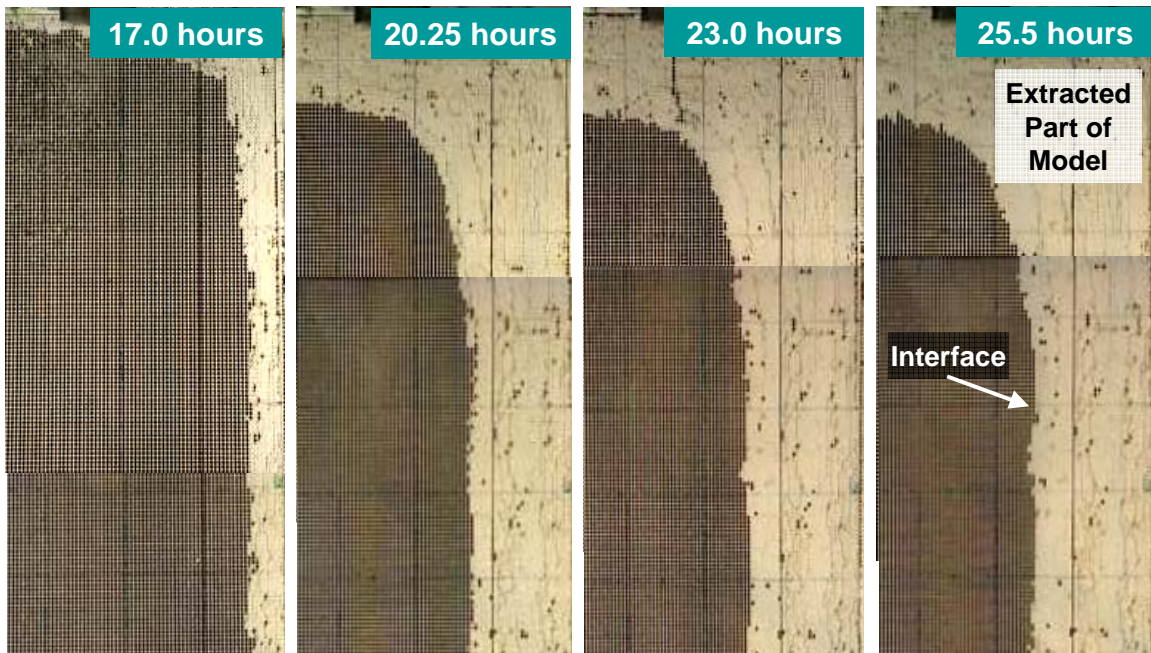
	Micromodels					
	OC-1 	DL-1 	DC-1 	SUDC-3 	M1-45 	M2-90 
C = consolidated U = unconsolidated	C	C	C	U	C	C
<b>Pore Dimensions (mm)</b>						
1) Pore to Pore	2.04	2.04	1.60	1.46	2.80	1.45
2) Pore Body Width	1.38	2.04	1.31	1.10	2.00	1.20
3) Pore Throat Width	0.45	0.67	0.49	0.39	0.80	0.25
4) Particle Size	1.59	0.99	1.11	1.06	2.00	1.20
5) Diffusion Distance	1.25	1.36	1.05	0.92	1.80	0.85
6) Flow Path	2.61	2.13	1.93	1.82	2.83	1.59
7) Pore Throat Length	0.66	n/a	0.29			
<b>Depth of Etching (mm)</b>						
Pore Body, $\delta_{etch}^P$	0.1244	0.2498	0.1281	n/a		
Pore Throat, $\delta_{etch}^T$	0.0809	0.0728	0.0649	n/a		
<b>Model</b>						
Length, L (cm)	30.4	30.4	30.4	28.9	28.2	20.8
Length, L (# pores)	149	149	190	181	72	155
Width, W (cm)	10.0	10.0	14.1	5.8	9.8	8.7
Width, W (# pores)	49	49	89	36	26	62
Pore Volume (cm <sup>3</sup> )	1.6	2.1	2.0			
<b>Porosity, <math>\phi</math></b>	0.42	0.28	0.36	0.38		
<b>Permeability, K (<math>\mu\text{m}^2</math>)</b>						
Constant Head Method	130	292	84			
Interface Advancement	129	291	91	n/a	45	66

Model DL-1 had the highest permeability and the length of the pore throats were negligible thus minimising the flow path. Model DC-1 had pores with comparable pore body width (dimension two) of model OC-1. However, the pore to pore distance (dimension one) and the diffusion radius (dimension five) were shorter in model DC-1. Other preliminary experiments have been conducted in unconsolidated glass micromodels using different solvents, as shown by model

SUDC-3. Models M1-45 and M2-90 were used in an earlier study by Chatzis (2002). The results discussed here focus on models OC-1, DC-1 and DL-1.

### 3.2.2.1 Interface Velocity / Sweep Efficiency

Once communication between the butane vapour and the bitumen saturated porous media was established, the solvent diffused into the heavy oil producing live oil and creating essentially three phases; heavy (undiluted) oil, live oil (with viscosity reduced) and solvent vapour. The position of the VAPEX (oil-solvent) interface was measured with time. The rate of interface advancement is akin to dead oil production and is a measure of economic viability of a formation. Figure 3.2.3 shows the VAPEX interface advancement over time for Model DC-1. Representative results are shown in Figure 3.2.4. Except for the top 10-15% of the micromodel, the VAPEX interface advanced linearly with time. The bitumen interface was actually ahead of the measured VAPEX interface due to the fact that the live oil drained down over the pores filled with heavy oil. The location of the interface appears uniform from a macroscopic perspective but at the pore scale, the interface position can vary by several pores. This is due to the way that the live oil drains at the pore scale, as discussed in 3.2.2.4 and 3.2.2.5. The average interface position per row (10 or 20 pores) is reported in Table 3.2.3.



**Figure 3.2.3: VAPEX Interface Advancement in Model DC-1**

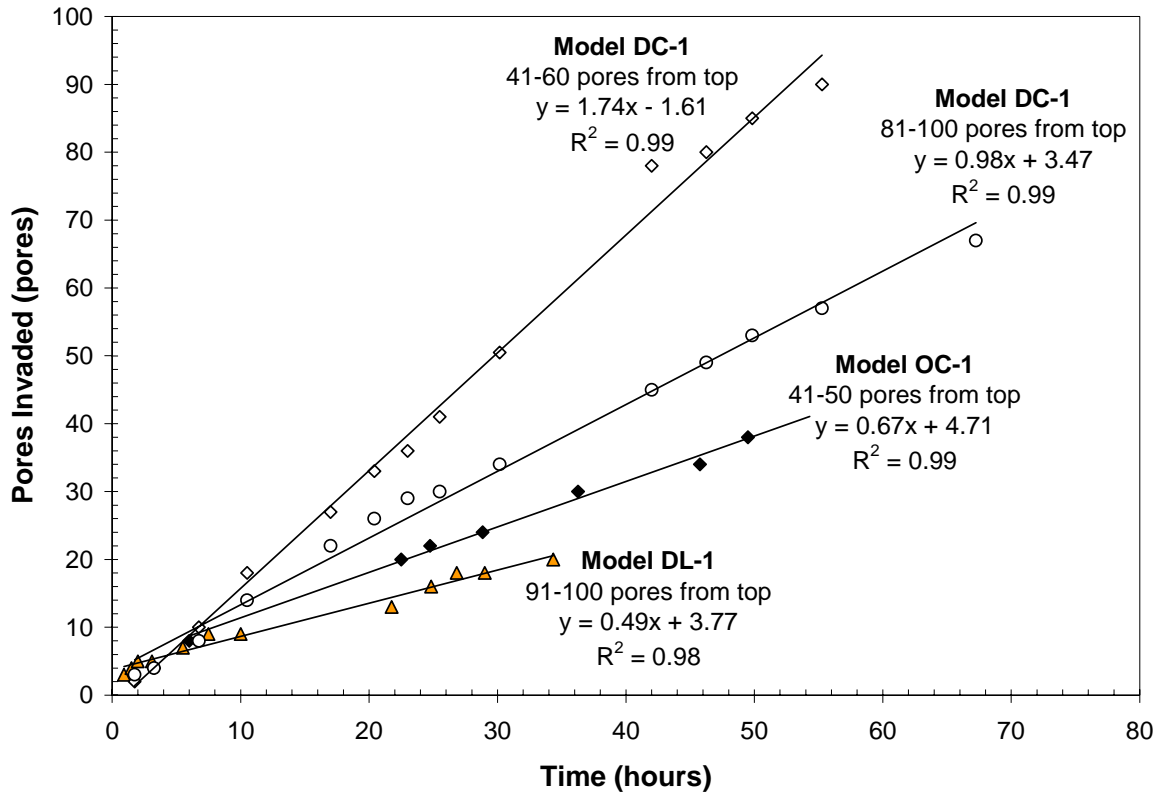


Figure 3.2.4: VAPEX Interface Advancement in Micromodels DL-1, DC-1 and OC-1

Table 3.2.3: VAPEX Interface Velocity ( $U_p^x$ ) and

	OC-1	DL-1	DC-1	SUDC-3	M1-45	M2-90
<b>Location in Model (pores/hour)</b>	<b>n-butane</b>	<b>n-butane</b>	<b>n-butane</b>	<b>n-pentane</b>	<b>n-butane</b>	<b>n-butane</b>
31-40 pores from top	0.73	0.82				
41-50 pores from top	0.67	0.77	1.74			
51-60 pores from top	0.58	0.67				
61-70 pores from top	0.59	0.64	1.24			
71-80 pores from top	0.59	0.57				
81-90 pores from top	0.62	0.57	0.98			
91-100 pores from top	0.60	0.48				
101-110 pores from top	0.59	0.52	0.87			
<b>Average (pores/hour)</b>	0.62	0.63	1.21		n/a	0.86
Using Pore to Pore distance (mm/hour)	1.27	1.28	1.93			
Using Pore Body Width (mm/hour)	0.86	1.28	1.58			

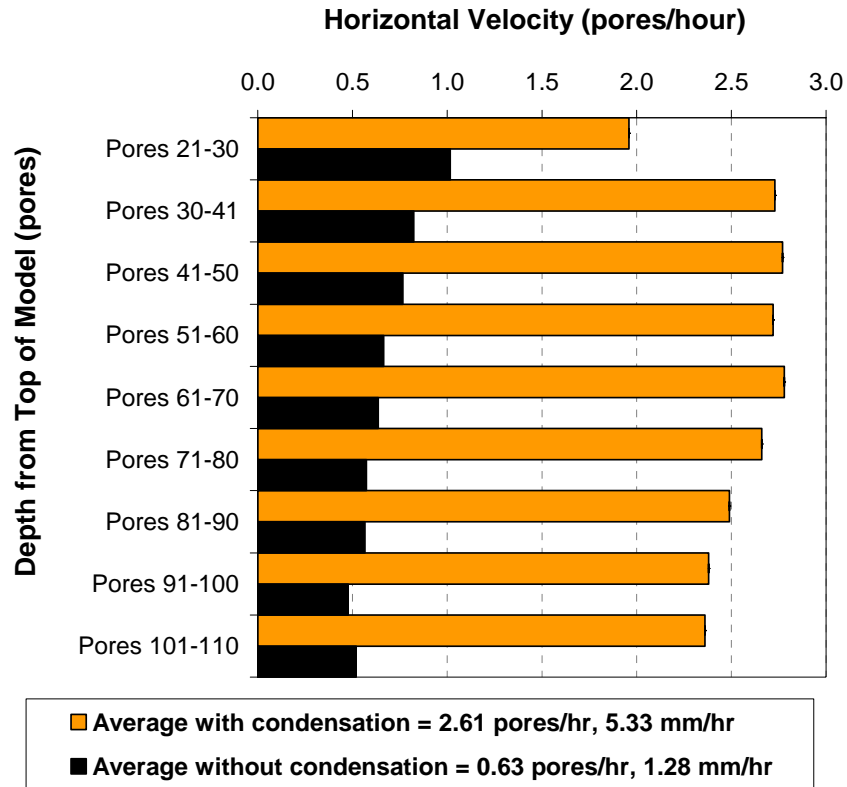


Figure 3.2.4 shows the interface velocity as a function of pores from the top for models DC-1, DL-1 and OC-1. Models OC-1 and DL-1 have similar high permeabilities yet model DC-1 exhibits a 50% increase in interface velocity. One would expect that the rate of interface advancement would be higher in high permeability models. The difference is the pore to pore distance which is only 1.60 mm compared to 2.04 mm in the other two models. The differentiating dimension appears to be the diffusion distance. The diffusion distance is defined as half the particle width plus the width of the pore throat. Alternatively, it is the distance from the midpoint of the pore throat to the far side of the pore throat connecting the pore with the one directly below it, i.e.

$$\text{Diffusion Distance} = 0.5(\text{Pore to Pore distance}) + 0.5(\text{Pore Throat width}) \quad (3.2.9)$$

The solvent needs to diffuse sufficiently into the pore so that the viscosity of the oil in the throat is also reduced. The live oil can then drain via drainage displacement once the capillary pressure is overcome. Capillary pressure is inversely proportional to the radius. The capillary pressure that must be overcome is the lowest in model DL-1 with a pore throat width of 0.67 mm. The capillary pressure is comparable in models OC-1 and DC-1 with pore throat widths of 0.45 mm and 0.49 mm respectively. One may think that the oil should drain more easily from model DL-1 but it has the greatest diffusion distance (1.36 mm compared to 1.25 mm and 1.05 mm in models OC-1 and DC-1 respectively). The oil also drains by film flow and both are discussed in more detail in the subsequent sections. In three dimensional porous networks, the reality is that film flow will contribute more to the drainage. One can conclude that at the pore scale, the diffusion distance and not the overall permeability that is the predominant dimension that effects how VAPEX sweeps or advances through the formation.

The same glass micromodel (Model DL-1), having a permeability of  $292 \mu\text{m}^2$ , was used in two experiments: one using butane vapour and the other where the butane condensed within the micromodel. The first water bath ( $23^\circ\text{C}$ ) contained the butane, and the glass micromodel was housed in the second water bath at  $25^\circ\text{C}$ . Since the vapour phase was 100% butane at its vapour pressure, then the slight increase in temperature prevented the butane vapour from condensing. The VAPEX interface was found to advance linearly with time. Figure 3.2.5 shows the rate at which the VAPEX interface advanced throughout the model. As shown, the average rate of VAPEX interface advancement for normal VAPEX was 0.63 pores/hour, while in the case of solvent condensation, the sweep rate was 4x greater at an average rate of 2.61 pores/hour.



**Figure 3.2.5: VAPEX Interface Velocity in model DL-1 with and without Condensation**

The results of this work in micromodels have fuelled further investigations into the behaviour of non-condensing VAPEX and condensing solvent processes. Tam (2007) performed a preliminary comparison of non-condensing and condensing solvent recovery in an 1123 Darcy unconsolidated glass bead system. She found that the rate of interface advancement was 30% faster in the condensing case and dead oil production was 36% more on a mass basis. Rezaei and Chatzis (2007 and 2008) have started a systematic comparison of non-condensing and condensing solvent recovery in unconsolidated glass bead models. Preliminary results indicate enhanced production rates when the solvent condenses at both low and high permeability and using low and high viscosity oil. They continue to investigate the effects of temperature coupled with permeability and oil viscosity to better understand the systematic effect of condensation on production rates.

The combination of the operating conditions, thermodynamic properties of the solvent and reservoir properties determines the phase of the solvent (liquid or vapour). Whether or not the solvent condenses in the porous media at the heavy oil/bitumen interface it affects the mass transfer, as well as the pore scale phenomena that take place. The pore scale mechanisms affect the mixing of the solvent, heavy oil and the gravity drainage of the live oil.

### 3.2.2.2 Mass Transfer Mechanisms at the Pore Scale

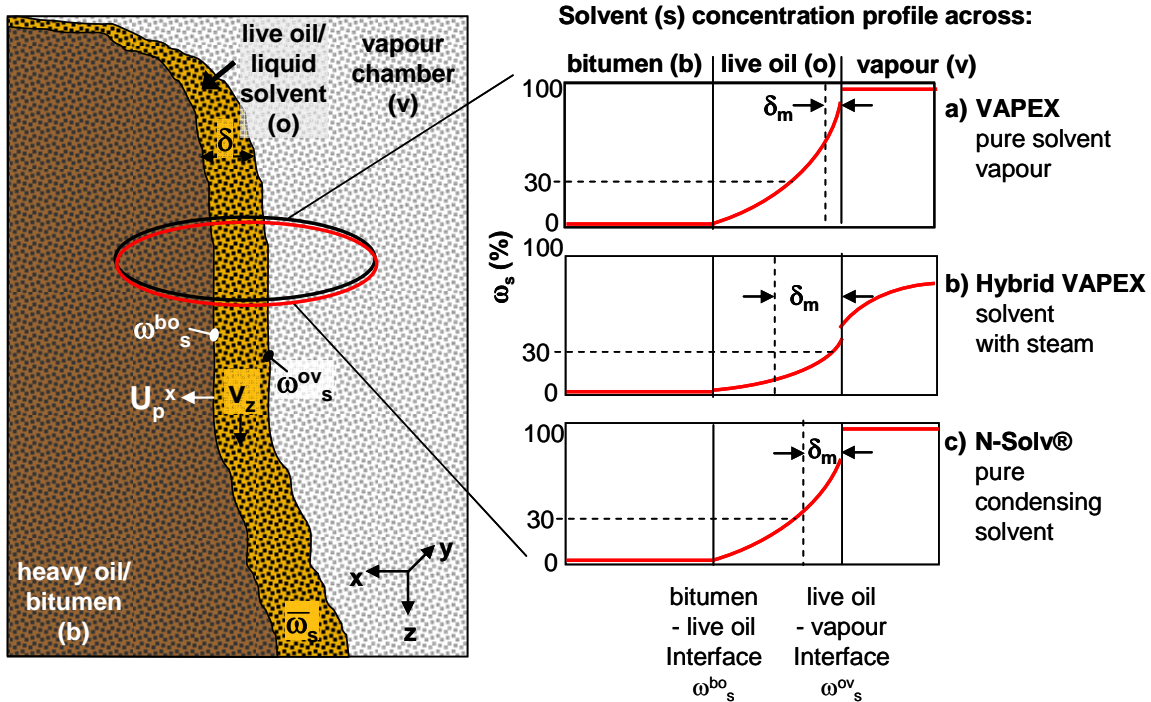
The mass transfer mechanisms at the pore scale of a solvent recovery process are different depending on whether the solvent condenses or not. This section aims to describe the mass transfer mechanisms present at the pore scale, by:

- first describing the solvent – bitumen interface in theory to better understand the nature of the complex interactions between mass transfer, viscosity reduction and gravity drainage;
- considering the impact of diffusion at the pore scale for both non-condensing and condensing processes;
- showing, through observations, that convective mixing is present at the pore scale and discussing the role of convection.

#### **The Solvent – Bitumen Interface**

The transport mechanisms involved in solvent processes are the mass transfer by diffusion and convection of the solvent into the heavy oil and vice versa, as well as gravity drainage of the solvent enhanced live oil. The live oil is mobilised when gravity forces are sufficient to overcome capillary and viscous forces. The predominant factor is the reduction of viscous drag due to the exponential viscosity reduction upon solvent mixing. The role of gravity (i.e. density difference) and capillary forces (i.e. capillary pressure) depend on the individual pore scale mechanisms. The goal of warm and hybrid VAPEX is to increase the rate of viscosity reduction in order to increase the rate of oil production. This is achieved through convective/capillary mixing and heat transfer.

Figure 3.2.6 shows the VAPEX interface and the qualitative solvent concentration profiles for VAPEX, N-Solv and hybrid VAPEX. This figure does not address the differences due to heat transfer or convective/capillary mixing between the different types of VAPEX, but aims to describe the solvent diffusion in the three cases: non-condensing solvent, condensing solvent and solvent mixed with steam. When heat is considered, the depth of the draining live oil probably increases, thus increasing production. This needs to be investigated further for completeness. The porous medium can be divided into three sections: the solvent chamber (to the right in Figure 3.2.6), the live oil/liquid film (Figure 3.2.6) and the heavy oil/bitumen (to the left in Figure 3.2.6). The heavy oil/bitumen is where no solvent exists. The solvent chamber on the right is the ‘swept’ portion of the porous medium through which the solvent vapour/steam must travel to the VAPEX interface. Regardless of the method employed, the heavy oil/bitumen portion remains unchanged.



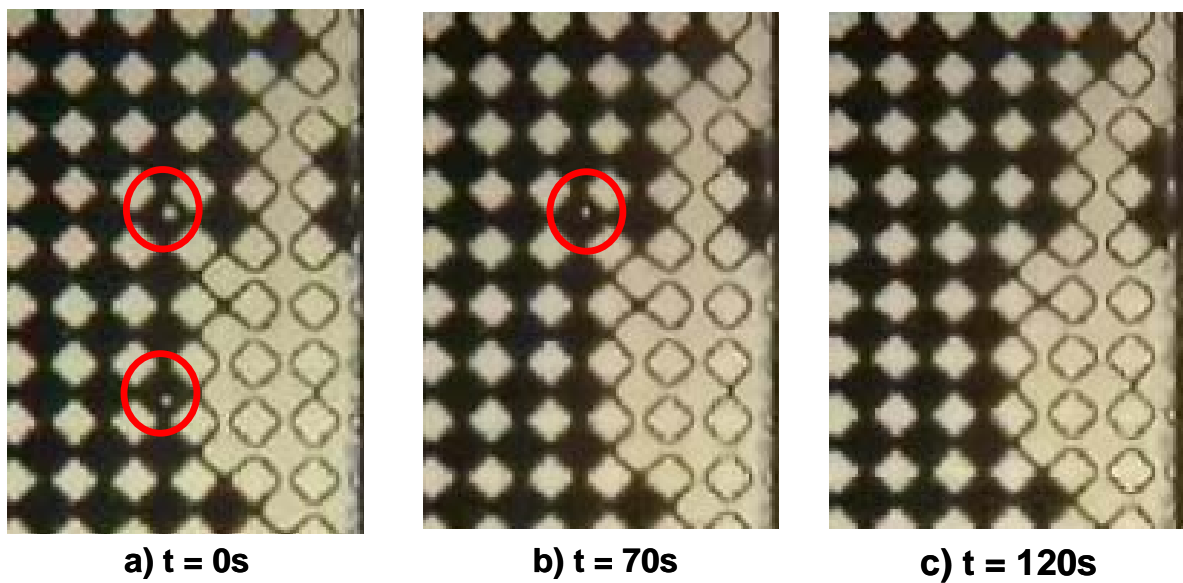
**Figure 3.2.6: The Solvent - Bitumen Interface**

If a non-condensing (VAPEX) or condensing (N-Solv) solvent process is employed (concentration profile a and c in Figure 3.2.6) using a pure solvent, then the concentration of the solvent in the vapour chamber is close to 100%. The maximum pressure, without adding an inert gas, is the solvent's vapour pressure at the specific temperature of the supply solvent. If the pressure is increased greater than the vapour pressure, or the temperature decreased, the solvent condenses to a liquid. Otherwise, if the solvent is mixed with an inert gas or steam (Figure 3.2.6b), then the mole fraction of solvent is less than one and is equal to the ratio of the partial pressure of the solvent over the total reservoir pressure ( $p_i/P_T$ ). The solvent concentration decreases from the point of injection towards the VAPEX interface where it diffuses/mixes with the oil. No assumptions are made at this point about the form of the concentration dependence on distance from the source. It would be presumptuous to assume the concentration profile is linear as that would imply steady state diffusion only with no net flux (Taylor and Krishna 1993). Thus, the solvent must diffuse through the stagnant gas region near the VAPEX interface in the solvent chamber. This condition causes reduced mass transfer of solvent.

The driving force for molecular diffusion is the concentration difference of the solvent at the live oil-vapour interface and the solvent concentration within the bitumen. The inert gas/steam layer and the tortuous pathway through the porous medium both act as a resistances to the solvent

transport through the vapour chamber. The live oil/condensed liquid film is the VAPEX interface. It is defined as the heavy oil/bitumen region containing solvent. It is here that solvent diffuses/mixes into the heavy oil/bitumen and where the live oil drains. The thickness or depth of the live oil film ( $\delta$ ) is not exactly known, but has been estimated (James and Chatzis 2004; Moghadam *et al.* 2009) to be on the order of a few pores deep for VAPEX. The solvent concentration across the depth of the live oil decreases from a maximum at the live oil-vapour interface ( $ov$ ) to a minimum at the bitumen-live oil interface ( $bo$ ) where the concentration is zero. The maximum concentration of solvent in the heavy oil at the given reservoir pressure and temperature is the solubility level for the given solvent concentration in the vapour phase adjacent to the interface ( $\omega_{ov}^s$ ). The mobile oil film ( $\delta_m$ ) is the portion of the live oil film in which the viscosity is sufficiently reduced to mobilize the oil under the force of gravity. The thickness of the mobile live oil film is not known either, nor its relation to the total live oil film thickness. How much further into the bitumen does the solvent diffuse before it starts to drain? What is the effect of the porous medium's permeability, porosity and/or connate water on the film thickness? Based on the molecular diffusion of the solvent only, one may argue that the film thickness can vary. However, the solvent mole fraction in the gas phase near the interface is higher for VAPEX and warm VAPEX than in hybrid VAPEX (with steam), so that the overall rate of mass transfer is greater for cases a and c in Figure 3.2.6.

### Diffusion at the Pore Scale



**Figure 3.2.7: Disappearing Trapped Solvent Vapour Bubbles Indicate Dilution by Diffusion with Non-Condensing Solvent**

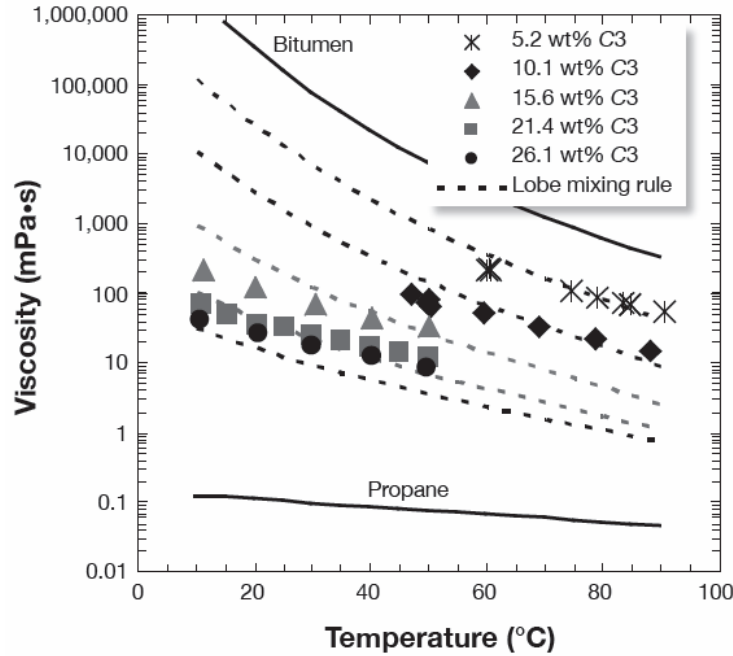
Researchers have been struggling with qualifying and quantifying the mass transfer and in particular the role of diffusion at the VAPEX interface since the first work published by Butler and Mokrys (1989, 1991) and Das (1995). Quantifying the diffusion of light hydrocarbon solvents has been an area much explored and is thoroughly discussed in the next chapter. There has never been any dispute that diffusion of solvent into the bitumen does occur but at what rate and how? The previous figure (Figure 3.2.7) shows that the diffusion of solvent into the bitumen occurs at the live oil – vapour interface as well as within the mobile live oil.

As the solvent vapour diffuses into the bitumen, the live oil becomes mobilised in the direction of gravity. The draining live oil often traps solvent vapour within it due to capillary phenomena of snap-off mechanisms. The trapped solvent vapour gives evidence of increased mass transfer within the live oil as well as the velocity at which the live oil drains (discussed further in the next section). The circled regions of Figure 3.2.7 show two such vapour bubbles trapped within the live oil. After 70s the first bubble has completely diffused into the live oil and likewise the second after 120s.

In a non-condensing solvent process the solvent diffuses into the bitumen. Once a live oil phase is created, the bitumen can counter-diffuse into the live oil. The oil's viscosity is reduced exponentially with the addition of solvent or heat and the effect is even more pronounced when both solvent and heat are combined. In discussing only the mass transfer aspects, Figure 3.2.8 (Badamchi-Zadeh *et al.* 2009a) illustrates the compounded effect of adding both solvent and heat to reduce the bitumen's viscosity. Assuming that the reservoir is 15°C, the raw bitumen viscosity is approximately 700,000 mPa.s. Adding 10% by mass of propane reduces the viscosity to approximately 6000 mPa.s. If the bitumen is heated to 50°C with no solvent, the viscosity is approximately 8000 mPa.s but by heating it to 50°C with 10% solvent by mass, the viscosity is only 73 mPa.s. Not only is the viscosity further reduced by increasing the temperature and adding solvent, the mass transfer mechanisms and rate are changed.

When liquid solvent at slightly higher temperatures is in contact with the heavy oil instead of solvent vapour at the reservoir temperature the mass transfer is increased. From a diffusion point of view, the rate of mass transfer is dependent on the diffusivity as well as the concentration gradient or driving force. As a liquid, the concentration gradient is initially one, from 100% solvent to 0% solvent, across a very short distance. When the light hydrocarbon solvent is in its vapour phase the driving force is initially the equilibrium interfacial concentration, i.e. the solubility which is pressure and temperature dependent. The maximum value is estimated to be

around 0.6 mass fraction for butane in Athabasca bitumen (see Chapter 3). Luo *et al.* (2007) and Badamchi-Zadeh *et al.* (2009) have found the solubility of propane to be much lower at 0.21 mass fraction in Lloydminster oil and 0.24 mass fraction in Athabasca bitumen respectively at 20°C and 800 kPa. The solubility is further decreased due to the reduction in partial pressure if another component is present in the gas phase, i.e. a non-condensable gas.



**Figure 3.2.8: Effect of Temperature and Solvent on the Viscosity of Athabasca Bitumen (Badamchi-Zadeh *et al.* 2009)**

Nenniger and Dunn (2008) make reference to the fact that it is more difficult to transfer solvent into the bitumen than bitumen into the liquid solvent. In a condensing solvent process, both solvent diffusion into the bitumen and bitumen into the solvent are possible. Let's look at propane and Athabasca bitumen at 15°C and 50°C, as illustrated in Figure 3.2.8. The Wilke-Chang correlation for small molecules diffusing through large molecules can be used to estimate the infinite dilution diffusivity of solvent into bitumen. At 15°C, the diffusivity of propane into bitumen is estimated to be  $5.3 \times 10^{-11} \text{ cm}^2/\text{s}$  yet at 50°C it is estimated to be  $5.2 \times 10^{-9} \text{ cm}^2/\text{s}$ . Increasing the temperature increases the diffusion of solvent into the bitumen by two orders of magnitude. Using the Stokes-Einstein equation to predict the infinite dilution of bitumen into propane (generally good for large round molecules diffusing into a solution of small molecules) the diffusion coefficients at 15°C and 50°C are estimated to be  $6.1 \times 10^{-5}$  and  $6.8 \times 10^{-5} \text{ cm}^2/\text{s}$  respectively. At a reservoir temperature of 15°C, condensing the solvent at the interface will create a counter-diffusion process where it is initially six orders of magnitude easier to move the

bitumen into the solvent than the reverse. Without condensation the bitumen cannot initially diffuse into the solvent until a sufficient solvent diffuses into the heavy oil to create conditions for reverse diffusion. At the same time, increasing the temperature increases the diffusion of solvent into bitumen due to viscosity reduction.

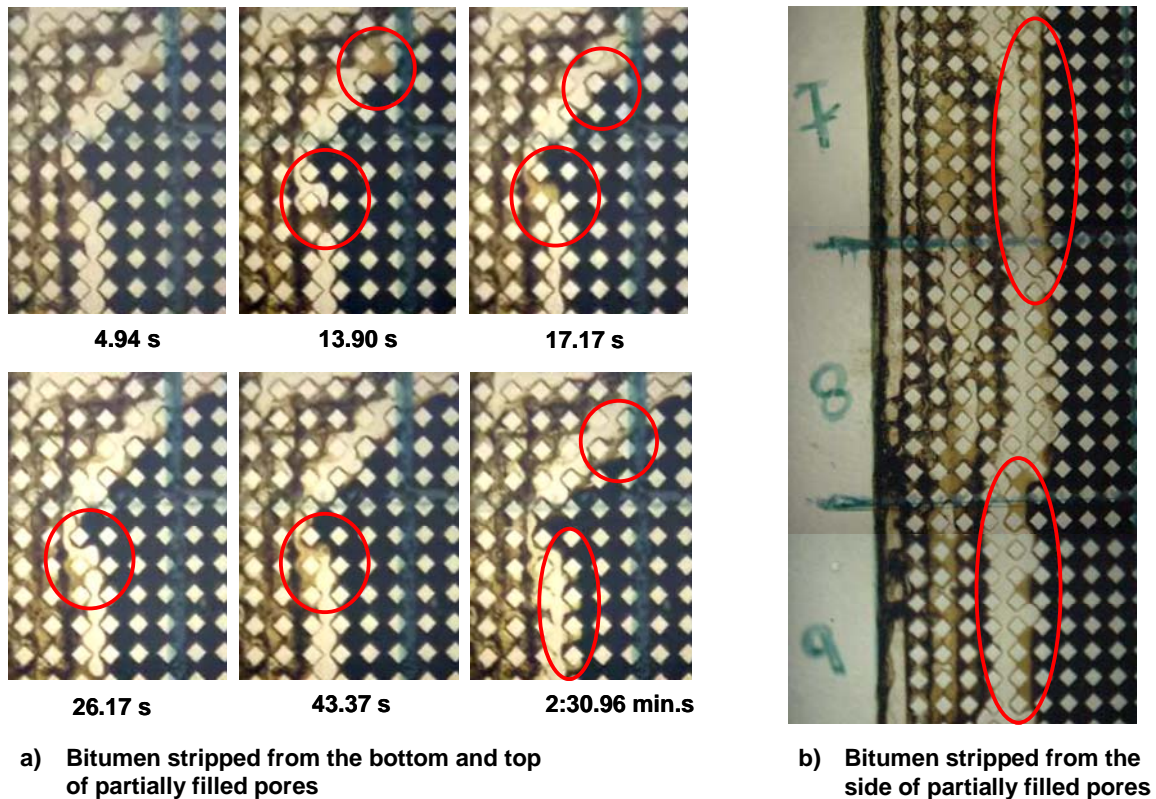
### **Convection at the Pore Scale**

Pore scale observations from condensing solvent experiment carried out in model DL-1 are shown in Figure 3.2.9. ‘Stripping’ of the bitumen by the liquid butane is observed in Figure 3.2.9a and b. In the series of six photographs of the same pores over a time span of two and a half minutes the three phases can be differentiated. The lightest represents a solvent vapour filled pore, the medium is butane condensate mixed with a little bitumen and the darkest is bitumen. The circled areas at 13.90, 17.17, 26.17 and 43.37 seconds show one pore partially filled with bitumen being stripped/washed by solvent flowing in the direction of gravity. The circled areas towards the top right at times 13.90, 17.17 and 2:30.96 illustrate solvent washing away a bitumen-filled pore from above. At time 2:30.96 in the lowest circle, it can be seen that the bitumen in the pores is starting to be stripped-off, when before that, these pores were fully saturated. The draining liquid butane not only strips the bitumen, but it also helps mix the bitumen and solvent. These phenomena are clearly shown in videos taken where the draining condensate has bitumen striations running through it while stripping the pore circled in Figure 3.2.9a (times 13.90, 17.17, 26.17 and 43.37).

The washing/stripping effect is also shown in the single photograph in Figure 3.2.9b, where the bitumen is in direct contact with the butane vapour (no live oil). A perfect vertical interface down the middle of the pore bodies has not been observed previously in normal VAPEX experiments conducted in glass micromodels. The perfect vertical segregation of the phases down the middle of the pore is possible because of the miscible nature of the bitumen and light liquid hydrocarbon solvent. It is possible that this type of interface exists in a normal VAPEX type process but that the difference between the live oil and bitumen cannot be detected due to the opacity of both the live oil and bitumen. It is clearly shown in the bottom circled area of Figure 3.2.9b the difference in interfacial contact between the bitumen and solvent vapour versus the bitumen and liquid condensate. The two pores at the top, one pore in the middle and three at the bottom of the bottom circle show the vertical interface separating the liquid condensate and bitumen. Whereas the two pores above and one pore below the middle pore of the bottom circle show liquid



(bitumen, live oil and/or condensate) in contact with solvent vapour. The shape of the interfaces is curved showing that capillary pressure differences influence the drainage sequence in pores.



**Figure 3.2.9: Stripping of Bitumen by Condensed Solvent – Convective Mass Transfer**

### 3.2.2.3 Asphaltene Precipitation

Figure 3.2.10 shows the comparison of the swept region of VAPEX and warm VAPEX experiments carried out in glass micromodels, respectively. The results from the two micromodels are directly comparable and the experiments were performed in model DL-1. The only difference is that the model and solvent were placed in the same water bath at 25°C to facilitate condensation. The solvent was maintained at 23°C, 2°C lower to operate in non-condensing (VAPEX) mode. The first photograph, in Figure 3.2.10a, shows the swept region of model DL-1 recovered using non-condensing n-butane. The residual oil is trapped in the occasional pore body (as discussed above) and there is no evidence of asphaltene precipitation. Figure 3.2.10b is a photograph of the same model when the butane was allowed to condense for the first half of the experiment. It shows vertical striations of precipitated asphaltenes which only

occurred when the solvent condensed. There is no asphaltene precipitation visible in the pores closer to the bitumen filled pores (on the right) when the solvent did not condense.

One question often pondered but not yet fully explored is the effect of asphaltene precipitation on the vertical permeability associated with the draining live oil. Some researchers believe that asphaltene precipitation will cause reduced vertical permeability and inhibit the drainage and subsequent production of live oil. Even if permeability is somewhat reduced in some pore throats and pore bodies, the overall effect of condensing the solvent will increase the interface advancement and production rates.



a) VAPEx showing no asphaltene precipitation in a glass micromodel



b) Asphaltene precipitation due to butane condensation

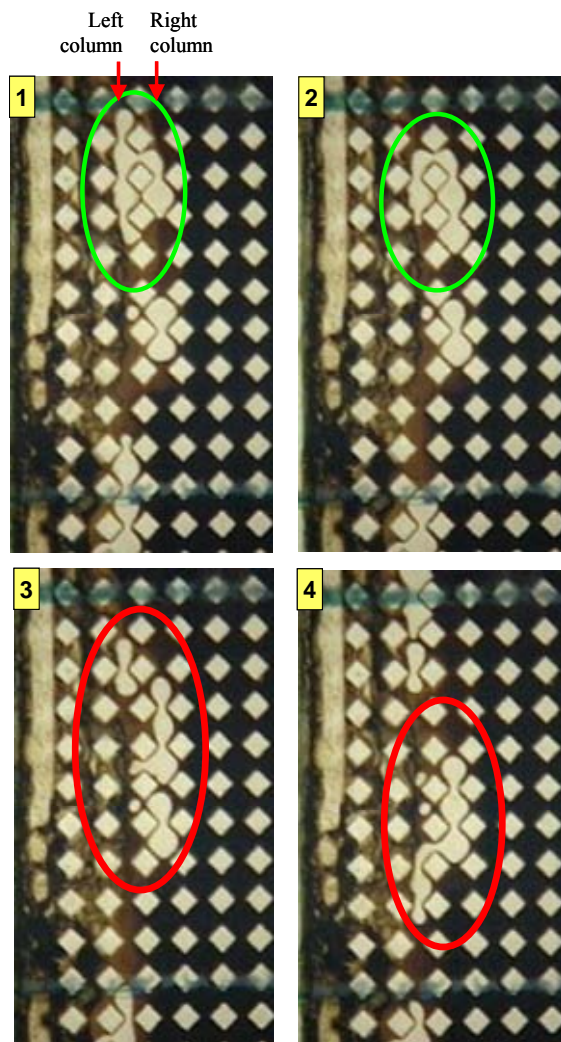
**Figure 3.2.10: Asphaltene Precipitation**

Asphaltenes precipitate once excess solvent is present. When a solvent process is operated below or slightly below the dew point of the solvent, there is generally not enough solvent mixed with the heavy oil to precipitate the asphaltenes where the produced live oil has on the order of 0.30-0.40 mass fraction solvent. When operating a condensing solvent process, the solvent to oil ratios are expected to be as high as 1.5 – 6 (Nenniger and Dunn 2008) and in these conditions, one would certainly anticipate asphaltene precipitation. The concentration profile at the pore scale needs to be addressed with respect to the precipitation of asphaltenes. Figure 3.2.6 shows the solvent-bitumen interface where the solvent vapour is separated from the bitumen by a layer of viscosity reduced “live” oil. From the observations in the pore scale micromodels, the live oil is on the order of one to three pores in width over which a concentration gradient exists, as shown in Figure 3.2.6. At the upper limit, the solvent concentration is one in the case of condensing solvent and the solubility limit in a non-condensing solvent process. Over the width of the live oil, the solvent concentration decreases to zero where the solvent has yet to mix with the pure bitumen. Excess solvent causing asphaltene precipitation is present at the live oil-solvent vapour boundary, i.e. at one side of the mobile live oil.

Drainage at the pore scale around the precipitated asphaltenes is shown in Figure 3.2.11. Butane vapour bubbles being mobilized downwards in the direction of gravity are deformed by the precipitated asphaltenes, as shown in photographs one, two, and four. Photographs one and two show the re-routing of the vapour bubble due to constrictions in the pore throat radius caused by asphaltene precipitation. Photographs three and four also depict the presence of asphaltenes in the “left” column of pores as shown by the deformed vapour bubbles. The vapour bubbles are not deformed in the “right” column of pores where asphaltenes are not yet present. Observations at the pore scale, shown in Figure 3.2.11, confirm that asphaltenes can reduce the permeability forcing the draining live oil to find another drainage pathway but only at the live oil-vapour interface. By the time the asphaltenes precipitate the live oil is already able to drain in the pores adjacent or ahead of the asphaltene deposition.

1. Solvent vapour bubbles are mobilised downwards in the direction of gravity due to the drainage of the live oil and liquid condensate in a glass micromodel porous medium. The bubbles move downwards in primarily two columns of pores, the “left” and “right”. Where indicated, the vapour bubble is not fully filling the pore space due to the presence of asphaltene precipitation.

2. The solvent vapour bubble does not have sufficient force to overcome the increased capillary force due to the reduction in pore throat size from asphaltene precipitation (in the left column of pores). Instead the gas bubble advances further downwards in the “right” column of pores.
3. The solvent bubble attempts to move into the pores to the left but due to the high aspect ratio, it snaps off in Photograph 4.
4. The two solvent vapour bubbles join. The portion of the vapour bubble travelling in the pores with asphaltene precipitation are deformed in their movement past the precipitated asphaltenes in the pore space. As shown in all photos, the bubbles travelling in the “right” column of pores are not deformed and fill the entire pore space.



**Figure 3.2.11: Live Oil Draining Around Precipitated Asphaltenes**

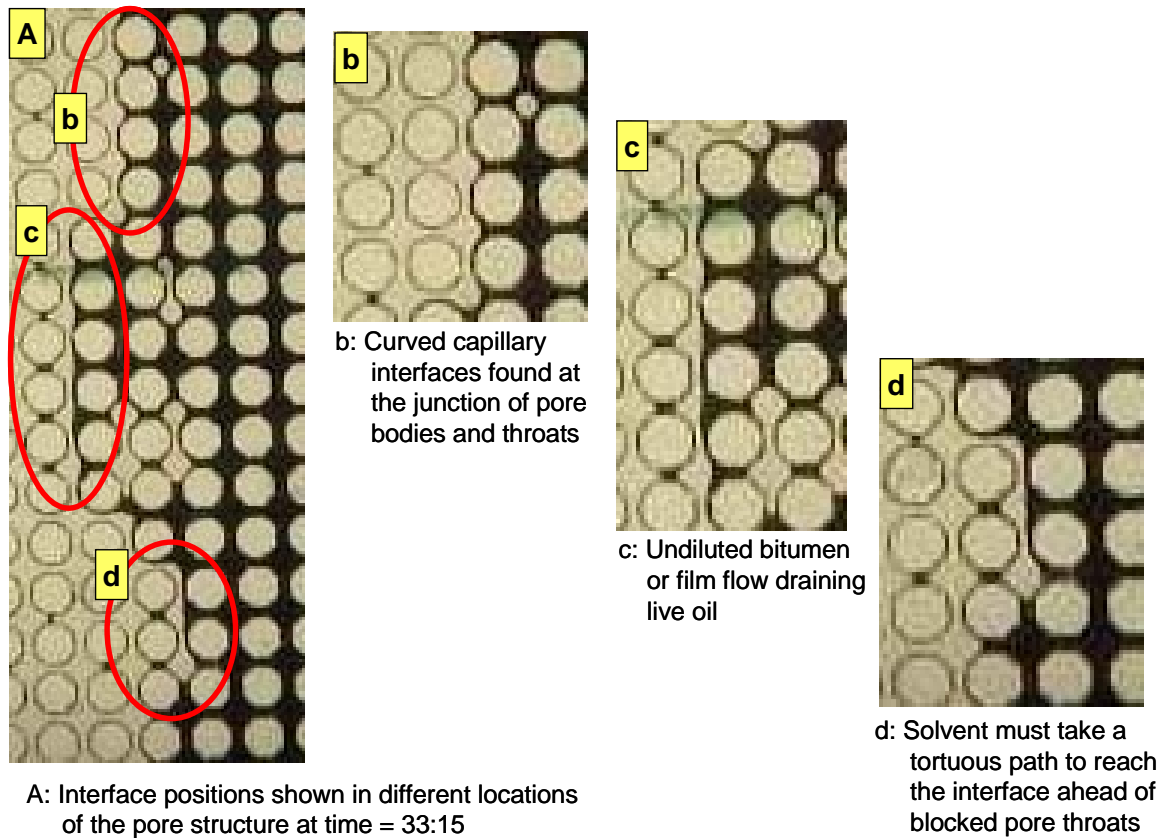
### 3.2.2.4 Drainage Mechanisms and Priority

A series of photographs shown in Figure 3.2.12 - Figure 3.2.17 the draining live oil in a VAPEX process. The photographs are explained in detail and are summarised as follows:

- Live oil drains by both capillary drainage displacement and film flow.
- Vapour-liquid interfaces exist primarily at the junction of pore bodies and throats indicative of the capillary pressure existing across the interface. However, less curved interface, advanced further into the pore body than the junction of the pore throat are observed for two reasons:
  - the interface exists between the solvent and undiluted bitumen, or
  - a film of live oil is draining over the interface dampening the curvature
- Solvent vapour can become trapped as bubbles within the draining live oil. The trapped solvent bubble can remain stationary or be mobilised if viscous and gravity forces are sufficient to overcome the buoyancy and capillary forces present. In either case the solvent vapour bubble can be absorbed into the bitumen/live oil phase.

The series of photographs are taken from video observations of model OC-1 and DC-1 during VAPEX experiments with non-condensing butane as the solvent. The location of the model OC-1 video and photographs were approximately 60 pores from the top of the model and 25 pores in from the well located on the left side of the model. The movie was taken 29 hours after the start of the experiment and is located on the tape at 28 minutes, 53 seconds. The photographs of pore scale events in model DC-1 in Figure 3.2.14 were taken at 17 hours and 10 minutes into the experiment at tape time 11:03. The video captured 90-110 pores down from the top and 53-70 pores in from the well located on the right side. The series of photographs of model DC-1 shown in Figure 3.2.15 through Figure 3.2.17 were taken near the start of the experiment at 3 hours 14 minutes at tape time 2:03 – 5:41 showing 121-140 pores from the top and only 4-6 pores in from the well on the right. The photographs of the video are referenced using the video clip time such that the first photograph is at time 33:15 indicating 33 seconds after the start of the video clip. The film time is noted for referencing, for physical understanding of the time scale, and to be able to calculate velocities of pore scale events.

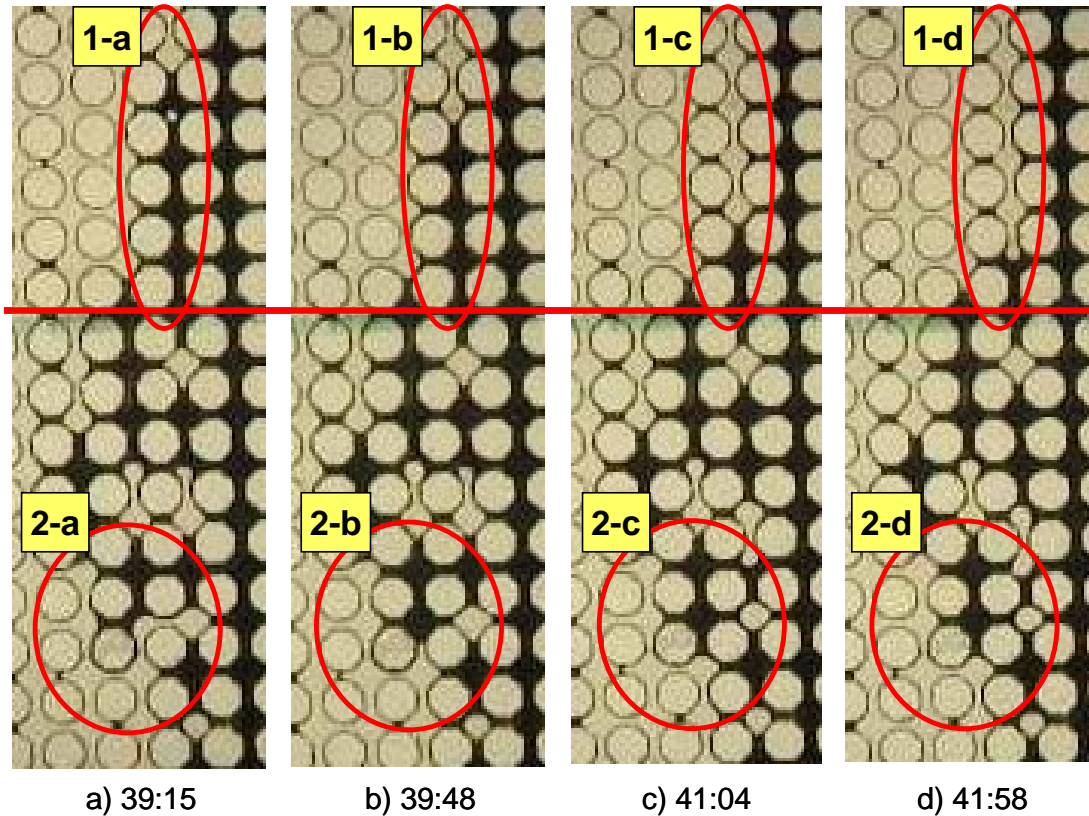
## Interface Positions



**Figure 3.2.12: Interface Positions during VAPEX Drainage in Model OC-1**

Figure 3.2.12 shows the first image of the series at time = 33:15 where the VAPEX interface is physically located in different parts of the pore structure. The first photograph in Figure 3.2.12A is an overview showing the general location of the details exploded in images b, c and d. Figure 3.2.12b shows curved capillary interface found at the junction of pore bodies and throats. Figure 3.2.12c shows that the VAPEX interface is not only found at the junction of pore bodies and throats. Here, it is observed that the oil phase is thicker around the solid particles to the right of butane filled pore bodies. This phenomenon can occur when the oil has not yet been diluted by solvent or when the live oil (diluted oil) drains in films creating the appearance of a thicker non-curved interface. Figure 3.2.12d shows that the interface is in front of a peak of oil filled throats which is joined to the rest of the vapour phase by the uppermost throat. A tortuous pathway is created through which the solvent must diffuse in order to reach the interface. This is especially relevant if an inert or non-condensable gas is present, as discussed in section 3.3.

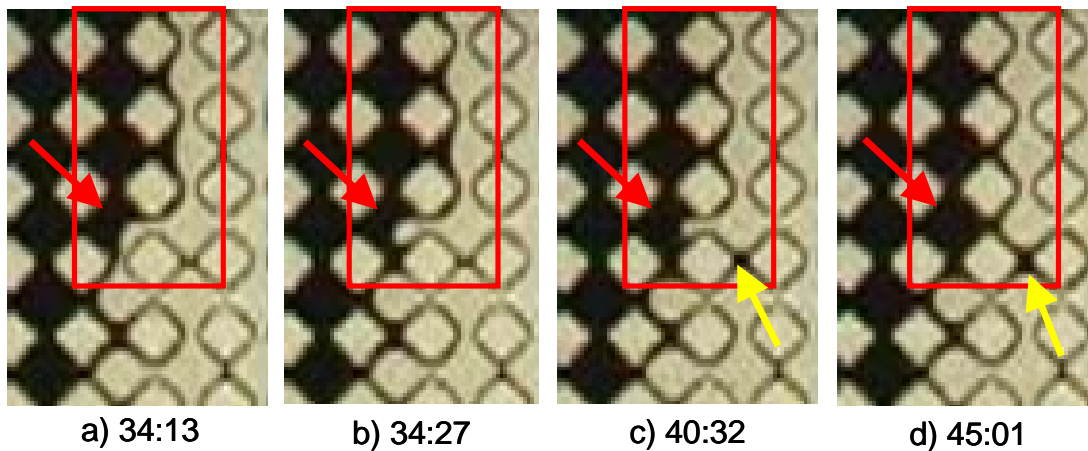
### Live Oil Drainage at the Interface



**Figure 3.2.13: Live Oil Drainage at the Interface of Model OC-1**

Live oil drainage is shown in the series of photographs in Figure 3.2.13. The focus of the first series (1-a through 1-d) shows drainage displacement mechanisms where the butane vapour invades the live oil filled pores. Drainage occurs when the non-wetting phase (butane) displaces wetting phase (live oil). Focus area 1-b shows that the butane has invaded one pore lower compared to focus area 1-a resulting in the trapped butane bubble visible in 1-a being reconnected with the continuous gas phase (solvent chamber). In the 2 minutes and 10 seconds elapsed from 1-c to 1-d, the butane vapour invaded two pores and was starting to invade the third pore located above the reference line. It is also interesting to note the position of the bitumen interface where it is located at the junction of the butane filled pore body and bitumen filled pore throat in focus areas 1-a through 1-c. This position is the equilibrium position where it requires a destabilisation of forces to overcome the capillary pressure and advance the butane into the next pore. Figure 3.2.13 focus area 1-d shows the butane – live oil interface moving through the pore throat into the next pore. This is a dynamic interface position due to the capillary instability and the interface will not stay there but establish itself in the pore body – pore throat junction like in focus areas 1-a through 1-c.

Although it is difficult to see in the series of photographs captured from the video, an important point to note is that as the live oil is draining from pores in one area, another area below is affected by the movement. The consequence of the drainage displacement occurring in the pores depicted in focus areas 1-a through 1-d is live oil draining by film flow occurring further down in focus areas 2-a to 2-d. In focus area 2-a there is partially filled pore in the centre with bitumen filling the upper left portion of the pore. This pore is filled in focus area 2-b from the film draining around the left side of the particles to the left of the centre pore. The result of the film flow drainage is that a one pore butane bubble becomes trapped (just to the right of the central pore in focus area 2-b). Drainage displacement mechanisms do not happen uniformly over the length of the live oil interface. Capillary drainage in one area can result in film flow in another area and vice versa.

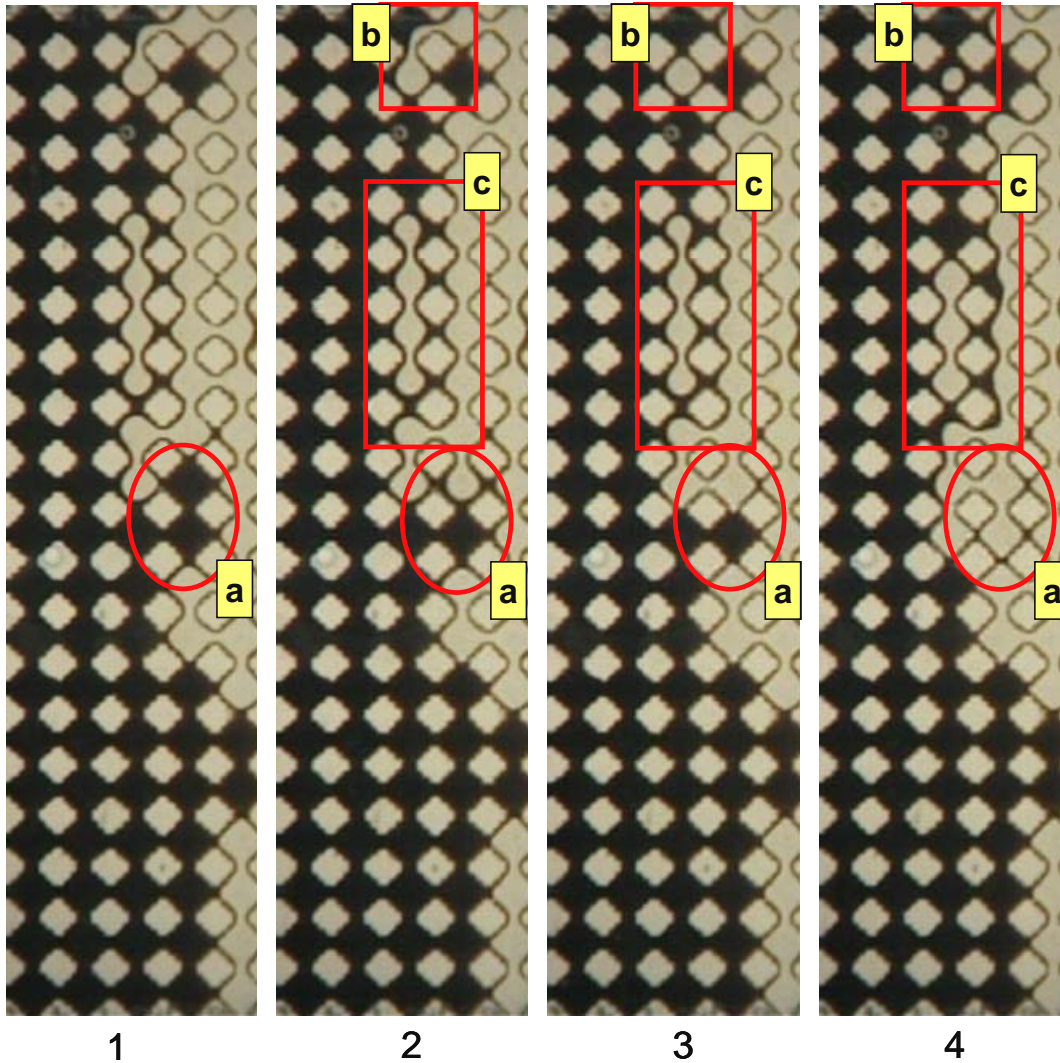


**Figure 3.2.14: Live Oil Drainage at the Interface of Model DC-1**

Figure 3.2.14 shows live oil draining by film flow in model DC-1. Note the thickness of the live oil at the vertical interface of the top two pores shown in the focus area. The film is the same thickness in Figure 3.2.14a and c but the pore pointed out by the downward facing (red) arrow is being filled with live oil from photograph a to c. In Figure 3.2.14d the pore is completely filled and the film thickness has decreased in the focus area. The consequence of the draining live oil was to fill the pore as well as the pore throat located at the bottom left of the focus area pointed out by the upward facing arrow (yellow).

Momentum transport at the pore scale does not happen in only one vertical column of pores. The interface can vary by a few pores. Observations show that oil filled pores protruding irregularly into the solvent chamber (the oil filled pores above focus area 2 in Figure 3.2.13) contain mobile live oil and not high viscosity raw bitumen.

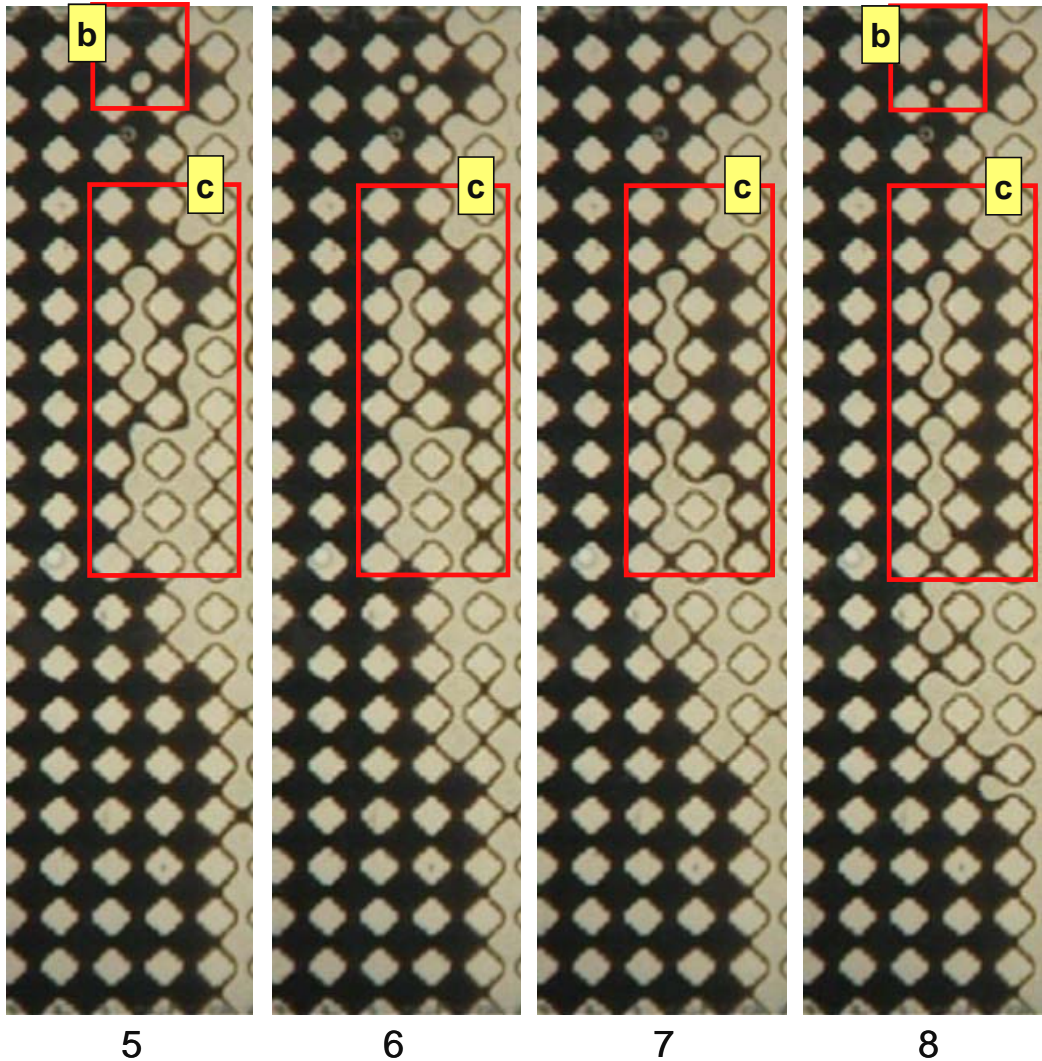




**Figure 3.2.15: Model DC-1 Bubble Formation during Live Oil Drainage 1/3 (series 7-1)**

The sequence of photos in Figure 3.2.15 show several pore scale events:

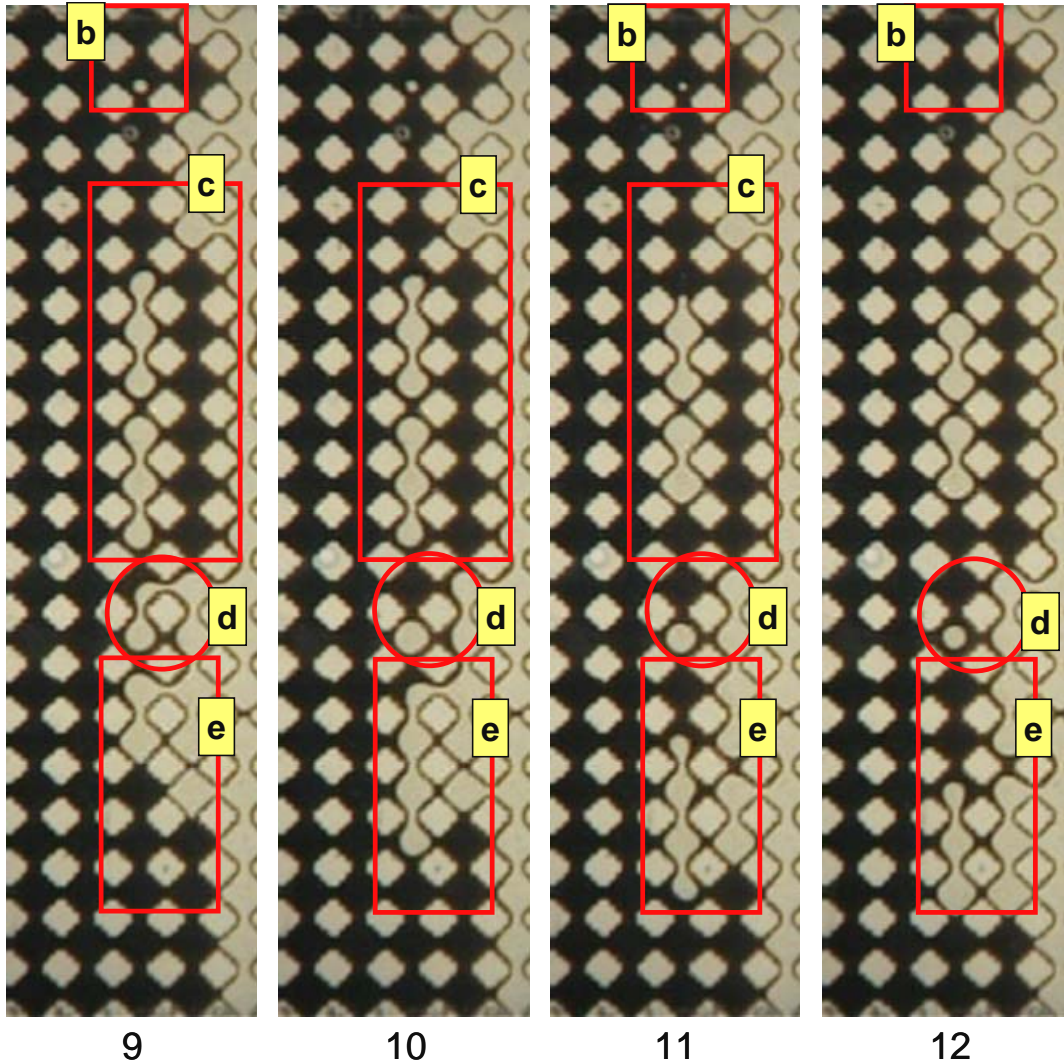
- a. The focus area (a) shows two pores initially filled with live oil in area (1-a). Areas (2-a) and (3-a) show the butane vapour draining the live oil from the top pore. In focus area (4-a) the bottom pore has also drained by drainage displacement.
- b. Focus area (b) shows the creation of a single pore butane bubble by film drainage in areas (2-b) and (3-b). The bubble is smaller in (4-b) due to diffusion into the oil.
- c. Focus area (c) shows the four pore bubble becoming a three pore bubble in (4-c) as well as film drainage on the oil filled throats to the right of the four pore bubble. Note the position of the oil-vapour interfaces on the right side of the horizontally oriented throats from (2-c) to (4-c).



**Figure 3.2.16: Model DC-1 Bubble Formation during Live Oil Drainage 2/3 (series 7-1)**

The sequence of photos in Figure 3.2.16 show several pore scale events:

- b. Focus area (b) in (5-b) and (8-b) shows the decreasing size of the original one pore bubble due to the mass transfer of the butane into the live oil phase.
- c. Focus area (c) shows the creation of a column of live oil filled pores to the right of the three pore bubble. Previously these pores were part of the solvent chamber and filled with butane as discussed and shown as part of Figure 3.2.15. Area (8-c) shows the result of gravity induced flow in the live oil filled pores. A second three pore bubble below the other three pore bubble is created.



**Figure 3.2.17: Model DC-1 Bubble Formation during Live Oil Drainage 3/3 (series 7-1)**

The sequence of photos in Figure 3.2.17 show several pore scale events:

- b. Focus area (b) continues to show the disappearance of the one pore bubble. It has been completely engulfed by the live oil in (12-d).
- c. Focus area (c) shows the two three pore bubbles being deformed into two pore bubbles in (11-c). The two pore bubbles shown in (8-c) have slightly larger diameters than their previous three pore versions.
- d. Focus area (9-d) shows the creation of another single pore bubble by film flow. Subsequently, it decreases in radius throughout (10-d), (11-d) and (12-d).
- e. In focus areas (9-e) and (10-e) movement downwards is observed by drainage displacement where vapour invades the two of the three bitumen filled pores on the bottom left. Film flow also occurs at the intersection of focus areas (10-d) and (10-e)

Again, a butane bubble is shown being trapped beneath the draining live oil in (10-e) and (11-e). Bubble mobilisation occurs by both drainage and imbibition. The head of the vapour bubble advances by drainage and the tail undergoes imbibition, as shown during the downward movement in (11-e) and (12-e).

In summary, one consequence of the draining live oil is that butane vapour can become trapped beneath the interface as shown in Figure 3.2.13 and Figure 3.2.15 through Figure 3.2.17. The trapped butane bubbles either remain stationary or are mobilised downwards in the direction of live oil drainage. During either event, the butane bubble can decrease in size due to mass transfer of the butane from the vapour to the oil phase by diffusion and convective mass transfer and/or be reconnected with the vapour phase and/or coalesce with other trapped butane bubbles if one or the other moves. The trapped vapour phase tends to remain stationary if the live oil velocity can not overcome the buoyancy forces of the bubble.

### 3.2.2.5 Depth of the Draining Live Oil

As just described in detail and shown through pore scale observations, the depth of the mobile live oil is not uniform over the length of solvent-bitumen interface, nor does it move uniformly. Locally, the interface can undulate one to three pores where in one area the already swept pores can become again filled with live oil and in other areas the live oil – solvent interface is more advanced. The difficulty is in differentiating between the live oil and the bitumen to determine the actual depth of the mobile live oil.

Mathematically, the depth of the mobile live oil can be calculated. However, a note of caution should be added that the calculated depth of mobile live oil would be an average only. Using an elemental mass/volumetric balance to equate the rate of linear advancement with the vertical drainage, the average depth of mobile live oil can be estimated. Experimentally, the pore velocity in the x-direction,  $U_p^x$ , is known and can be related to the Darcy velocity in the z-direction. Referring to Figure 3.2.18, the mass transfer and interface velocity moves in the x-direction perpendicular to area,  $A_{yz}$ . The live oil drains in the z-direction through area  $A_{xy}$ .

The volumetric flow rate of bitumen in the x-direction is related to the pore velocity  $U_p^x$ , the area  $A_{yz}$ , the porosity and the change in saturation  $\Delta S$ .

$$Q_b^x = U_p^x \phi A_{yz} \Delta S \quad (3.2.10)$$

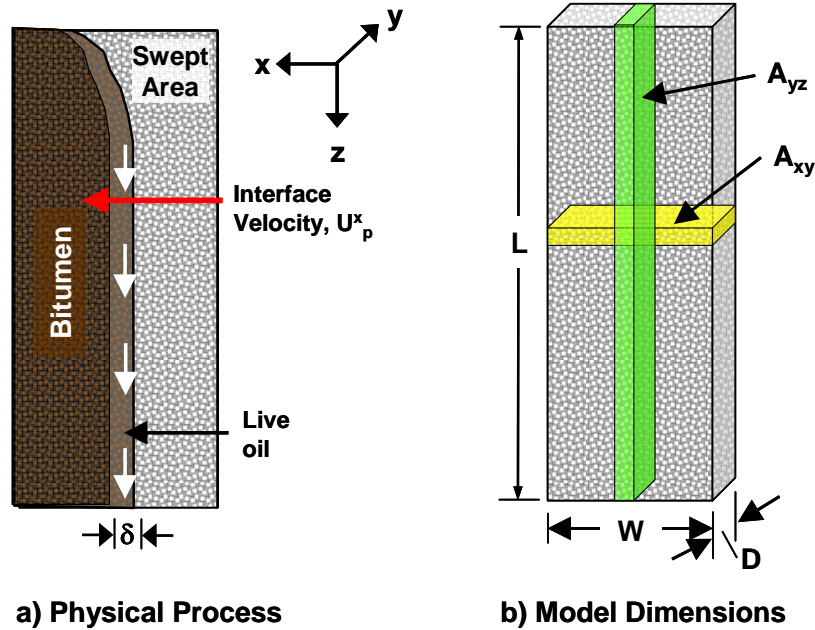
Darcy's law (equation 3.3.5) for the bitumen is given in the following equation.

$$Q_b^z = A_{xy} \frac{k \Delta \rho_{lo} g \sin \theta}{\mu_{lo}} (1 - v_s) \quad (3.2.11)$$

$\Delta \rho_{lo}$  is the difference in live oil density and butane vapour,  $k$  is the permeability,  $g$  is the gravitational constant,  $\phi$  is the dip angle,  $\mu_{lo}$  is the live oil viscosity and  $v_s$  is the volume fraction of solvent in the live oil. The physical and fluid properties used are shown in Table 3.2.1.

Therefore, the depth of the mobile bitumen can be estimated as:

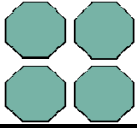
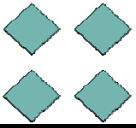
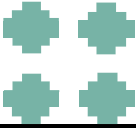
$$\delta_{film} = \frac{U_p^x \phi L_{model} \Delta S \mu_{lo}}{k \Delta \rho_{lo} g \sin \theta (1 - v_s)} \quad (3.2.12)$$



**Figure 3.2.18: Solvent Extraction in Two-Dimensional Models**

Using the relationship shown in equation 3.3.12, the depth of the draining bitumen and live oil can be found for the experimentally determined VAPEX interface velocities for the experiments conducted in the micromodels. The dip angle ( $\phi$ ) is assumed to be  $90^\circ$  and the change in saturation is assumed to be one with no residual oil. The viscosity is taken as 5 mPa.s, an average of results from previous experiments (James 2003; Oduntan 2001). The live oil was assumed to contain 0.30 mass fraction (0.425 volume fraction) solvent and the live oil density was determined using ideal mixing. The results of the calculations are shown in the following table.

**Table 3.2.4: Estimated Average Depth of the Draining Live Oil and Bitumen**

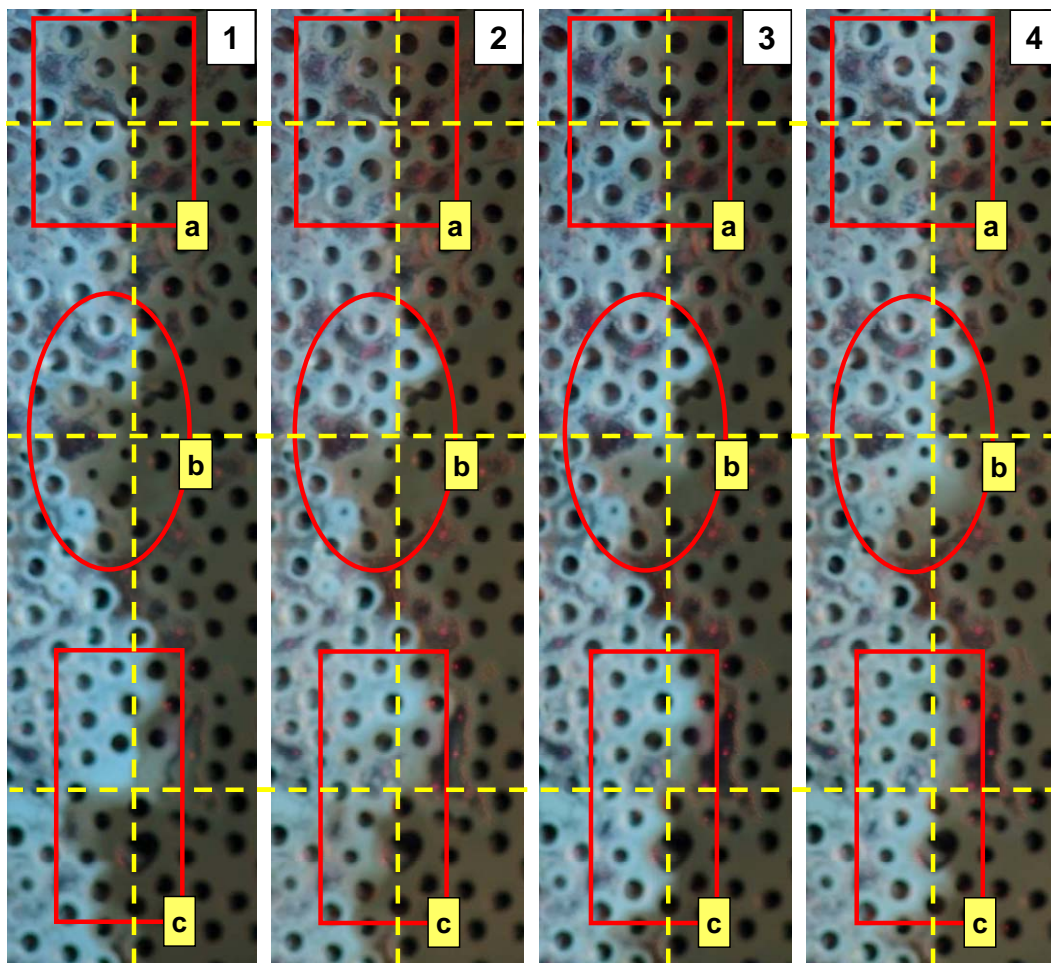
Micromodel Patterns	OC-1	DL-1	DC-1
			
<b>Summary of Dimensions</b>			
Pore to pore distance (mm)	2.04	2.04	1.60
Model length (cm)	30.4	30.4	30.4
Permeability (Darcy)	129	292	91
Porosity	0.42	0.28	0.36
Interface Velocity (pores/hr)	0.62	0.63	1.21
<b>Depth of the Mobile Phase</b>			
<b>Bitumen</b>			
(mm)	0.38	0.11	0.71
(pores)	0.28	0.05	0.54
<b>Live Oil</b>			
(mm)	0.66	0.19	1.24
(pores)	0.48	0.10	0.94

The results estimate that on average the depth of the mobile bitumen and live oil is less than one pore. This, of course, assumes that the mobile oil flows continuously and that the depth of the draining oil is of constant thickness. The prediction that the live oil only flows in one pore was inferred from VAPEX experiments using glass etched micromodels that were only one pore wide with film flow along two corners at most. In reality, the porous network is three-dimensional, where the piston-like drainage would probably still occur in one to two pores but the affect of film flow drainage is not adequately represented by the micromodel. There would be more than two corners, more likely four to six, depending on the pore shape that affect the film flow in three-dimensional porous networks.

Qualitatively, preliminary success has been achieved in visualising the depth of mobile live oil in consolidated and unconsolidated porous media using long wave UV light and a liquid solvent (Varsol®) spiked with an oil soluble florescent agent. This enabled the differentiation of pure solvent, live oil and pure bitumen as shown in Figure 3.2.19. The light blue area to the left is Varsol® with florescence, the brown to the right is bitumen, and the lighter brown colour highlighted in the focus area (a), (b), and (c) is the mobile live oil.

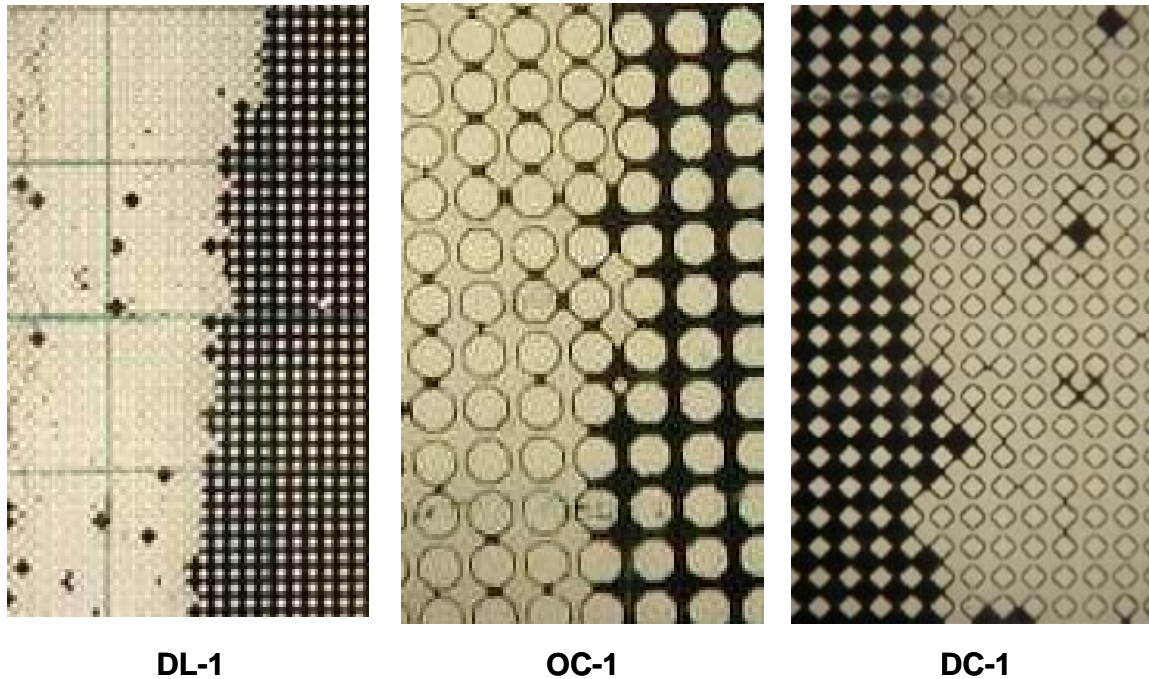
- a. Focus area (a) shows the mobile live oil initially in the upper left quadrant and over the four photographs it moves downward so that even the upper right quadrant is filled with solvent. The depth of the live oil that was mobilised was just over two pores.
- b. Focus area (b) shows movement of the three live oil filled pores that are originally located the left of the centre. Towards the top of the oval, to the right of the centre line, live oil is mobilised through one pore.
- c. The bottom left quadrant shows two pore-widths of live oil saturated pores in (1-c) that become filled with solvent in (4-c).

Observations shown in Figure 3.2.19 confirm the behaviour observed in the etched glass micromodels whereby the live oil does not drain in a continuous film but by capillary displacement mechanisms and film flow. The observations can also allow us to conclude that on average estimates of the depth of mobile live oil should not exceed one pore.



**Figure 3.2.19: Depth of Mobile Live Oil in Consolidated Media using Florescence**

### 3.2.2.6 Residual Oil



**Figure 3.2.20: Residual Oil Trapped in Extracted Parts of Models with Non-Condensing Solvent (VAPEX)**

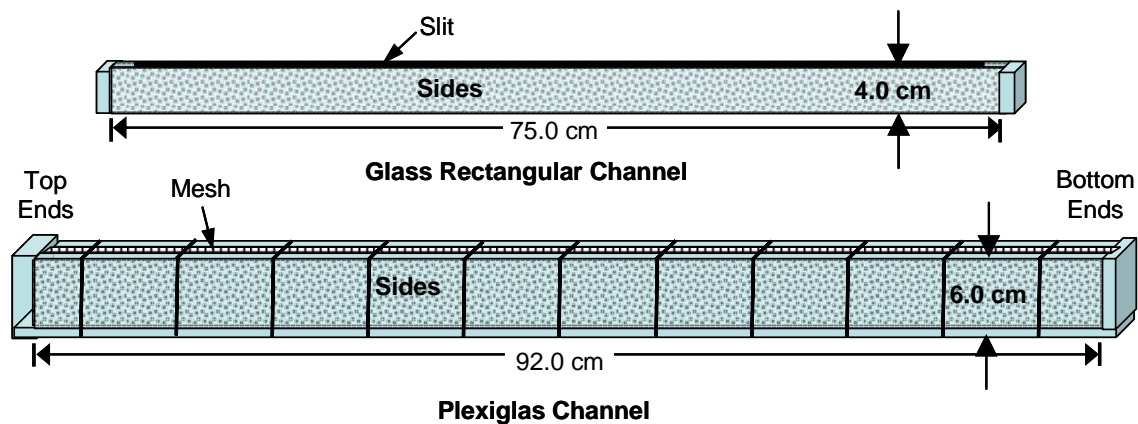
Figure 3.2.20 shows that the residual trapped oil was affected by the pore structure. Models DC-1 and DL-1, both with diamond shaped particles have shorter pore throat lengths compared to model OC-1. It is shown that the residual oil phase for models DL-1 and DC-1 was found primarily in pore bodies sporadically throughout the model. The residual saturation for the swept portion of model DL-1 was approximately 3.6%, depicted by the black, single pores filled with oil. The residual oil in model OC-1 was held preferentially in horizontally oriented pore throats, those found between vertically oriented particles or between two horizontally oriented pore bodies. In the field, the pore size distribution is not uniform and the pore throat lengths would be approximately equal to the particle size. Similar trapping could be envisioned in the field where residual oil would be found in some horizontally oriented pore throats and in pore bodies surrounded by pore throats with smaller diameters. Minimal trapping of residual oil from solvent based heavy oil recovery is a definite advantage. Results from laboratory scale VAPEX experiments indicate a residual oil of less than 10% is found (Oduntan 2001; Ramakrishnan 2002; James 2003; Friedrich 2006). Trapped residual oil is not observed in the glass micromodels when the solvent condenses due to the miscibility of the liquid solvent in bitumen, however asphaltenes do precipitate, as shown in Figure 3.2.10.



### 3.3 Effect of Non-Condensable Gas on VAPEX

The presence of a non-condensable should theoretically have a negative impact on production rates for solvent aided enhanced oil recovery processes. A non-condensable gas creates a diffusion boundary layer through which the solvent molecules must first diffuse to reach the bitumen interface. The partial pressure of the solvent is reduced with the presence of another gas phase thereby reducing the interfacial concentration (i.e. solubility) at the bitumen interface. The effect of different partial pressures of CO<sub>2</sub> and CH<sub>4</sub> was eluded to in a conference paper by Talbi and Maini (2004) and summarised in Table 2.2.1. Although the negative effect was difficult to decipher, production rates were shown to decrease with an increased partial pressure of either carbon dioxide or methane. The goal of this work was to perform a simple experiment to exemplify the detrimental effect of non-condensable gas on the VAPEX process.

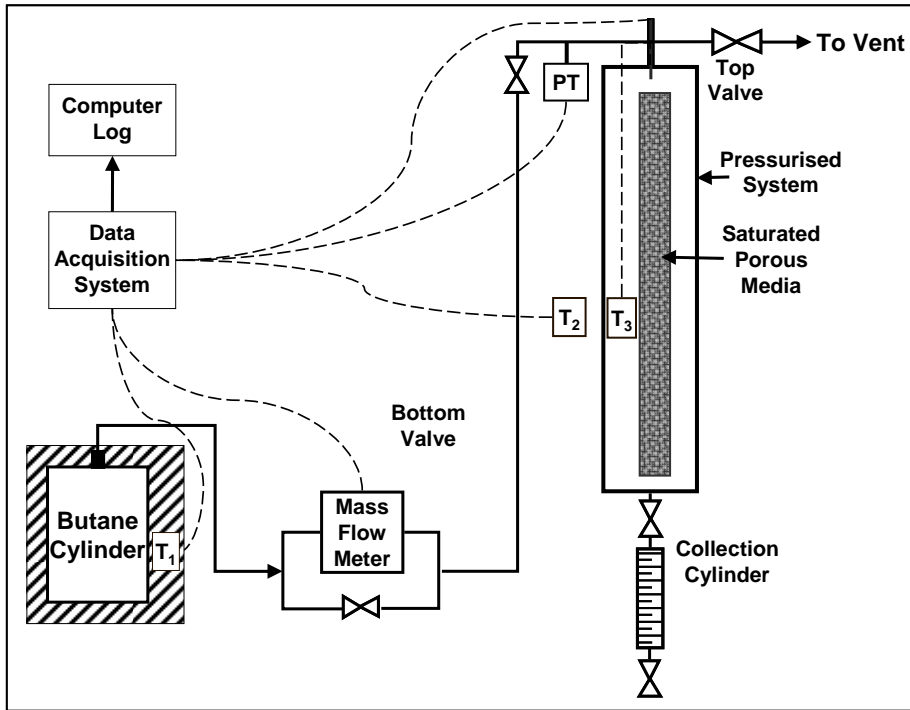
#### 3.3.1 Experimental Procedure using Unconsolidated Glass Beads



**Figure 3.3.1: Plexiglas Channels used for holding Unconsolidated Glass Beads**

The experimental procedure followed the same methodology used by James (2003) for investigating the rate of VAPEX interface advancement in unconsolidated media. Laboratory scale models consisting of fabricated Plexiglas® channels filled with oil saturated unconsolidated glass beads (shown in Figure 3.3.1) were housed in a pressurised system shown in Figure 3.3.2. Athabasca bitumen was used with a viscosity of 225,000 mPa.s and a density of 1.001 g/cm<sup>3</sup> at 22°C. The channels were saturated by placing them on their sides with the slit side facing up in a warm water bath at approximately 50-60°C. Approximately 1 cm depth of hot heavy oil (70-80°C) was poured into the channels. A layer of approximately 2-3 cm of 20-30 US mesh (0.5944 – 0.8407 mm diameter) glass beads heated to the same temperature was then evenly distributed over the heavy oil. The glass beads were allowed to gravity settle and more beads were added to

any under-saturated sections (visible by oil pooling above the beads) until unsaturated glass beads were left on the surface. The loose beads were then shaken out and the process repeated until the channel was filled. A wire mesh screen was then secured in place over the slit to prevent the formation from failing during the experiment.



**Figure 3.3.2: Experimental Set-up for Examining the Effect of Non-Condensable Gas**

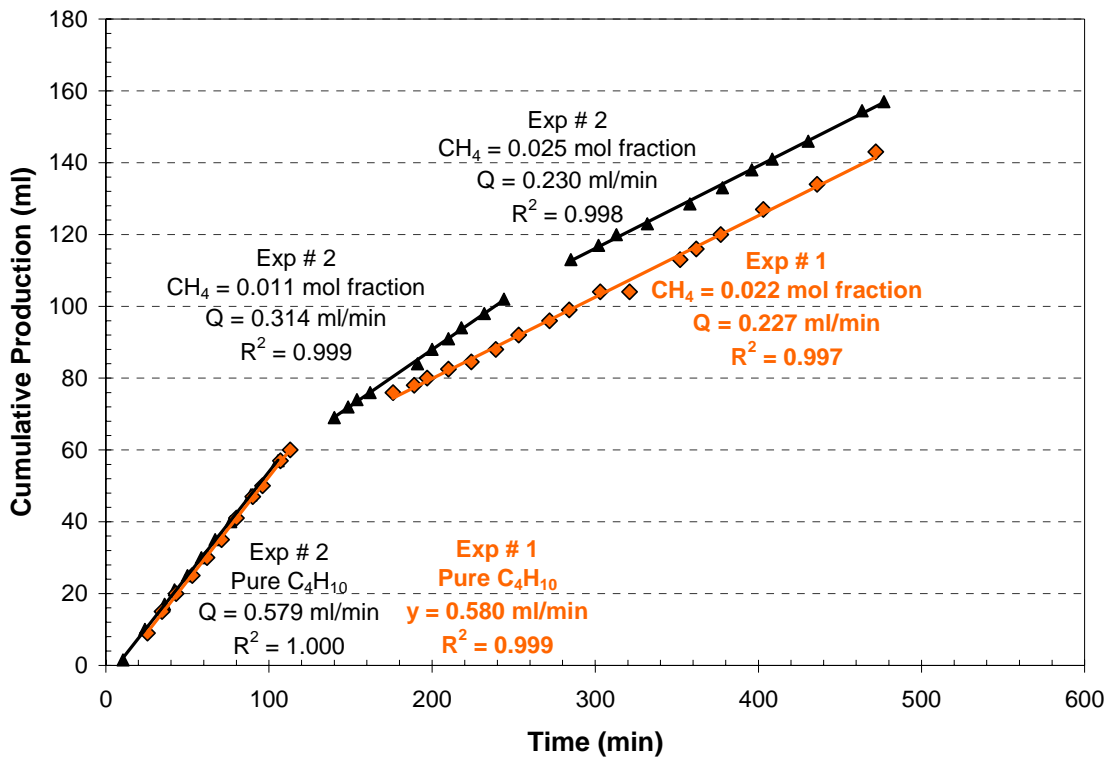
The experimental set-up shown in Figure 3.3.2 consists of a pressurised system made of a 8.89 cm (3.5" diameter) 1m long Plexiglas® tubing sealed at both ends and fit with a 0.635 cm (1/4" ) tube fitting at the bottom and a 1.27 cm (1/2") tube fitting at the top. The bottom is connected via a 2-way valve to a collection cylinder to measure the live oil produced with time. The butane cylinder, housed in a water bath, is connected via a mass flow meter to the top of the pressurised system where a pressure transducer measured the system pressure. The water bath, ambient, and system temperatures were measured using three T-type thermocouples. A data acquisition system recorded the temperature, pressure and butane flow rate.

The experiment was started by placing the saturated porous medium in the system housing and flushing the entire system with butane. The butane was connected to the bottom and flushed upwards in a gravity stable direction for 10 minutes. The butane was then reconnected to the top and the system pressurised to start the experiment. The goal of the experiment was to investigate the effect of non-condensable gas on VAPEX so the butane was kept 1-2°C lower than ambient to

ensure that it did not condense. Once steady state production was well established methane was added to the system. The system pressure was first decreased and then incrementally re-pressurised using methane. The system pressure was established again by re-connecting the butane. The concentration of methane in the system was calculated using the ideal gas law knowing the pressure difference and the void volume of the system and connected tubing.

### 3.3.2 Results and Discussion

The VAPEX experiment with the introduction of methane was repeated for consistency and the results are shown in Figure 3.3.3. The average butane and system temperatures for experiment #1 were 23.5 and 25.1°C respectively and 23.5 and 24.8°C for experiment #2. The average system pressure was 134.4 kPa (19.5 psig) for both experiments except during the methane addition. The temperature and pressure profiles are shown in Appendix B.



**Figure 3.3.3: Live Oil Production Rates with Methane Present**

Figure 3.3.3 demonstrates the effect of adding a small amount of methane to the system. Two experiments were performed with initial production rates of 0.580 and 0.579 cm<sup>3</sup>/min using pure butane at vapour pressures of 34.2 and 34.3 psia respectively. Once steady state production was established, the system pressure was decreased and methane was added to the solvent chamber.

The production rates dropped from 0.580 cm<sup>3</sup>/min to 0.227 cm<sup>3</sup>/min in experiment #1 when 2.2 mole % methane was present and in experiment #2 from 0.579 cm<sup>3</sup>/min to 0.230 cm<sup>3</sup>/min when 2.5 mole % methane was present. This constitutes a 61 and 60% decrease in production with the addition of only 2.2 - 2.5 mole % methane. This simple experiment shows very clearly the effect of solution gas on a VAPEX process.

The effect of non-condensable gas either as solution gas or added to the solvent upon injection would substantially decrease the effectiveness and efficiency of solvent extraction recovery. If propane was used as a solvent, whose vapour pressure at room temperature is around 850 kPa, the effect may be somewhat lessened by higher system pressure. The solubility of the solvent and methane would increase with increasing pressure yet the diffusion coefficient decreases with increasing pressure. However, the overall concentration would increase with increasing pressure thus increasing the driving force. Also, the two commonly proposed gases are methane and carbon dioxide, both of whose solubility increases slightly with increasing reservoir pressure. Nonetheless, solvent extraction production rates would be lessened in the presence of a non-condensable gas compared to using a pure solvent. The non-condensable gas would inhibit the mass transfer of solvent into the bitumen by two mechanisms. Firstly, due to the reduction of partial pressure from unity in the case of pure solvent to less than one when a non-condensable gas is present the solubility at the bitumen-solvent interface decreases. Secondly, the non-condensable gas in the solvent vapour chamber creates a mixture of gas molecules through which the injected solvent must first diffuse in order to reach the bitumen-solvent interface. The results of this simple experiment confirm the negative impact on production rates when a non-condensable gas is present. All efforts should be made to prevent the build-up of solution gas in the solvent chamber in any field operation. Based on these results, a non-condensable gas injected with the solvent would decrease the recovery efficiency of the heavy oil significantly.

## Chapter 4: One Dimensional Diffusion of n-Butane in Heavy Oil

In the late 1970s (Dunn *et al.* 1978) and again in the late 1980s (Butler and Mokrys 1989) the idea of producing Canada's heavy oil using solvent dilution was introduced. From these first ideas the enhanced oil recovery processes known as N-Solv and VAPEX were founded. There have been many permutations and computations of solvent aided recovery processes since then but some fundamental questions remain unsolved in trying to mathematically describe solvent aided recovery. Measuring the diffusivity of light hydrocarbon solvents in heavy oil has been of great interest. Butler and Mokrys (1991) and Das (1995) concluded that a much higher diffusion coefficient than estimated by theoretical predictions was required to match production rates from laboratory scale VAPEX experiments. Diffusivity of light hydrocarbon solvents in heavy oil research began in the mid to late 1990s and continues today exploring different techniques of measuring the diffusivity and refining over-simplified assumptions that were used initially by other researchers.

The one-dimensional diffusion work presented here is a culmination of several years work dating back to 2003 when the first preliminary diffusion experiments were performed. Contributions to the area of light hydrocarbon diffusion into heavy oil/bitumen include:

- The design and perfection of a simple one dimensional diffusion experiment to measure and independently validate the uptake of n-butane into bitumen and the swelling of the bitumen phase in time.
- An improved mathematical description of the diffusion of n-butane into heavy oil from first principles, without oversimplified assumptions. This was accomplished by considering:
  - the diffusivity and density are functions of the solvent concentration and cannot be assumed constant, and
  - the solvent concentration was assumed to be a function of position and time and numerically calculated.
- Determination that the concentration dependent molecular diffusivity of n-butane in heavy oil is a linear function of concentration.
- Validation of the mathematical model with experimental results.

Both the experimental and the numerical approach utilised are enlightening in their simplicity. The gravity stable one-dimensional diffusion experiment captures the swelling of the bitumen in time as butane vapour diffuses into it. The constant pressure solvent vapour is supplied from a leg of liquid butane which decreases in time. Mathematically, the partial differential equations

for the bitumen phase are derived from first principles: an overall mass balance, a mass balance on the solvent in the bitumen phase and an expression derived for the average velocity. A front fixing method first proposed by Landau (1950) simplifies the moving boundary problem by making the spatial coordinates dimensionless. The system of equations containing concentration dependent partial derivatives for the diffusivity and density are solved for using the method of lines implemented in Matlab (7.6.0). There are only two assumptions: 1) that the interfacial concentration is at thermodynamic equilibrium (solubility limit) and 2) the form of the diffusivity function is guessed. The diffusivity coefficient values were determined by using the least squares non-linear optimisation toolbox functionality in Matlab, where the objective function minimises the difference between the experimentally observed and the numerically predicted increase in bitumen height. The model was independently validated through the comparison of the predicted and experimental decrease in solvent height.

## **4.1 Literature**

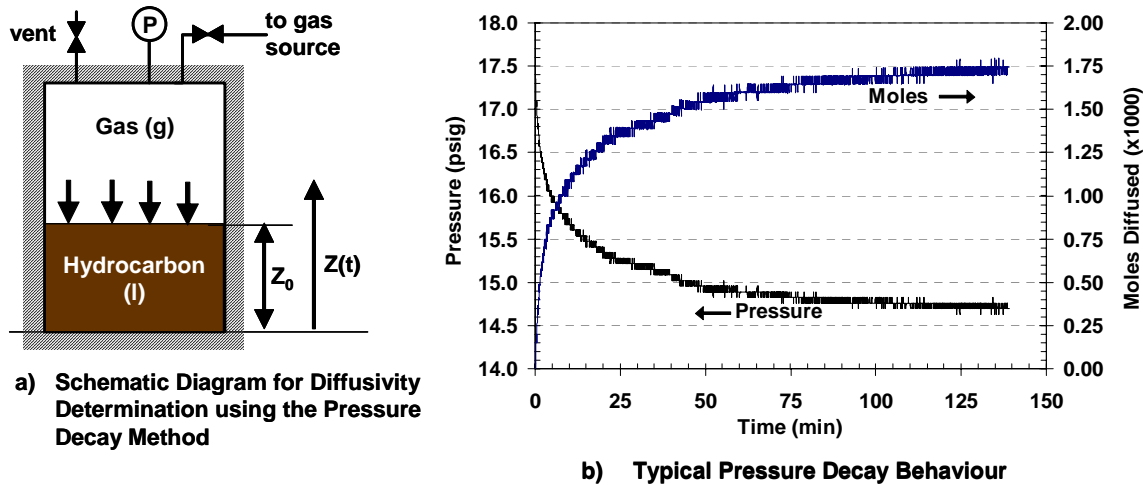
The overall understanding of experimental limitations and physical model assumptions for gas diffusion into bitumen has advanced quite significantly since the early pressure decay experiments and constant diffusivity models (Riazi 1996, Zhang *et al.* 2000, Upreti and Mehrotra 2002, Tharanivasan *et al.* 2006). The diffusion of a light hydrocarbon solvent into a heavy oil or bitumen is complex. The key findings include:

- The solubility of light hydrocarbons is sufficiently high so that assumptions for dilute conditions are invalid.
- The high solubility of the light hydrocarbon in heavy causes the bitumen phase to swell in time so that swelling of the oil cannot be ignored.
- The solubility of the light hydrocarbon in the heavy oil is proportional to the partial pressure of the solvent in the gas phase and the overall system pressure.
- The viscosity of the oil phase decreases exponentially when mixed with a light hydrocarbon solvent.
- There are large density gradients between the light solvent and the dense heavy oil.
- Experimental techniques are inhibited due to the opacity of the bitumen and the volatility of the light hydrocarbon solvents (that are of most interest to the recovery of heavy oil due to their thermodynamic behaviour at reservoir conditions).

### **4.1.1 Pressure Decay Methods**

The pressure decay method used for determining the diffusion of gases into heavy oil has been most recently employed in the studies by Upreti and Mehrotra (2002), Zhang *et al.* (2000) and

Riazi (1996). Experimentally, at time zero, the gas (A) is introduced into the constant temperature, constant volume chamber already containing the liquid hydrocarbon (B), as shown in Figure 4.1.1. The system pressure (P) is measured and decreases with time as component A diffuses into component B. The experimental technique has merit due to its simplicity. However, the mathematical development required to capture the pressure and composition dependent diffusivity as well as the changing interfacial concentration is at best very complex and has yet to be captured properly.



**Figure 4.1.1: Schematic Diagram of the Pressure Decay Method for Determining Diffusivities**

As the gas diffuses into the hydrocarbon, the hydrocarbon phase swells and the overall height ( $z$ ) increases with time. Zhang *et al.* (2000) assumed that the height was constant with time. Depending on the time period in question and the overall mass flux ( $\text{g}/\text{cm}^2 \cdot \text{s}$ ) this may or may not be true. The solubility of a gas in a liquid is a strong function of pressure and temperature. Temperature and solubility are inversely related while the solubility of a gas in a liquid increases with increasing pressure. The mass transfer model used to find the diffusivity must reflect the changing gas concentration at the interface while the pressure decreases in time.

Riazi (1996) also used the pressure decay method and the evaluation of the interface position to better predict the concentration dependent diffusivity of methane (g) into pentane (l). In the model development it is assumed that equilibrium always existed between the solvent vapour and oil phase and that the oil phase density is the product of the concentration of the oil phase ( $C_b$ ) and its molecular weight ( $M_b$ ). The numerical solution used a constant diffusivity that is assumed valid only during short time steps at which the thermodynamic conditions, liquid height and the

concentration of diffusing species are numerically evaluated. At each time step the concentrations and diffusion coefficient are updated based on the results from the previous time interval, including the changing saturation concentration at the interface boundary, which is a function of the thermodynamic conditions. The model calculates the time dependent composition of each phase, pressure and volume. Riazi found that the semi-analytical numerical model could accurately match experimental pressure decay results using several published diffusivity correlations within 5%. It is paradoxical that the diffusivity as a function of time was presented but no concentration dependence was presented. It is important to note that the diffusivity is dependent on the solvent gas pressure, so as the pressure declines, the diffusivity would change.

The experimental set-up used by Upreti and Mehrotra (2000) involved one-dimensional diffusion of carbon dioxide (CO<sub>2</sub>) in bitumen in the range of 25-90°C at 4 MPa initial pressure. The mass of carbon dioxide diffused in the liquid phase was measured using the pressure decay technique where the experiment was started at a given system pressure and the pressure decreased as the gas diffused into the heavy oil. Their method “utilises a comprehensive distributed parameter model of mass transfer and employs a functional optimisation technique to compute the concentration-dependent gas diffusivity. The calculation does not depend on empirical correlations. It incorporates the variation in the density of the gas-liquid mixture.” They assumed that the diffusivity is concentration dependent but pressure independent at a given concentration. However, the mathematical development suffered from one derivation flaw that was corrected by James (2003). Upreti and Mehrotra assumed a quasi-equilibrium interfacial concentration of solvent and heavy oil. They adjusted the solubility limit of equilibrium concentration at the gas-liquid interface with time to reflect the declining pressure. The results indicated that the diffusivity is a non-monotonic function of concentration. Upreti and Mehrotra found that the diffusivity of CO<sub>2</sub> in bitumen increases to a maximum value in the range of 0.007 – 0.010 mass fraction CO<sub>2</sub> and then decreases and levels off to a constant value (approximately  $0.185 \times 10^{-5}$  cm<sup>2</sup>/s). This is a rather unusual trend that they reason is plausible because the diffusivity would increase as the oil’s viscosity is decreased to a point beyond which additional CO<sub>2</sub> molecules already diffused in the bitumen hamper further diffusion. They also found that the diffusivity increased with increasing temperature. This finding agrees with the argument that diffusivity of a gas into a liquid is inversely proportional to the viscosity of the liquid phase, because as the temperature of the liquid increases, the viscosity decreases.

Zhang *et al.* (2000) performed pressure decay experiments using methane and CO<sub>2</sub> as diffusing species into Venezuelan heavy oil by measuring the pressure only. Experimentally, they



measured the pressure as a function of time without regard to ambient temperature fluctuations. Numerically, the transport equations were over-simplified but results were still reasonable. They assumed that the diffusivity was concentration independent and the change in interface height was small (and therefore negligible) although the experiments lasted for several days and the diameter of the test cell was only 2.5cm. Based on the constant diffusion coefficient and constant interface height, an analytical solution by Crank (1975) was employed for the time and position dependent concentration.

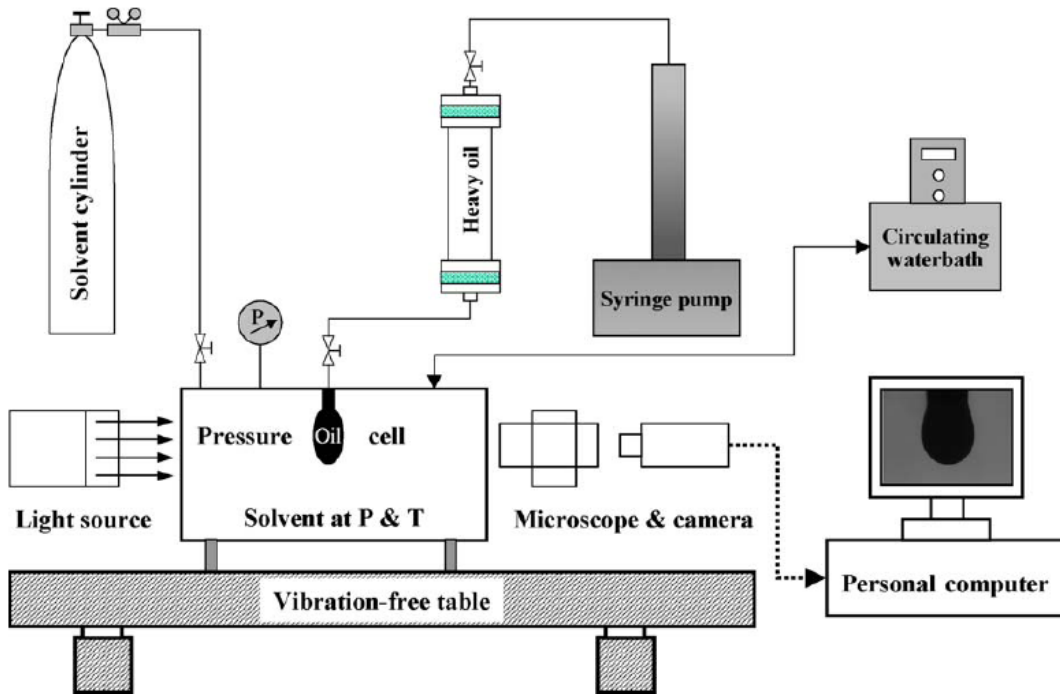
There is one inherent difficulty in developing a model based on pressure decay experiments; the use of boundary conditions. Normally, it is assumed that the heavy oil – solvent vapour interface instantly assumes the saturated equilibrium concentration of solvent at the given thermodynamic conditions. However, the concentration at the interface is dependent on pressure and if pressure decreases so does the interfacial concentration. Three choices of interfacial boundary conditions were compared by Tharanivasan *et al.* (2004): 1) the interface assumes the saturated solvent concentration at the equilibrium pressure regardless of whether or not the experiment reached equilibrium (Zhang *et al.* 2000); 2) the interfacial concentration is equal to the solubility concentration dependent on pressure (Upreti and Mehrotra 2000) and 3) the interface is not at equilibrium thus providing resistance to mass transfer. Tharanivasan *et al.* (2004) evaluated the three different boundary conditions using a constant diffusion coefficient model developed with an analytical solution and optimised to history match the results of the previously mentioned authors. It was determined that the non-equilibrium boundary condition worked best for the carbon dioxide-heavy oil system and the equilibrium boundary condition was most suitable for methane-oil systems although the results presented were almost independent of the boundary condition used. Physically, thermodynamic equilibrium should be maintained at the interface at all times.

#### **4.1.2 Dynamic Pendant Drop Volume Analysis (DPDVA)**

C. Yang and Gu (2005b, 2006a, 2006b, 2007) and D. Yang and Gu (2006, 2008) have developed a quick (one hour) visual technique to experimentally measure the swelling of an oil droplet in the presence of gas which they have called the pendant drop volume analysis (DPDVA). C. Yang and Gu (2005b, 2006a, 2006b, 2007) have focused on measuring the oil swelling factors and diffusion coefficients of carbon dioxide, methane, ethane, propane and three gas mixtures (mixture #1: 70% CO<sub>2</sub>, 30% C<sub>3</sub>H<sub>8</sub>; mixture #2: 70% CH<sub>4</sub>, 30% C<sub>3</sub>H<sub>8</sub> and mixture #3: 70% C<sub>2</sub>H<sub>6</sub>, 30% C<sub>3</sub>H<sub>8</sub>, (all in mole %)) in brine and heavy oil. They developed a mathematical model with

two different boundary conditions to try and obtain the diffusion coefficient and oil swelling factors. They used the changing pendant drop interfacial profile in part of the mathematical development but ignored its contribution on the diffusion process.

“Therefore, in this study, the influence of the shape and volume changes of the pendant drop on the diffusion process is neglected. It is assumed that the diffusion process occurs as if the pendant oil drop is stationary. It should be noted that the interfacial tension reduction and the oil-swelling effect are considered in predicting the dynamic interfacial profiles by solving the Laplace equation of capillarity.” (Yang, C. and Gu, Y. 2006a)



**Figure 4.1.2: Experimental Apparatus for the Dynamic Pendant Drop Volume Analysis (Yang, C. and Gu, Y. 2005a, 2005b, 2006a, 2006b, 2007)**

In the 2006a paper presented by C. Yang and Gu, the dimensionless form of the continuity equation cylindrical coordinates (shown in equation 4.1.1), assumes that the diffusivity is constant, the convection term is negligible and that the concentration profiles are independent of position around the pendant drop. The continuity equation along with the dimensionless forms of the initial and boundary conditions are solved simultaneously to find the average solvent concentration within the pendant drop and the interfacial solvent concentration assuming that the pendant drop does not change in size or shape during the measured diffusion time. The first boundary condition (shown in equation 4.1.2) assumes non-equilibrium at the bitumen-solvent

interface and the second assumes that solvent does not diffuse past a point of reference at the needle tip.

$$\frac{\partial c}{\partial t} = D \left[ \frac{1}{r} \frac{\partial}{\partial r} \left( r \frac{\partial c}{\partial r} \right) + \frac{\partial^2 c}{\partial z^2} \right] \rightarrow \frac{\partial C}{\partial \tau} = \frac{1}{R} \frac{\partial}{\partial R} \left( R \frac{\partial C}{\partial R} \right) + \frac{\partial^2 C}{\partial Z^2} \quad (4.1.1)$$

$$D \left( \frac{\partial c}{\partial r} n_r + \frac{\partial c}{\partial z} n_z \right) \Big|_{(r,z) \in \Gamma_l} = k \left( c_{sat} - c \Big|_{(r,z) \in \Gamma_l} \right) \quad (4.1.2)$$

The variables in equation 4.1.1 include the concentration  $c$ , the time  $t$ , the diffusivity  $D$ , radius  $r$  and length  $z$ .  $C$ ,  $\tau$ ,  $R$  and  $Z$  are the dimensionless concentration, time, radius and length.  $n_r$  and  $n_z$  are the  $r$  and  $z$  components of the outward normal vector to the droplet-gas interface,  $k$  is the mass transfer coefficient and  $c_{sat}$  is the solubility taken over the interface boundary domain. The authors made dimensionless equations 4.1.1 and 4.1.2 along with the boundary and initial conditions.

The mass transfer Biot number ( $k_D = k.r_n/D$ ) and the diffusivity,  $D$ , are initially guessed and optimised through minimising the difference between the measured and calculated  $z$  and  $r$  dimensions. Convection is ignored in the dimensionless continuity equation a constant diffusion coefficient is assumed. The average and interfacial solvent concentrations are used to determine the dynamic interfacial tension ( $\gamma$ ) and average density of the pendant drop from predetermined calibration curves. In my opinion, the methodology lacks independent validation of experimental measurement because the “measured” interfacial profile,  $z_m = z_m(r_m, t)$ , Bond number ( $Bo$ ) and the measured volume of the pendant drop ( $V_m$ ) are used to compute the “calculated” interfacial profile,  $z_c = z_c(r_c, t)$  from the following expressions (in dimensionless form):

$$Bo.Z = \frac{2}{\bar{R}_o} - \frac{\left| \frac{d^2 Z}{dR^2} \right|}{\left| 1 + \left( \frac{dZ}{dR} \right)^2 \right|^{3/2}} + \frac{\left| \frac{d^2 Z}{dR^2} \right|}{R \left| 1 + \left( \frac{dZ}{dR} \right)^2 \right|^{1/2}}, \quad \text{where } Bo = \frac{(\bar{\rho}_b(t) - \rho_s) g r_n^2}{\gamma(t)} \quad (4.1.3)$$

$$\int_0^{Z_d} \pi R^2 dZ = \frac{V_m}{r_n^3} = \bar{V}_m \quad (4.1.4)$$

$Z$ ,  $R$ ,  $\bar{R}_o$ , and  $\bar{V}_m$  are the dimensionless  $z$ -dimension, radius, principal radius of curvature and measured volume of the pendant drop. The difference between the “calculated” and “measured” normal distances from a measured radial position is minimised to find the mass transfer Biot

number and diffusion coefficient. They found and concluded that the diffusivity of CO<sub>2</sub> in brine is 1.81 x 10<sup>-5</sup> cm<sup>2</sup>/s at 3.6 MPa and 25°C and the diffusivity of CO<sub>2</sub> in heavy oil is 1.14 x 10<sup>-5</sup> cm<sup>2</sup>/s at 2.9 MPa and 25°C within the range of values found in the literature. In reality, the diffusion coefficient should not be considered constant, the swelling of the droplet needs to be accounted for, and the experimental measurements should be validated and not serve as input to finding the predicted values.

In the 2005b paper presented by C. Yang and Gu, the boundary condition and objective function are different. In this paper, they assume an equilibrium interfacial concentration to find the diffusivity of carbon dioxide in Lloydminster heavy oil ( $\rho = 0.988 \text{ g/cm}^3$  and  $\mu = 23,000 \text{ mPa}\cdot\text{s}$ ) at pressures of 2, 3, 4, 5, and 6 MPa at 23.9°C. After solving the set of equations, as above except that the boundary condition for the bitumen-solvent interface is a constant equilibrium concentration, the computed concentration profile is used to calculate the number of moles ( $n(t)$ ) diffused into the pendant drop at any time. The “calculated” volume ( $V_c$ ) of the heavy oil droplet is predicted using the following expression:

$$V_c(t) = V_o + v_{gas} MW_{gas} n(t) \quad (4.1.5)$$

$V_o$  is the initial volume of the droplet,  $MW_{gas}$  is the molecular weight of the gas and  $v_{gas}$  is the volume change per unit mass of gas dissolved at a constant pressure and temperature which is assumed constant. The potential issue arises from the value for the volume change per unit mass ( $v_{gas}$ ) which is calculated from the oil swelling factor ( $f_{sw}$ ) as shown in the following equation.

$$v_{gas} = \frac{f_{sw} - 1}{MW_{gas} c_{sat}} \quad (4.1.6)$$

The oil swelling factor is defined as the volume of saturated heavy oil at equilibrium conditions to the volume of solvent free heavy oil at normal pressure and temperature. During the diffusion process, equilibrium has only been reached at the interface and not throughout the oil droplet. Therefore, the equation should only be used at equilibrium if one were to be rigorous about the mathematical development.

The oil swelling factor and the diffusivity are initially guessed and then optimised by minimising the difference in the “measured” ( $V_m$ ) and “calculated” ( $V_c$ ) volumes of the oil droplet without considering the pendant drop swelling or a non-constant diffusivity on the results of the continuity equation solution. Their results indicate that the diffusivity and oil swelling factor increase with increasing pressure, as shown in Table 4.1.1.

C. Yang and Gu (2006b) present the same mathematical development using a constant solubility concentration at the oil droplet-solvent interface to find the diffusion coefficient and oil swelling factor for CO<sub>2</sub> (already presented in 2006a), CH<sub>4</sub>, C<sub>2</sub>H<sub>6</sub>, C<sub>3</sub>H<sub>8</sub> and three solvent mixtures in Lloydminster heavy oil at 23.9°C and different pressures that were smaller than the respective vapour pressures of the solvents. The results are shown in Table 4.1.1. It was concluded that the diffusivity and oil swelling factor increases for the respective solvent with increasing pressure, as theory would suggest. The same development, experimental procedure and results for propane in the Lloydminster heavy oil are presented in another paper published in the Journal of Canadian Petroleum Technology (Yang, C. and Gu, Y. 2007).

**Table 4.1.1: Diffusivity and Oil Swelling Factor Results for Different Solvents in Lloydminster Heavy Oil at 23.9°C (Yang, C. and Gu, Y 2006b)**

CO <sub>2</sub> ( $P_v^* = 6.28$ MPa)		
P = 2.0 - 6.0 MPa	$f_{sw} = 1.03 - 1.13$	$D_{sb} = 0.2 - 0.55 \times 10^{-5} \text{ cm}^2/\text{s}$
CH <sub>4</sub> ( $P_v^* = 31.38$ MPa)		
P = 6.0 - 14.0 MPa	$f_{sw} = 1.03 - 1.07$	$D_{sb} = 0.12 - 0.19 \times 10^{-5} \text{ cm}^2/\text{s}$
C <sub>2</sub> H <sub>6</sub> ( $P_v^* = 4.12$ MPa)		
P = 1.5 - 3.5 MPa	$f_{sw} = 1.09 - 1.315$	$D_{sb} = 0.13 - 0.77 \times 10^{-5} \text{ cm}^2/\text{s}$
C <sub>3</sub> H <sub>8</sub> ( $P_v^* = 0.93$ MPa)		
P = 0.4 - 0.9 MPa	$f_{sw} = 1.11 - 1.505$	$D_{sb} = 0.09 - 0.68 \times 10^{-5} \text{ cm}^2/\text{s}$
Mix #1 - 70 mol% CO <sub>2</sub> , 30 mol% C <sub>3</sub> H <sub>8</sub> ( $P_{dew}^* = 3.27$ MPa)		
P = 1.0 - 3.0 MPa	$f_{sw} = 1.09 - 1.48$	$D_{sb} = 0.08 - 0.82 \times 10^{-5} \text{ cm}^2/\text{s}$
Mix #2 - 70 mol% CH <sub>4</sub> , 30 mol% C <sub>3</sub> H <sub>8</sub> ( $P_{dew}^* = 4.79$ MPa)		
P = 2.0 - 4.5 MPa	$f_{sw} = 1.14 - 1.35$	$D_{sb} = 0.12 - 0.7 \times 10^{-5} \text{ cm}^2/\text{s}$
Mix #3 - 70 mol% C <sub>2</sub> H <sub>6</sub> , 30 mol% C <sub>3</sub> H <sub>8</sub> ( $P_{dew}^* = 2.19$ MPa)		
P = 0.75 - 2.0 MPa	$f_{sw} = 1.09 - 1.37$	$D_{sb} = 0.06 - 0.77 \times 10^{-5} \text{ cm}^2/\text{s}$
CO <sub>2</sub> in Weyburn Crude at 27°C (Yang, D. and Gu, Y. 2008)		
P = 0.1 - 5.0 MPa	$k = 0.88 - 8.41 \times 10^{-5} \text{ m/s}$	$D_{sb} = 0.47 - 2.49 \times 10^{-5} \text{ cm}^2/\text{s}$

Yang (D.) and Gu (2008) follow the same experimental and mathematical procedure as described in 2006 to find the diffusion coefficient and mass transfer coefficient for carbon dioxide in a Weyburn, Saskatchewan crude oil ( $\rho = 0.877 \text{ g/cm}^3$ ,  $\mu = 13 \text{ mPa}\cdot\text{s}$  at 27°C). The difference is that heavy oil instead of brine was used and the ADSA (axisymmetric drop shape analysis) was used to measure the dynamic interfacial tension at any time. Besides giving details for the

Galerkin finite element procedure used to solve the same set of equations as Yang, C. and Gu (2006a), they included a non-equilibrium boundary condition and the objective function compares the measured and calculated interfacial tensions instead of the interfacial profile. The “calculated” interfacial tension is determined from the solution of the differential equations for the average concentration profile of the solvent in the heavy oil droplet. They relate the dynamic interfacial tension to the transient interfacial concentration assuming it’s the same relationship as the equilibrium interfacial tension versus equilibrium concentration. Once the calculated interfacial tension is found, the diffusion coefficient is minimised for over a range of mass transfer coefficient values and then optimised over a wider range to find the global minimum. They reported mass transfer and diffusion coefficients at different pressures shown in the table above.

### **4.1.3 NMR and CAT Scanning**

Diffusion coefficients for liquid-liquid systems have been determined using medical imaging equipment, both NMR and x-ray CAY scanning. Wen and Kantzas (2005) and Wen *et al.* (2004, 2005) examined a range of solvents in different heavy oils/bitumens using NMR (pentane, hexane, heptane, toluene, kerosene and naphtha in Peace River, Atlee Buffalo, Edam and Cold Lake oils). The following papers present results using X-ray computer assisted tomography (CAT scanning) for measuring density profiles in the liquid-liquid systems, inferring concentration and calculating the diffusivity. As shown in Figure 4.1.3a, the liquid solvent is placed on top of a volume of heavy oil and the sample scanned to measure the x-ray attenuation for vertical cross sections in the diffused part of the system as a function of time. The concentration of the solvent in the heavy oil is calculated from the mixture density at each point in the solution, which is based on the x-ray attenuation. The advantage of using medical imaging equipment for determining diffusion coefficients in liquid-liquid systems is that the concentration profile is explicitly determined and not inferred like in the other techniques, assuming the mixing rule is well defined.

Ideal mixing was assumed until Luo *et al.* (2007) determined that there is an excess volume of mixing, as shown in Figure 4.1.3. An excess volume of mixing is indicative of deviation from ideal mixing. A negative excess volume of mixing arises from a mixture density greater than predicted from ideal mixing, and therefore a specific volume less than ideal. The concentration dependent diffusivity for heptane in heavy oil is shown in Figure 4.1.3b where the density of the oil is  $0.978 \text{ g/cm}^3$  at  $25^\circ\text{C}$  and the viscosity is approximately  $21,500 \text{ mPa}\cdot\text{s}$  at  $20^\circ\text{C}$ . The excess

volume of mixing helped but did not completely eliminate the time dependence. It should be expected that the diffusivity is concentration dependent but not time dependent for the same concentration. At higher heavy oil concentrations (from mass fraction 0.5 to 0.97) results show a linear dependence of diffusivity on heavy oil. Converting the heavy oil mass fraction to solvent mass fraction, the approximate linear function is  $D = 9.5 \times 10^{-6} \omega_S + 3.1 \times 10^{-6} \text{ cm}^2/\text{s}$ . This range of heavy oil concentration is of interest for solvent extraction processes because laboratory scale VAPEX experiments typically produce live oil with 0.30-0.40 solvent mass fraction.

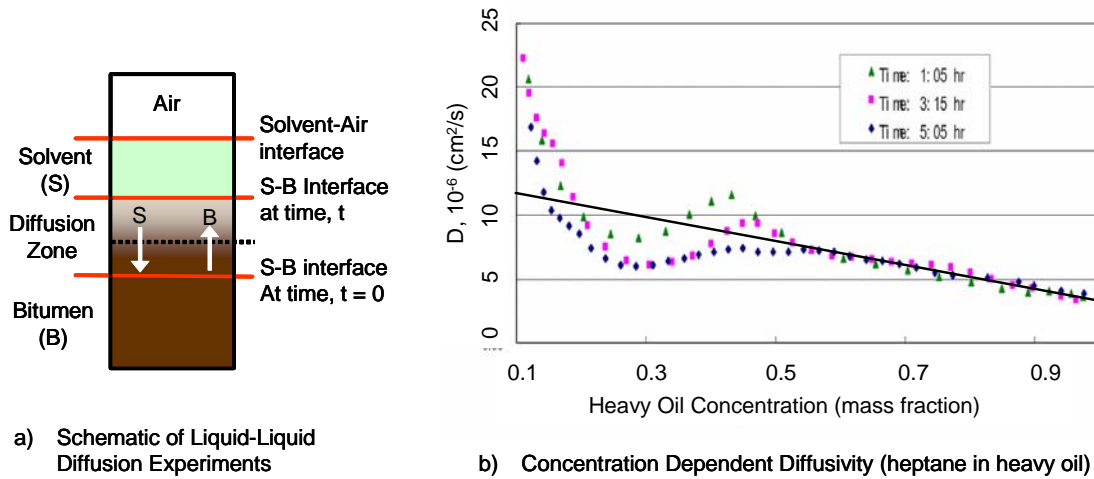


Figure 4.1.3: a) Experimental Schematic and b) Concentration Dependent Diffusivity for Heptane in Heavy Oil (Luo *et al.* 2007)

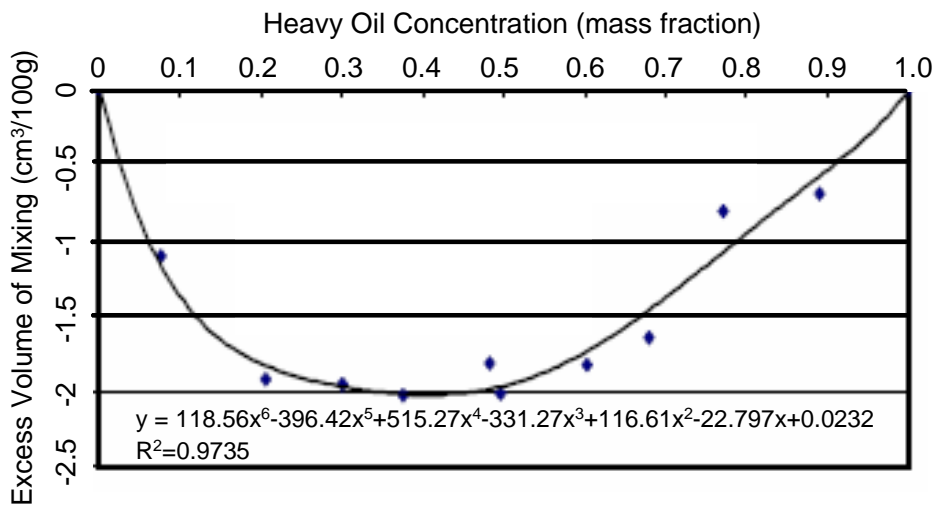
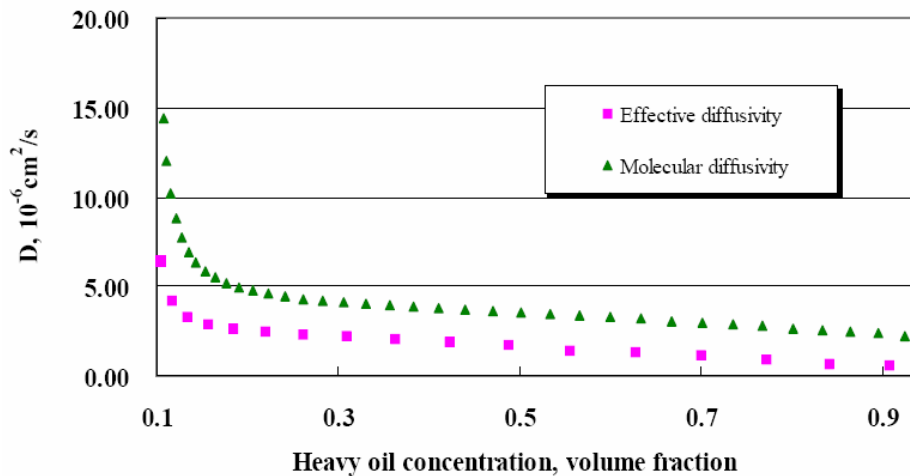


Figure 4.1.4: Excess Volume of Mixing for Heptane in Heavy Oil (Luo and Kantzas 2007)

In 2005, Salama and Kantzas monitored the diffusion of pentane, hexane, heptane and octane separately in the same heavy oil and in sand saturated with heavy oil. The calculated diffusivities show time dependence decreasing with log (time). What is interesting and expected is that the diffusivity in the presence of sand is lower than in bulk oil where the porosity and tortuosity of the porous media slows the rate of diffusion. Luo and Kantzas (2008) re-investigated the diffusion of liquid hydrocarbon solvents in the presence of sand, previously studied by Salama and Kantzas (2005) taking into consideration the volume change upon mixing. In a porous medium, it is expected that the tortuosity and the diffusion path length between pores would slow down the rate of diffusion and consequently the diffusivity is reported as an effective diffusivity ( $D_e$ ). The effective diffusivity is a function of the molecular diffusivity ( $D_{sb}^o$ ) and it takes into account the tortuosity expressed in terms of the formation resistivity factor (F) and in turn the porosity ( $\phi$ ) and cementation factor (m) for unconsolidated sand packs.

$$D_e = \frac{D_{sb}^o}{F} \rightarrow D_e = \frac{D_{sb}^o}{\phi^{-m}} \quad \text{where } F = \phi^{-m} \quad (4.1.7)$$

The time dependence of the diffusivity is reduced by taking into account the volume change on mixing and the authors conclude that the diffusivity in sand packs is less than in bulk liquids, as expected. They found a linear diffusivity (from 0.18 to 0.90 heavy oil volume fraction) with approximately the same dependence on solvent concentration as in the bulk liquid sample but with different limits, i.e. the slopes are equivalent, as shown in the following figure.



**Figure 4.1.5: Comparison of Effective and Molecular Diffusivities for a Homogeneous Sand Pack (Luo, H. and Kantzas, A. 2008)**



In 2007, Zhang and Shaw compared the mutual diffusion coefficients obtained from analysing compositional density profiles using two mathematical relationships for the mutual diffusivity. The density profiles were experimentally determined at the Tomographic Imaging and Porous Media Laboratory at the University of Calgary under Professor A. Kantzas. The first method involved relating the density profile to the volume fraction and determining the diffusivity using the following equation as per Oballa and Butler (1989), Das and Butler (1996) and Wen *et al.* (2004):

$$D_{sb,V_f} = -\frac{1}{2t} \left[ \frac{\partial x}{\partial V_f} \right]_{t,V_f} \int_0^{V_f} x \partial V_f \quad (4.1.8)$$

The results indicated that the diffusivity is different depending on the time over which it is evaluated and the authors attribute this to the fact that the diffusivity does not account for density gradients and that the results were acceptable at longer times when the density gradients are smaller. They then compared the diffusivity results using the above equation to results using an expression developed from the solvent continuity equation which maintains compositional variance of density and diffusivity, i.e. density and diffusivity are dependent on the solvent concentration. The solvent continuity was described using a single joint variable and the diffusivity is related to two coefficients, A and B using either a series approximation or a Taylor series expansion. The experimental composition profiles were used to optimise for the coefficients.

$$\frac{\partial D_{sb}}{\partial \omega_s} + D_{sb} \left\{ \frac{\partial \rho}{\partial \omega_s} \frac{1}{\rho} + \frac{\partial^2 \omega_s}{\partial \omega_s^2} \left/ \left( \frac{\partial \omega_s}{\partial x} \right)^2 \right. \right\} \quad (4.1.9)$$

$$\frac{\partial D_{sb}}{\partial \omega_s} + D_{sb} A(\omega_s) = B(\omega_s) \quad (4.1.10)$$

Neither the mathematical approach above nor data smoothing resulted in a diffusivity function independent of time. They suggested that if they considered time-invariant data, the mutual diffusion coefficient may be treated as constant in the range of  $1 \times 10^{-6}$  to  $2 \times 10^{-6}$  cm<sup>2</sup>/s for pentane and heptane in Athabasca and Cold Lake bitumen respectively. The data presented in their figures do not suggest a constant diffusion coefficient at all. As presented, Luo *et al.* (2007) resolved the time dependency by taking into account an excess volume upon mixing.

#### 4.1.4 Oil Phase Swelling

Riazi (1996) and recently Jamialahmadi *et al.* (2006) measured the swelling of the oil phase to determine the diffusivity of methane in liquid hydrocarbons. Jamialahmadi *et al.* investigated the diffusion of methane in do-decane at 45, 65 and 81°C and in a typical Iranian crude oil at 25 and 50°C and various pressures using both a constant diffusion coefficient and a viscosity dependent diffusivity. Experimentally, they monitored the change in height of the liquid oil phase as it swells due to the diffusion of the constant pressure CH<sub>4</sub>. Mathematically, equilibrium was assumed at the oil-gas interface and a no-flux boundary condition is used at the bottom of the one-dimensional diffusion cell. They related the change in volume (dV) per volume (V) to the change in the product of the average solvent concentration ( $\bar{C}_A$ ) and specific volume ( $v_A$ ), as shown in equation 4.1.8 and hence the average solvent concentration was related to the height at a given time compared to the initial height ( $Z_t/Z_0$ ).

$$\frac{dV}{V} = d(v_A \bar{C}_A) \rightarrow \bar{C}_A = \frac{1}{v_A} \ln \frac{V_t}{V_0} \rightarrow \bar{C}_A = \frac{1}{v_A} \ln \frac{Z_t}{Z_0} \quad (4.1.11)$$

Based on this equation and the integrated form of the continuity equation they arrived at an expression for the change in average concentration in time related to the difference in interfacial and average concentrations ( $C_{Ai} - \bar{C}_A$ ) plus the product of the diffusion coefficient (D) and the concentration gradient at the interface as shown in the following equation.

$$\frac{d\bar{C}_A}{dt} = (C_{Ai} - \bar{C}_A)v_A + \frac{D}{Z_0 \exp(v_A \bar{C}_A)} \left. \frac{\partial C_A}{\partial x} \right|_{Z_t} \quad (4.1.12)$$

The concentration gradient is unknown and so they assumed a power law concentration profile and developed it in terms of an adjustable parameter, a:

$$\left. \frac{\partial C_A}{\partial x} \right|_{Z_t} = \frac{(C_{Ai} - \bar{C}_A)(aC_{Ai} - \bar{C}_A)(1 - v_A \bar{C}_A)}{Z_0^2 \bar{C}_A} \quad (4.1.13)$$

Once the adjustable parameter, a, was optimised for by relating the average solvent concentration to the experimental height using equation 4.1.8, the left hand side of the following equation yielded a straight line with the diffusion coefficient as the slope. The  $\alpha$  coefficients are constants that are functions of the interfacial concentration, initial bitumen height and the coefficient a.

$$\frac{1}{\alpha_7} \ln \frac{(aC_{Ai} + \bar{C}_A)^{\alpha_1}}{(C_{Ai} + \bar{C}_A)^{\alpha_2} (1 - \bar{C}_A)^{\alpha_3/a}} + \frac{\alpha_4}{2a\alpha_7(1 - \bar{C}_A)^2} + \frac{\alpha_5}{a\alpha_7(1 - a\bar{C}_A)} + \frac{\alpha_6}{\alpha_7} = Dt \quad (4.1.14)$$

Using the above summarised methodology, the diffusion coefficient for methane in crude oil was shown to increase from approximately  $8.0 \times 10^{-5} \text{ cm}^2/\text{s}$  to  $13 \times 10^{-5} \text{ cm}^2/\text{s}$  in the range of approximately 4 – 28 MPa at 25°C.

The authors attempted to explore the effect of using a non-constant diffusivity by writing the partial derivatives of the continuity equation in terms of their equivalent finite differences and relating a variable,  $\lambda$ , to the diffusivity and the differential segment thickness,  $\Delta x$  resulting in a continuity equation of the form shown in equation 4.1.16.

$$\lambda = \frac{D.t}{(\Delta x)^2} \quad (4.1.15)$$

$$C_i^{j+1} = \frac{1}{1+2\lambda} \left[ C_i^j + \lambda (C_{i-1}^{j+1} + C_{i+1}^{j+1}) \right] \quad (4.1.16)$$

A successive substitution method was used to find the new diffusion based on the previous value. The results showed a time dependent rather than viscosity or concentration dependent diffusivity with an initial steep decrease towards a constant diffusion coefficient from 20 to 80 hours. The authors suggested that they found very good agreement between the experimental and predicted swelling at later times. This result is somewhat cyclical since the calculation is optimised to fit the experimental data. At earlier times the diffusion coefficient shows a time dependence which they attributed to an “incubation” period when both convection and diffusion are present. Although the continuity equation used ignores the convection term, so the statement is unjustified.

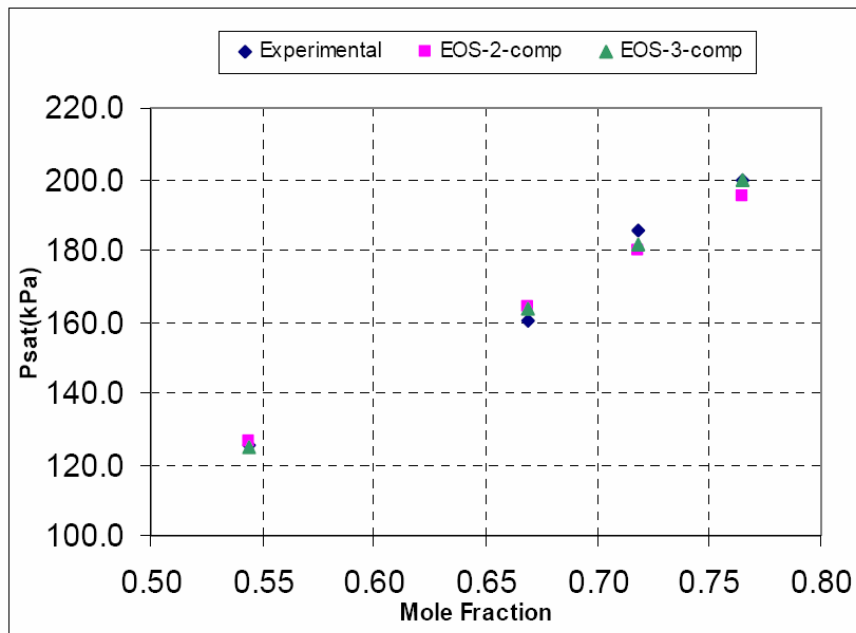
#### 4.1.5 Solubility in Heavy Oil

The pressure decay method (Riazi 1996, Zhang *et. al.* 2000, Upreti and Mehrotra 2002, Tharanivasan *et. al.* 2006), dynamic pendant drop volume analysis – DPDVA (Yang and Gu 2006; Luo *et al.* 2006) and the one dimensional diffusion methods (James *et al.* 2004, 2008 (and in this chapter); and Jamialahmadi *et al.* 2006) all require a boundary condition at the bitumen solvent interface. The boundary condition used is the solubility of the solvent in bitumen. The value of the solubility was determined experimentally (Luo *et al.* 2006; Jamialahmadi *et al.* 2006; Yazdani and Maini 2008; and Bademchi-Zadeh *et al.* 2009a, 2009b) and verified using the Peng-Robinson equation of state.

Luo and Gu (2007) as well as Yazdani and Maini (2008) found the solubility of propane in bitumen and n-butane in bitumen respectively. Luo and Gu (2007) presented their experimental

data found from their pendant drop method by showing the solubility (g solvent/100g of bitumen) as a function of equilibrium pressure at their experimental temperature of 23.9°C. Yazdani and Maini presented the equilibrium pressure as a function of the mole fraction of solvent in the heavy oil at their experimental temperature of 22°C. Both groups verified their experimental results using CMG’s WINPROP® software using the Peng-Robinson equation of state with good agreement. The specific oil/bitumen, in WINPROP®, is defined as function of the weight percent of the oil found in a broad range carbon group, i.e. < C21, or ≥ C21, the molecular weight of the group and the density of the group or component. Unfortunately, neither the temperature nor the oil used was equivalent to our study but the solubility limit (shown in Figure 4.1.6) at 200 kPa is shown to be only 0.77 mole fraction which seems low in comparison to section 4.4.5.

Recently, Bademchi-Zadeh *et al.* (2009) investigated the phase behaviour of propane in Athabasca bitumen including the viscosity, density and solubility. They compared two methods for experimentally determining the solubility: a step-wise and a continuous method at different temperatures (10, 20, 30, 40, 50°C). The maximum solubility reached is 0.8 mole fraction. They did report and compared experimental results to ideal mixing for density and the Lobe mixing rule for viscosity for different concentration propane-bitumen mixtures at different temperatures. It is interesting to see that the mixture density deviates from ideal mixing at higher (25.5 wt%) but otherwise the ideal mixing rule holds.



**Figure 4.1.6: Solubility of Butane in Frog Lake Bitumen (Yazdani and Maini 2007)**

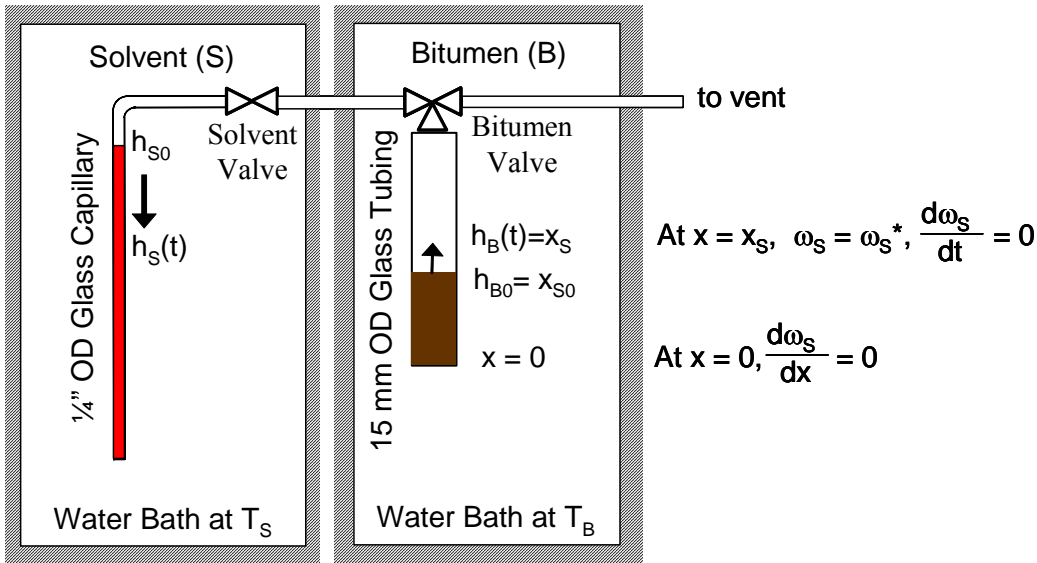
## **4.2 Experimental Procedure**

The experimental apparatus and procedure for determining the diffusivity of n-butane in heavy oil was designed and perfected over several years in order to obtain accurate and repeatable results. The experimental apparatus is shown in Figure 4.2.1 where the solvent mass transfer from the liquid butane phase into the bitumen was measured in time. As the butane diffused into the bitumen the change in height of both the bitumen swelling and the decrease in liquid solvent height were measured using a cathetometer.

An earlier design flaw of housing both the bitumen and solvent in the same water bath was overcome by using two water baths. Even when well stirred, slight temperature variations in the single water bath and/or the initial pressure drop from vacuum to the vapour pressure of n-butane could cause the solvent to condense somewhere in the line or in the bitumen tube. Erratic increases/decreases in the bitumen but mostly in the solvent were evidence of this phenomenon. The condensation issue was overcome by designing a two water bath system where the solvent was kept at a temperature less than the bitumen temperature. Between the two water baths, a short length of stainless steel tubing was insulated and heated with a low wattage incandescent bulb to ensure the solvent did not condense.

The temperature controllers and mixers were isolated from the water baths by placing the water baths on a vibration resistant table in order to reduce any convective mixing due to vibration. The water was circulated from the controller to the water bath by pumping the water to the bottom of the water bath and using overflow to return it to the controller. The solvent, bitumen, line between water baths, and the ambient temperatures were recorded during the diffusion experiments.

The Athabasca bitumen used in the diffusion tests was generously provided by Hatch™. The average bitumen molecular weight according to ASTM standard D2503 (analysed by Maxxam laboratories) was determined to be 557 g/mol. The density was measured using a pycnometer. The bitumen viscosity was determined using a Physica MCR 100 rheometer at different temperatures that were then fit with a power function and used to determine the viscosity at 26.3°C. The n-butane vapour pressure, density and viscosity were gathered from the National Institute of Standards Tables (NIST). The data and physical properties of the bitumen and solvent are shown in Table 4.2.1.



**Figure 4.2.1: Schematic Diagram of Solvent Diffusion into Heavy Oil**

Procedure-wise, most effort was involved in setting up the experiment. Knowing the mass of the empty bitumen tubes, bitumen was loaded into several tubes up to specific height and then weighed in order to obtain two replicate samples. In order to load the bitumen in the narrow inner diameter tube, 0.3175 cm (1/8”) stainless steel tubing filed to a needle tip at one end was attached to the bottom of a pressure cylinder housing the bitumen. The cylinder and its contents were heated to approximately 120°C (to reduce the bitumen viscosity) and then pressurised to 137.9 kPa (20 psig). The needle was placed into the bitumen tube and a needle valve opened until the required amount of bitumen was loaded into the tube. This methodology made it possible to load small bitumen samples without cleaning excess bitumen from the tube walls.

After assembling the bitumen and solvent tubes in the water bath, the system was allowed to equilibrate to temperature for several hours before starting the experiment. The temperature of the solvent water bath was maintained 1-2°C less than the bitumen water bath in order to ensure that the butane did not condense in the bitumen tube. Both, during the equilibration stage and during the experiment several temperatures were monitored including the solvent and bitumen controller water baths, the experimental solvent and bitumen water baths, ambient and the temperature of the line between the solvent and bitumen tanks. Temperatures were monitored using Omega type-T thermocouples connected to a Measurement Computing USB-TC 8-channel thermocouple data acquisition board. The temperatures were recorded at 0.5 or 1.0 minute intervals using LabVIEW version 7.1 software by National Instruments.

**Table 4.2.1: Experimental Data**

Measurement/Property	Run 1	Run 2
Average Solvent Temperature (°C)	24.9	24.9
Average Bitumen Temperature (°C)	26.3	26.3
<b>Mass of Bitumen</b>		
sample 1 (g)	1.33126	1.58222
sample 2 (g)	1.33076	1.58475
Average (g)	1.33101 ± 0.00025	1.58349 ± 0.00127
Vapour Pressure – n-butane at 24.9°C (psia)	35.177	
<b>Density (g/cm<sup>3</sup>)</b>		
n-butane (l) at 24.9°C	0.57295	
n-butane (l) at 26.3°C	0.57132	
Bitumen at 22°C	1.001	
<b>Viscosity</b>		
n-butane (l) at 26.3°C (mPa.s)	0.15645	
Bitumen at 26.3°C (mPa.s)	238,441	
<b>Molecular Weight (g/mol)</b>		
n-butane	58.12	
Bitumen	557	

Ensuring consistency between replicates and between experiments was predominately controlled through the start-up procedure. Flushing the system of air and establishing a vapour phase of pure butane was of paramount importance. Without the ability to flush the system from an inlet to outlet, a pure vapour phase was established through several cycles of filling the system to pressure using n-butane and then purging the system using vacuum. The solvent tube (up to the solvent valve, shown in Figure 4.2.1) contained liquid butane with the head space filled with pure solvent vapour before being connected to the bitumen tube. The bitumen tube initially contained liquid bitumen and air at atmospheric pressure. The first step was to connect the vent side of the three-way bitumen valve to vacuum for 10 seconds. The bitumen valve was then opened to the solvent to allow the bitumen tube to fill with butane vapour for 10 seconds. Subsequently, the bitumen valve was again turned to vacuum and the procedure continued for a total of five purge-fill sequences. After the final evacuation the bitumen tube was again filled with solvent which is released to atmosphere for five seconds before the bitumen valve was closed. This last step is to reduce the chance of solvent condensing on the bitumen when the experiment is started. The solvent vapour initially experiences instantaneous cooling due to sudden evaporation and pressure drop experienced when the bitumen valve is opened to start the diffusion experiment. Before

starting the experiment and immediately after opening the bitumen valve, the heights of the solvent and bitumen in both replicates were measured. It is important to take the heights again after opening the valve as the tube positions may have shifted slightly while opening the valve.

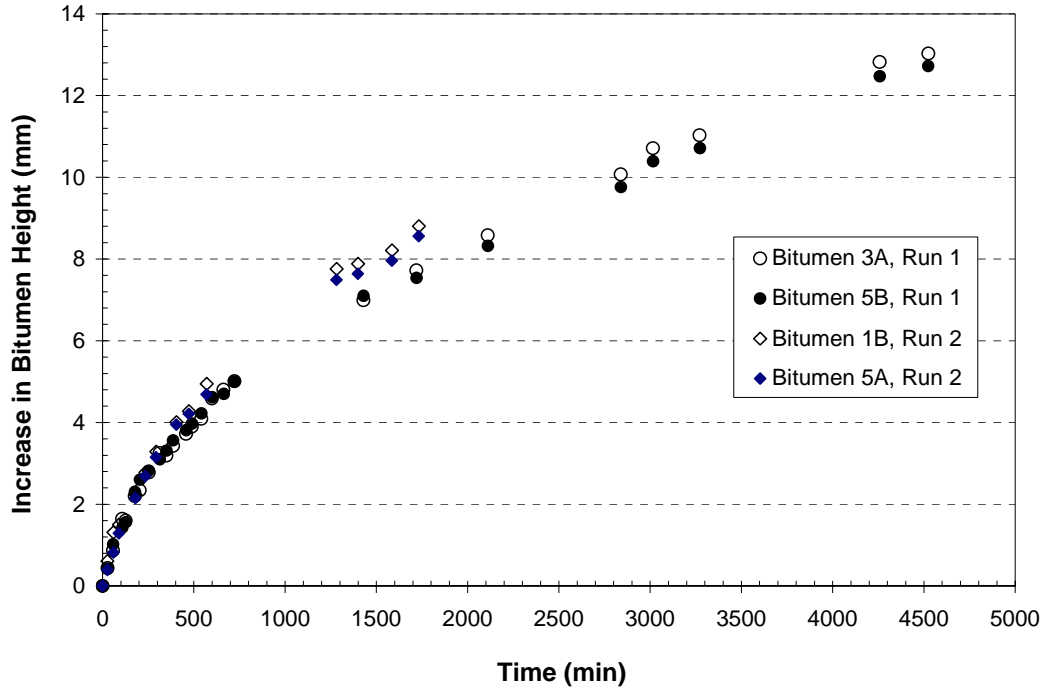
The experiment is started when the bitumen valves are opened to the solvent and at the same time the timer and data acquisition are started from zero. The solvent height is ideally recorded every 15-20 minutes. There is not sufficient change in the bitumen to record the height more frequently than every 45-60 minutes. The experimental run time is discretionary.

### **4.3 *Experimental Results***

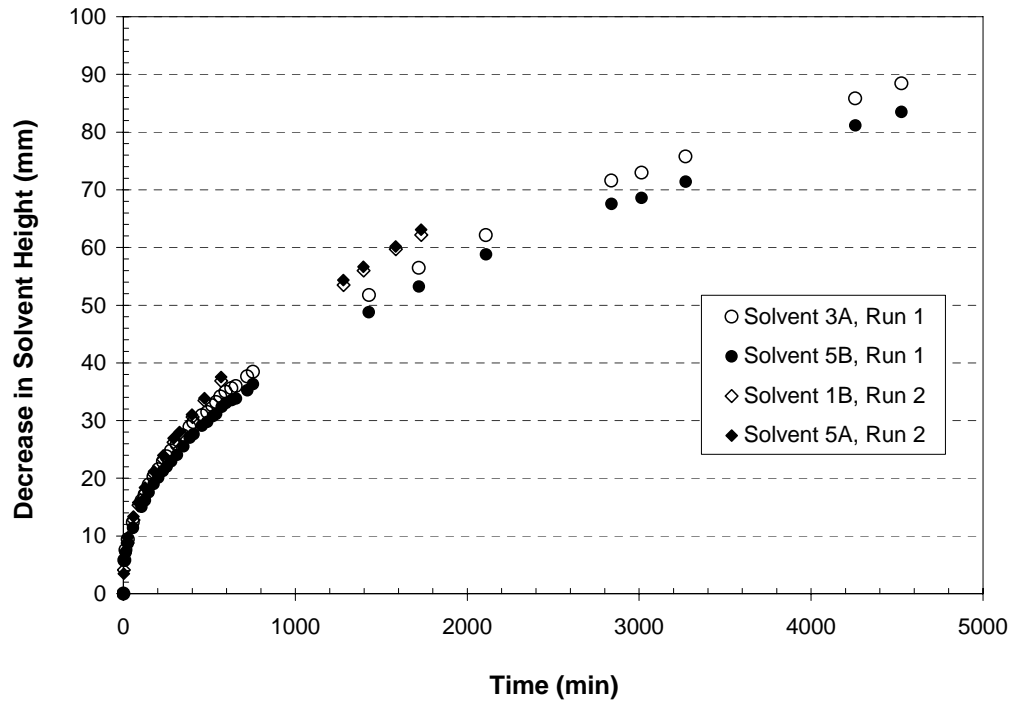
#### **4.3.1 Change in Bitumen and Solvent Heights**

Experimentally, the increase in bitumen and the decrease in liquid solvent are measured in time as shown in Figure 4.3.1 and Figure 4.3.2. A run consists of two replicate experiments where the two bitumen tubes contain the same mass of oil. Replicates are run simultaneously and should give identical results. Absolute height measurements are shown as changes in height from time zero, i.e. the increase in bitumen height and decrease in solvent height from time zero. Gaps in the data for the increase in bitumen height and the decrease in solvent height correspond with evenings and nights. As shown in the following two figures, the data points for both Run #2 (1B and 5A) experiments deviate from 1280 to 1732 minutes. This deviation is discussed in detail in the 4.3.2 Experimental Error section.





**Figure 4.3.1: Experimental Increase in Bitumen Height**

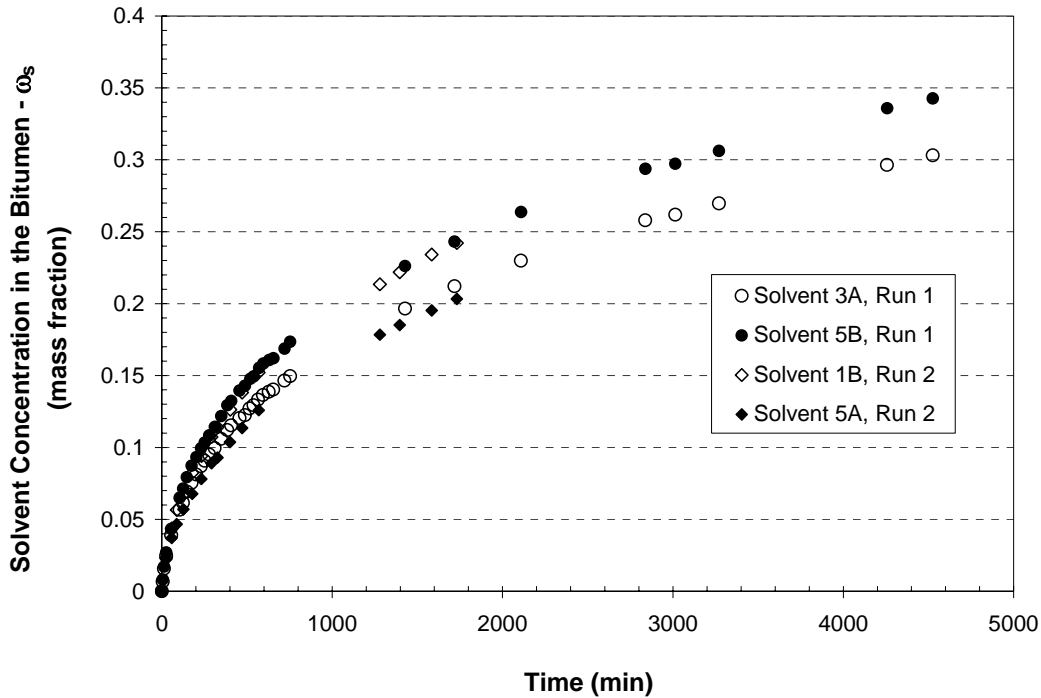


**Figure 4.3.2: Experimental Decrease in Solvent Height**

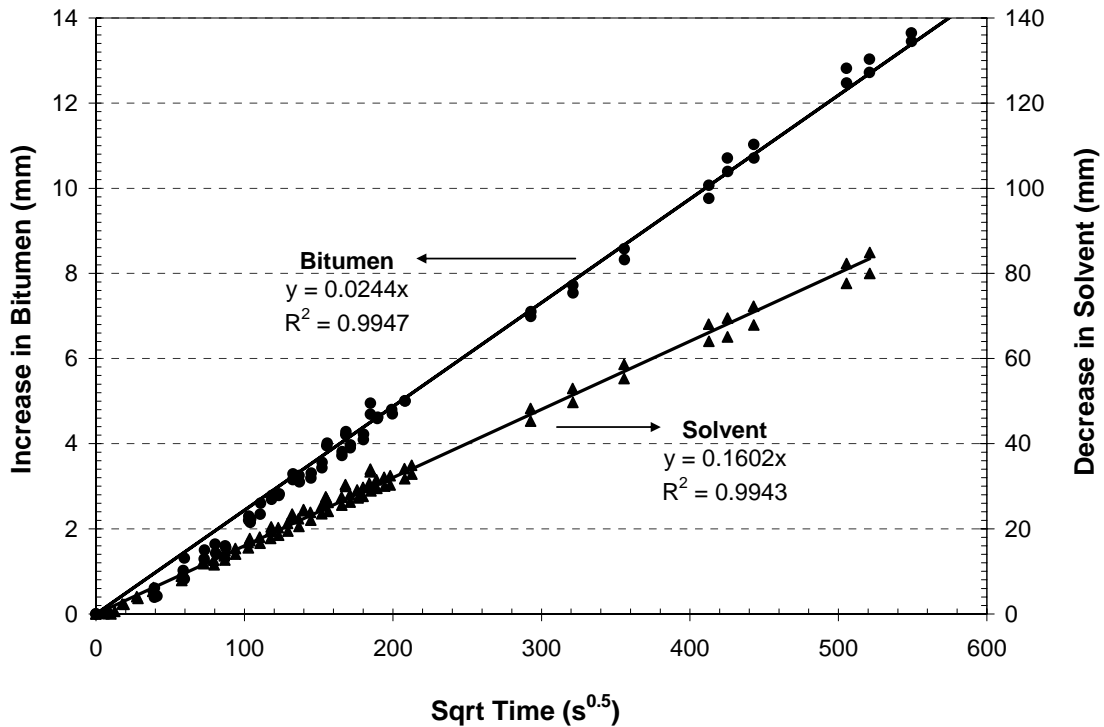
The mass of solvent and thus concentration of solvent in the bitumen phase can be calculated knowing the decrease in solvent height at any time. Figure 4.3.3 shows the overall solvent

concentration in the bitumen phase as a function of time. The maximum solvent concentration reached in 4500 minutes or 75 hours is 0.35 mass fraction or 0.84 mole fraction. Initially, upon starting the experiment, the solvent height suddenly decreases due to the butane filling the void space in the bitumen tube. This initial decrease is accounted for knowing the number of moles and thus mass required to fill the void volume from atmospheric to the vapour pressure of the solvent.

The increase in the bitumen and the decrease in the solvent have square root dependence with time as shown in Figure 4.3.4. The square root expression for the increase in bitumen height was used in the numerical model to compare the experimental to predicted increase in height. It should be noted that the last four experimental points from run #2 (shown in Figure 4.3.1 and Figure 4.3.2) are omitted from the correlation because they were considered outliers due to the temperature variation as explained in the subsequent Experimental Error section.



**Figure 4.3.3: Solvent Concentration in the Bitumen Phase as a Function of Time**

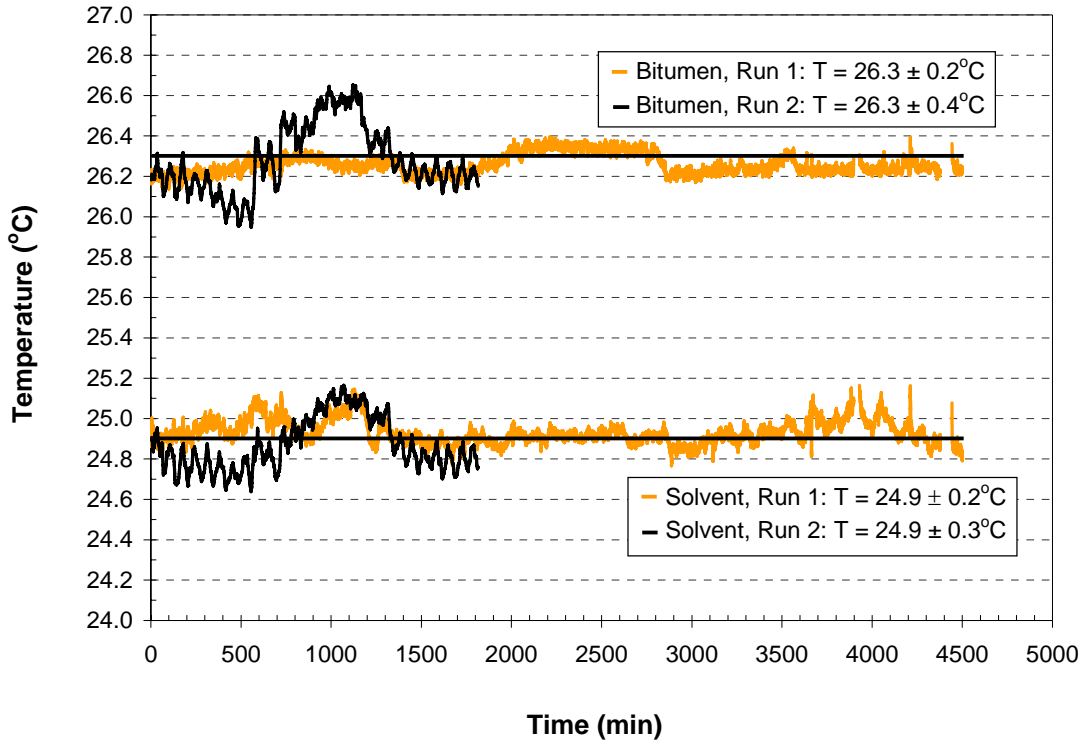


**Figure 4.3.4: Change in Height is Square Root Dependent on Time**

### 4.3.2 Experimental Error

The increase in bitumen and the decrease in solvent between the two runs correspond quite well. Fluctuations in the height readings are within the standard deviation of the replicates except for the last four measurements recorded for Run #2. These differences can be attributed to temperature fluctuations and not the precision of reading height measurements as shown from the temperature profiles in Figure 4.3.5. The increase in solvent and bitumen water bath temperatures between 750 to 1300 minutes could be the cause of the deviation in Run 2 data for the increase in bitumen (Figure 4.3.1) and decrease in solvent (Figure 4.3.2) heights observed between 1280 to 1732 minutes if there was a lag in response. The standard deviation in bitumen data between the two experiments during this time period is 0.54 mm. Likewise, the standard deviation between the two experiments for the solvent is 4.07 mm. At early times, up to 1280 minutes, the standard deviation is 0.19 mm for the bitumen and 2.08 mm for the solvent. The standard deviation for the bitumen and the solvent approximately doubles during the 1280 to 1732 minute range compared to earlier times. Clearly, the deviation between the two experimental runs is being affected by the temperature variation in the second experiment. It

would be preferential to have more responsive or finely tuned temperature controllers as well as having continuous data without time gaps.



**Figure 4.3.5: Temperature Profile for the Solvent and Bitumen Water Baths**

The error associated with replication of the experimental runs can be expressed as the standard deviation of the difference between the two replicates. The standard deviation for the difference in solvent decrease and for the difference in bitumen increase between the two replicates for both experimental runs are shown in Table 4.3.1. The standard deviation for the difference in height is less than 0.2 mm for the bitumen and solvent except for the Solvent Run #1. The 1.22 mm standard deviation for the Solvent Run #1 can't be explained but the difference in replicates appears to increase with time.

**Table 4.3.1: Average and Standard Deviation for the Differences in Height between the Replicate Experiments**

	Average Difference	Standard Deviation
<b>Solvent</b>		
Run 1	2.09 mm	1.22 mm
Run 2	0.62 mm	0.19 mm
<b>Bitumen</b>		
Run 1	0.16 mm	0.11 mm
Run 2	0.19 mm	0.12 mm

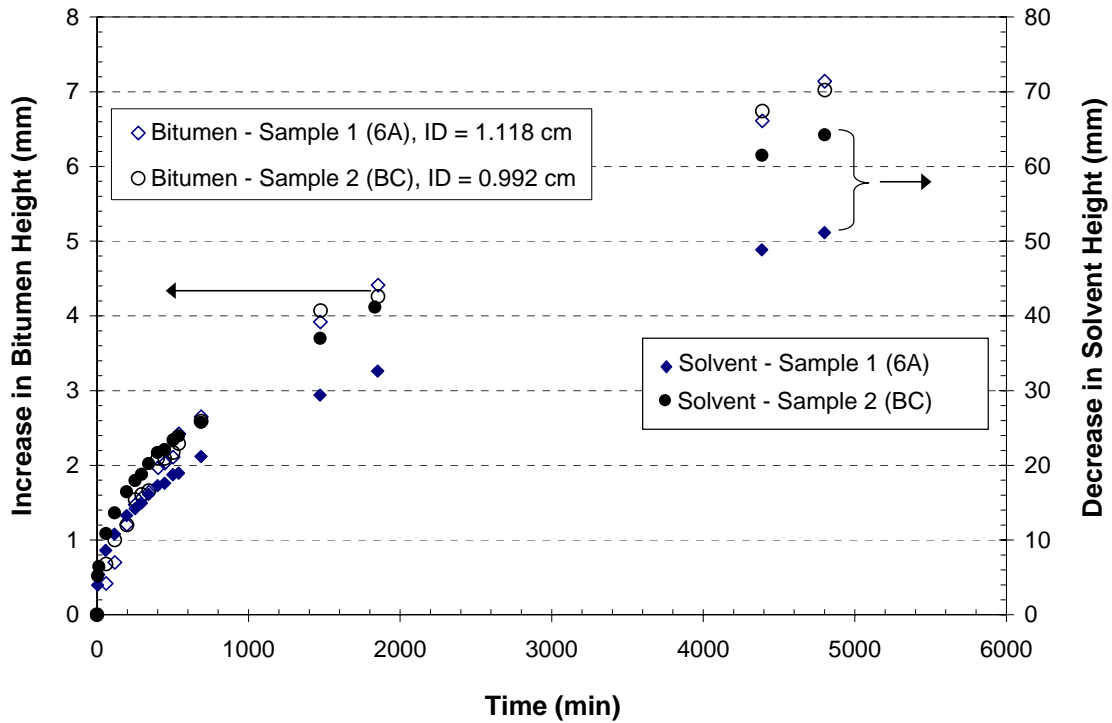
The precision in the height readings and the diameter of the bitumen and solvent tubes are shown in Table 4.3.2. One advantage of the experimental approach and mathematical model developed here is that it permits the monitoring of the change in height of the bitumen and solvent. Neither the experimental increase in bitumen nor the decrease in solvent is used as input into the mathematical model, as detailed in the next section. Error is minimised by comparing model prediction directly with the observed changes in height.

**Table 4.3.2: Experimental Error Propagation**

Measurement	Value (cm)	$\pm \delta d$ (cm)	Lower limit	Upper limit	Volume (cm <sup>3</sup> )	$\pm \delta V$ (cm <sup>3</sup> )	Source
<b>Height</b>	0.001	0.0005	0.0005	0.0015			Cathetometer precision
<b>Diameter</b>							
Small Bitumen	0.992	0.002	0.99	0.994	7.73E-04	3.9E-04	Average of measured values
Large Bitumen	1.118	0.008	1.11	1.126	9.82E-04	4.9E-04	Average of measured values
Solvent Capillary	0.3915	0.008	0.3835	0.3995	1.20E-04	6.0E-05	Average of measured values

Experimentally, independence of the increase in bitumen height on area was verified by running the diffusion experiment using different diameter bitumen tubes. The tubes used had inner diameters of  $1.118 \pm 0.008$  cm (bitumen tube 6A in Figure 4.3.6) and  $0.992 \pm 0.002$  cm (bitumen tube BC in Figure 4.3.6) resulting in a ratio of areas of 1.27 when the area of the larger tube is in the numerator. Figure 4.3.6 shows the experimental increase in bitumen height and decrease in solvent height. Over 4800 minutes, the increase in bitumen is the same irrespective of the area of the bitumen tube. Over the same time, the solvent for tube 6A (connected to the larger bitumen tube) decreased 64.24 mm while the solvent for tube BC (connected to the smaller bitumen tube) decreased 51.15 mm. The ratio of the decrease in solvent height is 1.26 which is in agreement with the ratio of bitumen tube areas.

The mathematical model, as described in the next section, assumes that the growth of the bitumen is independent of the cross-sectional area of the bitumen tube. The area of both the bitumen and the solvent is only used for the solvent mass balance. Once the system of equations is solved for the bitumen growth, and using the concentration of solvent at each nodal position within the bitumen, the mass of solvent and the corresponding decrease in solvent height is calculated knowing the area of the bitumen, area of the solvent and density of the liquid n-butane.



**Figure 4.3.6: Increase in Bitumen Height is Independent of Cross-Sectional Area**

#### 4.4 Mathematical Model

The mathematical model is a one-dimensional model that predicts the growth of the bitumen by guessing a diffusivity function and parameterizing the diffusivity function coefficients for which to optimise. The one-dimensional model (equations are developed with respect to the x-direction only) assumes neither a constant diffusivity nor a constant density as both vary with solvent concentration. The solvent concentration in the bitumen phase is a function of position and time. As the solvent diffuses into the bitumen, the bitumen swells with time and the viscosity of the bitumen exponentially decreases. The growth of the bitumen phase determined mathematically is compared to the growth of bitumen observed experimentally. The difference in bitumen growth (experimental – model) is minimised by optimising for the diffusivity function coefficients.

##### 4.4.1 Development of the Partial Differential Equations

The physical diffusion of solvent in heavy oil (shown in Figure 4.2.1) and the equations of continuity and mass conservation are used to develop the numerical model. Specifically, three equations make up the set of partial differential equations: 1) the solvent continuity equation, 2)

an expression to describe the mass average velocity ( $V^m$ ) in the solvent continuity equation derived from the solvent and overall continuity equations, and 3) the change in bitumen interface height derived from a macroscopic material balance on the solvent.

### **Solvent Continuity Equation**

The species continuity equation in a binary mixture without chemical reaction is shown in its fundamental form in equation 4.4.1 where the first term is the accumulation followed by the rate of net addition of solvent to bitumen due to convection in the second term and the rate of net addition by diffusion in the third term (Bird *et al.* 2002). The mass concentration of the solvent ( $\rho_s$ ) and the product of the overall phase density and mass average velocity ( $\rho V^m$ ) are shown in their differential forms where they are assumed to change with respect to time (t) and position (x) respectively. The mass average velocity is the average velocity of all species observed from a stationary point (Bird *et al.* 2002). The diffusivity of solvent (s) into bitumen (b) is denoted  $D_{sb}$  and  $\omega_s$  is the solvent mass fraction.

$$\frac{\partial(\rho_s)}{\partial t} + \frac{\partial}{\partial x}(\rho_s V^m) - \frac{\partial}{\partial x}\left(\rho D_{sb} \frac{\partial \omega_s}{\partial x}\right) = 0 \quad (4.4.1)$$

Sometimes, these terms can be assumed constant in cases of dilute diffusion or constant density systems. Neither is the case when a light hydrocarbon diffuses into heavy oil or bitumen to reach an average concentration of 0.3-0.4 mass fraction as found in laboratory scale VAPEX experiments (Oduntan 2001, James 2003, Friedrich 2005, Tam 2007). One can relate the mass concentration of the solvent ( $\rho_s$ ) to the mixture density and the solvent mass fraction, as follows:

$$\omega_s = \frac{\rho_s}{\rho_s + \rho_b} \rightarrow \rho_s = \omega_s \rho \quad (4.4.2)$$

The result of substituting equation 4.4.2 into equation 4.4.1 is:

$$\frac{\partial(\omega_s \rho)}{\partial t} + \frac{\partial}{\partial x}(\omega_s \rho V^m) - \frac{\partial}{\partial x}\left(\rho D_{sb} \frac{\partial \omega_s}{\partial x}\right) = 0 \quad (4.4.3)$$

Using the product rule, the first two terms are expanded to give:

$$\omega_s \frac{\partial \rho}{\partial t} + \rho \frac{\partial \omega_s}{\partial t} + \rho V^m \frac{\partial \omega_s}{\partial x} + \omega_s V^m \frac{\partial \rho}{\partial x} + \omega_s \rho \frac{\partial V^m}{\partial x} - \frac{\partial}{\partial x}\left(\rho D_{sb} \frac{\partial \omega_s}{\partial x}\right) = 0 \quad (4.4.4)$$

The overall continuity equation is the summation of the net accumulation and any changes in net accumulation due to convection.

$$\frac{\partial \rho}{\partial t} + \frac{\partial (\rho V^m)}{\partial x} = 0$$

$$\frac{\partial \rho}{\partial t} = -\rho \frac{\partial V^m}{\partial x} - V^m \frac{\partial \rho}{\partial x} \quad (4.4.5)$$

Substituting the overall continuity equation (equation 4.4.5) into the solvent continuity (equation 4.4.4) for  $\partial \rho / \partial t$  yields:

$$\rho \frac{\partial \omega_s}{\partial t} + \rho V^m \frac{\partial \omega_s}{\partial x} - \frac{\partial}{\partial x} \left( \rho D_{sb} \frac{\partial \omega_s}{\partial x} \right) = 0 \quad (4.4.6)$$

The solvent continuity shown in equation 4.4.6 relates the rate of overall increase of solvent in the bitumen phase to the rate of solvent addition by convection and by diffusion assuming there is no chemical reaction (Bird *et al.* 2002).  $\rho$  is the bitumen phase density ( $\text{kg/m}^3$ ,  $\text{g/cm}^3$ ),  $\omega_s$  is the solvent mass fraction,  $V^m$  (m/s, cm/s) is the mass average velocity and  $D_{sb}$  is the diffusivity of solvent into bitumen ( $\text{m}^2/\text{s}$ ,  $\text{cm}^2/\text{s}$ ). The product of the mass average velocity and the phase density ( $\rho V^m$ ) is the mass flux per unit volume ( $\text{kg/m}^2.\text{s}$ ,  $\text{g/cm}^2.\text{s}$ ). The solvent concentration is dependent on time and position within the bitumen phase. It is assumed that the diffusion of solvent into bitumen is a one-dimensional problem (in the downward x-direction) where the concentration is independent of the y and z coordinates.

$$\frac{\partial \omega_s}{\partial t} = -V^m \frac{\partial \omega_s}{\partial x} + \frac{1}{\rho} \frac{\partial}{\partial x} \left( \rho D_{sb} \frac{\partial \omega_s}{\partial x} \right) \quad (4.4.7)$$

Using the chain rule and assuming that the bitumen phase density ( $\rho$ ) and diffusivity ( $D_{sb}$ ) of solvent (s) into the bitumen (b) are both dependent on the solvent concentration, equation 4.4.7 becomes equation 4.4.8:

$$\frac{\partial \omega_s}{\partial t} = \frac{\partial \omega_s}{\partial x} \left[ \frac{D_{sb}}{\rho} \frac{\partial \rho}{\partial x} + \frac{\partial D_{sb}}{\partial x} - V^m \right] + D_{sb} \frac{\partial^2 \omega_s}{\partial x^2} \quad (4.4.8)$$

Ideal mixing is assumed and the bitumen phase density ( $\rho$ ) is shown in the following equation where  $v_s^*$  and  $v_b^*$  are the solvent and bitumen specific volumes ( $\text{cm}^3/\text{g}$ ).

$$\rho = \left[ \frac{1}{v_s^* \omega_s + v_b^* (1 - \omega_s)} \right]^{-1} \quad (4.4.9)$$

### **Mass Average Velocity, $V^m$**



The solvent continuity (equation 4.4.6) can be expressed in terms of  $\partial\rho/\partial t$  by multiplying the entire equation by  $\partial\rho/\partial\omega_s$  to yield:

$$\begin{aligned} \rho \frac{\partial\omega_s}{\partial t} \frac{\partial\rho}{\partial\omega_s} + \rho V^m \frac{\partial\omega_s}{\partial x} \frac{\partial\rho}{\partial\omega_s} - \frac{\partial\rho}{\partial\omega_s} \left[ \frac{\partial}{\partial x} \left( \rho D_{sb} \frac{\partial\omega_s}{\partial x} \right) \right] &= 0 \\ \rho \frac{\partial\rho}{\partial t} + \rho V^m \frac{\partial\rho}{\partial x} - \frac{\partial\rho}{\partial\omega_s} \left[ \frac{\partial}{\partial x} \left( \rho D_{sb} \frac{\partial\omega_s}{\partial x} \right) \right] &= 0 \end{aligned} \quad (4.4.10)$$

The expression in equation 4.4.5 for the overall continuity can be substituted into equation 4.4.10 and rearranged in terms of  $\partial V^m/\partial x$ :

$$\begin{aligned} \rho \left( -\rho \frac{\partial V^m}{\partial x} - V^m \frac{\partial\rho}{\partial x} \right) + \rho V^m \frac{\partial\rho}{\partial x} - \frac{\partial\rho}{\partial\omega_s} \left[ \frac{\partial}{\partial x} \left( \rho D_{sb} \frac{\partial\omega_s}{\partial x} \right) \right] &= 0 \\ -\rho^2 \frac{\partial V^m}{\partial x} - \rho V^m \frac{\partial\rho}{\partial x} + \rho V^m \frac{\partial\rho}{\partial x} - \frac{\partial\rho}{\partial\omega_s} \left[ \frac{\partial}{\partial x} \left( \rho D_{sb} \frac{\partial\omega_s}{\partial x} \right) \right] &= 0 \\ \frac{\partial V^m}{\partial x} = -\frac{1}{\rho^2} \frac{\partial\rho}{\partial\omega_s} \left[ \frac{\partial}{\partial x} \left( \rho D_{sb} \frac{\partial\omega_s}{\partial x} \right) \right] & \end{aligned} \quad (4.4.11)$$

The differential expression for the mass average velocity can be integrated over the range of  $x$ , i.e. over the height of bitumen at any given time:

$$V^m(x,t) = -\int_0^x \frac{1}{\rho^2} \frac{\partial\rho}{\partial\omega_s} \left[ \frac{\partial}{\partial x} \left( \rho D_{sb} \frac{\partial\omega_s}{\partial x} \right) \right] dx \quad (4.4.12)$$

The term  $1/\rho^2 \left( \partial\rho/\partial\omega_s \right)$  in the mass average velocity equation is simplified using the following integration rule:

$$-\frac{1}{\rho^2} \frac{\partial\rho}{\partial\omega_s} = \frac{\partial(1/\rho)}{\partial\omega_s} \quad (4.4.13)$$

Again, assuming ideal mixing, the change in density with respect to the solvent mass fraction can be related directly to the change in component specific volumes:

$$\begin{aligned} \frac{\partial(1/\rho)}{\partial\omega_s} &= \frac{\partial}{\partial\omega_s} \left[ \frac{1}{v_s^* \omega_s + v_b^* (1 - \omega_s)} \right]^{-1} = \frac{\partial}{\partial\omega_s} (v_s^* \omega_s + v_b^* - v_b^* \omega_s) \\ \frac{\partial(1/\rho)}{\partial\omega_s} &= (v_s^* - v_b^*) \end{aligned} \quad (4.4.14)$$

The resulting expression for the mass average velocity can be expanded using the chain rule to yield:

$$V^m(x,t) = (v_s^* - v_b^*) \int_0^x \left[ \frac{\partial}{\partial x} \left( \rho D_{sb} \frac{\partial \omega_s}{\partial x} \right) \right] dx \quad (4.4.15)$$

$$V^m(x,t) = (v_s^* - v_b^*) \int_0^x \left( D_{sb} \frac{\partial \rho}{\partial x} \frac{\partial \omega_s}{\partial x} + \rho \frac{\partial D_{sb}}{\partial x} \frac{\partial \omega_s}{\partial x} + \rho D_{sb} \frac{\partial^2 \omega_s}{\partial x^2} \right) dx \quad (4.4.16)$$

### **Increase in Bitumen Height**

The change in bitumen interface height, caused from the bitumen swelling from the addition of solvent, can be expressed as a function of solvent crossing the bitumen interface:

$$\frac{dm}{dt} = \frac{d}{dt} \left[ A \int_0^{x_s} \rho(x,t) dx \right] = A \left( \rho D_{sb} \frac{\partial \omega_s}{\partial x} \right) \Big|_{x=x_s} \quad (4.4.17)$$

The Leibniz integration rule is needed to perform the differentiation of the definite integral (shown in equation 4.4.17) where the limits of the integral are functions of the differentiable variable themselves. The Leibniz integration rule is as follows:

$$\frac{\partial}{\partial t} \int_{a(t)}^{b(t)} f(x,t) dx = \int_{a(t)}^{b(t)} \frac{\partial f}{\partial t} dx + \left( f(b,t) \frac{db}{dt} - f(a,t) \frac{da}{dt} \right) \quad (4.4.18)$$

The Leibniz rule applied to equation 4.4.17 is shown as:

$$\begin{aligned} \frac{d}{dt} \left[ A \int_0^{x_s(t)} \rho(x,t) dx \right] &= A \left[ \int_0^{x_s(t)} \frac{\partial \rho}{\partial t} dx + \rho(x_s,t) \frac{dx_s}{dt} - \rho(0,t) \frac{d0}{dt} \right] \\ \frac{d}{dt} \left[ A \int_0^{x_s(t)} \rho(x,t) dx \right] &= A \left[ \int_0^{x_s(t)} \frac{\partial \rho}{\partial t} dx + \rho(x_s,t) \frac{dx_s}{dt} \right] \end{aligned} \quad (4.4.19)$$

The result shown in equation 4.4.19 becomes the left hand side of equation 4.4.17 which is then isolated in terms of  $dx_s / dt$ , the change in bitumen interface height.

$$\begin{aligned} \int_0^{x_s(t)} \frac{\partial \rho}{\partial t} dx + \rho(x_s,t) \frac{dx_s}{dt} &= \left( \rho D_{sb} \frac{\partial \omega_s}{\partial x} \right) \Big|_{x=x_s} \\ \frac{dx_s}{dt} &= D_{sb} \frac{\partial \omega_s}{\partial x} \Big|_{x=x_s} - \frac{1}{\rho(x_s,t)} \int_0^{x_s(t)} \frac{\partial \rho}{\partial t} dx \end{aligned} \quad (4.4.20)$$

The partial derivative of the density with respect to time can be expressed as a definite derivative using the expression for ideal mixing.

$$\frac{\partial \rho}{\partial t} = \frac{d}{dt} \left( \frac{1}{\omega_s v_s^* + (1 - \omega_s) v_b^*} \right) \quad (4.4.21)$$

The quotient rule,

$$\frac{d}{dx} \left( \frac{f(x)}{g(x)} \right) = \frac{g(x) \frac{d}{dx} (f(x)) - f(x) \frac{d}{dx} (g(x))}{[g(x)]^2}, \quad (4.4.22)$$

is used to differentiate equation 4.4.21, to obtain:

$$\frac{\partial \rho}{\partial t} = \frac{- \left( (v_s^* - v_b^*) \frac{\partial \omega_s}{\partial t} \Big|_x \right)}{\left( \omega_s v_s^* + (1 - \omega_s) v_b^* \right)^2} = \frac{(v_b^* - v_s^*) \frac{\partial \omega_s}{\partial t} \Big|_x}{\left( \omega_s v_s^* + (1 - \omega_s) v_b^* \right)^2} \quad (4.4.23)$$

The inverse of the denominator is the density and in substituting it into equation 4.4.23, equation 4.4.24 is obtained for the partial derivative of the solution density with time.

$$\rho^2 = \frac{1}{\left( \omega_s v_s^* + (1 - \omega_s) v_b^* \right)^2}$$

$$\frac{\partial \rho}{\partial t} = \rho^2 (v_b^* - v_s^*) \frac{\partial \omega_s}{\partial t} \Big|_x \quad (4.4.24)$$

Finally, the result is substituted back into the expression for the change in bitumen height with time, equation 4.4.20, to yield:

$$\frac{dx_s}{dt} = \left( D_{sb} \frac{\partial \omega_s}{\partial x} \right) \Big|_{x=x_s} - \frac{(v_b^* - v_s^*) x_s(t)}{\rho(x_s, t)} \int_0^{x_s(t)} \rho^2 \frac{\partial \omega_s}{\partial t} \Big|_x dx \quad (4.4.25)$$

In summary, the predicted change in bitumen height is derived from equation 4.4.17 involving the product of the diffusivity, the concentration gradient at the bitumen-solvent interface and the density at the interface, which is constant due to the equilibrium concentration boundary condition. In the final form of this equation derived to explicitly calculate the change in interface height with time, shown in equation 4.4.25, the integrated density profile is expanded using the Leibniz integration rule, the definition for ideal mixture density and the quotient rule. The result is that the overall change in density with respect to time over the entire depth is derived in terms

of the density profile and the change in solvent mass fraction with respect to time which is subtracted from the product of the diffusivity and concentration gradient taken at the interface.

The partial differential equations for the solvent continuity, mass average velocity and the change in bitumen interface height (equations 4.4.8, 4.4.15 and 4.4.25, respectively) are transformed, discretized and simultaneously solved in Matlab (R2006a) to predict the change in bitumen height in time. The next sections discuss the transformation of the x-position variable and the discretization of the equations.

#### 4.4.2 Dimensionless Position ( $\xi=x/x_s(t)$ )

The depth or x-dimension in the set of partial differential equations developed in the previous section is made dimensionless in order to fix the bitumen height and spatial coordinates according to a “front-fixing method” first proposed by Landau (1950) and described by Crank (1984). Otherwise, without the transformation, the interface position would change with time. Resolving time derivatives with respect to a changing spatial coordinate is more complicated. The advantage of transforming the space coordinate to a fixed position is that the interface and the solution at the boundary are maintained at a fixed grid point. The x-dimension is made dimensionless by introducing a dimensionless variable  $\xi$ :

$$\xi = \frac{x}{x_s(t)} \quad (4.4.26)$$

The height of the bitumen interface ( $\xi$ ) is always equal to one and equation 4.4.27 shows the transformation of the required derivatives.

$$dx = x_s d\xi, \quad \frac{\partial \omega_s}{\partial x} = \frac{1}{x_s(t)} \frac{\partial \omega_s}{\partial \xi}, \quad \text{and} \quad \frac{\partial^2 \omega_s}{\partial x^2} = \frac{1}{x_s(t)^2} \frac{\partial^2 \omega_s}{\partial \xi^2} \quad (4.4.27)$$

The resulting set of partial differential equations as a function of dimensionless position ( $\xi$ ) comes from substituting equations 4.4.26 and 4.4.27 into equations 4.4.8, 4.4.15 and 4.4.25 respectively.

#### **Solvent Continuity Equation**

The solvent continuity is given by:

$$\frac{\partial \omega_s}{\partial t} \Big|_x = \frac{1}{x_s(t)} \frac{\partial \omega_s}{\partial \xi} \left[ \frac{D_{sb}}{\rho x_s(t)} \frac{\partial \rho}{\partial \xi} + \frac{1}{x_s(t)} \frac{\partial D_{sb}}{\partial \xi} - V^m \right] + \frac{D_{sb}}{(x_s(t))^2} \frac{\partial^2 \omega_s}{\partial \xi^2} \quad (4.4.28)$$

However, the partial derivative for the change in solvent concentration with respect to time at a given x-position,  $(\partial\omega_s/\partial t)|_x$ , must also be transformed to the partial derivative for the change in solvent concentration with respect to time for a given dimensionless  $\xi$ -position,  $(\partial\omega_s/\partial t)|_\xi$ . This is accomplished knowing the change in interface height with respect to time,  $(dx_s/dt)$ .

$$\frac{\partial\omega_s}{\partial t}\Big|_x = -\frac{\xi}{x_s(t)}\frac{dx_s}{dt}\frac{\partial\omega_s}{\partial\xi} + \frac{\partial\omega_s}{\partial t}\Big|_\xi \quad (4.4.29)$$

The solvent continuity equation (equation 4.4.8), at a given dimensionless  $\xi$ -position and in terms of dimensionless  $\xi$ , is shown in the following equation.

$$\begin{aligned} \frac{\partial\omega_s}{\partial t}\Big|_\xi &= \frac{\xi}{x_s(t)}\frac{\partial x_s}{\partial t}\frac{\partial\omega_s}{\partial\xi} + \frac{1}{x_s(t)}\frac{\partial\omega_s}{\partial\xi}\left[\frac{D_{sb}}{\rho x_s(t)}\frac{\partial\rho}{\partial\xi} + \frac{1}{x_s(t)}\frac{\partial D_{sb}}{\partial\xi} - V^m\right] \\ &+ \frac{D_{sb}}{(x_s(t))^2}\frac{\partial^2\omega_s}{\partial\xi^2} \end{aligned} \quad (4.4.30)$$

### **Mass Average Velocity, $V^m$**

The mass average velocity, in its differential and expanded forms (equations 4.4.15 and 4.4.16), in terms of dimensionless  $\xi$  are:

$$V^m(x,t) = (v_s^* - v_b^*) \int_0^\xi \left[ \frac{\partial}{\partial \xi} \left( \frac{\rho D_{sb}}{x_s(t)} \frac{\partial \omega_s}{\partial \xi} \right) \right] d\xi \quad (4.4.31)$$

$$V^m(x,t) = (v_s^* - v_b^*) \int_0^\xi \left( \frac{D_{sb}}{x_s(t)} \frac{\partial \rho}{\partial \xi} \frac{\partial \omega_s}{\partial \xi} + \frac{\rho}{x_s(t)} \frac{\partial D_{sb}}{\partial \xi} \frac{\partial \omega_s}{\partial \xi} + \frac{\rho D_{sb}}{x_s(t)} \frac{\partial^2 \omega_s}{\partial \xi^2} \right) d\xi \quad (4.4.32)$$

### **Increase in Bitumen Height**

The derivative for the change in bitumen interface height with respect to time, equation 4.4.25 is given in terms of dimensionless  $\xi$ . Equation 4.4.29 is used to transform the partial derivative for the mass fraction with respect to time.

$$\frac{dx_s}{dt} = \frac{D_{sb}}{x_s(t)} \frac{\partial \omega_s}{\partial \xi} \Big|_{\xi=1} - \frac{(v_b^* - v_s^*)}{\rho(x_s,t)} \int_0^1 \rho^2 \left[ \frac{-\xi}{x_s(t)} \frac{dx_s}{dt} \frac{\partial \omega_s}{\partial \xi} + \frac{\partial \omega_s}{\partial t} \Big|_{\xi} \right] x_s(t) d\xi \quad (4.4.33)$$

Equation 4.4.33 becomes an implicit equation where  $dx_s/dt$  exists on both the left and right hand sides of the equation. The right hand side is approximated using the results from the previous time step.

## **4.4.3 Discretized Set of Equations**

The method of lines is used to discretize dimensionless  $\xi$  and transform the set of partial differential equations (represented by equations 4.4.30, 4.4.32 and 4.4.33) to an approximate set of ordinary differential equations where the remaining independent variable is time. Equation 4.4.33 is discretized except for two terms on the right hand side; the change in solvent concentration with respect to time,  $\partial \omega_s / \partial t$ , and the change in interface height with respect to time,  $dx_s / dt$ . Numerically, the solvent continuity equation comes before the change in bitumen height and the result is used for the right hand side of equation 4.4.33.  $dx_s / dt$  is approximated from the last time step. The partial derivatives for density, solvent mass fraction, and diffusivity with respect to  $\xi$  ( $\partial \rho / \partial \xi$ ,  $\partial \omega_s / \partial \xi$ ,  $\partial^2 \omega_s / \partial \xi^2$ , and  $\partial D_{sb} / \partial \xi$ ) are discretized using the following finite difference methods. The domain over which the equations have been discretized is  $0 \leq x \leq x_s(t)$  or  $0 \leq \xi \leq 1$ , with  $n$  spatial segments and  $n+1$  nodes (i).

### **Central Difference Method:**

$$\frac{\partial \omega_s}{\partial \xi} = \frac{\omega_s^{i+1} - \omega_s^{i-1}}{2\Delta\xi} \quad (4.4.34)$$

### **3-Point Backwards Difference Method:**

$$\frac{\partial \omega_s}{\partial \xi} = \frac{3\omega_s^{i+1} - 4\omega_s^i + \omega_s^{i-1}}{2\Delta\xi} \quad (4.4.35)$$

### **2<sup>nd</sup> Order Central Difference Method:**

$$\frac{\partial^2 \omega_s}{\partial \xi^2} = \frac{\omega_s^{i+1} - 2\omega_s^i + \omega_s^{i-1}}{(\Delta\xi)^2} \quad (4.4.36)$$

### **2<sup>nd</sup> Order Backwards Difference Method:**

$$\frac{\partial^2 \omega_s}{\partial \xi^2} = \frac{2\omega_s^{i+1} - 5\omega_s^i + 4\omega_s^{i-1} - \omega_s^{i-2}}{(\Delta\xi)^2} \quad (4.4.37)$$

### **Solvent Continuity Equation**

The dimensionless  $\xi$  form of the solvent continuity (equation 4.4.30) becomes the following three equations in discrete form.

### **Positions Throughout the Bitumen Phase, for $i = 2:z$ :**

$$\begin{aligned} \frac{d\omega_s}{dt} \Big|_i &= \left[ \frac{(i-1)\Delta\xi}{x_s} \right] \left[ \frac{\omega_s^{i+1} - \omega_s^{i-1}}{2\Delta\xi} \right] \frac{dx_s}{dt} + \frac{1}{x_s} \left[ \frac{\omega_s^{i+1} - \omega_s^{i-1}}{2\Delta\xi} \right] * \\ &\left\{ \left( \frac{D_{sb}(\omega_s^i)}{\rho(\omega_s^i).x_s} \right) \left( \frac{\rho(\omega_s^{i+1}) - \rho(\omega_s^{i-1})}{2\Delta\xi} \right) + \frac{1}{x_s} \left( \frac{D_{sb}(\omega_s^{i+1}) - D_{sb}(\omega_s^{i-1})}{2\Delta\xi} \right) - V^m(\xi) \right\} \\ &+ \left( \frac{D_{sb}(\omega_s^i)}{(x_s)^2} \right) \left( \frac{\omega_s^{i+1} - 2\omega_s^i + \omega_s^{i-1}}{(\Delta\xi)^2} \right) \end{aligned} \quad (4.4.38)$$

### **No Flux Boundary, $\xi = 0, i = 1$ :**

$$\frac{d\omega_s}{dt} \Big|_{i=1} = \left( \frac{2D_{sb}(\omega_s^i)}{(x_s)^2} \right) \left( \frac{\omega_s^{i+1} - \omega_s^i}{(\Delta\xi)^2} \right) \quad (4.4.39)$$

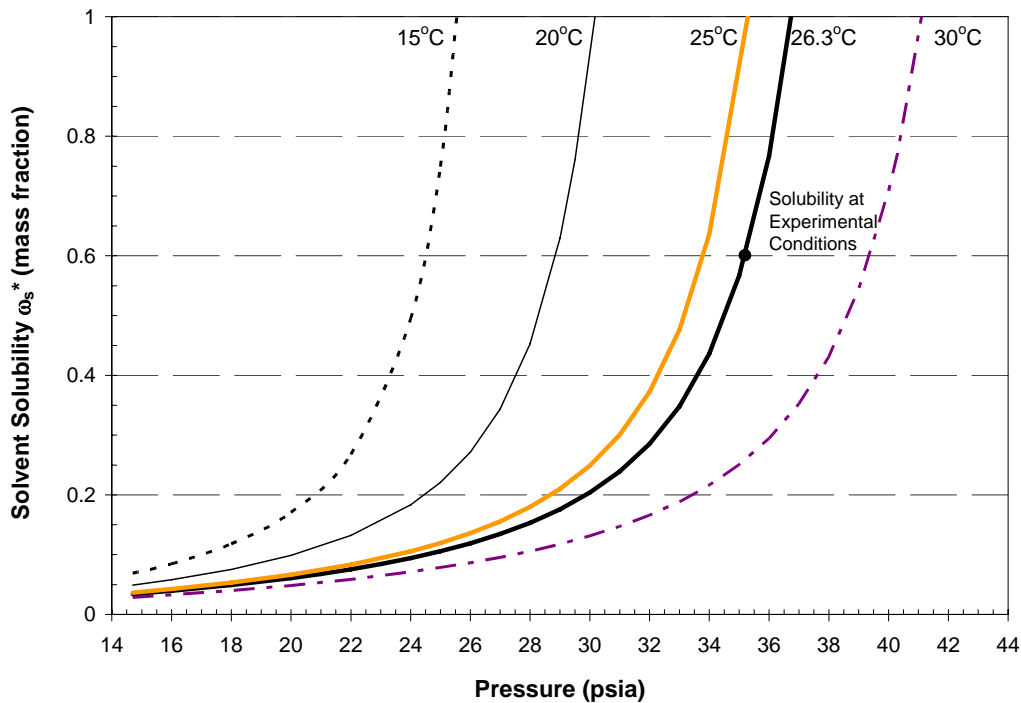
**At the Bitumen-Solvent Vapour Interface,  $\xi = 1, i = n+1$ :**

$$\left. \frac{d\omega_s}{dt} \right|_{i=n+1} = 0 \quad (4.4.40)$$

Another condition at the bitumen-solvent vapour interface is that the interfacial concentration ( $\omega_s^{n+1}$ ) is assumed to have reached equilibrium immediately after times greater than zero. The concentration at the interface is assumed to be the solubility ( $\omega_s^*$ ) of solvent in bitumen at the temperature of the bitumen and the vapour pressure of the solvent.

$$\omega_s^{n+1} = 0.6 \quad (4.4.41)$$

The solubility limit was estimated using the Peng-Robinson equation of state (PR EOS) in Aspen Plus (version 2006). The solubility mole fraction of n-butane in n-decane in the liquid phase at an equilibrium pressure of 30 psia (206.8 kPa) and 298K was in agreement with the liquid mole fraction predicted from known K-values (Kyle). An assay for Athabasca bitumen closely approximating the bitumen used was entered in Aspen and the solubility of n-butane in the bitumen was found to be 0.60 mass fraction or 0.95 mole fraction for the experimental temperature and pressure ( $T = 26.3^\circ\text{C}$ ,  $P = 242.5 \text{ kPa}$  or  $35.177 \text{ psia}$ ).



**Figure 4.4.1: Solubility Predicted using the PR EOS for n-Butane in Athabasca Bitumen**



The same diffusion apparatus was used to experimentally find the solubility of n-butane in the bitumen at the same experimental conditions. Instead of loading the bitumen in the bottom of the bitumen tube, a thin layer was smeared on the upper walls to increase the area for mass transfer. As the butane diffused into the bitumen it drained by gravity to the bottom of the vial thereby increasing mixing and thus mass transfer. Experimentally, the solubility was determined to be 0.6 mass fraction at 26.3°C and 35.177 psia.

### **Mass Average Velocity, $V^m$**

The mass average velocity in equation 4.4.32 is discretized using the trapezoidal rule combined with the difference approximations. The trapezoidal rule, with n being the number of segments, is given as:

$$\int_a^b f(x)dx \cong \left(\frac{h}{2}\right)(f(a)+f(b))+h\sum_{i=1}^n f(x_n) \quad \text{where } h = \frac{b-a}{n} \quad (4.4.42)$$

$$V^m \cong (v_s^* - v_b^*) \left(\frac{(i-1)\Delta\xi}{2(i-1)}\right)(f(a)+f(b))+\left(\frac{(i-1)\Delta\xi}{(i-1)}\right)\sum_{i=1}^n f(\xi_i) \quad (4.4.43)$$

$$f(a) = f(0) = 0 \quad (4.4.44)$$

$$\begin{aligned} f(\xi^i) = & \left(\frac{D_{sb}(\omega_s^i)}{x_s}\right) \left(\frac{\rho(\omega_s^{i+1}) - \rho(\omega_s^{i-1})}{2\Delta\xi}\right) \left(\frac{\omega_s^{i+1} - \omega_s^{i-1}}{2\Delta\xi}\right) + \\ & \left(\frac{\rho(\omega_s^i)}{x_s}\right) \left(\frac{D_{sb}(\omega_s^{i+1}) - D_{sb}(\omega_s^{i-1})}{2\Delta\xi}\right) \left(\frac{\omega_s^{i+1} - \omega_s^{i-1}}{2\Delta\xi}\right) + \\ & \left(\frac{\rho(\omega_s^i)D_{sb}(\omega_s^i)}{x_s}\right) \left(\frac{\omega_s^{i+1} - 2\omega_s^i + \omega_s^{i-1}}{(\Delta\xi)^2}\right) \end{aligned} \quad (4.4.45)$$

$$\begin{aligned} f(1) = & \left(\frac{D_{sb}(\omega_s^{n+1})}{x_s}\right) \left(\frac{3\rho(\omega_s^{n+1}) - 4\rho(\omega_s^n) + \rho(\omega_s^{n-1})}{2\Delta\xi}\right) \left(\frac{3\omega_s^{n+1} - 4\omega_s^n + \omega_s^{n-1}}{2\Delta\xi}\right) \\ & + \left(\frac{\rho(\omega_s^{n+1})}{x_s}\right) \left(\frac{3D_{sb}(\omega_s^{n+1}) - 4D_{sb}(\omega_s^n) + D_{sb}(\omega_s^{n-1})}{2\Delta\xi}\right) * \\ & \left(\frac{3\omega_s^{n+1} - 4\omega_s^n + \omega_s^{n-1}}{2\Delta\xi}\right) + \left(\frac{\rho(\omega_s^{n+1})D_{sb}(\omega_s^{n+1})}{x_s}\right) \left(\frac{\omega_s^{n+1} - 2\omega_s^n + \omega_s^{n-1}}{(\Delta\xi)^2}\right) \end{aligned} \quad (4.4.46)$$

The mass average velocity needs to be integrated from the no flux boundary at  $\xi = 0$ . The upper limit of the integral (b) is dependent on the position within the bitumen phase (node) being evaluated. If the  $\xi$  position is at a nodal position below the interface the central finite difference can be used, i.e. from node  $i = 2:n$ . However, at the interface,  $i = n+1$ , the backward difference method must be used. Logic is developed to handle the limit regardless of the numerical integration used for  $f(b)$ .

### **Increase in Bitumen Height**

Equation 4.4.33 for the increase in bitumen height is discretized using the trapezoidal rule and finite differences in a similar fashion as the mass average velocity, shown in the following equations (equations 4.4.47 - 4.4.51). However, the upper limit of the integral is always  $\xi = 1$  where backwards differences are used instead of central differences.

$$\frac{dx_s}{dt} = \left( \frac{D_{sb}(\omega_s^{n+1})}{x_s} \right) \left( \frac{3\omega_s^{n+1} - 4\omega_s^n + \omega_s^{n-1}}{2\Delta\xi} \right) - \frac{x_s(v_b^* - v_s^*)}{\rho(\omega_s^{n+1})} * \text{integral} \quad (4.4.47)$$

$$\text{integral} \cong \left( \frac{1}{2n} \right) (f(a) + f(b)) + \left( \frac{1}{n} \right) \sum_{i=2}^n f(\xi_i) \quad (4.4.48)$$

node 1

$$f(a) = f(0) = \rho(\omega_s^1)^2 \left( \frac{\partial \omega_s}{\partial t} \Big|_{\xi=0} \right) \quad (4.4.49)$$

node n+1

$$f(b) = f(1) = \rho(\omega_s^{n+1})^2 \left[ \frac{-1}{x_s} \left( \frac{dx_s}{dt} \right) \left( \frac{3\omega_s^{n+1} - 4\omega_s^n + \omega_s^{n-1}}{2\Delta\xi} \right) + \left( \frac{\partial \omega_s}{\partial t} \Big|_{\xi=1} \right) \right] \quad (4.4.50)$$

node  $i = 2:n$

$$f(\xi^i) = \rho(\omega_s^i)^2 \left[ \left( \frac{-(i-1)\Delta\xi}{x_s} \right) \left( \frac{dx_s}{dt} \right) \left( \frac{\omega_s^{i+1} - \omega_s^{i-1}}{2\Delta\xi} \right) + \left( \frac{\partial\omega_s}{\partial t} \Big|_{\xi=i} \right) \right] \quad (4.4.51)$$

#### 4.4.4 Change in Solvent Height

A macroscopic mass balance is used to predict the change in solvent height after the bitumen growth has been resolved for the entire time duration. The summation of the solvent concentration profile resolved for each discretized segment throughout the depth of the bitumen phase gives the mass of solvent in the bitumen at a given time.

$$m_s(t) = A_b \int_0^{x_s(t)} \rho\omega_s dx \quad (4.4.52)$$

The mass of solvent is used to calculate the predicted change in solvent height knowing the cross-sectional area of the bitumen tube ( $A_b$ ) and the cross-sectional area of the solvent capillary ( $A_s$ ) as well as the density of the solvent at the experimental conditions.

$$h_s(t) = \frac{m_s}{\rho_s A_s} \quad (4.4.53)$$

The two above equations are one of the key and unique features of this experimental and mathematical development. Once the discretized set of equations for the solvent continuity, mass average velocity and increase in bitumen height are solved for simultaneously (equations 4.4.30 – 4.4.51), the concentration and density profiles are used to predict the mass and subsequently decrease in liquid solvent height. The predicted decrease in solvent height (which is a result of the mathematical solution) is compared to the experimentally observed decrease in solvent height, as shown in Figure 4.6.2. This independent validation of the optimised mathematical solution differentiates the approach taken here compared to those reviewed in the Literature section.

#### 4.4.5 Numerical Model Methodology

The uniqueness in the overall approach used to find the diffusivity of solvent in bitumen is that the numerical results are independently validated! Trial and error was used to choose the type of diffusivity function where the predicted bitumen growth and solvent decrease were compared qualitatively to experimental results. The coefficients of the proposed diffusivity function are set as parameters for which to optimise. The difference in experimental and predicted growth of the bitumen is used as the objective function and minimised in order to optimise the linear diffusivity

coefficients  $p_1$  and  $p_2$ . When using the “lsqnonlin – least squares nonlinear” optimisation option in Matlab, the objective function is minimised automatically. The decrease in solvent is not used in the objective function and is used as independent validation of the solvent diffusivity.

$$D_{sb} = p_1 \omega_s + p_2 \quad (4.4.54)$$

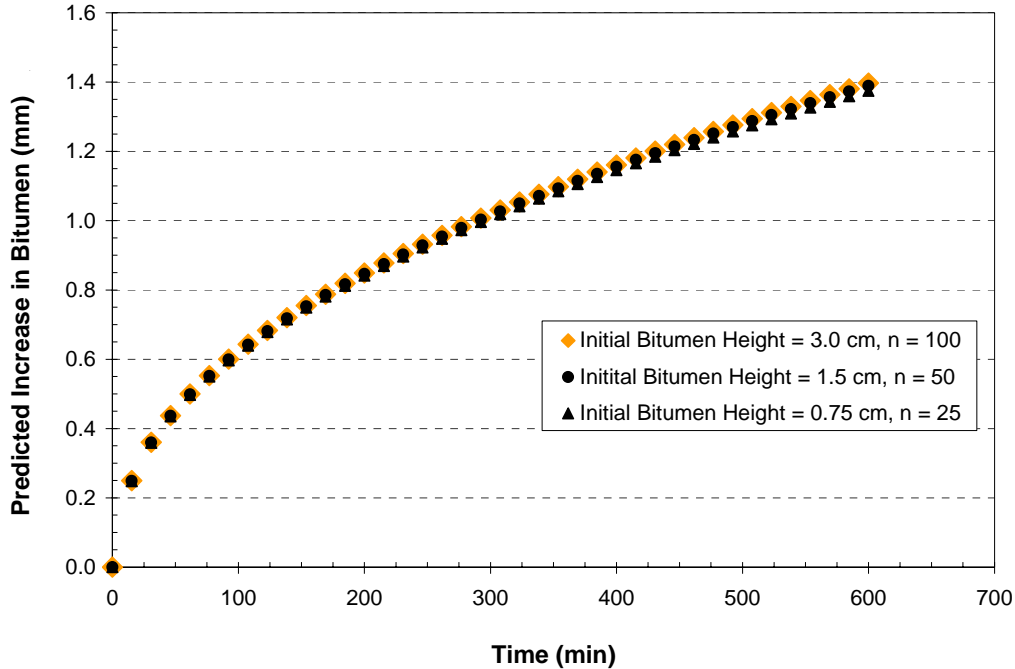
$$f_{objective} = \frac{(h_b)_{experimental} - (h_b)_{predicted}}{(h_b)_{experimental}} \quad (4.4.55)$$

Lower and upper bounds on the diffusivity coefficients were set to be  $1 \times 10^{-07}$  and  $1 \times 10^{-05}$  respectively. The optimisation terminates successfully when the log-likelihood objective function or parameter tolerances are minimised to less than  $1 \times 10^{-8}$ .

## 4.5 Model Validation

The numerical model was first validated to ensure consistent numerical results before being used to predict the diffusivity coefficients. Using a constant diffusivity of  $D_{sb} = 1 \times 10^{-5} \text{ cm}^2/\text{s}$ , the model results were compared to ensure that the increase in bitumen height and the concentration profile were equivalent, independent of number of nodes and initial height of bitumen. Figure 4.5.1 shows that the model predictions are equivalent independent of initial height of bitumen.

There are minimal differences in the predicted increase of bitumen height between the three initial heights used to validate the model. The difference increases slightly with time due to increasing solvent concentration throughout the bitumen and the evaluation of the derivatives at the nodes. However, at 600 minutes, the greatest difference between the 0.75 cm and 3.0 cm initial heights is only 0.022 mm, constituting a difference of 1.6%.



**Figure 4.5.1: Predicted Increase in Bitumen as a function of Time & Initial Height**

## 4.6 Comparison and Discussion

The mathematical model was used to optimise the linear diffusivity coefficients by minimising the difference in predicted bitumen increase and experimentally observed bitumen increase, as shown in equation 4.4.57. The resulting diffusivity for n-butane (at 24.9°C) in Athabasca bitumen (at 26.3°C) was found to be:

$$D_{sb} (cm^2 / s) = 4.78 \times 10^{-6} \omega_s + 4.91 \times 10^{-6} \quad (4.6.1)$$

The comparison between the experimental and model results for both the bitumen and the solvent are shown in Figure 4.6.1 and Figure 4.6.2 respectively. The optimisation, for the increase in bitumen height, terminated with a first order optimality of  $1.6 \times 10^{-3}$  and a sum of squared residuals of  $6.9 \times 10^{-3}$ . The coefficients found through the optimisation,  $p_1 = 4.78 \times 10^{-6}$  and  $p_2 = 4.91 \times 10^{-6}$  were verified independently by comparing the predicted decrease in solvent height with the experimentally observed values, as shown in Figure 4.6.2.

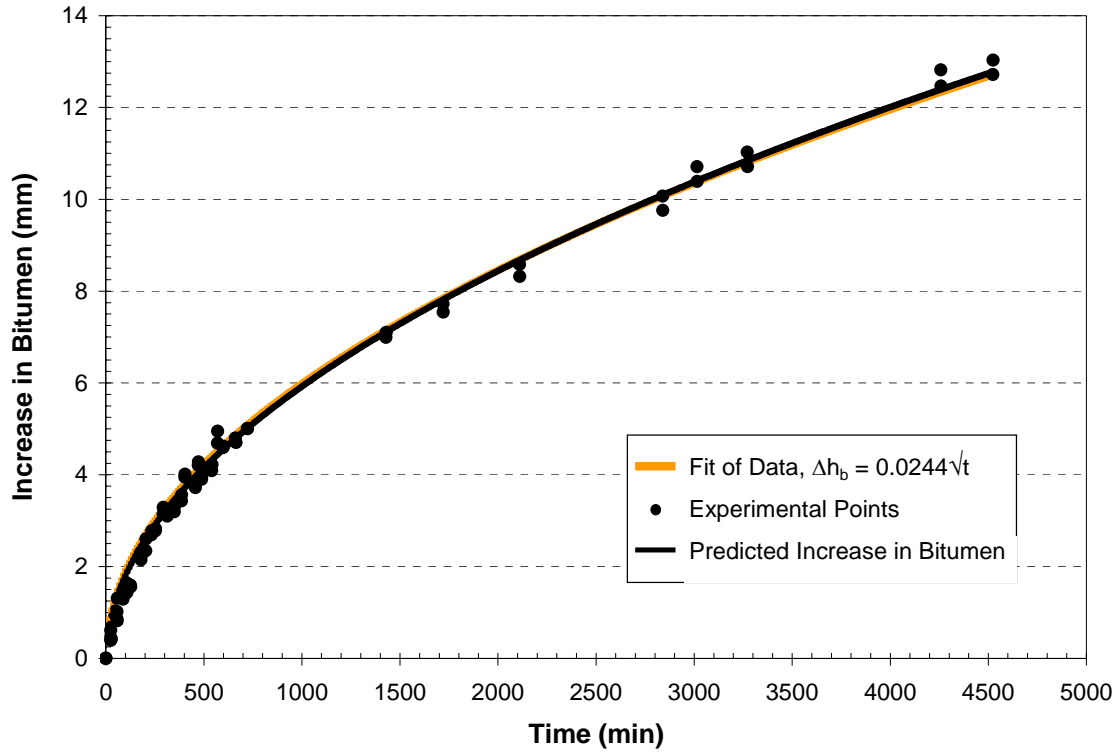


Figure 4.6.1: Bitumen Increase - Comparison of Experimental and Model Results

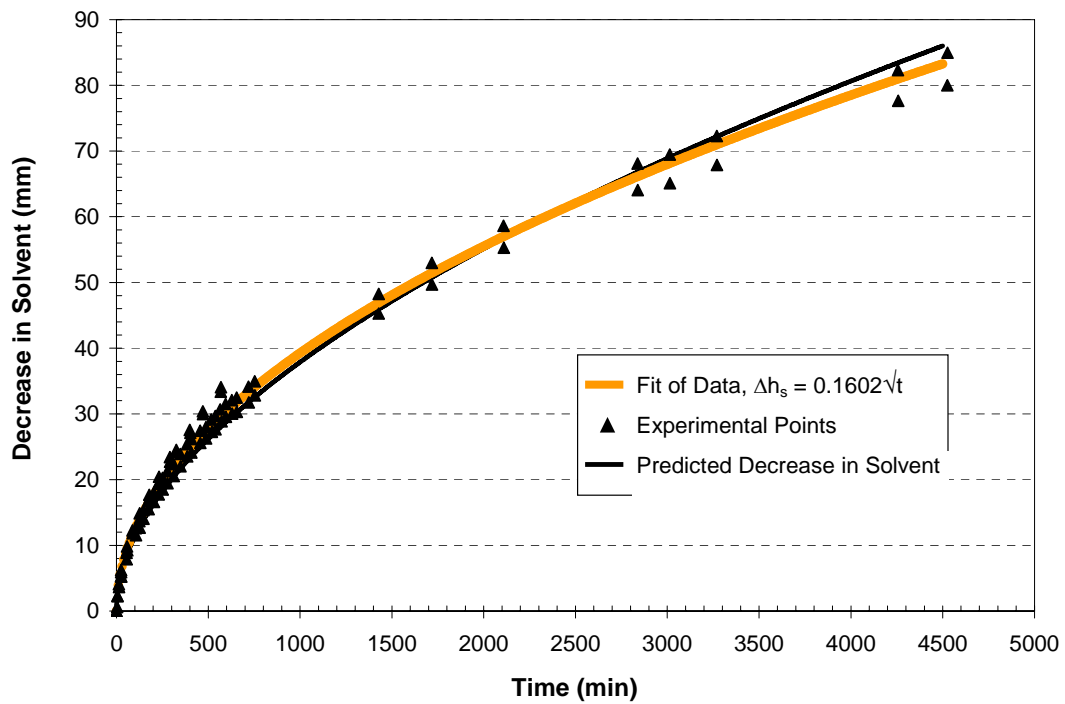
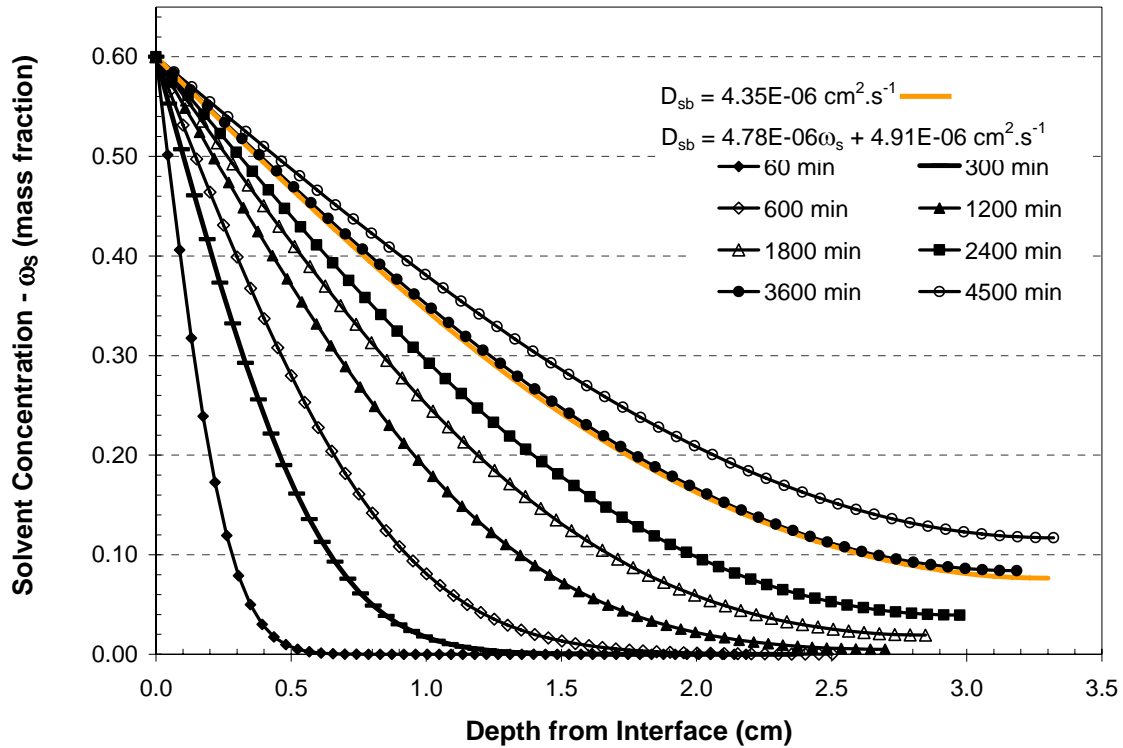


Figure 4.6.2: Solvent Decrease - Comparison of Experimental and Model Results



**Figure 4.6.3: Predicted Concentration Profiles**

The mathematically predicted decrease in solvent height from the macroscopic mass balance shown in equations 4.4.52 and 4.4.53 is compared with the experimentally observed decrease in solvent height. While slight variations in the diffusivity coefficients can fit the increase in bitumen, only the diffusivity given in equation 4.6.1 is able to independently predict the decrease in solvent as well (Figure 4.6.1 and Figure 4.6.2). Figure 4.6.3 shows the predicted concentration profiles at different times and clearly shows that the interfacial concentration at the bitumen-solvent interface is kept at its boundary condition of the solubility of n-butane in Athabasca bitumen at 26.3°C, i.e. 0.60 mass fraction. Initially, in the first 60 minutes, the solvent only reaches 0.5 cm from the bitumen-solvent interface including the 0.1 cm increase in height of the bitumen due to swelling. It is not until after 1200 minutes (20 hours) that the solvent reaches the no-flux boundary at the bottom of the bitumen tube. At the final time of 4500 minutes, the solvent concentration at the bottom has reached 0.11 mass fraction. The concentration profile for the best fit constant diffusion coefficient ( $4.35 \times 10^{-6} \text{ cm}^2/\text{s}$ ) is shown as reference where the optimised increase in bitumen height is shown in Figure 4.6.5. Figure 4.6.3 shows that the constant diffusivity at the final time of 4500 minutes has a concentration of solvent throughout the bitumen similar to the linear diffusivity at 3600 minutes. Despite the elevated concentration

profile, the diffusion coefficient is the “best fit” between the experimental and predicted increase in bitumen height (as shown in Figure 4.6.5). Figure 4.6.6 shows that the decrease in solvent height is clearly over-predicted using the optimised constant diffusion coefficient.

Two popular empirical models for estimating the mutual diffusivity of liquids are the Vignes (1966) and the Leffler and Cullinan (1970) equations shown in equations 4.6.2 and 4.6.3. The two extreme diffusivities,  $D_{sb}^o$  and  $D_{bs}^o$  should represent the infinite dilution diffusivity of the solvent into the bitumen and the bitumen into the solvent respectively.  $X_s$  and  $X_b$  are the mole fractions of solvent and bitumen respectively. The solvent, bitumen and mixture viscosities are shown as  $\mu_s$ ,  $\mu_b$  and  $\mu_{mix}$  respectively.  $\beta$  is a thermodynamic correction factor accounting for gradients in chemical potential rather than composition for non-ideal mixtures. In the case of ideal mixtures, assumed here,  $\beta$  is unity.

$$D_{sb} = D_{bs}^o X_s D_{sb}^o X_b \beta \quad (4.6.2)$$

$$D_{sb} \mu_{mix} = \left( D_{bs}^o \mu_s \right)^{X_s} \left( D_{sb}^o \mu_b \right)^{X_b} \beta \quad (4.6.3)$$

Both the Vignes and Leffler and Cullinan diffusivity equations were tried in the numerical model to determine the infinite dilution coefficients. The optimised coefficients are shown in Table 4.6.1. Figure 4.6.4 shows the diffusivities as a function of solvent concentration for the three optimised diffusivity functions. The infinite dilution diffusion coefficients can sometimes be estimated using the Stokes-Einstein equation or the Wilke-Chang equation that is based on the Stokes-Einstein equation (Bird *et al.* 2002). The Stokes-Einstein equation was derived for large hard spherical molecules diffusing into a low molecular weight liquid and thus  $D_{bs}^o$  is estimated to be  $4.32 \times 10^{-5} \text{ cm}^2/\text{s}$ . The optimised infinite dilution diffusion coefficients of  $7.54 \times 10^{-6}$  and  $9.05 \times 10^{-6} \text{ cm}^2/\text{s}$  for the respective Vignes and Leffler and Cullinan correlations are on the same order of magnitude. Using the Wilke-Chang correlation, the infinite dilution diffusivity for solvent into bitumen,  $D_{sb}^o$ , is predicted to be  $1.41 \times 10^{-10} \text{ cm}^2/\text{s}$ . This is several orders of magnitude smaller than the optimised parameter using either the Vignes or Leffler and Cullinan correlations.

Figure 4.6.4 shows that the optimised diffusivity functions are quite different over the range of solvent concentration. At the two extremes, the diffusivity coefficients represent the infinite

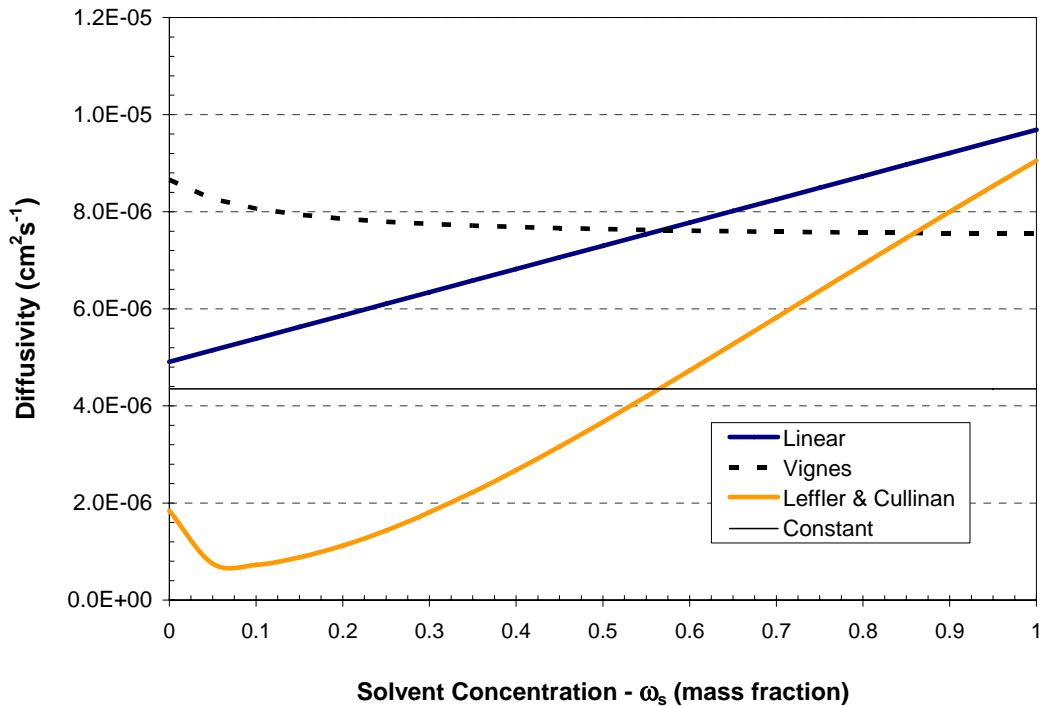


dilution diffusivity in the Vignes and Leffler and Cullinan equations. The lower limit of the linear diffusivity is the constant coefficient and at 100% solvent, the diffusivity is the addition of the two coefficients. Going from zero solvent concentration to the solubility limit,  $0 \leq \omega_s \leq 0.6$ , Figure 4.6.4 shows that the predicted diffusivity using the Vignes equation and the linear diffusivity are much closer in agreement. The Leffler and Cullinan diffusivity drops an order of magnitude, from zero to 0.05 solvent mass fraction, due to the effect of the viscosities. The different forms of the diffusivity function affects less the swelling of the bitumen and more the required solvent.

**Table 4.6.1: Optimised Diffusion Coefficients**

	$p_1$ (cm <sup>2</sup> /s)	$p_2$ (cm <sup>2</sup> /s)
Linear	$4.78 \times 10^{-6}$	$4.91 \times 10^{-6}$
Constant	$4.35 \times 10^{-6}$	
Vignes (1966)*	$8.66 \times 10^{-6}$	$7.54 \times 10^{-6}$
Leffler and Cullinan (1970)*	$9.04 \times 10^{-6}$	$9.05 \times 10^{-6}$

\*  $p_1 = D_{sb}^o$  and  $p_2 = D_{bs}^o$  are the infinite dilution coefficients for the Vignes and Leffler and Cullinan equations.



**Figure 4.6.4: Optimised Diffusivity Functions as per Table 4.6.1**

The predicted increase in bitumen height and decrease in solvent height for the three optimised diffusivities are shown in Figure 4.6.5 and Figure 4.6.6. Figure 4.6.5 illustrates that the bitumen growth can also be predicted using the Vignes equation or the Leffler and Cullinan equation. Whereas, Figure 4.6.6 shows that the Vignes equation reasonably predicts the solvent decrease at early times but not later. The Leffler and Cullinan equation does not predict the decrease in solvent even though it accounts for the component viscosities as well as the mixture viscosity. It is possible to predict the bitumen swelling in time using more than one diffusivity function. This is due to the fact that the change in bitumen height is predicted from the product of the diffusivity and concentration gradient at the interface less the change in overall density with respect to time as shown in equation 4.4.21 and explained directly thereafter. Even though the concentration and thus density profiles differ for different diffusivity functions, as shown in Figure 4.6.7, the change in predicted bitumen height with respect to time can be the same for different diffusivities. The predicted decrease in solvent height is calculated from a simple mass balance. Equations 4.4.50 and 4.4.51 show that the predicted solvent decrease is simply the product of the solvent mass fraction and mixture density integrated over the depth of bitumen. The unique diffusivity is deciphered when the calculated decrease in solvent independently predicts the experimentally observed decrease in liquid solvent.

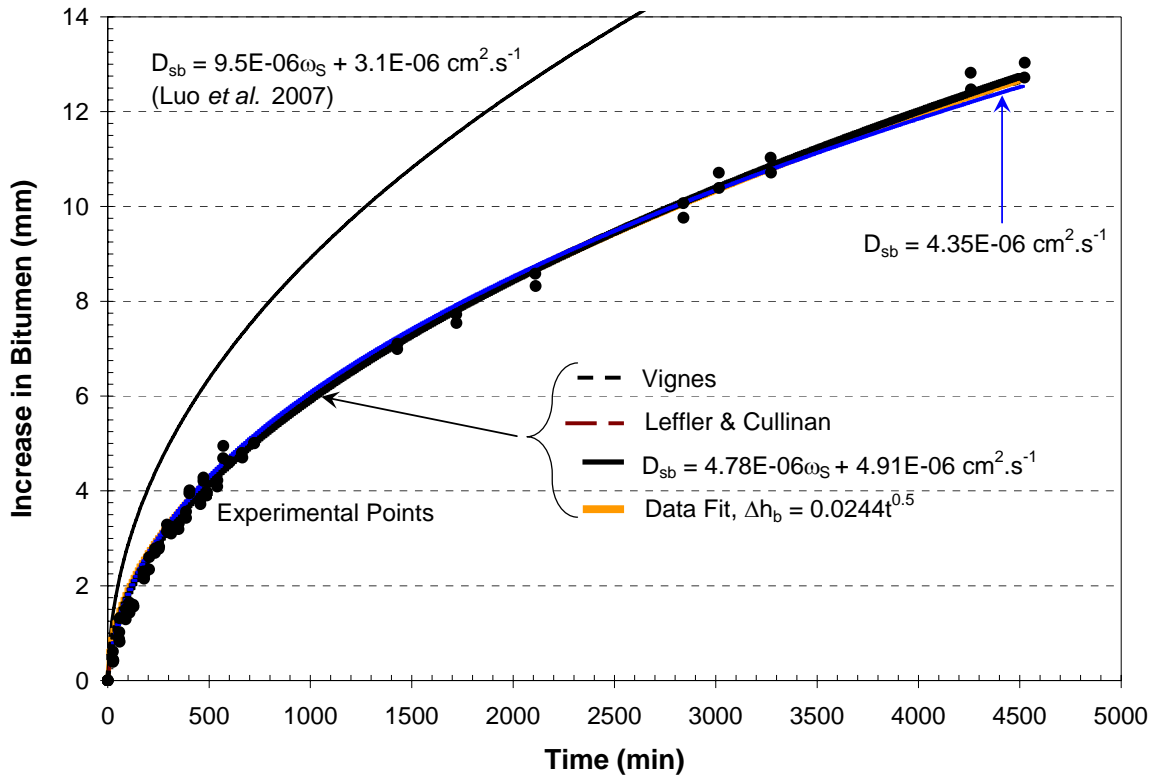


Figure 4.6.5: Comparison of the Increase in Bitumen using Different Diffusivities

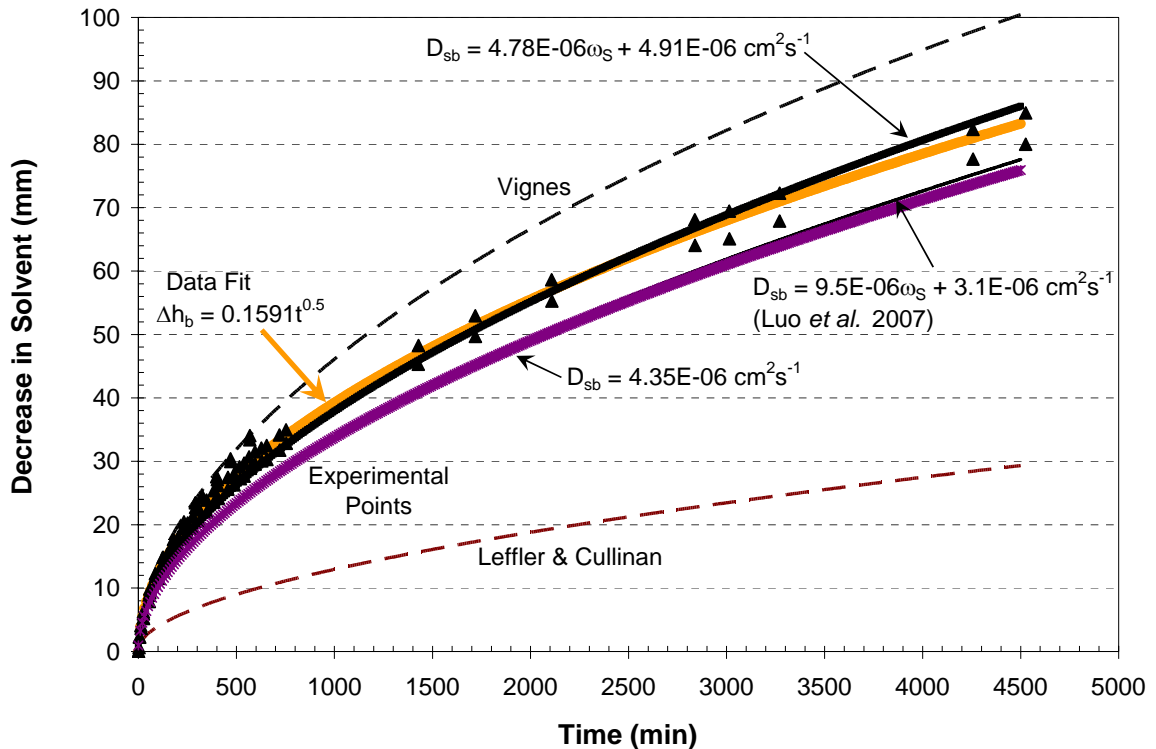
The significant findings detailed in the experimental procedure/results and mathematical development include:

The concentration dependent diffusivity for n-butane in Athabasca bitumen at 26.3°C and a vapour pressure of 35.2 psia was found to be linear and independently validated as:

$$D_{sb} \text{ (cm}^2 \text{ / s)} = 4.78 \times 10^{-06} \omega_s + 4.91 \times 10^{-06}$$

The mathematical model is developed directly from theory without using oversimplified assumptions or complicated mathematical manipulations. Specifically, the continuity equation maintains both the diffusion and convection terms and is developed in terms of a concentration dependent diffusivity.

The methodology clearly shows that it is possible to fit the bitumen swelling with more than one diffusivity function and that even a constant diffusion coefficient can reasonably fit the experimentally measured increase in bitumen height. However, the predicted decrease in liquid solvent height (i.e., the solvent uptake) explicitly and independently validated the true diffusivity function.



**Figure 4.6.6: Comparison of the Decrease in Solvent using Different Diffusivities**

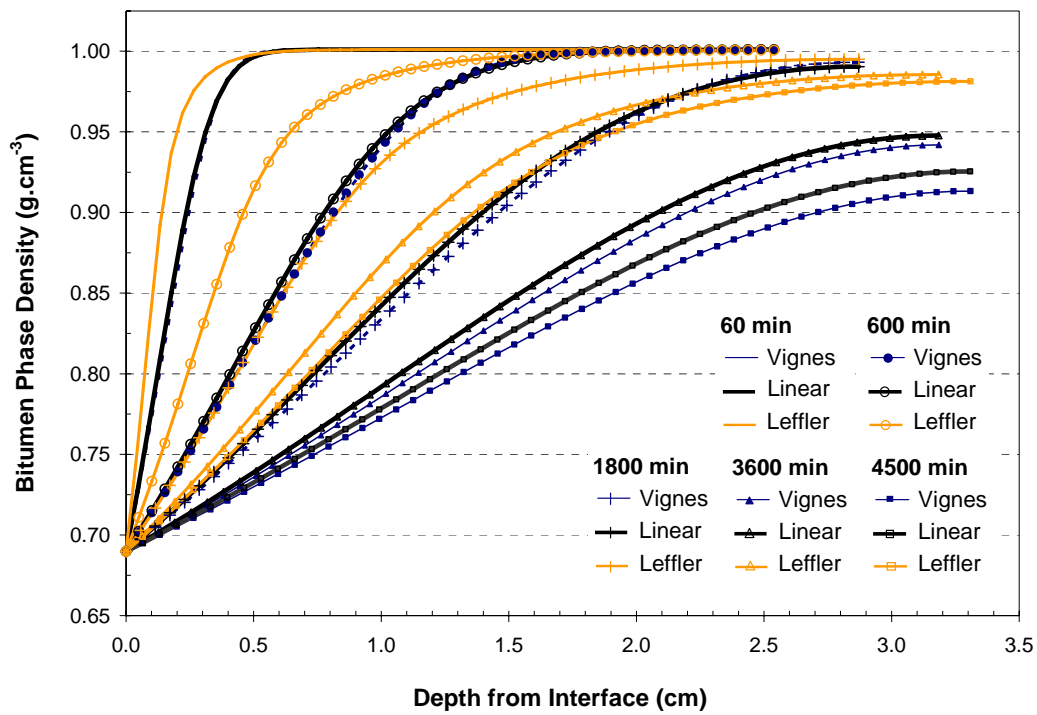


Figure 4.6.7: Comparison of Bitumen Phase Density using Different Diffusivities

# Chapter 5: Conclusions and Recommendations

## 5.1 Conclusions

The mass transfer mechanisms during the solvent recovery of heavy oil were investigated by specially designed experiments and mathematical analysis of the diffusion process.

Using etched glass micromodels, the solvent recovery of heavy oil was observed at the pore scale for both non-condensing (VAPEX) and condensing (N-Solv) solvent recovery methods. When solvent makes contact with the bitumen via a line source, the bitumen-solvent interface advances linearly with time at a constant sweep rate (interface velocity). Depending on the pore structure and the permeability, the sweep rate advances more quickly at the top of the model, as observed in unconsolidated laboratory scale models and etched glass micromodels.

The rate of interface advancement in the micromodels was observed to be over four times greater when the solvent condensed at the bitumen surface, as in the case of N-Solv® compared to VAPEX.

Mass transfer during the solvent recovery of heavy oil is by convective mass transfer and diffusion. Solvent diffuses into the bitumen and bitumen into the gravity draining live oil.

Convective mass transfer was observed and documented at the pore scale, confirming that mass transfer is not by diffusion alone. Although only observed in condensing solvent experiments due to the opacity of the oil, convection would play a role in non-condensing solvent recovery as well. The difference being the concentration gradient of the draining film through which the bitumen is leached away from the interface. Convection is enhanced by capillary displacement mechanisms of drainage and imbibition.

Live oil drains primarily by two mechanisms: drainage displacement mechanisms where there is periodic movement of the live oil from pore to pore and by film flow in the corners of the pores and pore throats already invaded by the solvent.

In-situ upgrading via asphaltene precipitation was only observed when the solvent condensed. Asphaltene precipitation was observed to occur at the tailing side (closer to the solvent chamber rather than the bitumen interface) therefore not creating any reduction in permeability that would affect the draining live oil.

The depth of the mobilised, solvent enriched, live oil was observed to be on average one pore deep and it was confirmed by calculation. However, the mobilised live oil can in some places be 2-3 pores deep and in others only the thickness of a draining film.

Residual oil was observed to be less than 5% in the micromodels. The location of the residual oil was found to depend on the pore structure. The oil was trapped in the occasional pore body when pore throats were very short and in horizontally oriented pore throats when the pore throat length was on the order of a particle diameter, as would be the case for unconsolidated sandstone.

Non-condensable gas in the form of solution gas or injected along with the solvent would have a detrimental impact on production rates compared to using a pure solvent.

A combined experimental-modelling approach was developed to find the concentration dependent diffusivity of light hydrocarbon solvents in heavy oil without the need of cost-prohibitive imaging equipment to measure the concentration profiles.

A simple experiment was developed to monitor the rate of solvent uptake and bitumen swelling for the one-dimensional diffusion of solvent in heavy oil. The rate of mass transfer of butane in Athabasca bitumen at 25°C was experimentally measured.

A one-dimensional diffusion model was mathematically formulated to predict the bitumen swelling in time. The model was developed from first principles and incorporates a concentration dependent diffusivity, assumes the mixture density follows ideal mixing and that the bitumen phase swells as butane diffuses into it. Simplifying assumptions result in inaccurate diffusivity values. A front fixing method was used to create a new dimensionless depth of the bitumen in order to overcome the discretization issues associated with a moving boundary. The method of lines was used to solve the set of partial differential equations and predict the bitumen swelling dependent on the diffusivity used. The difference in the predicted and experimentally determined bitumen swelling was optimised using least squares non-linear regression to optimise for the coefficients of the assumed form of the diffusivity function. **The diffusivity of butane in bitumen at 25°C was found to be:**

$$D_{sb} = 4.78 \times 10^{-6} \omega_s + 4.91 \times 10^{-6} \text{ cm}^2/\text{s}.$$

The differentiating element and uniqueness of the approach used here is that the diffusivity is independently validated using the solvent mass balance. One can optimise for the coefficients of other possible forms of the diffusivity function, including a constant diffusion coefficient. However, the results do not accurately match the solvent uptake even when the bitumen swelling is matched.

## **5.2 Recommendations**

Asphaltene precipitation needs to be more thoroughly investigated using a dynamic controlled experiment to determine when and where asphaltenes precipitate during the solvent recovery process.

Quantifying the overall mass transfer using a mass transfer coefficient approach has merit and needs to be further analysed and explored.

The one-dimensional diffusion experiment reported in this thesis should be used to measure the bitumen swelling and solvent uptake at different temperatures, and vapour pressures, using different viscosity oils and solvents. This will enable the development of better data base to mathematically describe the diffusivity as a function of composition, bitumen/solvent pair and temperature conditions.

## References

- Allen, J.C. & Redford, A.D. 1976. Combination solvent-noncondensable gas injection method for recovering petroleum from viscous petroleum-containing formations including tar sand deposits, United States Patent No. 4109720, Texaco, New York, August 29, 1978, US application No. 740281, November 9, 1976.
- Allen, J.C. 1974. Gaseous solvent heavy oil recovery, Canadian Patent No. 446874, February 28, 1974.
- Awang, M. and Farouq Ali, S.M. 1980. Hot-Solvent Miscible Displacement, *Proceedings: 31<sup>st</sup> Annual Technical Meeting of the Petroleum Society of CIM*, Calgary AB, May 25-28, 1980, paper 80-31-29.
- Badamchi-Zadeh, A., Yarranton, H.W., Svrcek, W.Y., and Maini, B.B. 2009a. Phase Behaviour and Physical Property Measurements for VAPEX Solvents: Part I. Propane and Athabasca Bitumen. *Journal of Canadian Petroleum Technology*, 48(1), 54-61.
- Badamchi-Zadeh, A., Yarranton, H.W., Svrcek, W.Y., and Maini, B.B. 2009b. Phase Behaviour and Physical Property Measurements for VAPEX Solvents: Part II. Propane Carbon Dioxide and Athabasca Bitumen. *Journal of Canadian Petroleum Technology*, 48(3), 57-65.
- Bird, B.R., Stewart, W.E. and Lightfoot, E.N. 2002. Transport Phenomena, 2<sup>nd</sup> edition, John Wiley and Sons, Toronto.
- Boustani, A. and Maini, B. 2001. The Role of Diffusion and Convective Dispersion in Vapour Extraction Process, *Journal of Canadian Petroleum Technology*, 40(4), 68-77.
- Butler, R.M. 2001. Some recent developments in SAGD, *Journal of Canadian Petroleum Technology*, 40(1), 18-22.
- Butler, R.M. and Jiang, Q. 2000. Improved Recovery of Heavy Oil by VAPEX with Widely Spaced Horizontal Injectors and Producers, *Journal of Canadian Petroleum Technology*, 39(1), 48-56.
- Butler, R.M. and Mokrys, I.J. 1989. The Rise of Interfering Solvent Chambers: Solvent Analog Model of Steam Assisted Gravity Drainage. *Journal of Canadian Petroleum Technology*, 32(3).
- Butler, R.M. and Mokrys, I.J. 1991. A New Process (VAPEX) for Recovering Heavy Oils using Hot Water and Hydrocarbon Vapour. *Journal of Canadian Petroleum Technology*, 30(1).
- Butler, R.M. and Mokrys, I.J. 1993. Recovery of Heavy Oils Using Vapourized Hydrocarbon Solvents: Further Development of the Vapex Process. *Journal of Canadian Petroleum Technology*, 32(6).
- Butler, R.M., and Mokrys, I.J. 1998. Closed-loop Extraction Methods of Heavy Oils and Bitumens Underlain by Aquifers: The Vapex Process, *Journal of Canadian Petroleum Technology*, 37(4).
- CAPP - Canadian Association of Petroleum Producers. 2009. Oil Sands, [www.capp.ca/canadaIndustry/oilSands](http://www.capp.ca/canadaIndustry/oilSands) (accessed 22 April 2009).
- Chatzis, I. 1980. Ph.D. Dissertation, University of Waterloo, Waterloo, ON, Canada
- Chatzis, I., 2002. Pore Scale Mechanisms of Heavy Oil Recovery using the VAPEX Process. *Proceedings: International Symposium of Society of Core Analysts*, Monterey, CA, September 2002.
- Chatzis, I. and Dullien, F.A.L. 1983. *Journal of Colloid and Interfacial Sciences*, 91, 199.
- Chatzis, I. and Dullien, F.A.L. 1985. *ICE*, 25, 47.
- Crank, J. 1975. The Mathematics of Diffusion. 2<sup>nd</sup> edition, Clarendon Press, Oxford, England.
- Crank, J. 1984. Free and Moving Boundary Problems. Clarendon Press, Oxford, England.
- Das, S.K. 1995. In Situ Recovery of Heavy Oil and Bitumen Using Vapourized Hydrocarbon Solvents, Ph.D. Dissertation, University of Calgary, Calgary, AB, Canada.



- Das, S.K. 1998. VAPEX: an efficient process for the recovery of heavy oil and bitumen, SPE 50941, 232-237.
- Das, S.K. 2002. VAPEX- A Unique Canadian Technology. *Journal of Canadian Petroleum Technology* **41**(8), 32-34.
- Das, S.K. and Butler, R.M. 1996a. Countercurrent extraction of heavy oil and bitumen, SPE 37094.
- Das, S.K. and Butler, R.M. 1996b. Diffusion Coefficients of Propane and Butane in Peace River Bitumen. *Canadian Journal of Chemical Engineering*, **74**, 986-992.
- Das, S.K. and Butler, R.M. 1998. Mechanism of the Vapour Extraction Process for Heavy Oil and Bitumen. *Journal of Petroleum Science and Engineering*, **21**, 43-69.
- Deng, X. 2005. Recovery Performance and Economics of Steam/Propane Hybrid Process. *Proceedings: SPE International Thermal Operations and Heavy Oil Symposium*, Calgary, AB, 1-3 November 2005, paper SPE 97760.
- Dunn, S.G., Neniger, E.H. and Rajan, V.S.V. 1989. A Study of Bitumen Recovery by Gravity Drainage Using Low-Temperature Soluble-Gas Injection. *Canadian Journal of Chemical Engineering*, **67**, 978-991.
- Dusseault, M. 2006. Introduction to the New Oil Production Technologies (not just for heavy oil!). New Oil Production Technologies for EARTH 634: Geomechanics - In Situ Process (Power Point presentation).
- EIA - Energy Information Administration. 2008. International Energy Outlook. Report #:DOE/EIA-0484(2008), Department of Energy, United States Government, <http://www.eia.doe.gov/oiaf/ieo> (accessed 14 April 2009).
- Einstein, Norman. 2006. Athabasca Oil Sands map. [http://commons.wikimedia.org/wiki/File:Athabasca\\_Oil\\_Sands\\_map.png](http://commons.wikimedia.org/wiki/File:Athabasca_Oil_Sands_map.png) (accessed 15 April 2008).
- El-Haj, R., Lohi, R. and Upreti, S.R. 2009. Experimental Determination of Butane Dispersion in Vapor Extraction of Heavy Oil and Bitumen. *Journal of Petroleum Science and Engineering*, *accepted manuscript*.
- Farouq Ali, A. 1976. Bitumen Recovery from Oil Sands, Using Solvents in Conjunction with Steam. *Journal of Canadian Petroleum Technology*, **3**(11).
- Farouq Ali, A. and Snyder, S.G. 1973. Miscible Thermal Methods Applied to a Two-Dimensional, Vertical Tar Sand Pack, With Restricted Fluid Entry. *Journal of Canadian Petroleum Technology*, **4**(1) 20-26.
- Ferguson, M.A., Mamora, D.D. & Goite, J.G. 2001. Steam-propane injection for production enhancement of heavy Morichal oil, SPE 69689.
- Frauenfeld, T.W., Deng, X., and Jossy, C. 2006. Economic Analysis of Thermal Solvent Processes. *Proceedings: Canadian International Petroleum Conference*, Calgary, AB, 13-15 June 2006, paper 2006-164.
- Friedrich, K.J. 2005. Effects of a Non-Condensable Gas on the Vapex Process, Masters Thesis, University of Waterloo, Waterloo, ON, Canada.
- Gotie, J.G., Mamora, D.D. and Ferguson, A.M. 2001. Experimental study of Morichal heavy oil recovery using combined steam and propane injection, SPE 69566.
- Hayduk, W., Castaneda, R., Bromfield, H. and Perras R.R. 1973. Diffusivities of Propane in Normal Paraffin, Chlorobenzene, and Butanol Solvents; *AIChE Journal*, **19**(4) 859-861.
- Hines, Anthony, L. and Maddox, Robert, N. 1985. Mass Transfer Fundamentals and Applications. Prentice-Hall, Inc. New Jersey.
- Haghighat, P. and Maini, B.B. 2008. Role of Asphaltene Precipitation in Vapex Process. *Proceedings: Canadian International Petroleum Conference*, Calgary, AB, June 17-19, 2008, Paper 2008-087.
- James, L.A. 2003. A Closer Look at VAPEX, Masters Thesis, University of Waterloo, Waterloo, ON, Canada.

- James, L.A. and Chatzis, I. 2004. Details of Gravity Drainage of Heavy Oil during Vapour Extraction. *Proceedings: International Symposium of Society of Core Analysts*, Abu Dhabi, UAE, 5-9 October, 2004.
- James, L.A., Rezaei, N. and Chatzis I. 2008. VAPEX, Warm VAPEX and Hybrid VAPEX – The State of Enhanced Oil Recovery for In Situ Heavy Oils in Canada. *Journal of Canadian Petroleum Technology*, 47(4), 12-18.
- Jamialahmadi, M., Emadi, M., and Müller-Steinhagen, H. 2006. Diffusion Coefficients of Methane in Liquid Hydrocarbons at High Pressure and Temperature. *Journal of Petroleum Science and Engineering*, 53(1-2), 47-60.
- Jiang, Q., Recovery of Heavy Oil and Bitumen Using VAPEX Process in Homogeneous and Heterogenous Reservoirs. PhD Dissertation, University of Calgary, Calgary, AB, Canada, 1996.
- Jin, W. 1999. Heavy Oil Recovery Using the VAPEX Process, Masters Thesis, University of Waterloo, Waterloo, ON, Canada, 1999.
- Karmaker, K., Maini, B.B. 2003. Experimental investigation of oil drainage rates in the VAPEX process for heavy oil and bitumen reservoirs, SPE 84198.
- Karnaker, K. and Maini, B.B., 2003. Applicability of Vapor Extraction Process to Problematic Viscous Oil Reservoirs, SPE 84034.
- Kyle, B.G. 1992. Chemical and Process Thermodynamics. 2<sup>nd</sup> Edition, Prentice Hall, Inc. New Jersey.
- Landau, H.G. 1950. Heat Conduction in a Melting Solid. *Quarterly of Applied Mathematics*. 8(1), 81-94.
- Leffler, John and Cullinan, H.T. 1970. Variation of Liquid Diffusion Coefficients with Composition. *Binary Systems. Industrial and Engineering Chemistry Fundamentals*, 9(1), 84-88.
- Lemmon, E.W., McLinden M.O. and D.G. Friend. Thermophysical Properties of Fluid Systems in NIST Chemistry WebBook, NIST Standard Reference Database Number 69, Eds. P.J. Linstrom and W.G. Mallard, National Institute of Standards and Technology, Gaithersburg MD, 20899, <http://webbook.nist.gov>, (retrieved September 2, 2008).
- Luhning, R.W., Das, S.K., Fisher, L.J., Bakker, J., Grabowski, J., Engleman, J.R., Wong, S., Sullivan, L. A., and Boyle, H. A. 2003. Full Scale VAPEX Process -Climate Change Advantage and Economic Consequences. *Journal of Canadian Petroleum Technology*, 42(2), 29-34.
- Luo, H., Kryuchkov, S. and Kantzas, A. 2007. The Effect of Volume Changes Due to Mixing on Diffusion Coefficient Determination in Heavy Oil and Hydrocarbon Solvent System. *Proceedings: SPE Annual Technical Conference and Exhibition*, 11-14 November 2007, Anaheim, California, U.S.A., paper SPE 110522.
- Luo, H. and Kantzas, A. 2008. Investigation of Diffusion Coefficients of Heavy Oil and Hydrocarbon Solvent Systems in Potous Media. *Proceedings: SPE Improved Oil Recovery Symposium*, 19-23 April 2008, Tulsa, Oklahoma, USA, paper SPE 113995.
- Luo, P. and Gu, Y. 2005. Effects of Asphaltene Precipitation and Solvent Concentration on Heavy-Oil Viscosity. *Proceedings: SPE/PS-CIM/CHOA International Thermal Operations and Heavy Oil Symposium*, 1-3 November 2005, Calgary, Alberta, Canada, paper SPE 97778.
- Luo, P., Yang, C. and Gu, Y. 2007. Enhanced Solvent Dissolution into In-Situ Upgraded Heavy Oil Under Different Pressures. *Fluid Phase Equilibria*, 252, 143-151.
- Mamora, D.D., Rivero, J.A., Hendroyono, A. & Venturini, G.J. 2003. Experimental and simulation studies of steam-propane injection for the Hamaca and Duri fields, SPE 84201.
- Moghadam, S., Nobakht, M. and Gu, Y. 2009. Theoretical and Physical Modeling of a Solvent Vapour Extraction (VAPEX) Process for Heavy Oil Recovery. *Journal of Petroleum Science and Engineering*, accepted.

- Mokrys, I.J. and Butler, R.M., 1993. In-Situ Upgrading of Heavy Oil and Bitumen by Propane Deasphalting: The VAPEX Process, Proceedings: *Production Operations Symposium*, Oklahoma City, OK, 21-23 March 1993, SPE 25452.
- Nenniger, E.H. Canadian Patent CA1059432, 1979. Hydrocarbon recovery, Hatch & Associates, 31 July 1979.
- Nenniger, John, Canadian Patent CA2299790, 2008. Method and Apparatus for Stimulating Heavy Oil Production. Filed: 23-Feb-2000.
- Nenniger, J.E. and Dunn, S.G. How Fast is Solvent Based Gravity Drainage? *Proceedings: Canadian International Petroleum Conference*, 17-19 June 2008, Calgary, Alberta, Canada, Paper 2008-139.
- Nenniger, John and Nenniger, Emil, Canadian Patent CA2351148, 2008. Method and Apparatus for Stimulating Heavy Oil Production. Filed 21-Jun-2001.
- Nenniger, John and Nenniger, Emil, United States Patent US6883607B2, 2005. Method and Apparatus for Stimulating Heavy Oil Production. Filed 20-Jun-2002.
- Oduntan, A.R. 2001. Heavy Oil Recovery Using the VAPEX Process: Scale Up and Mass Transfer Issues. Masters Thesis, University of Waterloo, Waterloo, Canada.
- Oduntan, A.R. and Chatzis I. 2001. Heavy Oil Recovery Using the VAPEX Process: Scale-Up Issues. *Proceedings: Canadian International Petroleum Conference*, Calgary, Alberta, paper 2001-127.
- Radler, M. 2002. Worldwide Reserves Increase as Production Holds Steady. *Oil and Gas Journal*, 100 (2), 113-116.
- Radler, M. 2008. New estimates boost worldwide oil, gas reserves. *Oil and Gas Journal*, 106 (48).
- Ramakrishnan, Venkatesh, 2003. In situ Recovery of Heavy Oil by VAPEX using Propane. Masters Thesis, University of Waterloo, Waterloo, Canada.
- Rezaei, N. and Chatzis, I. 2007. Incorporation of heat in the VAPEX process: warm VAPEX. *Proceedings: Canadian International Petroleum Conference*, Calgary, AB, June 12-14, 2007, Paper 2007-133.
- Rezaei, N. and Chatzis, I. 2008. Warm VAPEX; a Thermally Enhanced Vapor Extraction Process. *Proceedings: Canadian International Petroleum Conference*, Calgary, AB, June 17-19, 2008, Paper 2008-191.
- Riazi, M.R. 1996. A New Method for Experimental Measurement of Diffusion Coefficients in Reservoir Fluids. *Journal of Petroleum Science and Engineering*, **14**, 236-260.
- Rivero, J.A. & Mamora, D.D. 2002. Production acceleration and injectivity enhancement using steam-propane injection for Hamaca extra-heavy oil, SPE 75129.
- Salama, D. and Kantzas, A. 2005. Monitoring of Diffusion of Heavy Oil with Hydrocarbon Solvents in the Presence of Sand. *Proceedings: SPE/PS-CIM/CHOA International Thermal Operations and Heavy Oil Symposium*, 1-3 November 2005, Calgary, Alberta, Canada, paper SPE 97855-MS.
- Shu, W.R. 1984. A Viscosity Correlation for Mixtures of Heavy Oil, Bitumen and Petroleum Fraction. *Society of Petroleum Engineers*, **24**(3), 277-282.
- Singhal, A.K., Das, S.K., Leggitt, S.M., Kasraie, M. & Ito, Y. 1996. Screening of Reservoirs for Exploitation by Application of Steam Assisted Gravity Drainage/VAPEX Processes. SPE 37144.
- Smalley, C. 2000. Heavy Oil and Viscous Oil Chapter from *Modern Petroleum Technology*. R.A. Dawe, ed, John Wiley and Sons Ltd.
- Talbi, K., and Maini, B.B. 2004. Further Investigation of CO<sub>2</sub> Based VAPEX for the Recovery of Heavy Oils and Bitumen. *Proceedings: Canadian International Petroleum Conference*, Calgary, AB, Paper 2004-270.
- Tam, S. 2007. VAPEX Experiments in an Annular Packing of Glass Beads and the Numerical Simulation of VAPEX using Comsol®. Masters Thesis, University of Waterloo, Waterloo, Canada.

- Taylor, R. and Krishna, R. 1993. Multicomponent Mass Transfer. John Wiley & Sons, Inc. New York.
- Tharanivasan, A.K., Yang, C., Gu, Y. 2004. Comparison of Three Different Interface Mass Transfer Models used in the Experimental Measurement of Solvent Diffusivity in Heavy Oil. *Journal of Petroleum Science and Engineering*, **44**, 269-282.
- Upreti, S.R., and Mehrotra, A.K. 2000. Experimental Measurement of Gas Diffusivity in Bitumen: Results for Carbon Dioxide. *Industrial and Engineering Chemistry Research*, **39**, 1080-1087.
- Vignes, Alain. 1966. Diffusion in Binary Systems. Variation of Diffusion Coefficient with Composition. *Industrial and Engineering Chemistry Fundamentals*, **5**(2), 189-199.
- Wen, Y. and Kantzas, A. 2004. Evaluation of Heavy Oil/Bitumen-Solvent Mixture Viscosity Models. *Proceedings: Canadian International Petroleum Conference*, 8-10 June 2004, Calgary, Alberta, Canada, Paper 2004-065.
- Wen, Y., Kantzas, A. and Wang, G.J. 2004. Estimation of Diffusion Coefficients in Bitumen Solvent Mixtures Using X-Ray CAT Scanning and Low Field NMR. *Proceedings: Canadian International Petroleum Conference*, 8-10 June 2004, Calgary, Alberta, Canada, Paper 2004-270.
- Yang, C. and Gu, Y. 2005a. Effects of Heavy-Oil/Solvent Interfacial Tension on Gravity Drainage in the Vapor Extraction (Vapex) Process. *Proceedings: SPE/PS-CIM/CHOA International Thermal Operations and Heavy Oil Symposium*, 1-3 November 2005, Calgary, Alberta, Canada, paper SPE PS2005-406.
- Yang, C. and Gu, Y. 2005b. New Experimental Technique for Measuring Gas Diffusivity in Heavy Oil by the Dynamic Pendant Drop Volume Analysis (DPDVA). *Industrial and Engineering Chemistry Research*, **44**, 4474-4483.
- Yang, C. and Gu, Y. 2006a. A New Method for Measuring Solvent Diffusivity in Heavy Oil by Dynamic Pendant Drop Shape Analysis (DPDSA). *Society Of Petroleum Engineers Journal*, **11**(1), 48-57.
- Yang, C. and Gu, Y. 2006b. Diffusion Coefficients and Oil Swelling Factors of Carbon Dioxide, Methane, Ethane, Propane, and their Mixtures in Heavy Oil. *Fluid Phase Equilibria*, **243**, 64-73.
- Yang, C. and Gu, Y. 2007. A Novel Experimental Technique for Studying Solvent Mass Transfer and Oil-Swelling Effect in the Vapour Extraction (VAPEX) Process. *Journal of Canadian Petroleum Technology*, **46**(9), 44-48.
- Yang, D. and Gu, Y. 2006. Dynamic Interfacial Tension Method for Measuring Gas Diffusion Coefficient and Interface Mass Transfer Coefficient in a Liquid. *Industrial and Engineering Chemistry Research*, **45**, 4999-5008.
- Yang, D. and Gu, Y. 2008. Determination of Diffusion Coefficients and Interface Mass-Transfer Coefficients of the Crude Oil-CO<sub>2</sub> System by Analysis of the Dynamic and Equilibrium Interfacial Tensions. *Industrial and Engineering Chemistry Research*, **47**, 5447-5455.
- Yazdani, A.J. and Maini, B.B. 2005. Effect of Drainage Height and Grain Size on Production Rates in the Vapex Process: Experimental Study. *SPE Reservoir Evaluation and Engineering*, June 2005, 205-213, Paper SPE-89409-PA.
- Yazdani, A.J. and Maini, B.B. 2006. Further Investigation on Drainage Height Effect on Production Rate in Vapex. *Proceedings: SPE Annual Technical Conference and Exhibition*, San Antonio, TX, September 24-27, 2006, SPE 101684.
- Zhang, X. and Shaw, J.M. 2007. Liquid-phase Mutual Diffusion Coefficients for Heavy Oil + Light Hydrocarbon Mixtures. *Petroleum Science and Technology*, **25**, 773-790.
- Zhang, Y.P., Hyndman, C.L., and Maini, B.B. 2000. Measurement of Gas Diffusivity in Heavy Oils. *Journal of Petroleum Science and Engineering*, **26**, 37-47, 2000.
- Zhao, L. 2004. Steam alternating solvent process, SPE 86957.

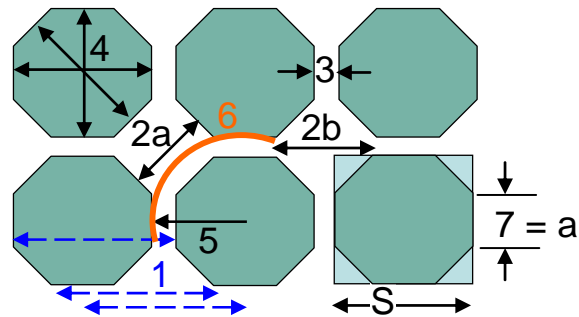
# Appendix A: Micromodel Characterisation

**Table A.1: Physical Constants used in the Micromodel Characterisation**

Physical Constants	
$\theta_{\text{water-air, adv}} (^{\circ})$	27
$\theta_{\text{water-air, rec}} (^{\circ})$	0
$\sigma_{\text{toluene-air}}$ (dynes/cm)	28.17
$\sigma_{\text{water-air}}$ (dynes/cm)	72
$\theta_{\text{toluene-air}} (^{\circ})$	0
$g$ (cm/s <sup>2</sup> )	981
$\rho_{\text{water}}$ (g/cm <sup>3</sup> )	1
$\rho_{\text{air}}$ (g/cm <sup>3</sup> )	0.001
$\rho_{\text{toluene}}$ (g/cm <sup>3</sup> )	0.866
$\mu_{\text{water}}$ (cP)	1
$\mu_{\text{toluene}}$ (cP)	0.588

**Table A.2: Model OC-1 Dimensions**

Model Dimensions	
<b>Pore Dimensions (mm)</b>	
(1) Pore to Pore (3) + (4)	2.04
(2a) Pore Body	1.28
(2b) Pore Body (1) - (7)	1.38
(3) Pore Throat Width	0.45
(4) Particle Size	1.59
(5) Diffusion Distance $0.5 \cdot (4) + (3)$	1.245
(6) Flow Path $0.25 \cdot (2\pi r) + (7)$ $0.5 \cdot \pi \cdot (5) + (7)$	2.61
(7) Pore Throat Length $S/2.414$ $(4)/2.414$	0.66
<b>Model</b>	
Length (cm)	30.4
Length (# pores)	149
Width (cm)	10.0
Width (# pores)	49



**Model OC-1**

**Table A.3: Model OC-1 Capillary Heights**

Distance from Left edge (cm)	Water Imbibition $h_c^{imb}$ (cm)	Water Drainage $h_c^{dr}$ (cm)	Toluene Imbibition $h_c^{imb}$ (cm)
0	13.5	21.1	6.0
1	12.5	19.6	6.0
2	10.6	19.8	6.0
3	11.9	18.6	6.0
4	12.6	19.5	6.0
5	11.8	19.5	5.8
6	11.8	19.3	5.8
7	11.4	18.9	5.8
8	10.9	18.2	5.8
9	9.9	18.3	5.6
9.8	10.1	17.2	5.6
$h_c^{avg}$ (cm)	11.55	19.09	5.85
$r_{eq}$ (cm)	0.01134	0.007	0.01134
$\delta_{etch}$ (cm)	0.01244	0.00809	0.01244
$A_x$ (cm <sup>2</sup> )	0.124	0.081	0.124
$P_c$ (g/cm s <sup>2</sup> )			4968

**Table A.4: Model OC-1 Constant Water Head Permeability Measurements**

	Trial 1	Trial 2	Trial 3
Water Head (cm)	113.9	102.4	93.4
Head Loss (mm)	0	0	0
Time (s)	Mass (g)	Mass (g)	Mass (g)
20	0.66	0.61	0.93
40	1.31	1.21	1.45
60	2.01	1.83	1.94
80	2.71	2.45	2.45
100	3.41	3.08	2.97
120	4.12	3.7	3.51
140	4.82	4.32	4.01
160	5.54	4.94	4.54
180	6.75	5.56	5.07
Q (cm <sup>3</sup> /s)	0.037	0.031	0.026
R <sup>2</sup>	0.995	1.000	1.000
$\Delta P/l$ (g/cm <sup>2</sup> .s <sup>2</sup> )	3675.5	3304.4	3014.0

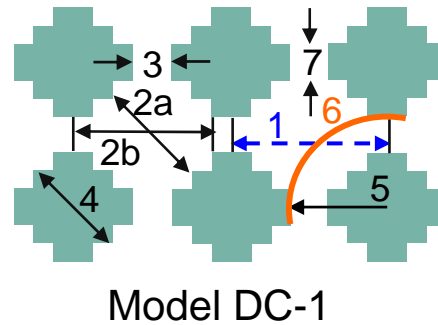
slope (Q vs $\Delta P/l$ ) (cm <sup>5</sup> .s/g)	1.63922E-05
R <sup>2</sup>	0.998
$K^{imb}$ (Darcy)	132

**Table A.5: Model OC-1 Advancing Interface Permeability Measurements**

Trial 1			Trial 2		
Time (s)	Interface Position (cm)	$X^2$ (cm <sup>2</sup> )	Time (s)	Interface Position (cm)	$X^2$ (cm <sup>2</sup> )
26	5	25	10	2.6	6.76
40	7	49	34	4.5	20.25
55	8.5	72.25	49	7	49
68	10	100	61	8.5	72.25
77	11.5	132.25	75	10	100
91	13	169	82	11	121
103	14	196	94	12.5	156.25
			112	13.5	182.25
			124	14.5	210.25
slope (cm <sup>2</sup> /s)		2.2756			2.1495
R <sup>2</sup>		0.9848			0.9949
K (Darcy)		135			127
K <sub>avg</sub> (Darcy)		131			

**Table A.6: Model DC-1 Dimensions**

Model Dimensions	
<b>Pore Dimensions (mm)</b>	
(1) Pore to Pore (3) + (4)	1.6
(2a) Pore Body	1.34
(2b) Pore Body (1) - (7)	1.31
(3) Pore Throat Width	0.49
(4) Particle Size	1.11
(5) Diffusion Distance 0.5*(4) + (3)	1.045
(6) Flow Path 0.25*(2πr) + (7) 0.5*PI*(5) + (7)	1.93
(7) Pore Throat Length	0.29
<b>Model</b>	
Length (cm)	30.4
Length (# pores)	190
Width (cm)	14.1
Width (# pores)	89



**Table A.7: Model DC-1 Capillary Heights**

Distance from Left edge (cm)	Water Imbibition	Water Drainage	Toluene Imbibition, $h_c^{imb}$ (cm)		
	$h_c^{imb}$ (cm)	$h_c^{dr}$ (cm)	Reference Height = 70.7 cm	Reference Height = 81.5 cm	Reference Height = 88.8 cm
0	11.8	24.4	7.1	7.5	8.2
1	11.8	24.2	7.7	8	8.6
2	10.0	23.8	8.0	7.9	8.7
3	11.3	22.5	7.8	8.1	8.7
4	12.1	22.6	8.1	8.2	8.3
5	11.7	23.4	8.1	8.3	8.3
6	11.5	22.5	8.1	8.2	8.6
7	11.8	22	8.3	8.2	8.4
8	10.7	22.1	8.3	8.5	8.5
9	10.3	23.1	9.6	8.6	8.6
10	10.3	23.3	10.0	8.9	8.7
11	10.5	22.5	8.7	9.6	8.7
12	11.8	22.6	8.8	8.7	8.6
13	11.3	22.5	8.9	8.7	8.9
13.8	11.1	21.1	9.1	8.6	8.2
$h_c^{avg}$ (cm)	11.20	22.84	8.52		
$r_{eq}$ (cm)	0.01169	0.006	0.00779		
$\delta_{etch}$ (cm)	0.01281	0.00649	0.00827		
$A_x$ (cm <sup>2</sup> )	0.181	0.092	0.117		
$P_c$ (g/cm s <sup>2</sup> )			7229		

**Table A.8: Model DC-1 Constant Water Head Permeability Measurements**

	Trial 1	Trial 2	Trial 3
Water Head (cm)	114.1	102.5	89.3
Head Loss (mm)	0	0	0
Time (s)	Mass (g)	Mass (g)	Mass (g)
20	0.97	0.86	0.78
40	1.91	1.70	1.53
60	2.86	2.52	2.27
80	3.85	3.35	3.01
100	4.85	4.18	3.77
120	5.84	5.00	4.49
140	6.83	5.86	5.24
160	7.83	6.69	5.95
180	8.84	7.53	6.69
Q (cm <sup>3</sup> /s)	<b>0.049</b>	<b>0.042</b>	<b>0.037</b>
R <sup>2</sup>	1.000	1.000	1.000
$\Delta P/l$ (g/cm <sup>2</sup> .s <sup>2</sup> )	<b>3682.0</b>	<b>3307.6</b>	<b>2881.7</b>
slope (Q vs $\Delta P/l$ ) (cm <sup>5</sup> .s/g)	<b>1.5363E-05</b>		
R <sup>2</sup>	0.970		
$K^{imb}$ (Darcy)	<b>85</b>		

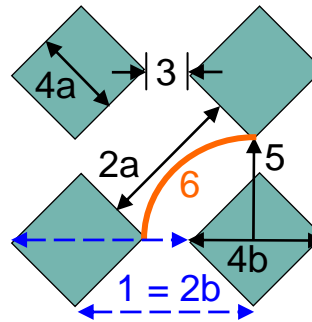


**Table A.9: Model DC-1 Advancing Interface Permeability Measurements**

Trial 2		Trial 4		Trial 5	
Time (s)	X <sup>2</sup> (cm <sup>2</sup> )	Time (s)	X <sup>2</sup> (cm <sup>2</sup> )	Time (s)	X <sup>2</sup> (cm <sup>2</sup> )
0	0.0	0	46.2	0	23.0
5	6.3	5	56.3	5	30.3
10	9.0	10	67.2	10	34.8
15	16.0	15	70.6	15	37.2
20	27.0	20	79.2	20	43.6
25	29.2	25	86.5	25	49.0
30	36.0	30	96.0	30	56.3
35	42.3	35	106.1	35	64.0
40	53.3	40	118.8	40	72.3
45	56.3	45	127.7	45	81.0
50	60.8	50	136.9	50	86.5
55	64.0	55	148.8	55	96.0
60	68.9	60	156.3	60	108.2
65	82.8	65	161.3	65	118.8
70	90.3	70	169.0	70	130.0
75	106.1	75	182.3	75	144.0
80	110.3	80	193.2	80	161.3
85	125.4	85	196.0	85	176.9
90	134.6	90	207.4	90	182.3
95	151.3	95	222.0	95	198.8
100	158.8	100	231.0	105	216.1
105	171.6	105	246.5	110	231.0
110	182.3	110	259.2	120	256.0
115	193.2	120	275.6	130	272.3
120	204.5	130	289.0	140	295.8
125	213.2	140	331.2	150	327.6
135	225.0	150	346.0	160	349.7
145	249.6	160	372.5	170	380.3
155	269.0	170	416.2	180	416.2
165	306.3	180	436.8	190	441.0
175	342.3	190	462.3	200	466.6
185	361.0	200	479.6	210	484.0
195	380.3	210	501.8	220	506.3
205	400.0	220	529.0	230	529.0
215	420.3	230	542.9	240	552.3
225	449.4	240	552.3	250	566.4
235	466.6	250	576.0	260	590.5
245	501.8	260	585.6	270	600.3
255	533.6	270	605.2	280	605.2
270	566.4	280	650.3	290	635.0
285	585.6	290	650.3	300	655.4
300	610.1	300	691.7	310	681.2
315	640.1	310	707.6	320	702.3
330	676.0	320	739.8	330	723.6
345	702.3	330	750.8	340	745.3
360	761.8	340	767.3	350	756.3
375	812.3	350	795.2	360	789.6
390	841.0	360	818.0	370	823.7
		370	835.2	380	852.6
		380	858.5	390	882.1
		390	882.1		
<b>slope (cm<sup>2</sup>/s)</b>	2.2812		2.2187		2.2818
<b>R<sup>2</sup></b>	0.9981		0.9983		0.9968
<b>K (Darcy)</b>	<b>93</b>		<b>90</b>		<b>93</b>
<b>K<sub>avg</sub> (Darcy)</b>	<b>92</b>				

**Table A.10: Model DL-1 Dimensions**

Model Dimensions	
<b>Pore Dimensions (mm)</b>	
(1) Pore to Pore (3) + (4b)	2.04
(2a) Pore Body	1.91
(2b) Pore Body (2b) = (1)	2.04
(3) Pore Throat Width	0.67
(4a) Particle Size	0.99
(4b) Particle Size	1.37
(5) Diffusion Distance $0.5 \cdot (4b) + (3)$	1.36
(6) Flow Path $0.25 \cdot (2\pi r)$ $0.5 \cdot \pi \cdot (5)$	2.13
(7) Pore Throat Length $S/2.414$ $(4)/2.414$	n/a
<b>Model</b>	
Length (cm)	30.4
Length (# pores)	149
Width (cm)	10.0
Width (# pores)	49



**Model DL-1**

**Table A.11: Model DL-1 Capillary Heights**

Distance from Left edge (cm)	Water Imbibition $h_c^{imb}$ (cm)	Water Drainage $h_c^{dr}$ (cm)	Toluene Imbibition, $h_c^{imb}$ (cm)		
			Reference Height = 70.9 cm	Reference Height = 80.8 cm	Reference Height = 89.0 cm
0	5.2	15.7	5.8	5.5	6.7
1	5.4	17.9	6.5	6.3	7.6
2	5.7	18.8	6.9	6.7	7.5
3	5.9	19.0	7.2	7.1	7.6
4	6.0	19.8	7.3	7.2	7.6
5	5.5	20.0	7.1	7.1	7.7
6	6.3	21.0	7.4	7.7	7.8
7	6.0	21.5	7.5	7.7	7.7
8	6.2	21.4	7.4	7.8	7.9
9	6.3	21.7	7.5	7.9	8
9.8	6.7	22.5	7.5	8	8
$h_c^{avg}$ (cm)	5.93	19.94	7.51		
$r_{eq}$ (cm)	0.02209	0.007	0.00884		
$\delta_{etch}$ (cm)	0.02498	0.00728	0.00927		
$A_x$ (cm <sup>2</sup> )	0.250	0.073	0.093		
$P_c$ (g/cm s <sup>2</sup> )			6374		

**Table A.12: Model DL-1 Constant Water Head Permeability Measurements**

	<b>Trial 1</b>	<b>Trial 2</b>	<b>Trial 3</b>	<b>Trial 4</b>
<b>Water Head (cm)</b>	<b>126.6</b>	<b>119.5</b>	<b>114.2</b>	<b>107</b>
<b>Head Loss (mm)</b>	<b>2</b>	<b>2</b>	<b>2</b>	<b>2</b>
<b>Time (s)</b>	<b>Mass (g)</b>	<b>Mass (g)</b>	<b>Mass (g)</b>	<b>Mass (g)</b>
0	0.00	0.01	0.00	0.00
20	3.77	4.03	3.97	3.46
40	8.31	8.12	7.92	6.90
60	12.71	12.28	11.74	10.41
80	17.29	16.42	15.57	13.83
100	21.98	20.61	19.44	17.35
120	25.96	24.61	23.27	20.76
140	30.31	28.73	27.08	24.26
160	34.73	32.80	30.83	27.64
180	39.11	36.83	34.61	31.00
<b>Q (cm<sup>3</sup>/s)</b>	<b>0.219</b>	<b>0.205</b>	<b>0.192</b>	<b>0.173</b>
<b>R<sup>2</sup></b>	<b>1.000</b>	<b>1.000</b>	<b>1.000</b>	<b>1.000</b>
<b><math>\Delta P/l</math> (g/cm<sup>2</sup>.s<sup>2</sup>)</b>	<b>4085.3</b>	<b>3856.2</b>	<b>3685.2</b>	<b>3452.9</b>

<b>slope (Q vs <math>\Delta P/l</math>)</b> <b>(cm<sup>5</sup>.s/g)</b>	<b>7.3780E-05</b>
<b>R<sup>2</sup></b>	<b>0.994</b>
<b>K<sup>imb</sup> (Darcy)</b>	<b>295</b>

**Table A.13: Model DL-1 Advancing Interface Permeability Measurements**

Trial 1			Trial 2		
Time (s)	Interface Position (cm)	X <sup>2</sup> (cm <sup>2</sup> )	Time (s)	Interface Position (cm)	X <sup>2</sup> (cm <sup>2</sup> )
20	10	100	25	10.2	104.04
25	11.4	129.96	30	11.2	125.44
30	12.6	158.76	35	12.3	151.29
35	13.4	179.56	40	13.4	179.56
40	14.4	207.36	45	14.2	201.64
45	15.2	231.04	50	14.9	222.01
50	16.3	265.69	55	16	256
55	17.6	309.76	60	16.8	282.24
60	18.4	338.56	65	17.8	316.84
65	19.7	388.09	70	18.8	353.44
70	20.3	412.09	75	19.8	392.04
75	21.2	449.44	80	20.7	428.49
80	21.9	479.61	85	21.3	453.69
85	23.3	542.89	90	22.2	492.84
90	23.7	561.69	95	22.8	519.84
95	24.1	580.81	100	23.5	552.25
100	24.8	615.04	105	24.1	580.81
105	25.7	660.49	110	24.7	610.09
110	26.2	686.44	115	25.5	650.25
115	26.9	723.61	120	26	676
120	27.3	745.29	125	26.9	723.61
125	27.8	772.84	130	27.3	745.29
130	28.1	789.61	135	27.7	767.29
135	28.7	823.69	140	28.2	795.24
140	29.1	846.81			
slope (cm <sup>2</sup> /s)		<b>6.5149</b>			<b>6.2594</b>
R <sup>2</sup>		<b>0.9968</b>			<b>0.9980</b>
K (Darcy)		<b>300</b>			<b>289</b>
K <sub>avg</sub> (Darcy)		<b>295</b>			

# Appendix B: Effect of Non-Condensable Gas on VAPEX

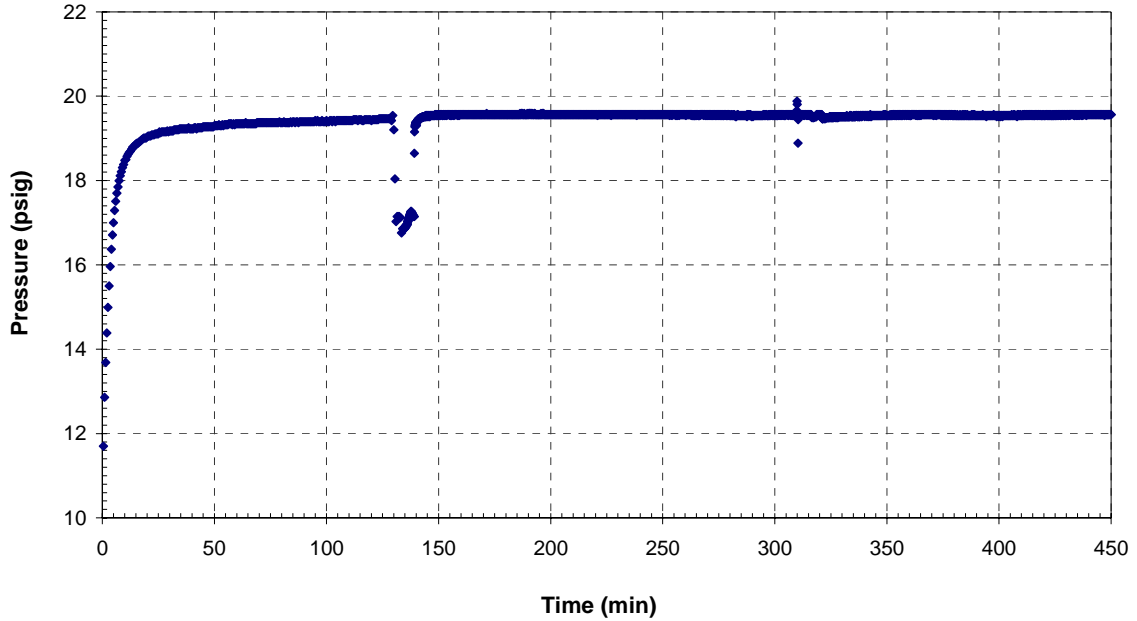


Figure B.1: System Pressure during NCG VAPEX Experiment #1

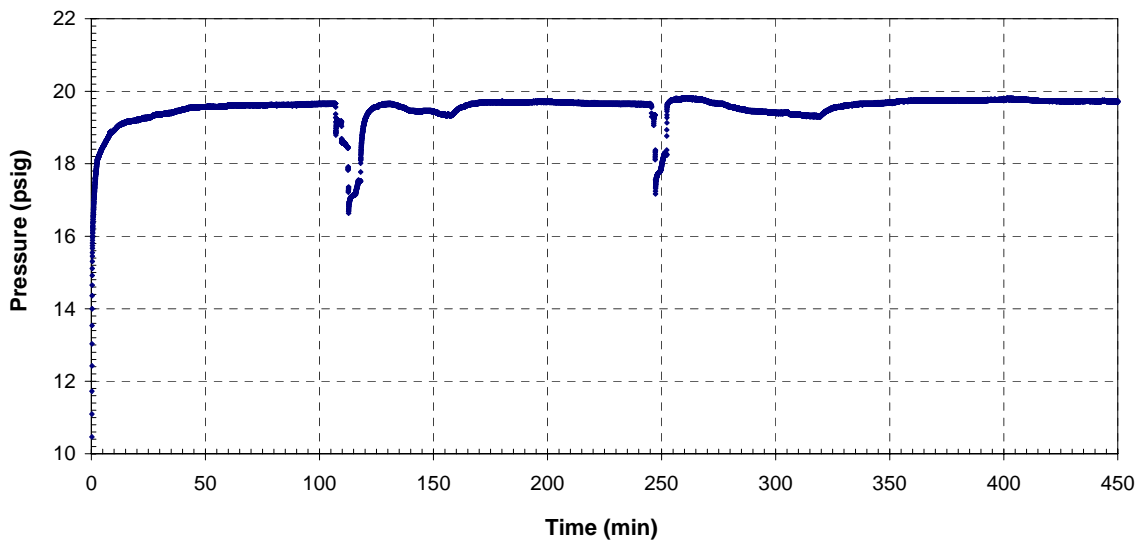
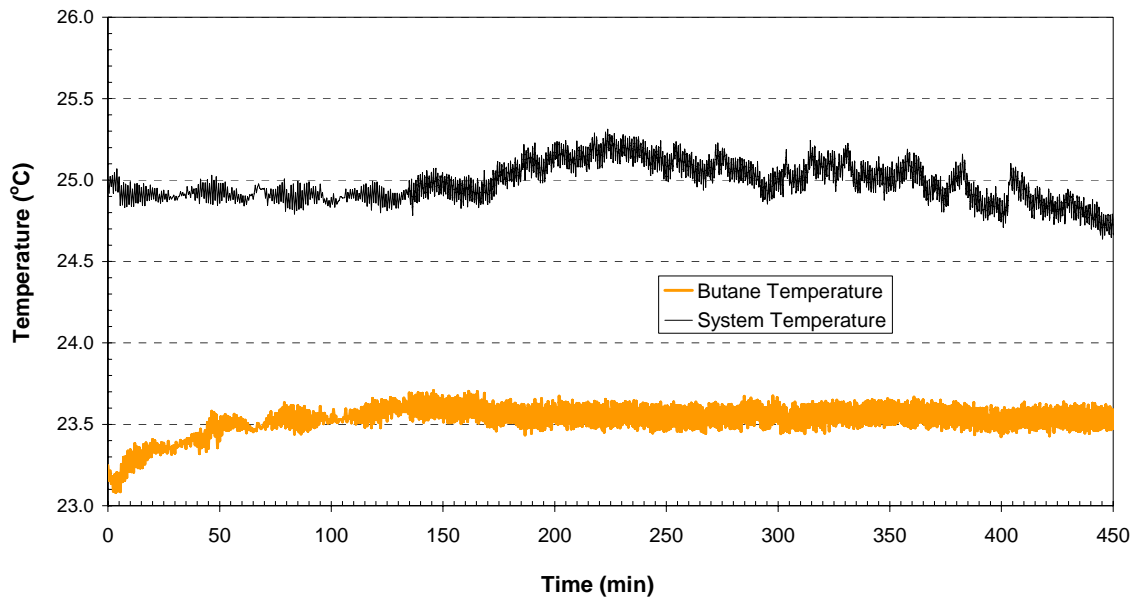
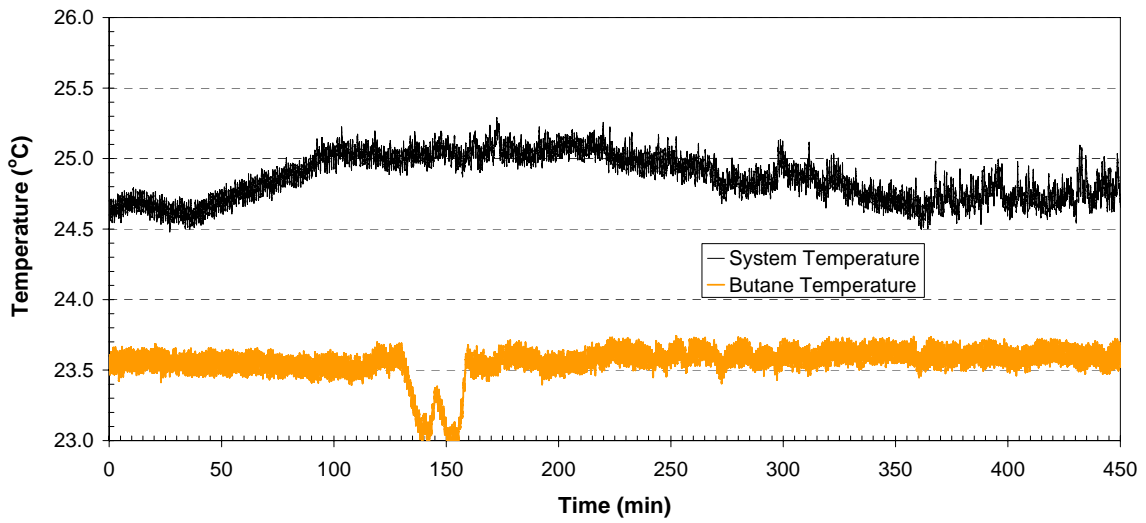


Figure B.2: System Pressure during NCG VAPEX Experiment #2



**Figure B.3: System and Butane Temperatures during NCG VAPEX Experiment #1**



**Figure B.4: System and Butane Temperatures during NCG VAPEX Experiment #2**